THE DISSERTATION COMMITTEE FOR LISA ELANNA BURRIS CERTIFIES THAT THIS IS THE APPROVED VERSION OF THE FOLLOWING DISSERTATION:

INCREASING THE REACTIVITY OF NATURAL ZEOLITES USED AS SUPPLEMENTARY CEMENTITIOUS MATERIALS

Committee:

Maria Juenger, Supervisor

Raissa Ferron

David Fowler

Lynn Katz

Howard Liljestrand

Kitty Milliken

INCREASING THE REACTIVITY OF NATURAL ZEOLITES USED AS SUPPLEMENTARY CEMENTITIOUS MATERIALS

by

LISA ELANNA BURRIS, B.S.A.E.; M.S.

DISSERTATION

Presented to the Faculty of the Graduate School of

The University of Texas at Austin

in Partial Fulfillment

of the Requirements

for the Degree of

DOCTOR OF PHILOSOPHY

THE UNIVERSITY OF TEXAS AT AUSTIN

AUGUST 2014

Dedication

To my husband, Joe, my best friend and biggest supporter.

Acknowledgements

Thank you first to my advisor Dr. Maria Juenger, without whom this graduate school experience would not have been possible. I am incredibly thankful for her professional and personal mentorship, her endless well of research ideas, her constant support, and her ever-hopeful nature. I will be forever thankful to her for being willing to take a chance on a girl from Kansas.

I am also grateful to Dr. Kyle Riding, who not only introduced me to the world of concrete materials research, but has also been one of my biggest supporters along this path, as well as my best example of what it looks like to be a successful young faculty member. I would be remiss to not acknowledge Dr. Robert Peterman, who hired me as an undergraduate research assistant at a time when I wasn't even sure engineering was the path for me, as well as his graduate students, Sarah Larson and Jake Perkins, under who's guidance I discovered my love for research work and my place in the world of civil engineering.

Thank you to my committee members, especially to Dr. Lynn Katz, who opened her labs to me and provided me with so much insight about zeolites and knowledge about water chemistry, as well as to many of her graduate students, Ellison Carter, Anne Mikelonis, Joon Han, and Clayton Ernst, who taught me to use, and trusted me with, their equipment. Thank you also to Dr. Donggao Zhao in the Jackson School, for use of his SEM and carbon coater.

Thank you also to all the folks at 18B who've helped me, through help with my actual research, but also through companionship, friendship, and commiseration. I am fortunate to have had the chance to get to know, learn from, and work with so many wonderful friends and colleagues, including Zeynep Basaran, Sriramya Nair, Saamiya Seraj, Fred Aguayo, Mitchell Dornak, Trevor Williamson, Dongyeop Han, Anthony Garcia, Eric Gianinni, JC Montelongo, and Stephen Stacey. I'd especially like to thank Mike Rung for all his help troubleshooting equipment and for some great chats about good food, politics, and "the way Austin used to be" on our way to and from picking up research specimens in Houston and just in general around the lab. Thank you also to Sherian Williams, who was always available and willing to help with even the most obscure tasks and orders, and also brings the best dishes to lab picnics. I'd also like to thank Chris Clement, not only for passing on to me a small bit of his endless mechanical and technical knowledge, but also for his friendship, and a great traditional Texan banana pudding recipe. I would like to thank Katy Aughenbaugh, for being so welcoming to me from my first day visiting Austin to tour the lab, as well as for always being willing to share her extensive knowledge of SEM sample prep, XRD, and Rietveld techniques, and for all the great times decorating cookies, sewing, and just hanging out, doing and discussing girlie things.

I would like to thank my family, especially Judith and Gregory Beck, my mother and father, for 28+ years of love, advice and financial, mental, and spiritual support. Now, you can finally tell people that you daughter has graduated from college!

Finally, I would like to thank my husband, and best friend, Joe. For giving up a job you loved to move down to Austin, Texas with me, for picking up the slack at home and supplying me with food and love during the dark days of dissertation writing, for always being up to try something new, and for being willing to sacrifice your time and tire tread to enable me to pursue my dreams. Hopefully this is only the beginning of many new adventures for us.

INCREASING THE REACTIVITY OF NATURAL ZEOLITES USED AS SUPPLEMENTARY CEMENTITIOUS MATERIALS

Lisa Elanna Burris, PhD

The University of Texas at Austin, 2014

Supervisor: Maria Juenger

This work examined the effects of thermal and chemical treatments on zeolite reactivity and determined the zeolite properties governing the development of compressive strengths and pozzolanic reactivity. Zeolites are naturally occurring aluminosilicate minerals found abundantly around the world. Incorporation of zeolites in cement mixtures has been shown by past research to increase concrete's compressive strength and durability. In addition, use of zeolites as SCMs can decrease the environmental impact and energy demands associated with cement production for reinforced concrete structures. Further, in contrast to man-made SCMs such as fly ash, zeolite minerals provide a reliable and readily available SCM source, not affected by the production limits and regulations of unrelated industries such as the coal power industry.

In this work, six sources of naturally occurring clinoptilolite zeolite were examined. The zeolites were first characterized using x-ray fluorescence, quantitative x-ray diffraction, thermal analysis, particle size analysis, pore size distribution and surface area analysis, and scanning electron microscopy. Cation exchange capacity was also tested for one of the zeolites. Following comprehensive material characterization, the

pozzolanic reactivity of the natural zeolites was determined by measuring the quantity of calcium hydroxide in paste after 28 or 90 days, by measuring calcium hydroxide consumption of the zeolite in solution and by tracking the development of strengths of zeolite-cement mortars. Pretreatments that attempted to increase the reactivity of the zeolites, including calcination, acid treatment, milling and cation exchange, were then tested and evaluated using the same methods of material characterization and testing mentioned previously. Last, the results of the reactivity testing were reanalyzed to determine which properties of natural zeolites, including particle size, nitrogen-available surface area, and composition, govern the development of compressive strengths, pozzolanic reactivity and improved cement hydration parameters of pastes and mortars using natural zeolites as SCMs. Pretreatment testing showed that milling and acid-treatment successfully increased the reactivity of zeolites used as SCMs. Additionally, particle size was shown to be the dominant property in determining the development of compressive strengths while particle size and surface area of the zeolites contributed to zeolite pozzolanic reactivity.

Table of Contents

List of Tables

List of Figures

Chapter 1: Introduction

Natural zeolites are aluminosilicate minerals prevalent throughout the world. Prior research has shown zeolites to be feasible for use as supplementary cementitious materials (SCMs), replacing a portion of the cement in concrete while still generating similar or improved concrete properties (Lilkov et al. 2011, Perraki et al. 2010, Ahmadi and Shekarchi 2010, Janotka and Krajci 2008). Natural zeolites have been shown to be pozzolanic, reacting with calcium hydroxide and water in cementitious systems to create more C-S-H[1] binding phase (Lilkov et al. 2011, Perraki et al. 2010). Zeolites improve many concrete properties when included as part of the cementitious binder including resistance to alkali silica reaction, sulfate attack, and penetration by chlorides (Ahmadi and Shekarchi 2010, Janotka and Krajci 2008). However, understanding of the mechanisms governing zeolite reactions in cementitious materials is limited and several disadvantages are associated with the use of natural zeolites in cementitious mixtures: properties generated by cementitious mixtures using natural zeolites can vary greatly depending on zeolite source (Ackley et al. 2003); mixtures using natural zeolites have been shown to produce lower concrete compressive strengths, especially at early ages (Ahmadi and Shekarchi 2010, Lilkov et al. 2011b); and, ranging from $70-$200/ton (Novinskie, G., Bunger, P., Hodnett, D., Admire, C., personal communications,

[1] Cement chemistry uses its own set of abbreviated notations: C = CaO, A = Al_2O_3, S = SiO, H = H_2O, F = Fe_2O_3. C-S-H, a poorly crystalline calcium silicate hydrate, is one of the products of cement hydration, the other being calcium hydroxide. The dashes in the C-S-H notation indicate that no particular composition is implied. The stoichiometry of C-S-H varies depending on many factors including the composition of the materials present during hydration, the stage of hydration and the quantity of water present for hydration, but the general formula is 1.5-1.9$CaO.SiO_2.nH_2O$, with n dependent on relative humidity and temperature. (Taylor 1997, Shehata et al. 1999, Lothenbach et al. 2011)

November 2011), natural zeolite has a higher cost than several of the commonly used SCMs such as fly ash (~$40/ton) (ARTBA 2011).

The research presented in this dissertation provides improved understanding of the interactions of natural zeolites and constituents of cementitious systems during initial cement hydration reactions as well as over the long term in hydrated pastes and mortars. It also furthers understanding of the effect of treatment techniques on the physical and chemical properties of natural zeolites and how those properties affect the performance of cementitious systems in which natural zeolites are used as supplementary cementitious materials (SCMs). The findings of this work shed light on how zeolites interact with cement and will also help engineers create higher durability concrete using zeolites. However, this research not only increases the knowledge of how zeolites affect cementitious systems, but also furthers understanding of how other potential SCMs will behave when used in similar situations; for example, this research may improve the understanding of the role material composition plays on system performance compared to particle size or surface, or what effect cations contributed from the SCM have on the kinetics of the cement hydration reactions. This research also increases understanding of how pretreatments, common in other industries such as water and gas purification (Wang and Peng 2013, Ackley et al. 2003, Kesraoul-Ouki et al. 1993, Perez-Ramirez et al. 2003, Athanasiadis and Helmreich 2005, Faghihian and Bowman 2005, Ivanova and Koumanova 2009) and catalysis (Matias 2009, Beers et al. 2003, Triantafillidis 2001, Unveren 2005), affect the properties of aluminosilicate minerals for use as SCMs. This

understanding will also allow future concrete mixtures to be engineered without requiring trial-and-error testing and long-term property testing to achieve desired performance.

1.1 MOTIVATION

Cement production accounts for 31.6 Tg of CO_2 emissions each year in the U.S., making it one of the largest contributors to CO_2 emissions in the country (EPA 2013). Cement industry emissions account for around 5% of global CO_2 emissions (Barcelo 2014). The emissions associated with cement production come from two sources: "process" emissions that result from decarbonation of limestone ($CaCO_3$), one of the primary raw materials used to make cement, and emissions resulting from the energy needed to heat and run the kiln.

Concrete is a composite material consisting of three main components: binder (cement and SCMs), water, and rock (coarse and fine aggregates). One solution to reducing CO_2 emissions associated with concrete construction is to use supplementary cementitious materials. SCMs lower CO_2 emissions by offsetting the quantity of cement needed per ton of concrete while providing comparable, or improved, concrete properties. Figure 1.1 shows an example of SCM use in concrete.

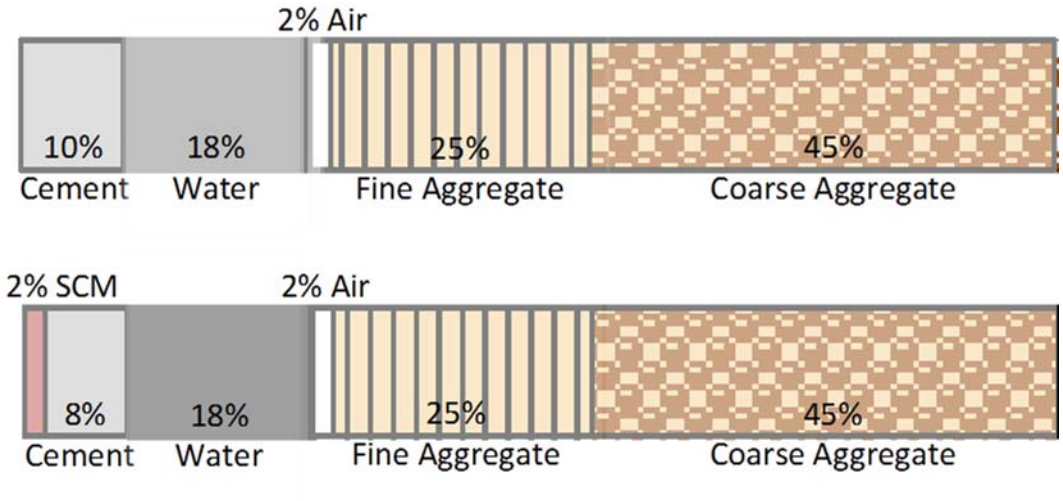

Figure 1.1 - Typical concrete makeup without SCMs (top) and with SCMs (bottom). (Adapted from Kosmatka et al. 2003)

The idea of using natural zeolites as SCMs is not new (Colella et al. 2001), but zeolites have not been highly utilized in U.S. concrete construction due to the abundant availability of inexpensive, man-made pozzolans such as fly ash. Fly ash, a by-product of the coal burning electric power industry, is by far the most used SCM, with nearly 11.4 million tons used in cement and concrete applications in the U.S. on an annual basis (Obla et al. 2012). While fly ash is an inexpensive and effective material for use, either as an SCM or in blended cements, its availability and compositional stability have been threatened by recent EPA standards imposed on energy production facilities (Naranjo and Lukefahr 2012). Further, fly ash is not available in all regions of the world, especially less developed areas. It is essential that the construction industry investigates and develops new SCM sources that are not affected by environmental regulations and are readily available throughout the world. Natural zeolite, a mineral prevalent worldwide, has been proposed as one material that may be able to supplement the use of fly ash in concrete.

1.2 RESEARCH OBJECTIVES

In the research presented in this dissertation the chemical and physical properties of six sources of natural zeolite were characterized, and their effects on the chemical and mechanical performance of cementitious mixtures using natural zeolites as SCMs was determined. Pretreatments, including calcination, soaking in acid, ball milling and exchanging the zeolite's cations to create a homoionic zeolite form, were then employed in an attempt to increase the reactivity of the zeolite. In order to determine if pretreatment techniques were successful, the relative reactivities of the untreated and treated materials were tracked by three methods: (1) measuring the amount of calcium hydroxide converted to calcium silicate hydrate (C-S-H) in zeolite-cement pastes relative to the calcium hydroxide present in cement-only pastes; (2) measuring the amount of calcium hydroxide consumed by the untreated and treated zeolites in a heated calcium hydroxide aqueous solution; and (3) comparing the compressive strengths developed in mortar cubes composed of sand and cement with and without treated or untreated zeolites. Changes in reactivity were then linked to changes induced by the pretreatments in: material phases, relative crystallinity, particle size, and surface area or pore size distribution.

In summary, this work had two primary objectives:

1. Determine the factors that control the performance of zeolites in cementitious mixtures.
2. Determine if pretreatments such as calcination, acid treatment, milling and cation exchange can be used to increase the reactivity of zeolites used as SCMs.

1.3 DISSERTATION ORGANIZATION

This dissertation is organized into several sections. First, background information about the history, current usage, and availability of natural zeolites, as well as the properties of zeolite-cement mixtures, including compressive strengths, durability and pozzolanicity, are presented in Chapter 2. General methods and materials used throughout this work are presented in Chapter 3. Methods specific to a particular treatment or type of analysis, however, are presented in their respective chapters, for example, the procedure for acid treatment is presented in the chapter covering acid treatment, Chapter 5. The results of zeolite pretreatment testing are described in Chapters 4-7, with calcination covered in Chapter 4, acid treatment in Chapter 5, milling in Chapter 6, and cation exchange in Chapter 7. Chapter 8 presents an overview of the data collected from pretreatment testing, attempts to discern what physical properties dominate the performance of zeolites in cementitious systems, and develops relationships for predicting the performance of zeolite-cement mixtures. Conclusions and suggestions for future work are contained in Chapter 9. Several appendices follow the conclusions that addressed questions related to the reactivity of natural zeolites used as SCMs, but did not directly fit into the scope of the main body of this dissertation. Appendix A explores the applicability of the Chapelle test as a measure of zeolite reactivity, while Appendix B investigates the use of zeolites with high limestone cements, and the influence of the filler effect compared to pozzolanic reactivity on performance of zeolite-cement systems. Appendix C provides insight into the relationships between cation-exchanged zeolites and hydration kinetics shown in isothermal calorimetry testing, showing the effect of

added cations to the zeolite-cement pastes. Finally, Appendix D shows an attempt to quantify zeolite reactivity by measuring the rate of dissolution when the zeolite is exposed to a simulated pore solution.

Chapter 2: Background

2.1 General Zeolite Background Information

Zeolites are hydrated crystalline aluminosilicate minerals. The crystalline framework consists of silicate and aluminate tetrahedra that link together, forming defined size pore openings (Bongdanov et al. 2009). Zeolites are highly porous, with pore volume often consisting of as much as 50% of the total volume (Pabalan and Bertetti 2001). Zeolite tuffs typically form when volcanic glasses are altered through interaction with interstitial fluids at temperatures and pressures that are high, but less than those required for metamorphic transitions. This interaction produces several different products including crystalline zeolites, quartz, cristobalite, aragonite, thenardite, smectite, unaltered volcanic glass, halite, calcite, feldspar, montmorillonite, non-crystalline aluminosilicate gels and hydrated iron oxides (Colella et al. 2001; Pabalan and Bertetti 2001; Sprynskyy et al. 2006). As a result, natural zeolites are rarely found in pure form, but the deposits in which they are found are often more than 70% zeolite (Sprynskyy et al. 2006).

Over 40 types of natural zeolites exist, with the most common being clinoptilolite, chabazite and mordenite. This work focused solely on clinoptilolite zeolite. Clinoptilolite is a member of the heulandite family of zeolites and is differentiated from heulandite by the ratio of silicon to aluminum in the crystal. A Si/Al ratio greater than 4 indicates the presence of clinoptilolite, while a Si/Al ratio less than 4 is representative of heulandite (Perraki et al. 2005). In addition to a higher Si/Al ratio, clinoptilolite also has a greater thermal stability than heulandite (Perraki et al. 2003; Sprynskyy et al. 2006). The typical

formula for clinoptilolite is $(Na,K)_6(Al_6Si_{30}O_{72})\bullet 28H_20$. Clinoptilolite compositions vary widely within the ranges of 58.5-70.6% SiO_2, 9.7-21.54% Al_2O_3 and 1.3-3.8% CaO. Some example chemical compositions for clinoptilolites reported in the literature are shown in Table 1. The clinoptilolite zeolite's average void volume is 34% (Sprynskyy et al. 2006).

Table 2.1 - Typical clinoptilolite compositions

Source	Location	CaO	SiO_2	Al_2O_3	Fe_2O_3	MgO	Na_2O	K_2O
Ahmadi 2010	Iran	1.68	67.79	13.66	1.44	1.2	2.04	1.42
Bilim 2011	Turkey	3.87	63.01	10.72	2.68	1.07	0.23	3.8
Gordon 2008	California	1.27	67.81	21.54	-	0.39	3.05	3.75
Lilkov 2010	Bulgaria	6.73	62.74	9.68	0.74	2.9	0.29	2.79
Lilkov 2011	New Mexico	2.97	70.39	11.24	1.28	1.13	-	3.23
Mertens 2009	Ecuador	3.71	58.48	15.52	2.24	0.32	0.96	2.07
	Turkey	1.88	62.09	12.35	1.15	0.21	1.18	4.17
	Serbia	3.37	64.14	11.26	0.97	0.22	1.01	1.01
Naiqian 1998	China	2.64	67.71	11.22	1.12	1.1	1.55	2.65
	Japan	2.54	70.17	11.81	1.61	0.52	2.73	1.91
Perraki 2005	Greece	3.01	67.24	12.66	0.15	0.49	0.48	1.62
Perraki 2010	Greece	3.52	70.61	10.83	0.48	0.62	0.52	1.95
Ortega 2000	Greece	3.8	67.9	11.9	1.2	1.1	0.4	1.5

2.1.1 Sources in the USA

According to the USGS, in 2011, USA had a zeolite production of 65,400 metric tons, and world production was estimated to range between 2.8 to 3.3 million metric tons. Seven US companies currently mine zeolites, with reserves in Arizona, California, Idaho,

Nevada, New Mexico, Oregon and Texas [USGS mineral yearbook 2011]. The major producers in the USA are: St. Cloud Mining, Inc. in Arizona, California and New Mexico, UOP LLC in Arizona, KMI Zeolite Inc. in California, Bear River Zeolite Co., Inc., Steelhead Specialty Minerals, Inc. and Teague Mineral Products Co. in Idaho, and Zeotech Corp. in Texas (USGS mineral yearbook 2011). "World reserves are not determined but are expected to be large" (USGS mineral commodity summary 2011).

2.1.2 Zeolite Uses

Zeolites are used in many industries as molecular sieves, but zeolites used in industrial applications are most often synthesized in order to decrease the amount of material impurities and control opening sizes. Natural zeolites have many uses including: animal feed, pet litter, odor control, water purification, wastewater treatment, fungicide or pesticide carrier, gas absorbent, fertilizer carrier, oil absorbent, desiccant, catalyst and control of ammonia in aquaculture systems (Bongdanov et al. 2009) (USGS mineral yearbook 2011).

2.1.3 The History of Zeolites used in Cementitious Mixtures

Zeolitic tuffs were used in building materials as pozzolans as far back as ancient Rome (Mielenz et al. 1951). In modern times, zeolites have been used extensively throughout Europe and Asia as SCMs and in blended cements (USGS mineral yearbook 2011). In 1989 about $7x10^7$ tons of blended cement were manufactured in China containing 10-30% natural zeolite (USGS mineral yearbook 2011). Expanded zeolitic tuffs have also been used as a source of lightweight aggregate and incorporated into

pozzolan-cements in the US (Colella et al. 2001), as well as into some well-recognized U.S. structures, such as the Los Angeles Aqueduct (Mumpton 1999).

2.2 PERFORMANCE OF ZEOLITE AS AN SCM

2.2.1 Pozzolanic Capacity of Zeolites

When cement reacts with water the two primary resultant products are C-S-H and calcium hydroxide. Of these two products, C-S-H is generally preferred over calcium hydroxide because it provides the strength of the hydrated solid material. One way zeolites interact within the cementitious system is through the pozzolanic reaction, which produces C-S-H In the pozzolanic reaction, silica and alumina react with calcium hydroxide to form additional hydrate phases, primarily C-S-H. Thus, in a zeolite-cement paste, lower calcium hydroxide content correlates with higher quantities of C-S-H and also indicates higher pozzolanic reactivity of the zeolite. The pozzolanic reaction is shown in Equations 3.1-3.5 (Shi and Day 2000). In the first step, shown in Equation 3.1, hydrolysis of calcium hydroxide increases the system pH. The high pH pore solution then dissolves and depolymerizes the zeolite's silicate and aluminate species, shown in Equations 3.2 and 3.3. In the final step, shown in Equations 3.4 and 3.5, Ca^{2+} ions and the silicate or aluminate species meet and reform into C-S-H or C_4AH_{13} hydrates, or mixtures of these. It is generally assumed that the pozzolanic reaction is a relatively long-term reaction, and can continue for up to 90 days after mixing.

$$Ca(OH)_2 \rightarrow Ca^{2+} + 2OH^- \quad (3.1)$$

$$Si\text{-}O\text{-}Si + 3OH^- \rightarrow [SiO(OH)_3]^- \quad (3.2)$$

$$Si\text{-}O\text{-}Al + 7OH^- \rightarrow [SiO(OH)_3]^- + [Al(OH)_4]^- \quad (3.3)$$

$$Y[SiO(OH)_3]^- + XCa^{2+} + (Z - X - Y)H_2O + (2X - Y)OH^- \rightarrow C_X\text{–}S_Y\text{–}H_Z \quad (3.4)$$

$$2[Al(OH)_4]^- + 4Ca^{2+} + 6H_2O + 6OH^- \rightarrow C_4AH_{13} \quad (3.5)$$

Published research has shown encouraging evidence of good pozzolanic capacity of zeolites in cement mixtures (Lilkov et al. 2011a; Ortega et al. 2000; Perraki et al. 2010). When clinoptilolite was mixed into a paste with solids consisting of 20% clinoptilolite, 80% CaO and water added to create a water-to-solids ratio of 0.30, Ortega et al. (2000) showed that the paste reacted and hardened. When cured at 50°C, the compressive strength was 5380 psi at 28 days. Other studies found that when zeolites were used to replace cement at a replacement level of 5-10% by weight, calcium hydroxide contents were lower in zeolite-cement pastes than neat pastes at all times tested (Lilkov et al. 2011a; Perraki et al. 2010). For all pastes, calcium hydroxide contents continued to decline over time indicating that more calcium hydroxide was consumed by the zeolites than was produced by cement hydration (Lilkov et al. 2011a; Perraki et al. 2010). Additionally, the total amount of C-S-H and calcium aluminate hydration products per gram of cement was greater in zeolite-cement pastes versus the ordinary portland cement paste reference (Lilkov et al. 2011a).

The zeolitic pozzolanic reaction has been found to begin after 2-3 days (Snellings et al. 2010) and continue for up to one year, as demonstrated by Lilkov et al. (2011b), who found that at 10% replacement, no calcium hydroxide remained in samples after 365 days. However, it has been suggested that nearly all of the zeolite that will react in a zeolite-cement paste does so within 3 days (Gordon et al. 2011). Compared to mixtures

containing fly ash, zeolite-cement mixtures were found to have greater degrees of reaction at all times after 3 days (Poon et al. 2006). Particle size distribution, external specific surface area, and zeolite crystal structure were found to influence the reaction rate of early zeolite pozzolanic reactivity (Mertens et al. 2009; Snellings et al. 2010) while Si/Al ratio dictates later age pozzolanicity due to the availability of free silica to drive the pozzolanic reaction (Mertens et al. 2009).

In general, as a result of the pozzolanic reaction, use of SCMs results in greater quantities of C-S-H, as calcium hydroxide is converted into C-S-H, and lower porosity, as pozzolanic reaction products fill the mixture's pores (Lothenbach et al. 2011). As a result, use of SCMs often translates into better performing materials, with increased compressive strengths and better durability in aggressive environments, such as those containing sulfates or chlorides (Lothenbach et al. 2011). The subsequent sections present, in greater detail, the effect of zeolites on the performance of zeolite-cement pastes, mortars and concretes.

2.2.2 Compressive Strength

The effect of the replacement of cement with zeolite on compressive strength is disputed in the literature. Ahmadi and Shekarchi (2010) tested replacement rates from 5-20% by weight of cement and saw increases in concrete strength versus a control, cement-only concrete at all times after three days and all replacement levels; the optimum replacement level, based on strengths at 90 days, was found to be 15%. Other researchers saw a reduction in compressive strength development with increasing replacement of cement with zeolite, although these reductions often decreased over time as compared to

the portland cement-only concrete (Caputo et al. 2008; Janotka and Krajči 2008; Lilkov et al. 2011c; Perraki et al. 2010; Poon et al. 1999). Use of 20% zeolite-80% cement concrete resulted in lower strengths at all ages compared to 100% cement concrete, while 10% cement-replacement by zeolite resulted in an increase in strength at 28 and 90 days (Perraki et al. 2010). All zeolite-cement mortars studied by Lilkov et al. (2011c) showed reduced compressive and flexural strengths at 28 days, with a diminished effect after 180 days. Similarly, Poon et al. (1999) saw a reduction in 3 and 7-day compressive strengths for zeolite-containing cement pastes compared to the cement-only, but the strengths of the zeolite and cement-only mixtures were equivalent at 28 days. Zeolites contribute to strengths more effectively when used at low water-to-cement ratios (w/cm) compared to higher w/cm mixtures (Poon et al. 1999). Particle size also has a marked effect on compressive strengths, with decreasing zeolite particle size leading to increasing compressive strengths in mortars (Rosell-Lam et al. 2011).

2.2.3 Alkali Silica Reaction

Natural zeolites have been shown to behave similarly to fly ash in controlling expansion due to alkali silica reaction (ASR) (Ahmadi and Shekarchi 2010; Karakurt and Topçu 2011). At 20-40% cement replacement levels, zeolite mortars met the ASTM C 1567 (2011) expansion limit and had comparable expansions to mixtures containing similar fly ash replacement levels despite highly reactive aggregates and equivalent alkali contents up to 2.2% (Ahmadi and Shekarchi 2010). In other studies, mortars containing only 10% replacement of cement with zeolite were also below the ASTM C 1567 (2011) expansion limit at 14 days, as the standard requires, and even as long as 90 and 180 days

(Karakurt and Topçu 2011; Naiqian and Tingyu 1998).

2.2.4 Sulfate Resistance

Zeolite-cements perform similarly to high sulfate resistant cements with regard to resistance to sulfate attack (Janotka and Krajči 2008; Janotka et al. 2011; Karakurt and Topçu 2011). After 6 months of exposure to a 10% Na_2SO_4 solution, Karakurt and Topçu (2011) found that the expansion due to sulfate attack in mortar bars with a 30% replacement of cement with zeolite was 0.017%, less than half the 0.05% expansion limit for sulfate-resistant cements called for in ASTM C1157 (2011). Additionally, no evidence was found of ettringite, one of the primary products of the sulfate-cement reaction, in scanning electron microscopy (SEM) images of the zeolite-cement mortar (Karakurt and Topçu 2011). Janotka et al. (2011) saw similar results, with mortars with 15% replacement of cement with zeolite showing less than 0.5% expansion after 6 months of exposure to a 5% Na_2SO_4 solution and less expansion at all times up to a year, than the high sulfate resistant cement also used in the study. The increased resistance to sulfate attack in zeolite-cement mortars is theorized to be a result of the finer pore structure resulting from use of zeolite-cements (Janotka et al. 2011) as well as chemical interactions leading to the development of different hydration products and lower amounts of calcium hydroxide in the mixtures.

2.2.5 Other Durability Factors

Water sorption, oxygen permeability and chloride permeability were all reduced with the replacement of cement by zeolites, up to 20% (Ahmadi and Shekarchi 2010;

Bilim 2011; Lilkov et al. 2011c). Natural zeolite also increased the electrical resistivity of the concrete, signifying a reduction in pore solution ionic concentration and a finer pore distribution (Ahmadi and Shekarchi 2010; Bilim 2011; Lilkov et al. 2011c). As a result of the late onset of the pozzolanic reaction relative to the hydration of the cement-only mortar, specific pore volume of zeolite-cement mortars was greater at 28 days than the cement-only mortar, but the pore volume decreased between 28-180 days relative to the control, cement-only mortars (Lilkov et al. 2011c). Reduced carbonation depths were also seen in cement-zeolite pastes relative to control pastes, with the minimum depth of carbonation achieved with a 30% replacement level (Bilim 2011). Zeolite-cement concrete performed better than control specimens subject to freezing and thawing up to a 5% replacement level. Higher replacement levels, however, produced concrete with diminished freeze-thaw resistance (Bilim 2011).

2.2.6 Heat of Hydration

Understanding of how an SCM affects the cumulative heat of hydration released by a SCM-cement mixture can increase understanding of the reactions occurring in the mixture (Lothenbach et al. 2011; Schindler and Folliard 2005), help quantify the degree of hydration over time (Branco et al. 1992; Schindler and Folliard 2005), and determines whether the mixture can be used for large scale structures, like dams (Branco et al. 1992). Previous research indicates that replacement of cement with zeolite results in lower heat of hydration, with no significant reduction in setting time (Lilkov et al. 2011a; Mozgawa et al. 2011; Perraki et al. 2010). This occurs because in the first few hours of hydration zeolites adsorb water and slow dissolution of the cement grains. Replacement of cement

with zeolite may result in an advance in the onset of the acceleration period of cement hydration (Snellings et al. 2010). Greater total heat released after two days of hydration in zeolite-cement pastes relative to cement-only paste evidences high chemical solubility of the zeolites and a quick onset of the pozzolanic reaction (Lilkov et al. 2011a).

2.2.7 Water Demand

Water demand is not directly related to the pozzolanic reactivity of the zeolitic material, however it represents one of the greatest challenges to utilizing zeolites as SCMs. Zeolite cements have a substantially increased water demand relative to neat pastes, primarily due to the material's high surface area and porous structure (Yilmaz et al. 2009). Water demand in pastes increases proportional to the dosage of zeolite (Ahmadi and Shekarchi 2010; Bilim 2011; Lilkov et al. 2011b; Perraki et al. 2010). However, no problems have been encountered when using superplasticizers to overcome the higher water demand of the zeolite-cement mixtures (Ahmadi and Shekarchi 2010).

2.3 SUMMARY

In summary, zeolites have been shown by other researchers to work well in cementitious systems. Published research has shown encouraging evidence of good pozzolanic capacity of zeolites in cement mixtures (Lilkov et al. 2011c; Ortega et al. 2000; Perraki et al. 2010), and natural zeolites have been shown to adequately control ASR (Ahmadi and Shekarchi 2010; Karakurt and Topçu 2011) and sulfate attack (Janotka and Krajči 2008; Janotka et al. 2011; Karakurt and Topçu 2011). The effect of the replacement of cement with zeolite on compressive strength is not as positive, with

several researchers showing reductions in compressive strength development with replacement of cement with zeolite, especially at early ages (Caputo et al. 2008; Janotka and Krajči 2008; Lilkov et al. 2011c; Perraki et al. 2010; Poon et al. 1999). For this reason improving the reactivity of natural zeolites used as SCMs could be highly beneficial, creating a material that both yields high strengths and good durability.

Chapter 3: Methods and Materials

3.1 General Test Methods

The overall goal of this work was to increase zeolite-cementitious system performance by increasing the reactivity of the zeolites through pretreatments. For each zeolite pretreatment examined, there was a common set of tests performed on the zeolite and zeolite-cement pastes and mortars, described in this chapter. Zeolite testing procedures were divided into two main categories: characterization (physical and chemical) and reactivity testing. Characterization testing was performed in order to increase the understanding of what aspects of the zeolite primarily control its performance in cementitious systems and to determine quick testing methods to determine zeolite reactivity without full-scale performance testing in the future.

Physical and chemical characterization included phase and relative percent crystallinity testing using X-ray diffraction, specific surface area and pore size distribution testing using nitrogen adsorption and the BET and BJH models, particle size characterization using laser diffraction, and thermogravimetric analysis to aid in understanding changes to zeolite crystal structure and stability. Zeolite reactivity testing included measurement of the amount of calcium hydroxide in cement and cement-zeolite pastes, the Chapelle test, an accelerated measurement of material pozzolanicity, and compressive strengths of cement and cement-zeolite mortars. In addition to characterization and reactivity testing, the effect of untreated and pretreated zeolites on cement hydration was measured using isothermal calorimetry. The general testing methods used for multiple zeolite pretreatments are outlined in sections 3.1.1–3.1.3.

Additional tests that are specific to a certain pretreatment are described in the corresponding pretreatment chapter.

3.1.1 Zeolite Physical and Chemical Characterization Testing Methods

Zeolite characterization was completed in order to determine what primary factors contributed to changes in zeolite reactivity in cementitious systems. Characterization testing tracked changes from pretreatments in the phases present in the zeolite samples, as well as particle size, surface area and pore sizes.

3.1.1.1 X-Ray Diffraction (XRD)

X-ray diffraction (XRD) was used to determine the crystalline phases present in each sample, in addition to gauging the effectiveness of reducing crystallinity and the amount of non-zeolite minerals present in the systems by the pretreatments. Amorphous material is known to be very pozzolanically reactive (Naceri and Hamina 2009; Sabir et al. 2001). whereas many of the minerals that form in the same environment with zeolites, such as clays, silicates and plagioclase minerals, are inert in cementitious mixtures (Lawrence et al. 2003; Fernández, Vigil de la Villa, Garcia et al. 2011). Therefore, increasing the amorphous fraction of the zeolite material, in addition to removing inert phases, may result in an increase in reactivity (Habert et al. 2008).

XRD samples were prepared by grinding the treated sample to a powder passing the No. 325 sieve (44 μm) using a ceramic mortar. Each specimen was then pressed into plastic XRD sample holders using a glass plate such that the plane of the specimen

surface was even with the edge of the sample holder in order to create a specimen face in the focusing circle of the powder diffractometer (Reynolds, Jr. 1989).

X-ray diffraction scans were performed using a Siemens D500 x-ray diffractometer, using a copper x-ray source producing Ni-filtered CuKα radiation. The diffractometer was operated at 40 kV and 30 mA with scans taken from 5-70° 2θ with a step size of 0.2° 2θ and a 2 second dwell time. The diffractometer was configured with 4° soller slits and 1° anti-scatter slits on both the beam and detector sides, a 1° divergence slit on the beam side and a 0.15mm receiving slit and 0.6mm detector slit on the detector side. Cu K-β radiation was removed before reaching the detector by a graphite monochromator. Crystalline phases present in each zeolite were determined using files from the inorganic crystal structure database (Bergerhoff and Brown 1987) and Jade MDI software package (Downs and Hall-Wallace 2003). Relative crystallinity was qualitatively gauged according to the reduction of the peak heights of each phase compared to other phases present in the material. In general, lower peak heights correlate with lower sample crystalline content (McCarthy et al. 1988).

3.1.1.2 Specific Surface Area and Pore Size Distribution

Greater material surface area has been shown to correlate with increased pozzolanic reactivity in other SCMs (Lothenbach et al. 2011; Shi et al. 2005), as more of the material is in contact with the pore solution and reaction products of the cementitious system. It was hypothesized that increasing zeolite surface area would also result in increased reactivity, so zeolite surface area was measured and compared to changes in the performance of zeolite-cement mixtures. Pore size distributions were studied in order to

gain an understanding of changes occurring in the zeolite that resulted in changes in zeolite surface area. Due to the large internal surface area inherent in the zeolite crystal structure, surface area and particle size were assumed to be independent of each other for the purposes of this work.

Surface area data was obtained for all samples using a Micromeritics ASAP 2020 Surface Area and Porosimetry Analyzer. Prior to measurement, zeolite samples and the sample tubes were individually weighed to microgram precision. The raw zeolite samples were then degassed for 12 hours at 100°C and a pressure of 500 μmHg or less. Pretreated samples were degassed for 6 hours at 300°C and a pressure of 500 μmHg or less. Samples were heated individually during degassing using a heating mantle with a Type K thermocouple controlled by the nitrogen adsorption testing software program. Degassing temperatures varied and are reported in the chapters for the samples discussed therein. After degassing, samples were reweighed, and this value was used as the sample mass for analysis. Nitrogen adsorption was tracked using high purity nitrogen as the adsorbate with liquid nitrogen used as the coolant. All the values of the adsorbed volume reported at the isotherm are equal to the equivalent gas volume in standard pressure and temperature (273K, 1 atm). The surface area and pore size distribution was calculated from N_2 adsorption-desorption isotherms recorded at the temperature of liquid nitrogen (77K). The BET equation, shown in Equation 3.1, was used to determine the specific surface area for linear points from p/p_0 from 0.05 – 0.3:

$$\frac{1}{W((P_0/P)-1)} = \frac{1}{W_m C} + \frac{C-1}{W_m C}\left(\frac{P}{P_0}\right) \tag{3.1}$$

where, W is the weight of gas absorbed, P/P_0 is the relative pressure, W_m is the weight of adsorbate as a monolayer, and C is the BET constant. As many points from this range were used in the calculation of sample surface area while maintaining a coefficient of variation >0.9999. T-plots generated using de Boer's equation, shown in Equation 3.2, were used to determine the external surface area of the zeolite samples.

$$a(t) = \frac{M}{\rho} \cdot \left(\frac{n}{t}\right) \quad (3.2)$$

where a(t) is the specific surface area, t is the standard multilayer thickness on the reference non-porous material at the corresponding $p/p°$, n is the amount of nitrogen adsorbed, and M and ρ are 28.01 g/mol, and 0.809 g/cm^3 for nitrogen at 77 K, respectively.

For this study, nitrogen-available internal surface area (hereafter, internal surface area) of each sample was calculated as the difference between the total nitrogen-available surface area determined by BET and the external surface area calculated using a t-plot.

The Barrett, Joyner and Halenda (BJH) model was used to determine pore size distributions. This model is based on the Kelvin model for pore filling, and calculates the quantity of pores in each size range using the adsorption isotherm and Equation 3.3:

$$\ln(P/P_0) = -\frac{2V\gamma}{rRT}\cos\phi \quad (3.3)$$

where V is the molar volume of the liquid, γ is the liquid's surface tension, r is pore radius and Φ is contact angle (usually zero), R is the gas constant and T is the temperature of the sample.

3.1.1.3 Particle Size Analysis

Changes to material particle sizes were tracked in order to determine the effect of pretreatments on the particle size distribution of the zeolite, as well as the role particle size plays in the generation of cement-zeolite system properties. In general, smaller particle size leads to faster and greater hydration due to increased nucleation of hydration products (Kadri et al. 2009) as well as higher compressive strengths (Aini et al. 2013; Day and Shi 1994). Therefore it was hypothesized that particle size played a significant role in each sample's performance in zeolite-cement systems.

Particle size distributions were obtained using a Malvern 2000 Laser Particle Size Analyzer. Enough sample was added to 1L of distilled water to generate 5-15% obscuration and was ultrasonicated for 60 seconds in order to reduce particle agglomeration. The instrument default optical parameters were used for all materials, with a refractive index of 1.5026 and 1.33 used for the zeolites and water, respectively. Measurements were taken in triplicate over 10 seconds using both a HeNe red gas laser and a LED blue light in a reverse Fourier convergent beam lens arrangement. The laser light scattering measurements were analyzed by the Malvern software using Mie Scattering Theory and Fraunhofer Diffraction Theory in order to generate an average particle size distribution data for each sample.

Particle size data for each sample is presented by three different methods: 1) d_{10}, d_{50} and d_{90} distribution points and, 2) a percent smaller than chart, and 3) a chart of the percent volume present for each particle size. The d_{10}, d_{50} and d_{90} distribution points correspond to the particle size where 10, 50 or 90 percent of the distribution, respectively,

has a smaller particle size than the stated value. The d_{10}, d_{50} and d_{90} values help to describe what is happening to the finest, median and coarsest values of the material and give a discrete value to an otherwise more complicated distribution, shown by the percent smaller chart. The figure showing the cumulative percentage of material smaller than each particle size is the traditional reporting method for particle size distributions and gives a good picture of major shifts in particle sizes. When comparing materials in this chart type, smaller materials appear further to the left, with larger particle size materials on the right. The d_{10}, d_{50} and d_{90} values can also be approximated from this chart type. The third particle size figure shows the distributions of particles by volume. While large shifts in particle size may be more difficult to interpret, small changes in particular volume fractions of the sample are much easier to visualize using this method. This analysis is especially helpful when changes occur in the finest volume fractions of the material, which often do no account for significant quantities of the overall sample volume, and are therefore often difficult to discern from a percent smaller chart.

3.1.1.4 Thermogravimetric Analysis of Raw Zeolites

Thermogravimetric analysis was used to determine differences in crystallographic properties of the zeolites by tracking mass loss of the material (Pane and Hansen 2005). Mass losses in minerals with increased temperature are the result of many processes, such as dehydration, dehydroxlyation or combustion, and can be used to characterize components present according to the temperatures at which these changes occur (Borrachero et al. 2008). Research has shown that for zeolites, mass losses up to 300°C are due to the dehydration of three types of water, loosely bound, strongly bound and

zeolitic water (Knowlton et al. 1981). Variations in the quantity of water lost can be attributed to variations in size of non-framework cations, with the presence of smaller cations corresponding to higher quantities of zeolitic water (Alver et al. 2009; Khaleghian-Moghadam and Seyedeyn-Azad 2009). Above 500°C zeolitic mass loss is due to dehydroxlyation of hydroxyl groups associated with defect sites in the zeolite framework (Khaleghian-Moghadam and Seyedeyn-Azad 2009). This reaction can continues up to 800°C, but generally slows due to the strong bonds of the molecules being removed at high temperatures and the zeolite cages (Khaleghian-Moghadam and Seyedeyn-Azad 2009).

In order to track the mass loss with temperature, each raw zeolite was ignited to 1000°C using a Mettler Toledo Thermogravimetric Analyzer. The mass change of approximately 20 mg samples was recorded as samples were heated at a temperature ramp rate of 20°C/min in a nitrogen environment. The total mass loss was measured and the differential of the mass loss versus time curve and the energy input tracked using Differential Scanning Calorimetry (DSC) curve were used to investigate changes to the zeolite with increasing temperature.

3.1.2 Zeolite Reactivity Testing

Changes to zeolite pozzolanic reactivity before and after pretreatments were tracked through several methods of measuring the pozzolanic reaction: measurement of the calcium hydroxide ($Ca(OH)_2$) content of zeolite-cement pastes; the Chapelle test, which measures the amount of calcium consumed by a sample in aqueous solution; compressive strength testing of zeolite-cement mortars; and through changes to the

material when exposed to a simulated pore solution. All pastes and mortar mixtures used a 20% replacement by mass of cement with zeolite or quartz. All paste and mortar samples used the cement described in section 3.2.1. All mortar samples used the sand described in section 3.2.2.

3.1.2.1 Determination of Calcium Hydroxide Content using Thermogravimetric Analysis

The calcium hydroxide (also portlandite) content of hydrated cement-zeolite pastes was determined for pastes using raw and pretreated zeolites. Samples for calcium hydroxide content measurement were prepared with a w/cm of 0.4, and a 20% replacement of cement with zeolite. Before the addition of water, the cement and zeolite were mixed together by hand for 30 seconds. The cement, zeolite and water samples were then mixed by hand for two minutes and each sample was sealed in 14g (0.5 oz) individual plastic cup and cured at 23°C. At 28 or 90 days after mixing, the sample was removed from the cup, the edges of each sample were removed, the remaining sample mass was recorded and the sample was crushed to pass the No. 8 sieve. The sample was dried under vacuum for seven days to stop hydration. After seven days the sample was reweighed to determine the mass loss of water in the system and then ground to pass the No. 100 (149 μm) sieve. Each sample was then heated to 1000°C at a temperature ramp rate of 20°C/min in a nitrogen environment in a Mettler Toledo Thermogravimetric Analyzer. The mass change of approximately 20 mg samples was recorded as samples were heated.

The amount of calcium hydroxide present in the sample was calculated from the amount of mass lost from approximately 450°C to 550°C, which corresponds to the dehydration of $Ca(OH)_2$ according to Equation 3.6 (Ramachandran 2001):

$$Ca(OH)_2 \leftrightarrows CaO + H_2O \quad (3.6)$$

It was assumed that one mole of $Ca(OH)_2$ was present for each mole of H_2O lost in this range. The dehydration temperatures used were tailored to each specific sample using the inflection points on the differential thermogravimetric analysis curves to determine the start and end of dehydration for each sample.

3.1.2.2 Chapelle Testing

The Chappelle test for pozzolanic reactivity, based on the French standard NF P 18-513, (2010) measured the amount of $Ca(OH)_2$ consumed by the material in a saturated calcium solution, and was also used to evaluate the pozzolanicity of the materials before and after calcination. This test attempts to measure the relative strength of the pozzolanic reaction in 16 hours, as opposed to the 56 to 90 days normally required, through increased temperature and contact between Ca^{2+} and the pozzolan in solution. The Chapelle test was designed for use with metakaolin, and was tested in this study to determine its suitability for predicting zeolite pozzolanic performance.

In the Chapelle test a 1g sample of the pozzolan was combined with 2g CaO and 250 mL distilled water and heated at 85°C for 16 hours. The solution was then cooled to room temperature and combined with 60g of sucrose and an additional 250 mL of distilled water for 15 minutes in order to slow the reaction between the calcium and pozzolan. Finally, the mixture was filtered using a Buchner funnel and titrated with 0.1M

hydrochloric acid to determine the amount of $Ca(OH)_2$ remaining in solution. Results are given in grams of $Ca(OH)_2$ consumed per gram of sample initially added to the solution.

3.1.2.3 Compressive Strength Testing

The influence of zeolites on compressive strength was tested on mortars of cement and either raw or pretreated zeolites. All zeolite-cement mortars used a 20% substitution by mass of zeolite for cement. Mortars using a 20% substitution of cement with a finely ground quartz were used to understand whether differences between zeolite-containing mortars and cement-only control mortars were occurring due to a filler effect or from contributions of the zeolite (Moosberg-Bustnes et al. 2004). Two-inch mortar cubes, mixed in accordance with ASTM C305 (2011), were cast at a water to cementitious materials ratio (w/cm) of 0.51, in order to provide adequate workability for the high water demand zeolite mixtures. The cubes were removed from the molds after 24 hours and stored in limewater at 23°C until tested. Compressive strengths were obtained 1, 3, 7, 28 and 90 days after mixing following the procedures of ASTM C109 (2011).

3.1.3 Influence of Zeolite on Cement Hydration Testing

3.1.3.1 Isothermal Calorimetry

Isothermal calorimetry was used to compare the initial rate of hydration of cement pastes with 0% or 20% zeolite replacement of raw or pretreated zeolites. Calorimetry provides information on how SCMs affect the hydration of cement. For example, an SCM that retards cement hydration will cause a time delay in the start of the fastest

period of heat released, known as the acceleratory period. Fillers that affect nucleation and growth will change the rate of the acceleratory period, noted by a change in slope during this period, or a change in the peak rate of heat production at the end of the acceleratory period (Oey et al. 2013a). SCMs can also affect the aluminate reactions, changing the magnitude of reactions, as well as their timing, (Lerch 1946; Lothenbach et al. 2011).

Heat evolution was tracked per gram of cement in a TAM AIR (Thermometric) calorimeter for ten-gram paste samples prepared with a w/cm of 0.4, and a 20% replacement of cement with zeolite. Samples were mixed for two minutes and placed into vials according to ASTM C1679 (2009). Heat evolution was tracked for 72 hours.

A typical rate of heat evolution curve for an OPC paste is shown in Figure 3.1. Five periods are generally recognized to take place during cement hydration. Period 1 is the initial dissolution period. A large amount of heat is released during this period due to the initial wetting and dissolution of aluminate phases, C_3S, and CaO (Bullard et al. 2011). The reaction quickly slows and the mixture enters the induction period, Period 2. The induction period occurs as a result of slow reactions (Thomas et al. 2009) Period 3, the acceleratory period, begins when the hydration reactions speed up and become nucleation controlled. Precipitation of hydration products increases, leading to solidification and densification. Two peaks often occur during the acceleration phase attributed to the separate reactions of C_3S and C_3A, which often occur at different times. The quantity of gypsum present controls the timing of the C_3A peak (Lerch 1946; Minard et al. 2007). Cementitious mixtures are generally designed to have enough gypsum, or

calcium sulfate, present to delay the C_3A peak until after the C_3S peak, as early gypsum depletion can disrupt C_3S hydration and additionally result in a flash set of the cement mixture (Odler 2004; Lerch 1946). In this work it will be assumed, unless otherwise noted, that all mixtures have sufficient gypsum to delay the C_3A peak until after the C_3S peak occurs. The first C_3S peak will be used for quantification of the maximum rate of heat evolution of mixtures, discussed in more detail later in this section. In period 4 the rate of hydration reactions slow, partially due to space constraints as further hydration products fill in voids, but also due to a shift in the rate controlling mechanism from nucleation and growth-controlled reactions to diffusion-controlled reactions (Bullard et al. 2011). The reaction continues until it runs out of reactants and space, at which point it enters period 5, steady state conditions, where hydration continues at a very slow rate.

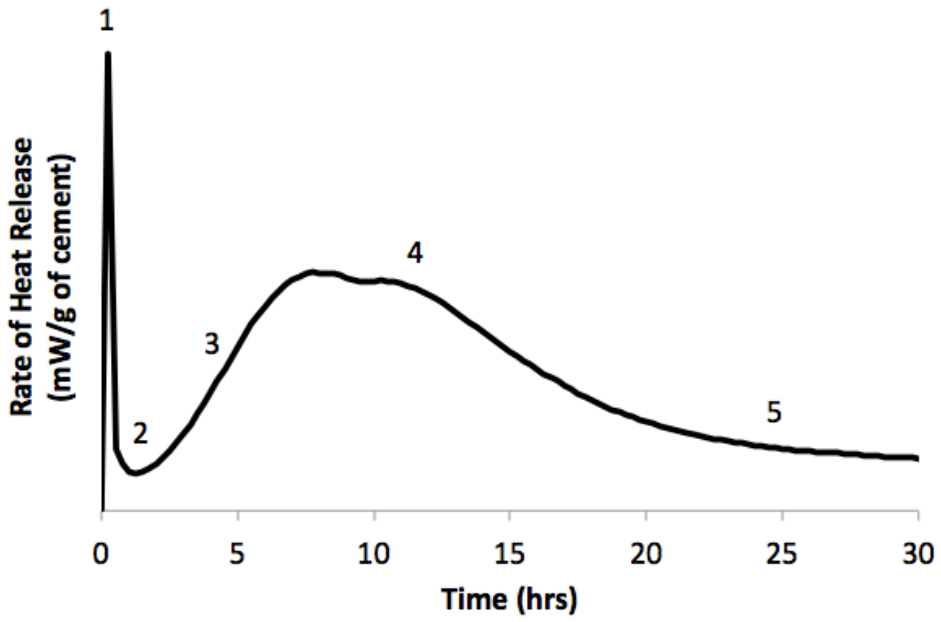

Figure 3.1 - Typical OPC hydration curve. Periods of hydration: 1-initial dissolution, 2-induction, 3-acceleratory, 4-decceleratory, 5-steady state

Several parameters were investigated using isothermal calorimetry in order to understand how the incorporation of untreated or treated zeolites affected cement hydration. These parameters include: 1) the slope of the rate of heat evolution versus time curve during the acceleration period, referred to in this work as the rate of reaction in the acceleration period; 2) the time required for the mixture to enter the acceleration period (i.e. the end of the induction period); 3) the time required for the mixture to reach its peak rate of heat release (for the presumed C_3S peak); 4) the magnitude of the rate of heat evolution at the peak; and 5) the cumulative heat released over 72 hours. Each of these parameters supplies a different piece of information about the kinetics of hydration of the cementitious paste.

Previous work has shown the time for a mixture to enter the acceleration period to be proportional to the ability of C-S-H particles to nucleate and grow in the mixture. Introduction of filler materials has lessened or eliminated the induction period by providing nucleation sites for the precipitation of hydration product in studies by Oey et al. (2013) and Thomas et al. (2009). Higher surface area materials were also shown to generally correlate with greater nucleation and acceleration rates (Bullard et al. 2011; Cheung et al. 2011). The time of the start of the acceleration period was determined for all mixtures in this study as the point at which the minimum rate of heat evolution occurred following the initial, period 1, peak.

Bullard et al. (2011) and Thomas et al. (2009) hypothesized that the time to the maximum rate of heat release peak occurs as growth is slowed by the impingement of hydration products. Thomas et al. (2009) showed that the presence of fillers resulted in a

reduction in the time to the maximum heat release peak, and additionally reduced the time to the start of the acceleration period by providing immediate availability of nucleation sites. Fillers decreased the time to the peak rate of heat release because they promoted growth of cement hydrates on surfaces other than the surface of the cement grains, allowing more regions of hydration products to grow at the same time also leading to a faster reduction in available space for continued growth (Thomas et al. 2009). As the reduction in the rate of heat release occurred due to the impingement of hydration products, the time to the peak rate of heat release has also been suggested for use in inferring set times for mixtures (Odler 2004). The time of the maximum rate of heat evolution was determined for all mixtures in this study as the time to the first maximum occurring after the start of the acceleration period. In cases where the C_3S and C_3A peaks overlapped and the maximum rate of heat evolution for the C_3S peak could not be definitively determined, the time the peak occurred was visually estimated.

The slope of the heat release versus time curve during the acceleration period has been used by other researchers to describe the rate of hydration of the mixture (Oey et al. 2013a). The rate of reaction during the acceleration period has been shown to be an amalgamation of several chemical processes, including dissolution of cement phases, movement of moisture through the cement paste and along the surfaces of solids, precipitation of solids from dissolved phases, growth of the precipitated solids, complexation of ions in solution and adsorption of ions at solid-liquid interfaces, all occurring at roughly the same time (Bullard et al. 2011). The rate of reaction during the acceleration period resulting from the previously mentioned processes has been shown to

be dependent on the surface area of the cement and SCMs (if used), as well as the calcium concentration in solution (Thomas et al. 2009). In this study, since the acceleration period isn't completely linear, the slope of the acceleration period was standardized by using the slope at the time halfway between the time at which the acceleration period began and the time the maximum rate of heat evolution occurred.

The maximum rate of heat evolution can be used to compare the amount of growth occurring during hydration during the acceleration period. Thomas et al. (2009) demonstrated that when heat releases are normalized by the quantity of cement, an inert filler material generated a greater maximum rate of heat release because the filler had nucleated a greater quantity of growth regions than what would have developed in a cement-only paste (Thomas et al. 2009). Additionally, use of filler materials resulted in hydration of a greater proportion of the volume of cement in the mixture, as nucleation occurred in pore spaces between cement grains rather than directly on the surface where C-S-H growth would slow further cement grain dissolution (Thomas et al. 2009). Therefore, in this study, heat evolution rates greater than those generated by the cement-only paste indicated that the SCM increased the regions of hydration and total quantity of C_3S dissolved and hydrated, while heat evolution rates less than that generated by the cement-only paste indicated SCM interference with cement hydration reactions. Discussion of the mechanisms that cause SCMs to interfere with cement hydration reactions was outside the scope of this study. For all mixtures investigated in this study, the maximum rate of heat release peak was taken as the rate of heat evolution at the first maximum occurring after the start of the acceleration period. In cases where the C_3S and

C_3A peaks overlapped and the maximum rate of heat evolution for the C_3S peak could not be definitively determined, the magnitude of the peak was visually estimated.

Finally, cumulative heat evolution over 72 hours was used to discern whether differences in isothermal calorimetry curves occurred as a result of the filler effect only or if other properties of the zeolite (cations, pozzolanic reaction, etc.) provided extra contributions to hydration of the mixtures. Lothenbach et al. (2011) saw that substitution of fillers in cement pastes resulted in greater cumulative heat release because of the presence of extra space for hydration products to fill. Therefore it was expected that even if the zeolites tested in this study were inert, zeolite-cement pastes should release greater cumulative amounts of heat than the cement-only paste. Generation of higher cumulative evolved heat by a zeolite-cement mixture compared to a paste using a 20% substitution of cement paste with quartz filler indicated that the zeolites increased the rate of reaction of the cement through a reaction or mechanism other than the filler effect. Equal cumulative heat evolution by the zeolite-cement and quartz-cement pastes indicated that the zeolite acted only as filler material, and zeolite-cement pastes releasing lower cumulative heat than the quartz-cement paste, even if the cumulative heat was still greater than for the cement-only pastes, indicated that heat increases resulting for the filler effect were offset by interferences of the zeolite with the cement hydration reactions. The cumulative heat evolved was calculated for each mixture using the heat release measured every three minutes by isothermal calorimetry and applying the trapezoidal rule.

If pretreatments improve zeolite interactions with cement hydration, we should expect to see increases in the rate of reaction during the acceleration period, decreases in

the time to the start of the acceleration period and time to the maximum rate of heat release, an increased maximum rate of heat release and greater cumulative heat evolved than for a comparable quartz-cement paste.

3.2 MATERIALS

3.2.1 Cement

As ASTM C150 Type I/II Texas Lehigh cement, referred to hereafter as 'ordinary portland cement' (OPC), was used for all pastes and mortars in this work. The chemical and physical properties of the cement are shown in Table 3.1. The particle size distribution of the cement is shown in Figure 3.2

Table 3.1 - Oxide compositions of the cement, in percent, determined using XRF

SiO_2	Al_2O_3	Fe_2O_3	CaO	MgO	SO_3	Na_2O	K_2O
19.36	5.13	2.53	63.17	1.03	3.22	0.09	0.88

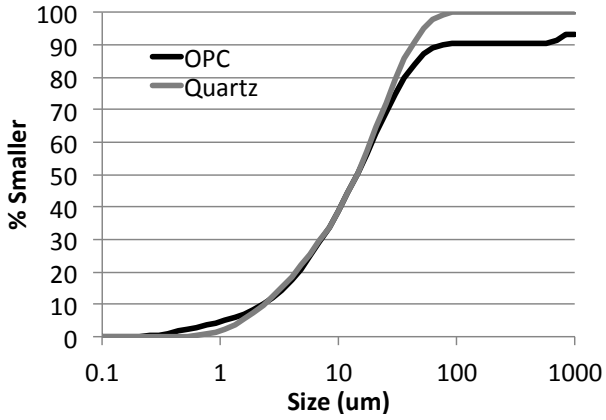

Figure 3.2 - Particle size distribution of OPC and quartz filler

3.2.2 Sand

An ASTM C109 (2009) graded Ottawa sand, certified to meet the ASTM C778 (2013) "graded sand" standard, was used for all mortars in this work.

3.2.3 Quartz Filler

A quartz filler (Old Hickory, Clay World) was used throughout this work to help differentiate between improvements due to filler effect and those occurring as a result of the pozzolanic reaction. The particle size distribution for the sample used is shown in Figure 3.2.

3.2.4 Natural Zeolites

The source location and composition of the six zeolite sources used throughout this work are shown in Table 3.2. The sources of zeolites used in this study were chosen in order to investigate the viability of several deposits of zeolites in the Texas region and compare them with zeolites from more traditional zeolite mining operation locations, such as Idaho. The composition of all zeolite samples is similar, and consists of approximately 65% silica and 10% alumina. Other elements present besides silicon and aluminum primarily represent the non-framework cations that reside in the zeolite pore structure. The SiO_2/AlO_3 ratio of all of the samples is > 4.5, indicating that all of the zeolites are clinoptilolite zeolite, as opposed to its very compositionally similar cousin, heulandite.

The phases present in each zeolite sample, determined by XRD, are shown in Table 3.3 and Figures 3.2 to 3.8. All of the zeolites primarily consist of clinoptilolite zeolite, but several also contain two other zeolites, heulandite and stilbite, as well as several impure phases including quartz, cristobalite, albite, anorthite, illite, biotite, potassian halite, and stellerite. Of these minerals only halite is soluble in water (Crawford 2009).

Table 3.2 - Zeolite source locations and composition

Zeolite Source	Location	CaO (%)	SiO_2 (%)	Al_2O_3 (%)	Fe_2O_3 (%)	MgO (%)	Na_2O (%)	K_2O (%)	SiO_2/ AlO_3
Zeo Inc (Z)	Preston, ID	2.52	65.29	10.90	2.36	0.59	0.52	4.82	5.99
Bear River (B)	Preston, ID	2.98	64.13	10.98	2.03	0.68	0.43	4.16	5.84
Max 30LM (L)	Tilden, TX	2.23	66.39	11.07	1.28	0.88	0.67	4.21	6.00
Max 30T (T)	Tilden, TX	2.21	62.23	11.88	1.12	0.64	1.00	1.68	5.24
Clean Age Minerals (C)	Marfa, TX	5.50	63.99	13.08	2.38	0.90	3.57	2.63	4.89
Alamitos (A)	El Paso, TX	6.90	63.80	12.84	2.29	1.07	3.07	2.52	4.97

Table 3.3 - Phases present in the natural zeolites

Zeolite	Phases	
Z	Clinoptilolite	Heulandite, K-exchanged
	Illite	Cristobalite
	Quartz	
B	Clinoptilolite	Potassium Halite
	Quartz	Biotite
	Cristobalite	Stilbite
L	Clinoptilolite	Heulandite, K-exchanged
	Quartz	Cristobalite
T	Clinoptilolite	Illite-2M1
	Quartz	Cristobalite
	Biotite	
C	Clinoptilolite	Heulandite, K-exchanged
	Anorthite	Albite
	Quartz	Stellerite
	Cristobalite	Biotite
A	Clinoptilolite	Heulandite, K-exchanged
	Albite	Anorthite
	Quartz	Cristobalite
	Biotite	Illite-2M1

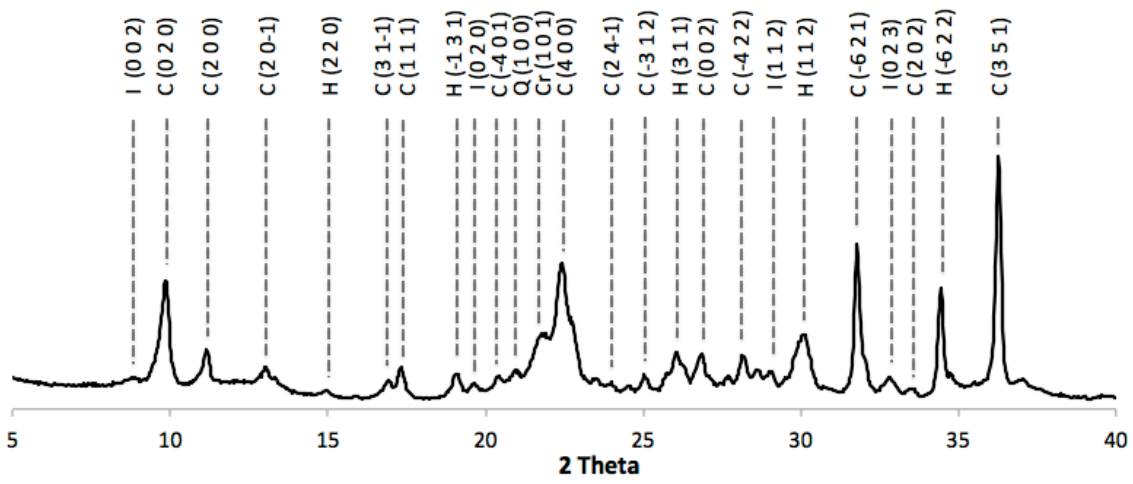

Figure 3.3 - Phases present in zeolite Z (C = clinoptilolite, H = heulandite, I = illite, Q = quartz, Cr = cristobalite). Numbers in parenthesis indicate the d-spacing of the reflection.

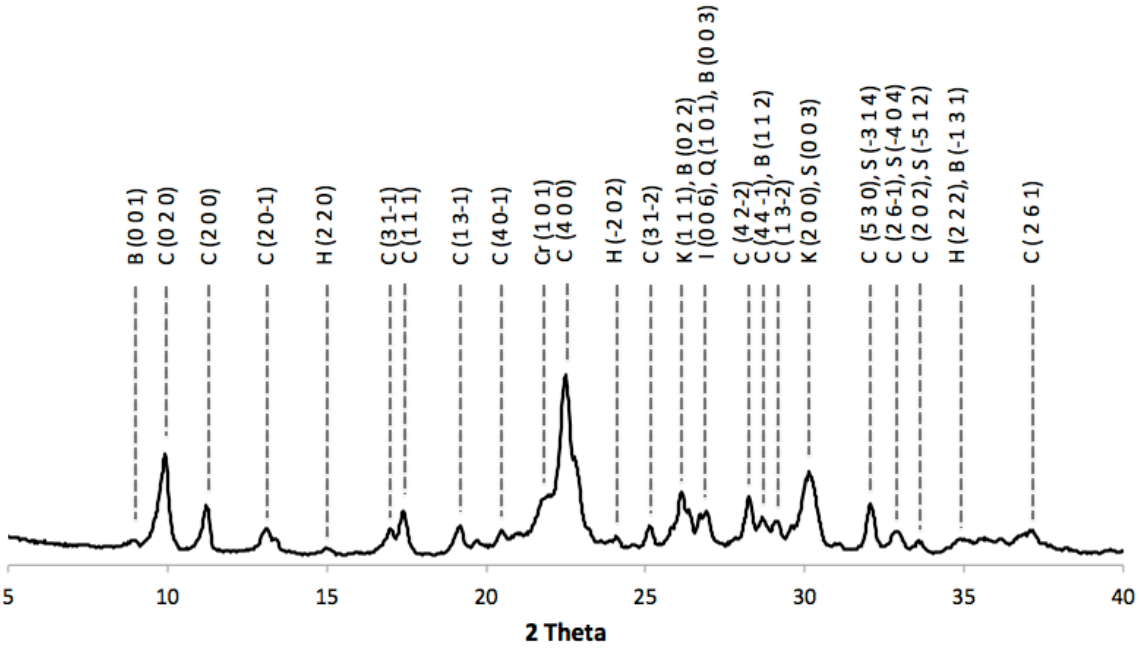

Figure 3.4 - Phases present in zeolite B (C = clinoptilolite, H = heulandite, Cr = cristobalite, K = potassian halite, B = biotite, I = illite). Numbers in parenthesis indicate the d-spacing of the reflection.

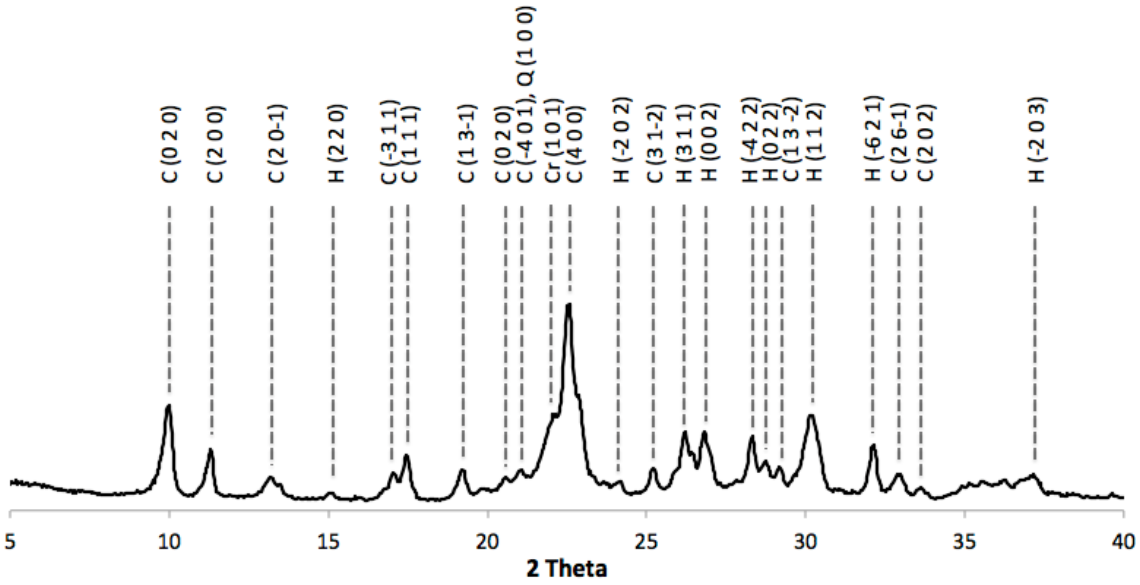

Figure 3.5 - Phases present in zeolite L (C = cristobalite, H = heulandite, Q = quartz, Cr = cristobalite). Numbers in parenthesis indicate the d-spacing of the reflection.

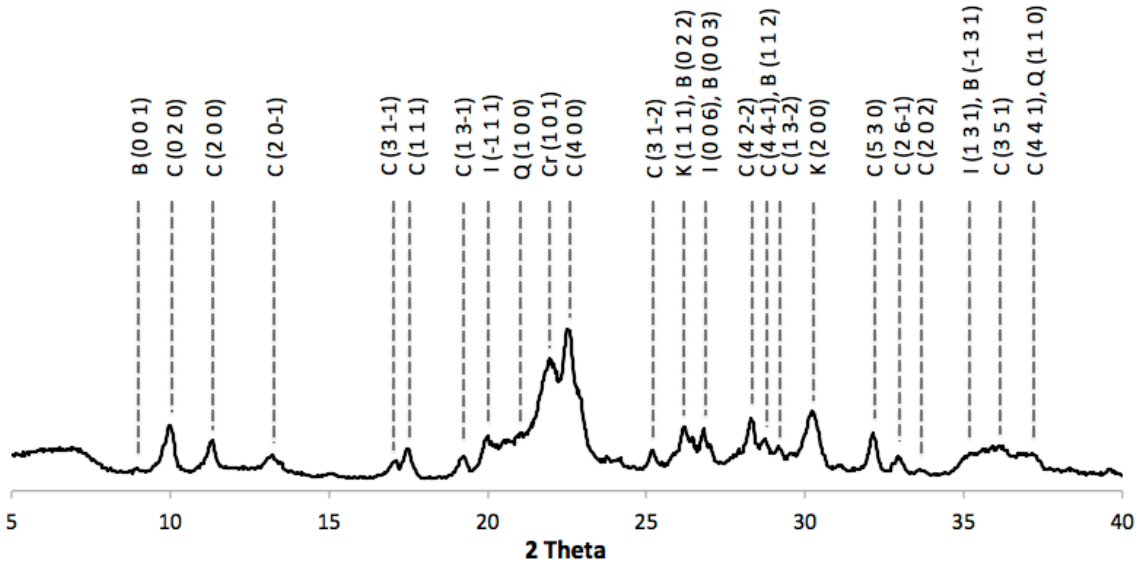

Figure 3.6 - Phases present in zeolite T (C = clinoptilolite, I = illite, Q = quartz, K = potassian halite, B = biotite). Numbers in parenthesis indicate the d-spacing of the reflection.

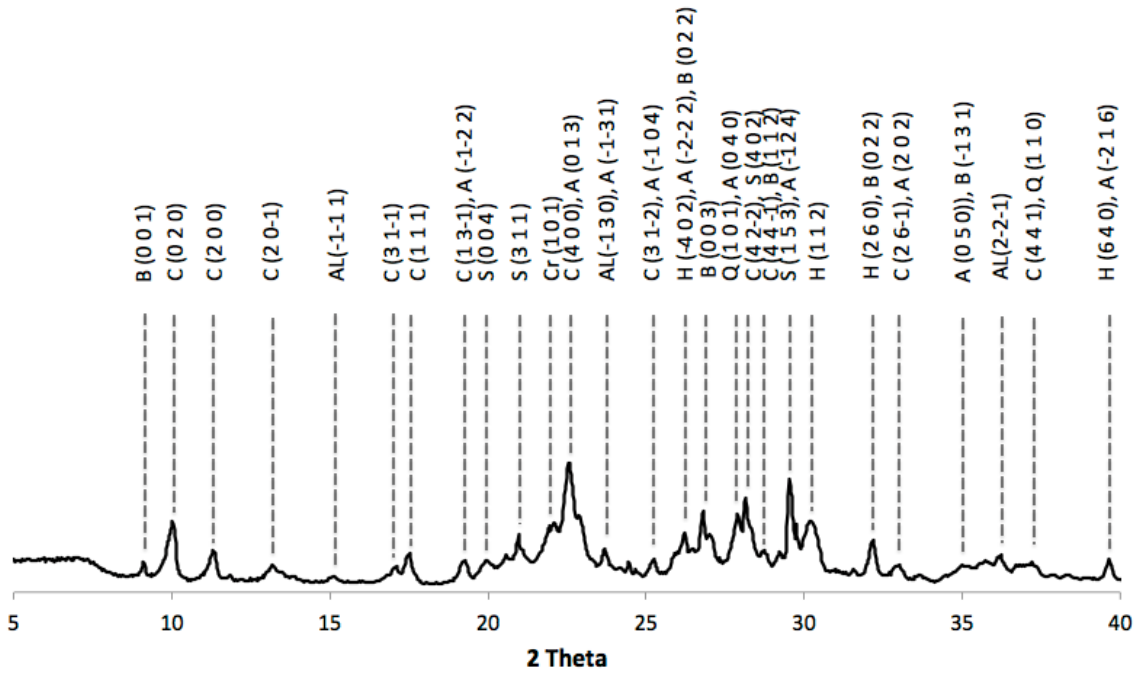

Figure 3.7 - Phases present in zeolite C (C = clinoptilolite, B = biotite, A = anorthite, AL = ablite, S = stellerite, Cr = cristobalite, H = heulandite, Q = quartz). Numbers in parenthesis indicate the d-spacing of the reflection.

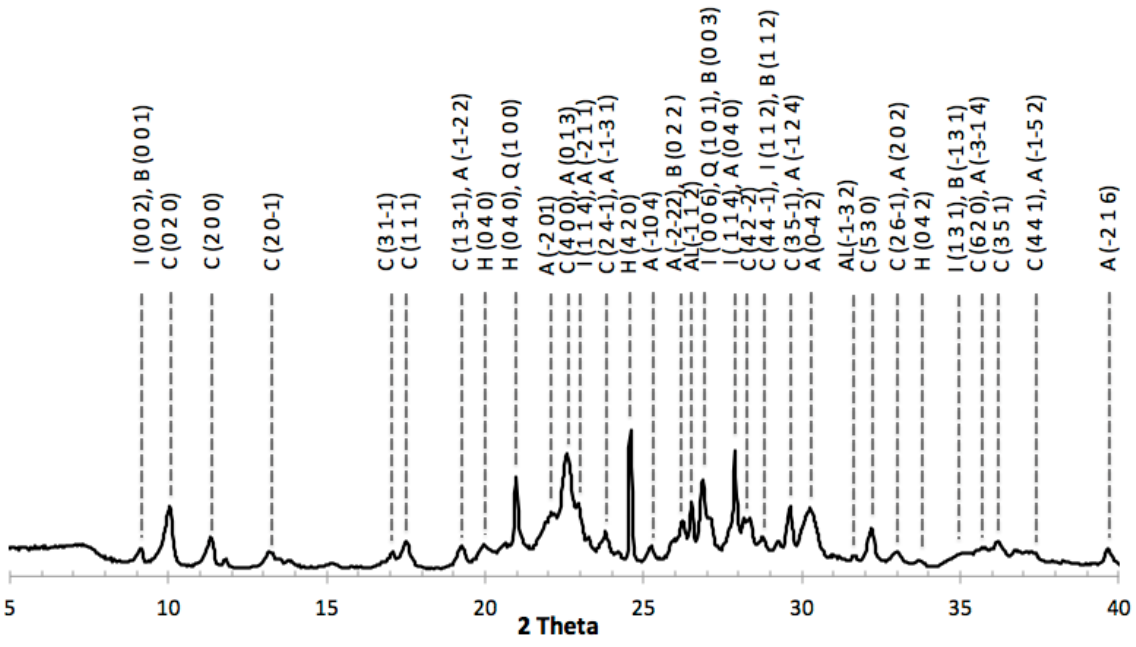

Figure 3.8 - Phases present in zeolite A (I = illite, C = clinoptilolite, H = heulandite, A = anorthite, B = biotite, AL = albite, Q = quartz). Numbers in parenthesis indicate the d-spacing of the reflection.

Figures 3.9 to 3.14 show the mass loss and differential mass loss of each sample as it was heated from 23-1000°C. Sample dehydration due to loss of water in zeolite cavities and bound to non-framework cations is indicated by a broad mass loss peak from 23°C to approximately 200°C, but can occur up to as high as 500°C depending on zeolite charge density and cation content (Erdogan et al. 2010, Khaleghian-Moghadam and Seyedeyn-Azad 2009). Water lost after 185°C is referred to as "zeolitic" water and has high entropy (58-72 J/mole/degree) compared to other types of adsorbed water (Knowlton et al. 1981). The mass loss occurring in zeolite B at approximately 300°C, is likely due to decomposition of the stilbite zeolite in the sample, which is significantly affected by temperature change, and undergoes several phase transitions between 145-470°C, leading to thermal destruction of the mineral (Aumento 1966). The mass loss at temperatures greater than 500°C can often be attributed to dehydroxlyation of hydroxyl groups strongly bound to defect sites within the zeolite framework, (Khaleghian-Moghadam and Seyedeyn-Azad 2009) but may also be due, in part, to the presence of illite clay, which loses significant mass between 500-700°C (Fernández, Vigil de la Villa, Garcia et al. 2011). Endothermic peaks corresponding to the temperature of the mass losses between 500-700°C, suggest that a phase change is linked to the mass loss. Lastly, a very small gain in mass occurs at approximately 935°C in all samples. This change likely indicates structural collapse of the zeolite and transformation of the zeolite to an amorphous phase (Khaleghian-Moghadam and Seyedeyn-Azad 2009). The endothermic peaks in the DSC curves at 935°C confirm this hypothesis

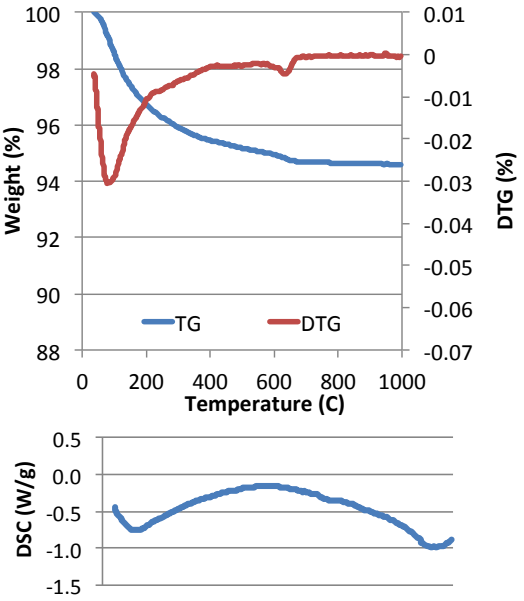

Figure 3.9 - TG/DTG and DSC of zeolite Z.

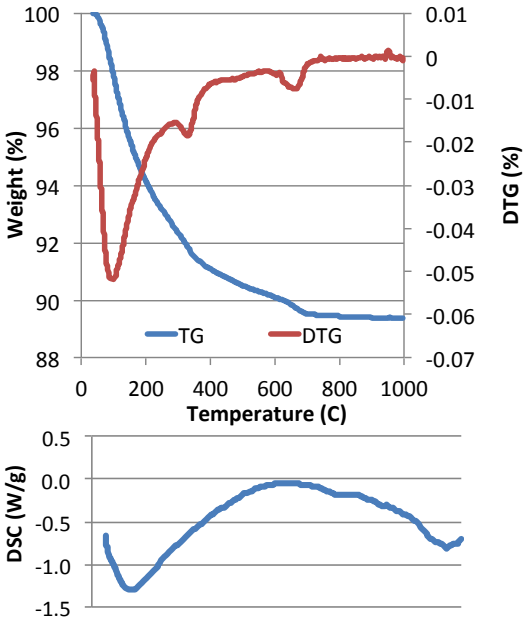

Figure 3.10 - TG/DTG and DSC of zeolite B

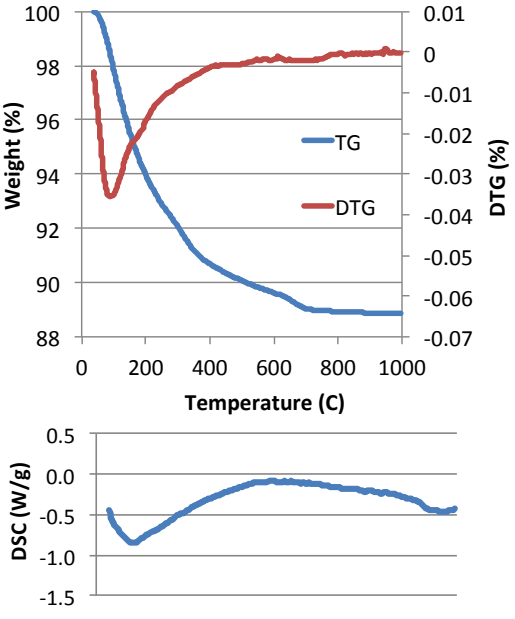

Figure 3.11 - TG/DTG and DSC of zeolite L

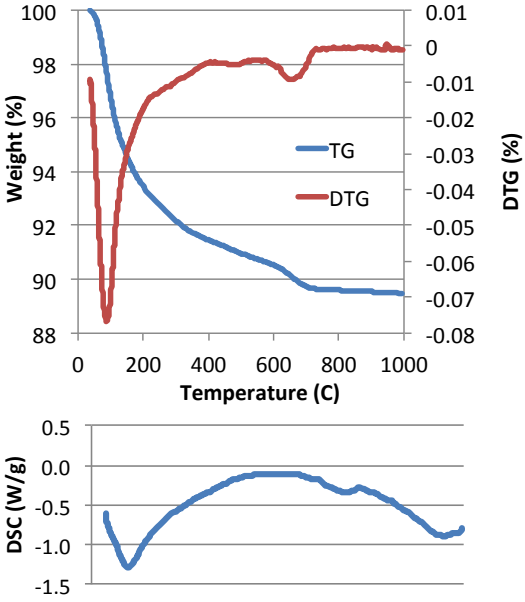

Figure 3.12 - TG/DTG and DSC of zeolite T

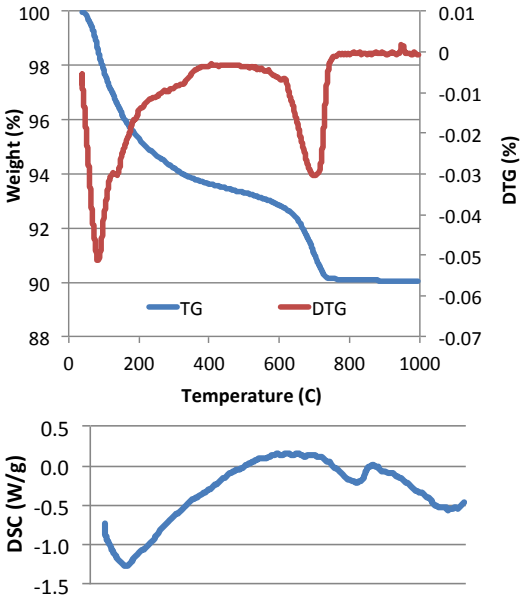

Figure 3.13 - TG/DTG and DSC of zeolite C

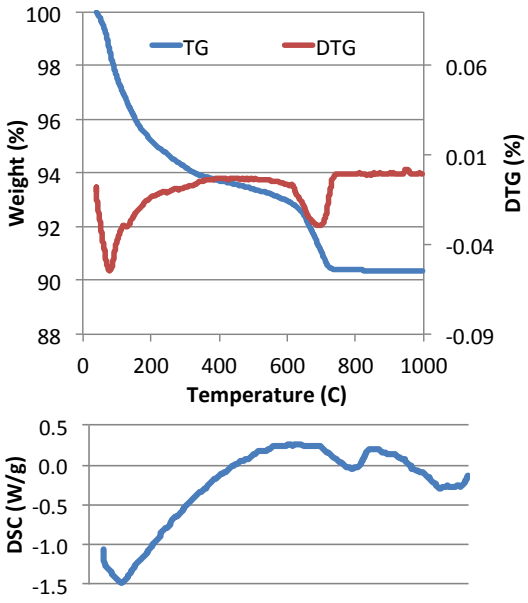

Figure 3.14 - TG/DTG and DSC of zeolite

Chapter 4: Zeolite Pretreatment Methods to Increase the Reactivity of Zeolites for Use as SCMs – Calcination

4.1 Introduction and Literature Review

Calcination pretreatments have been used to improve the properties of zeolites used in industries such as water treatment and catalysis (Beers 2003; Perez-Ramirez et al. 2003; Tao et al. 2006). Studies have indicated that calcination pretreatments can induce changes in zeolites such as reduced crystallinity and greater amorphous content (Ates and Hardacre 2012; Duvarcı et al. 2007; Johnson et al. 2003) that may benefit the reactivity of zeolites for use in cementitious mixtures as well. In addition, calcination pretreatments have been utilized to increase the reactivity of other naturally occurring materials, such as clays, for use as SCMs (Sabir et al. 2001; Taylor-Lange et al. 2012). The reactivity of calcined zeolites has been examined in saturated calcium solutions, with results suggesting that calcination could increase the reactivity of zeolites (Elaiopoulos et al. 2010; Habert et al. 2008; Janotka and Krajči 2008; Liebig and Althaus 1998; Perraki et al. 2005; Fernández et al. 2011). However, while these studies all suggest that calcination could be used to improve the performance of zeolites used in cementitious mixtures, the ”optimum temperature” for calcination suggested by researchers varies widely.

Several studies have shown that calcination results in a destabilization of the zeolite crystal structure, a loss of crystallinity and an increase in amorphous content. Perraki et al. (2005) used X-ray diffraction (XRD) to demonstrate that reduction in the crystallinity of heulandite zeolite begins around 400°C and that the zeolite is fully decomposed by 500°C. The loss of zeolitic phases was accompanied by an increase in amorphous content of the sample at 500°C (Perraki et al. 2005). This conclusion was

supported by Liebig and Althaus (1998), who showed that phillipsite zeolite breaks down "well below 500°C." The results of Habert et al. (2008) were similar, showing that the complete structural collapse of phillipsite and heulandite zeolites occurs at 350°C and 450°C, respectively.

However, other researchers reported differing results. Elaiopoulos et al. (2010) measured loss of crystallinity using XRD and found that at 500°C the crystallinity of heulandite and mordenite zeolite was only reduced 30-35%. Calcination to 750°C decreased crystallinity further, to 50%. Scanning electron microscopy (SEM) showed that crystals remained intact and showed no trace of structural collapse as high as temperatures of 850°C. Ates and Hardacre (2012) did not see a reduction in zeolite phases measured by XRD and accompanying increase in amorphous content until after heating past 600°C, while Durvaci et al. (2007) did not evidence changes in a zeolitic tuff crystal structure using XRD until after calcination at 800°C, although changes to crystal structure were inferred from water losses measured using thermogravimetric analysis (TGA) from 120-750°C. Using energy dispersive x-ray diffraction, which is similar to XRD, but utilizes polychromatic photons as the radiation source, Johnson et al. (2003) also showed that water loss alters clinoptilolite crystal structure at temperatures as low as 200°C, but did not see full structural collapse of the zeolite until 920-1000°C, depending on the specific cation-exchanged form of the zeolite. Likewise, Fernandez et al. (2011) did not see any significant changes in the mordenite zeolite phases until 900°C, when the material became almost completely X-ray amorphous. However, by 1000°C the zeolite sample had recrystallized into chemically inert and alkali resistant cristobalite.

Investigations of the changes to surface area, particle size and zeolite surface morphology after calcination did not seem to suggest that calcination could improve the reactivity of zeolites for use as SCMS. Using N_2 adsorption, Ates and Hardacre (2012) found that calcination of zeolites resulted in lower surface area and a reduction in porosity. They concluded that these changes were due to agglomeration and sintering of zeolite particles as well as blocking of the zeolite channels by amorphous material. The work of Elaiopoulos et al. (2010) supports these claims; SEM imaging showed agglomerations of particles and nitrogen adsorption also found reductions in zeolite surface area inversely proportional to calcination temperature.

Several researchers have demonstrated that zeolite performance can be improved by calcination, although the optimum temperature is not agreed upon. Perraki et al. (2005) tested the abilities of zeolites to consume Ca^{2+} in solution using the Chapelle test. It was found that the zeolite consumed the most Ca^{2+} after calcination at 400°C. Fernandez et al. (2011) tested the Ca^{2+} consumption of zeolites in a saturated Ca^{2+} solution stirred at 40°C for 7 days. This testing found that calcium consumption increased for zeolites calcined at 300 and 400°C, with the 300°C calcined zeolites showing the greatest improvement in Ca^{2+} consumption. Cornejo et al. (2013) calcined and then milled two types of zeolite, one mordenite sample and one clinoptilolite-heulandite-mordenite sample, and found that heating to 800°C followed by milling for 48 minutes significantly increased compressive strengths of mortars with 15% cement replacement with either of the zeolites. In contrast to these results, Fernandez et al. (2011) showed that calcination temperatures of 500°C or greater reduced the Ca^{2+} consumption ability of the zeolite relative to the untreated zeolite, with temperature inversely correlated with Ca^{2+}

consumption. The results of Liebig and Althaus (1998) demonstrated a similar trend, showing that calcination at 500°C increased the amount of Ca^{2+} fixed by zeolite in a saturated Ca^{2+} solution over 90 days. When the zeolite was calcined at 800°C, the amount of Ca^{2+} consumed by the zeolite was reduced compared to the amount consumed by the 500°C calcined sample, although it was similar to the amount consumed by the untreated zeolite sample.

These results suggest that zeolite calcination could influence its performance as an SCM, but the studies fail to agree on the conditions that yield the best results, nor do they provide a clear understanding of the effect of calcination on zeolite structure, crystallinity and performance in cementitious systems. Accordingly, the study presented in this chapter attempted to determine the optimal calcination conditions for treating zeolites for use in cementitious systems. Six sources of zeolites were calcined at several temperatures (300, 500, 800, and 956°C), each of which has been indicated in the literature to be the temperature at which the zeolite crystal structure is most destabilized and thus creates the most reactive zeolite. Further, the study presented in this chapter investigated the physical changes in the zeolite materials after heat treatment using XRD, nitrogen adsorption, laser diffraction and SEM. Those changes were linked the properties of cementitious mixtures incorporating those zeolites, measured through calcium hydroxide contents, compressive strengths and isothermal calorimetry, in order to characterize changes in reactivity, pozzolanicity, and effect of the zeolite on early age cement hydration, and to determine which properties are most responsible for zeolite reactivity in cementitious systems.

4.2 EXPERIMENTAL METHODS AND MATERIALS

4.2.1 Zeolite Sample Preparation

The six sources of zeolite shown in Table 3.3 in Chapter 3 were used for calcination testing. The zeolites were used in the form they were received and were not ground, washed or dried before testing.

Calcined samples were prepared by heating approximately 50g of zeolite to 300°C, 500°C, 800°C or 965°C in a covered ceramic crucible in a Lindberg/Blue M 150 furnace. Samples were heated at 5°C per minute and held at the designated temperature for five hours to ensure completion of any chemical or structural changes occurring in the zeolites. After 5 hours the samples were then cooled to room temperature in the furnace at approximately 5°C per minute.

4.2.2 Zeolite Physical and Chemical Characterization Testing

Characterization testing was completed in order to determine what characteristics influenced zeolite reactivity in cementitious systems. Characterization testing tracked changes in the crystalline phases present in the zeolite samples after calcination, as well as particle size, surface area and pore sizes, as discussed in Chapter 3.

4.2.2.1 Scanning Electron Microscopy (SEM)

Scanning electron microscopy (SEM) was used to determine if sintering and particle agglomeration were occurring with higher calcination temperatures and to obtain images of particle morphology. In order to prepare samples for SEM imaging, zeolite powders were sonicated for 30 seconds in a glass beaker immersed in the water of a Buehler Ultramet 2003 Sonic Cleaner in order to disperse the powders and reduce

particle agglomeration. Each zeolite sample was then dusted and pressed into double-sided Ted Pella carbon tape applied to SEM platforms. The samples were sprayed with compressed air to remove loose particles and coated with carbon using a LADD Research Industries carbon evaporator to create a conductive surface and prevent charging by the electron beam. This step helped prevent electrons from the microscope's electron beam from building up on the sample surface, since the zeolite samples themselves were non-conductive. SEM imaging was conducted using a JEOL JSM-6490 scanning electron microscope at an accelerating voltage of 20 kV, spot size of 50 and working distance of approximately 10 mm.

4.2.3 Calcination Treatment Testing Methods: Reactivity Testing

Changes to zeolite pozzolanic reactivity after calcination were tracked through two methods of measuring the pozzolanic reaction as described in Chapter 3: measurement of the calcium hydroxide content of hydrated zeolite-cement pastes and measurement of the amount of calcium consumed by a zeolite in aqueous solution, through the Chapelle test.

4.3 RESULTS

4.3.1 Physical and Chemical Characterization Testing Results

4.3.1.1 XRD Phase Analysis/Relative Amount of Crystallinity

The changes in the crystalline phases present in each zeolite sample with calcination are shown in Figures 4.1 to 4.6. Table 4.1 shows the phases present in each sample before calcination and after calcination at 965°C. As shown in Figure 4.1, the zeolite Z sample appears mostly unchanged after calcination at 300°C. However,

decomposition of the zeolite phases, indicated by a reduction in peak heights, can be clearly seen after calcination of the samples at 500°C, as the heights of all zeolite peaks decreased noticeably. Likewise, at 500°C, decomposition of a montmorillonite phase, indicated by the peak at 19° 2θ, also begins, indicated by a decrease in peak height. A halite phase peak at 30° 2θ responds similarly, decreasing in height with increasing calcination temperature, beginning with calcination at 500°C. The only peak that does not change with calcination temperature is the cristobalite peak at 22° 2θ. The cristobalite peak at 22° 2θ becomes more prominent with higher calcination temperatures, and is the only prominent peak remaining in the 965°C calcined sample. Although only cristobalite remains after calcination at 965°C, other phases are present in the sample even after calcination at 800°C, although much less prominently than in the original, untreated sample.

Zeolite B, shown in Figure 4.2, follows a trend similar to zeolite Z. Calcination results in the decomposition of nearly all crystalline phases present in the sample, beginning between 300 and 500°C. In the zeolite B sample only the silica phases of low quartz and cristobalite are present in the sample after calcination at 965°C.

Zeolites L and T, shown in Figures 4.3 and 4.4, again show a similar decomposition of zeolite phases proportional to higher calcination temperatures. Several different forms of low quartz and cristobalite were present in the samples after calcination at 965°C.

Calcination affected zeolite C, shown in Figure 4.5, a little differently than the previous samples, due to the presence of albite in the sample, shown by the large peak at 28.0° 2θ. The zeolite and illite clay phases initially present in the sample follow the same

pattern as in other zeolite samples, with decomposition beginning after 300°C and complete before 965°C, but the albite phase is unaffected by calcination temperature. Cristobalite, low quartz and albite phases remain in the sample after calcination at 965°C.

Calcination of zeolite A, shown in Figure 4.6, is similar to zeolite C, with the addition of another plagioclase feldspar phase, anorthite, in the sample. Both the albite and anorthite phase XRD reflections are present throughout all calcination samples, while the zeolite and clay phases present in the untreated sample decompose proportional to calcination temperature. After calcination at 965°C albite, anorthite, high and low quartz and cristobalite phases remain in the sample.

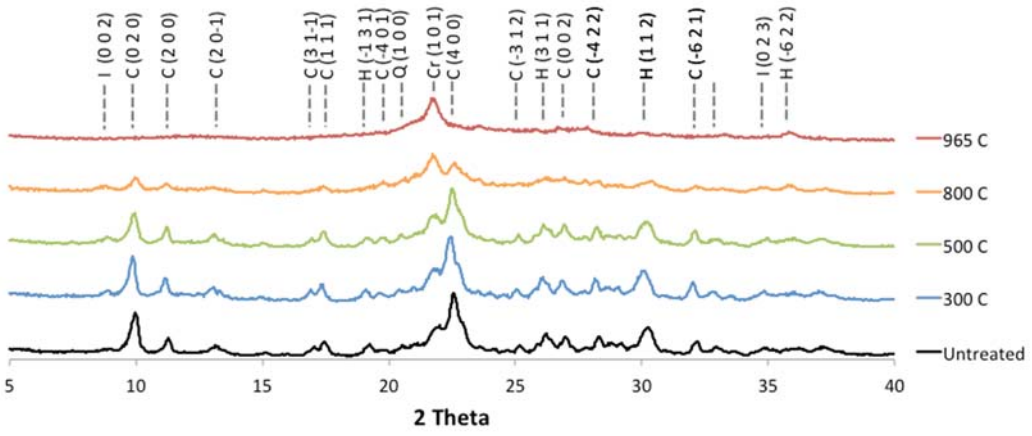

Figure 4.1 - Phases present in the zeolite Z sample before and after calcination. (C = clinoptilolite, H = heulandite, I = illite, Q = quartz, Cr = cristobalite). Numbers in parenthesis indicate the d-spacing of the reflection.

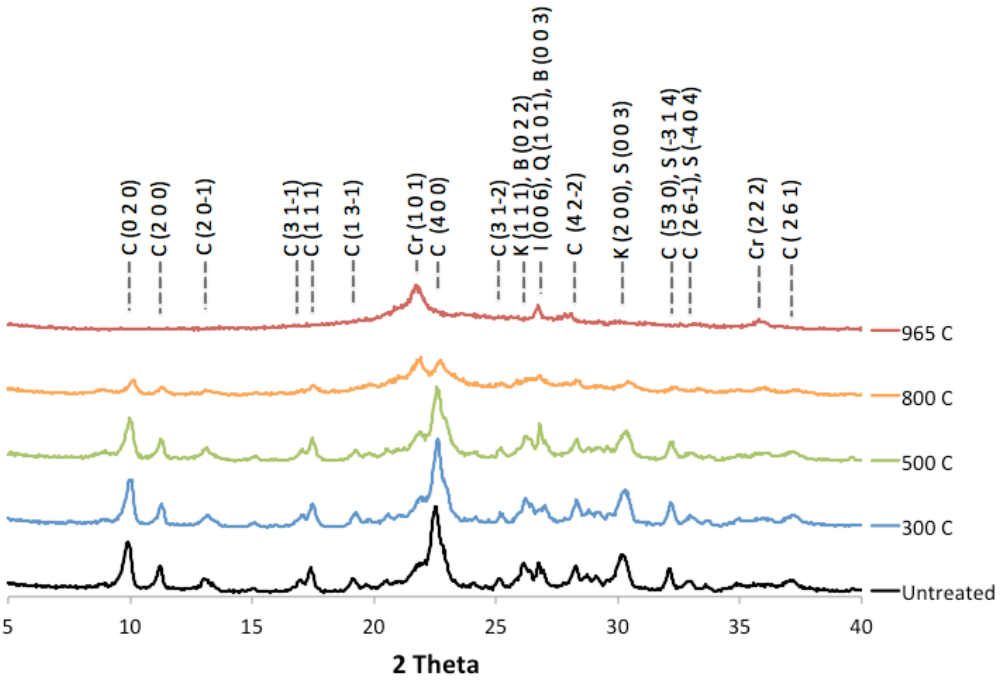

Figure 4.2 - Phases present in the zeolite B sample before and after calcination. (C = clinoptilolite, H = heulandite, Cr = cristobalite, K = potassian halite, B = biotite, I = illite). Numbers in parenthesis indicate the d-spacing of the reflection.

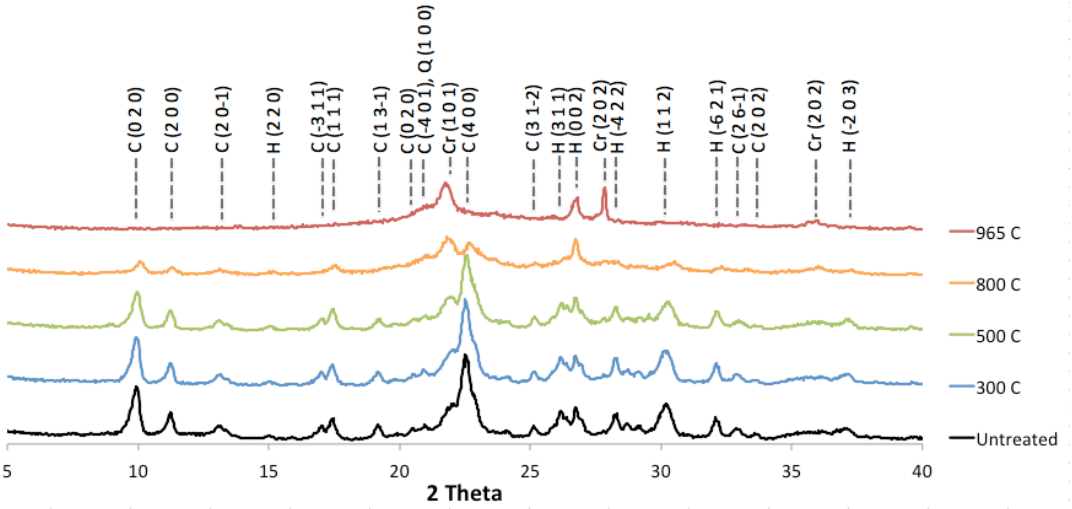

Figure 4.3 - Phases present in the zeolite L sample before and after calcination. (C = cristobalite, H = heulandite, Q = quartz, Cr = cristobalite). Numbers in parenthesis indicate the d-spacing of the reflection.

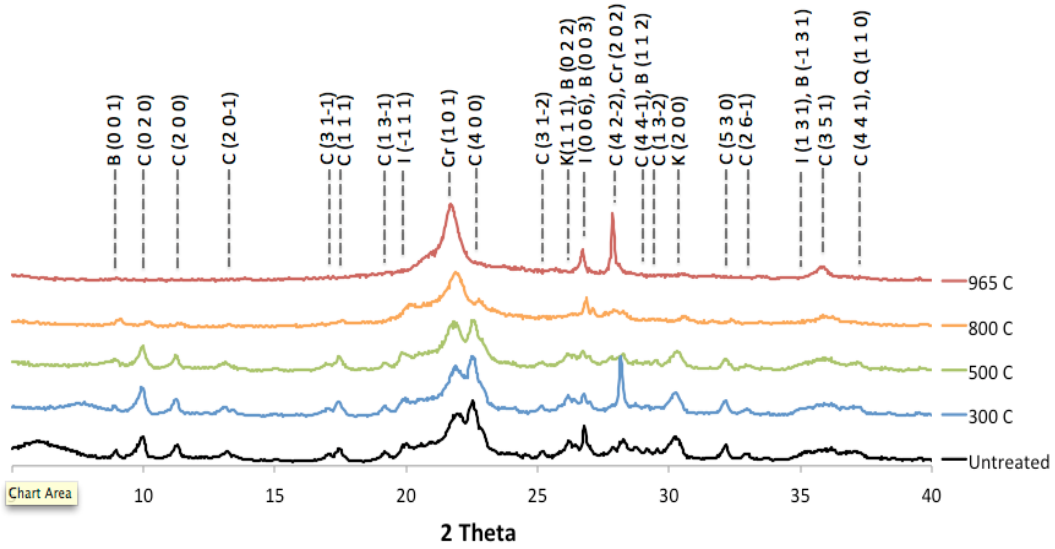

Figure 4.4 - Phases present in the zeolite T sample before and after calcination. (C = clinoptilolite, I = illite, Q = quartz, K = potassian halite, B = biotite), Numbers in parenthesis indicate the d-spacing of the reflection.

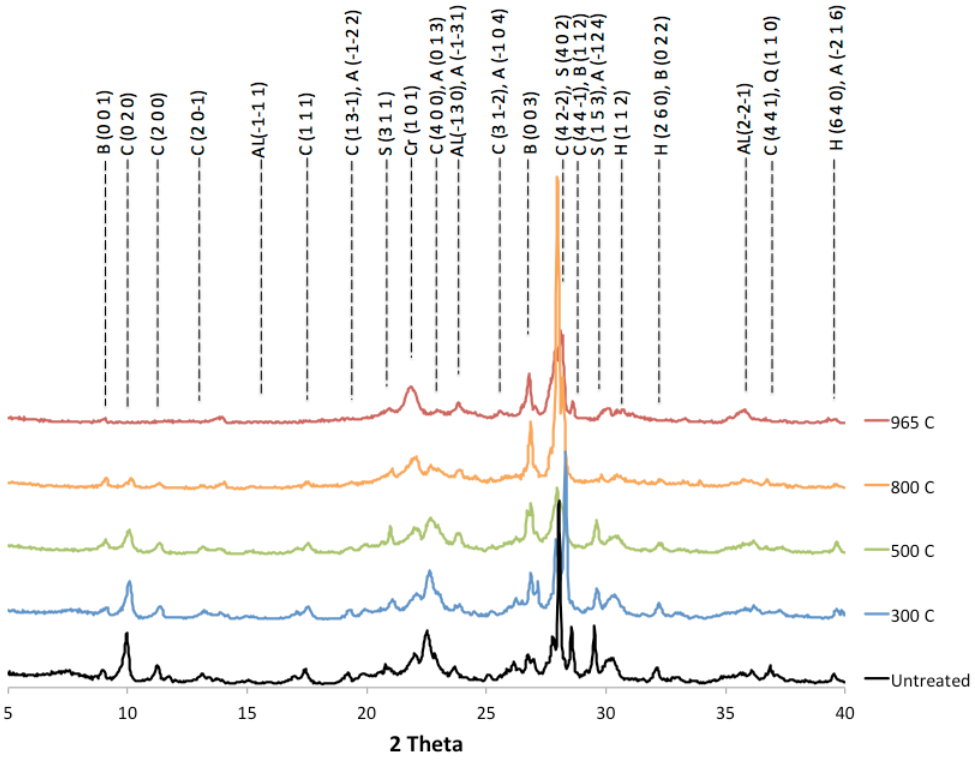

Figure 4.5 - Phases present in the zeolite C sample before and after calcination. (C = clinoptilolite, B = biotite, A = anorthite, AL = ablite, S = stellerite, Cr = cristobalite, H = heulandite, Q = quartz). Numbers in parenthesis indicate the d-spacing of the reflection

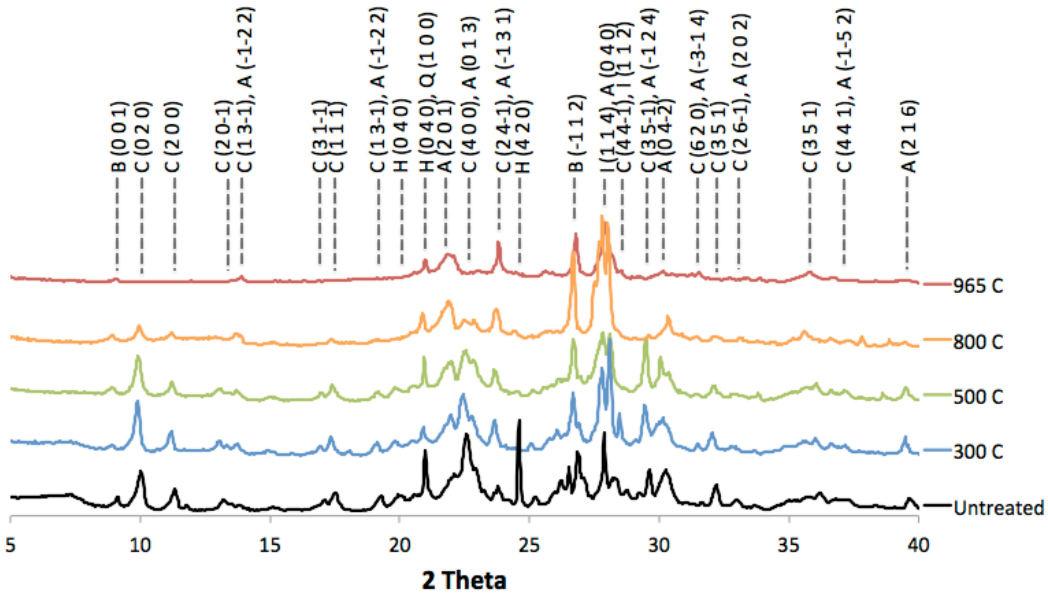

Figure 4.6 - Phases present in the zeolite A sample before and after calcination. (I = illite, C = clinoptilolite, H = heulandite, A = anorthite, B = biotite, AL = albite, Q = quartz). Numbers in parenthesis indicate the d-spacing of the reflection.

Table 4.1 - Phases present before calcination and after calcination at 965°C

Zeolite	Phases Present Before Calcination		Phases Present After Calcination at 965°C
Z	Clinoptilolite Illite Quartz	Heulandite, K-exchanged Cristobalite	Cristobalite Quartz
B	Clinoptilolite Quartz Cristobalite	Potassium Halite Biotite Stilbite	Cristobalite Quartz
L	Clinoptilolite Quartz	Heulandite, K-exchanged Cristobalite	Cristobalite Quartz
T	Clinoptilolite Quartz Biotite	Illite-2M1 Cristobalite	Cristobalite Quartz
C	Clinoptilolite Anorthite Quartz Cristobalite	Heulandite, K-exchanged Albite Stellerite Biotite	Cristobalite Quartz Anorthite Albite
A	Clinoptilolite Albite Quartz Biotite	Heulandite, K-exchanged Anorthite Cristobalite Illite-2M1	Cristobalite Quartz Anorthite Albite

4.3.1.2 Surface Area and Pore Size Distributions

The changes to surface area and the pore sizes of the zeolites with calcination are shown in Figures 4.7 to 4.18. Zeolites are commonly known to be microporous materials, but as the filling of pores less than 2 nm in size typically occurs at pressures much lower than was measured in this study (Bae et al. 2010), the BET surface area reported in this study does not include surfaces of zeolite nanopores. For this reason, in this study the surface areas determined using nitrogen adsorption could be thought of as ”nitrogen-available specific surface area,” but for simplicity will simply be called “surface area” or “nitrogen surface area” in this dissertation. Similarly, the BJH model is only applicable for pores larger than 2 nm in size, therefore only changes due to calcination in zeolite pores greater than this size were examined.

Figure 4.7 shows the effect of calcination on the nitrogen-available surface area, the external surface area and the internal surface area of zeolite Z. Calcination at temperatures greater than 300°C progressively lowers the external surface area of the zeolite, with the largest reduction occurring between 800 and 965°C. Internal surface area was nearly unchanged by calcination until 965°C, when it was reduced to very low levels. This suggests that calcination results in sintering of the zeolite particles until 965°C, at which time the pores begin to fill. This assertion is supported by Figure 4.8, which shows the pore size distribution of the untreated and calcined Z zeolite samples and indicates that higher calcination temperatures result in a reduction in the small, ~2-7 nm diameter, pores. After calcination at 965°C nearly all porosity of the material was eliminated in the zeolite Z samples.

Zeolite B, shown in Figures 4.9 and 4.10 exhibited a trend in decreasing nitrogen-available surface area with increasing calcination temperature similar to zeolite Z. However, unlike zeolite Z, the external surface area remained stable with calcination while the internal porosity of the zeolite was filled at much lower temperatures, beginning at 500°C. At 965°C both internal and external surface area were significantly reduced. The pore size distribution data shows that the zeolite's small pores, ~2-7 nm, filled progressively with increasing calcination temperatures up to 500°C. Above 500°C, the ~7-30 nm pores began to fill, and, after calcination at 965°C, nearly all of the pores of the material were filled, resulting in the large drop in measured surface area. Zeolite L, shown in Figures 4.11 and 4.12, followed very similar trends in the reduction of surface area to those seen with the calcination treatment of zeolite B.

Zeolite T, shown in Figures 4.13 and 4.14 had the greatest quantity of surface area of the untreated zeolites, likely a result of its significantly greater quantities of small pores, as seen in Figure 4.14. The changes in surface area with calcination were very similar to both zeolites B and L, however, zeolite T appeared to have stability at greater temperatures than many of the other zeolite samples, with its porosity not reduced until after heating to temperatures greater than 500°C. However, after calcination at 800°C, the ~2-7 nm pores of the zeolite were substantially reduced, to levels similar to the other zeolite samples, and were nearly eliminated after calcination at 965°C.

Both the external and internal surface area of zeolite C were reduced with calcination, while porosity changes with calcination of zeolite C were similar to the effects seen in zeolites B and L and are shown in Figures 4.15 and 4.16. However, zeolite

C appeared to have slightly greater stability at higher temperatures, with very little reduction in porosity until temperatures greater than 500°C.

The changes to the nitrogen-available surface area of zeolite A, shown in Figures 4.17 and 4.18 did not fit the trends exhibited by the other zeolites. The pore size distribution data, shown in Figure 4.18, indicates that calcination at 500°C created significant porosity in the sample. However, the surface area of the sample was reduced from 300°C to 500°C, so it is possible that the creation of ~7-30 nm pores may have been paired with infilling of pores. Although unexpected, this effect was repeatable as the same results occurred in triplicate samples. The reduction in the nitrogen-available surface area of zeolite A appeared to be primarily due to changes in the external surface area of the sample.

In general, calcination resulted in a significant reduction in specific surface area of the zeolites, a reduction in pore volume, and an overall increase in pore diameter. For half of the zeolites, reductions in nitrogen-available surface area were a result of changes to external surface area, while other zeolites showed changes primarily in the sample's internal surface area. One sample showed similar reductions in both internal and external surface area. It is unclear by what mechanism surface area is reduced with higher calcination temperatures, though the trend towards reduction in total nitrogen-available surface area with calcination is consistent across all zeolite samples. The pore size distribution plots show that, for most samples, calcination resulted in an infilling of the particles' small, ~2-7 nm, pores with very little change to the larger, ~7-30 nm, pores, followed by a reduction of the total volume of all pores with further increase in temperature.

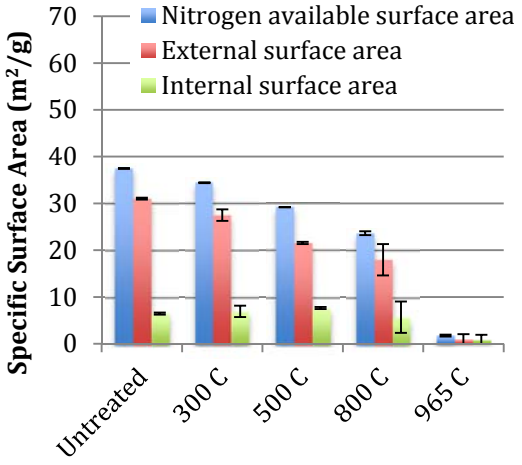

Figure 4.7 - Nitrogen-available specific surface area of untreated and calcined zeolite Z

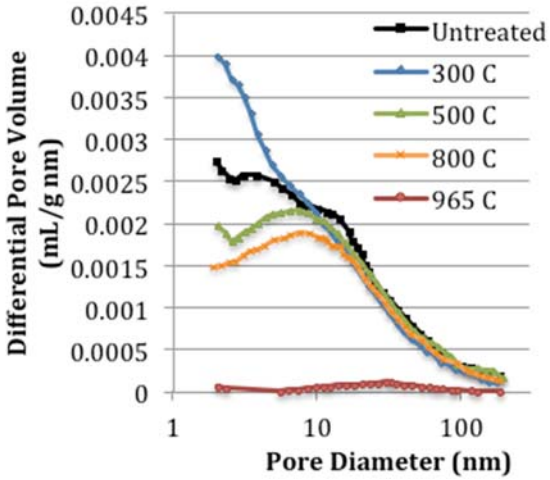

Figure 4.8 - Pore size distribution of untreated and calcined zeolite Z

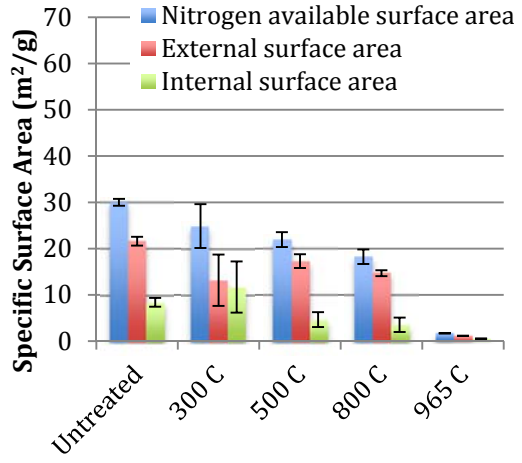

Figure 4.9 - Nitrogen-available specific surface area of untreated and calcined zeolite B

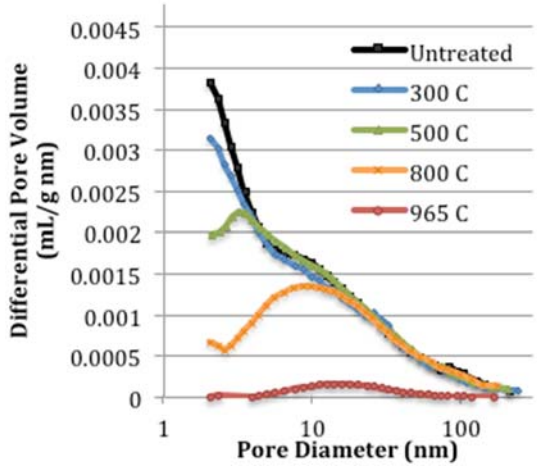

Figure 4.10 - Pore size distribution of untreated and calcined zeolite B

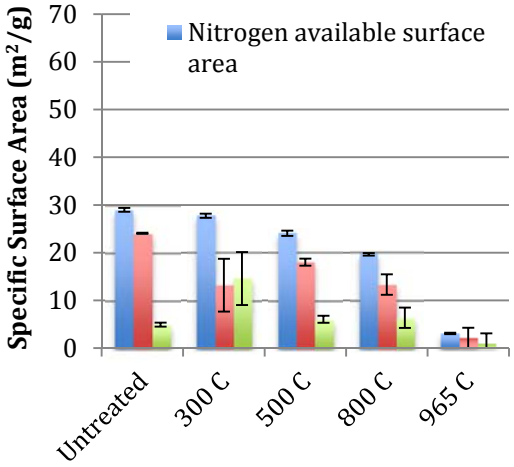

Figure 4.11 - Nitrogen-available specific surface area of untreated and calcined zeolite L

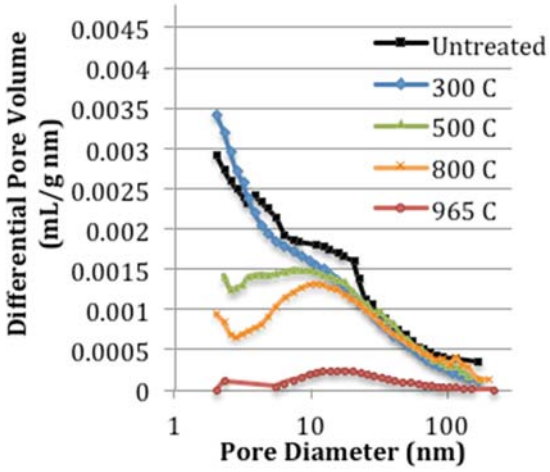

Figure 4.12 - Pore size distribution of untreated and calcined zeolite L

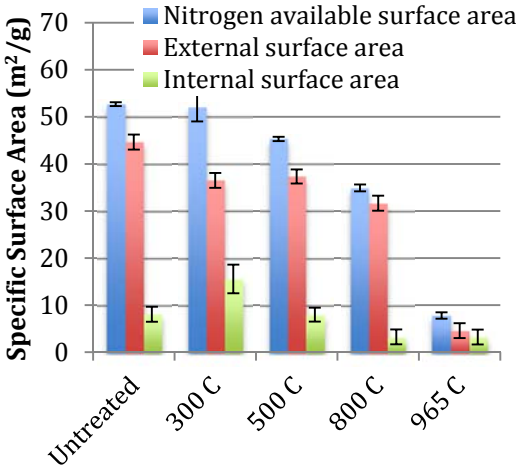

Figure 4.13 - Nitrogen-available specific surface area of untreated and calcined zeolite T

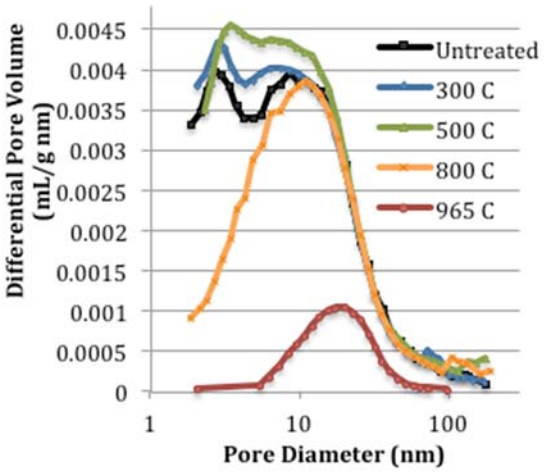

Figure 4.14 - Pore size distribution of untreated and calcined zeolite T

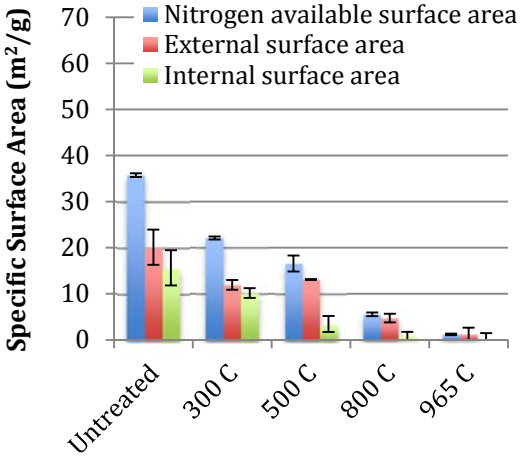

Figure4.15 - Nitrogen-available specific surface area of untreated and calcined zeolite C

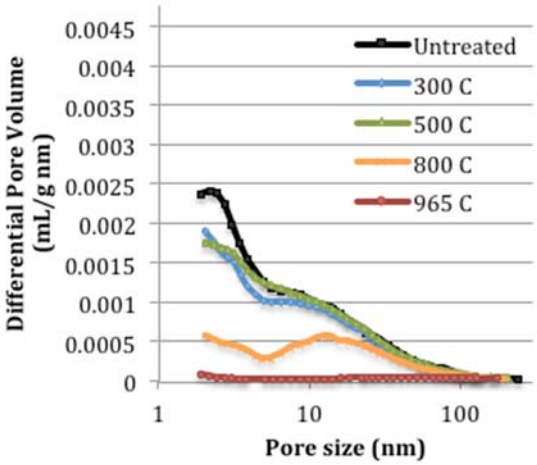

Figure4.16 - Pore size distribution of untreated and calcined zeolite C

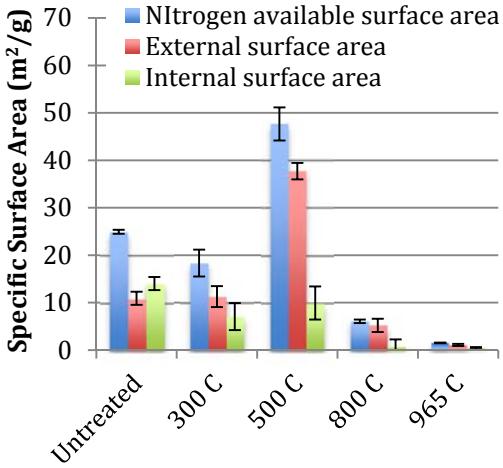

Figure4.17 - Nitrogen-available specific surface area of untreated and calcined zeolite A

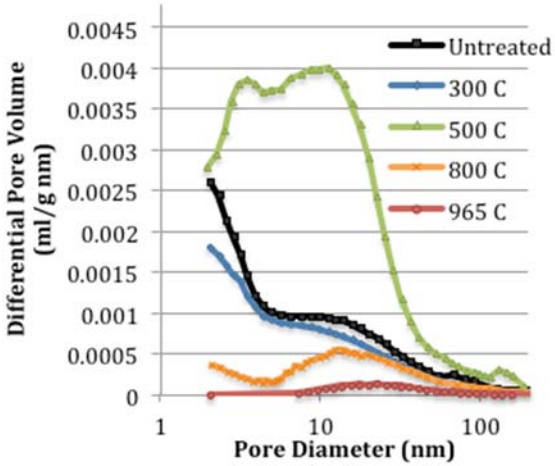

Figure 4.18 - Pore size distribution of untreated and calcined zeolite A

4.3.1.3 Particle Size

The changes in particle sizes after calcination at 300, 500, 800 or 965°C are shown in Tables 4.2 to 4.7 and Figures 4.19 to 4.24. In nearly all cases calcination increased the average zeolite particle size. Correspondingly, the volume of fine particles was also reduced in all samples with increasing calcination temperatures. This effect became particularly evident after calcination at 500°C, but is noticeable to a small degree after calcination at 300°C in some samples, such as zeolite T and B. The exception to this effect is seen in zeolite Z, shown in Table 4.2 and Figure 4.19. This zeolite showed very little change in particle size at temperatures lower than 965°C. Particle size data for the 965°C sample for this zeolite is not shown because after calcination the sample was obtained from the oven in one large, solid block and had to be chipped apart and reground before use. The particle size results after the calcination of zeolite B are shown in (a) cumulative particle size distribution, (b) volumetric particle size distribution Table 4.3. Calcination decreased the amount of fine, 0.75-7 μm material, but otherwise had very little effect on the sample's particle size distribution. Calcination of zeolite L reduced the size of particles throughout the range of the particle size distribution of the zeolite sample, as shown in Table 4.4 and Figure 4.21. As shown in Table 4.5 and Figure 4.22, calcination of zeolite T initially resulted in an overall decrease in particle size, despite an increase in the d_{90} particle size. Treatment at 500°C resulted in an increase in the quantity of particles in the ~7-30 μm range, but continued to reduce the size ~200-800 μm particles. Calcination at 800°C resulted in a significant increase in the ~200-800 μm, particles and reduction in the quantity of ~7-30 μm particles. Further calcination to 965°C did not appear to have any additional effect on particles.

For zeolite C, only the zeolite particles ranging from ~30-300 µm, shown in Table 4.6 and Figure 4.23, were affected by calcination at 300°C, with the volume of these particles present in the sample having been slightly reduced by calcination. However, calcination temperatures greater than 300°C noticeably increased the size of particles throughout the range of the particle size distribution of the zeolite sample up to 800°C, especially increasing particles in the ~70-600 µm range. Very little change to the zeolite C particle size distribution resulted from calcination at 965°C.

Calcination of zeolite A, shown in Table 4.7 and Figure 4.24, showed similar results to calcination of zeolite T, discussed previously. Calcination at 300 and 500°C resulted in a decrease in overall particle size, shifting the general distribution of particles lower. Calcination at 800°C resulted in a significant increase in the volume of ~50-600 µm, particles, with very little additional change resulting from further calcination to 965°C.

Table 4.2 - Particle sizes of zeolite Z before and after calcination

Calcination Temperature (°C)	Particle Sizes (µm)		
	d_{10}	d_{50}	d_{90}
0	1.9	6.4	16.0
300	1.5	7.1	16.2
500	1.8	6.5	20.1
800	1.6	6.9	15.2

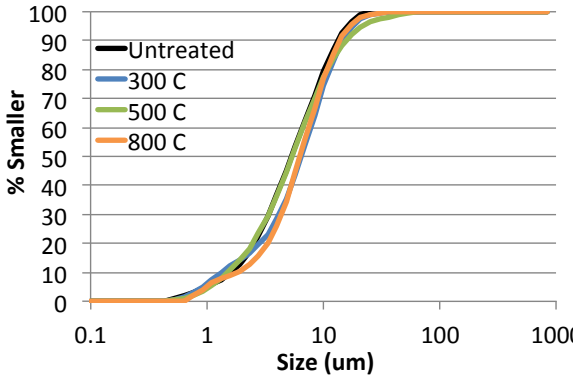

(a)

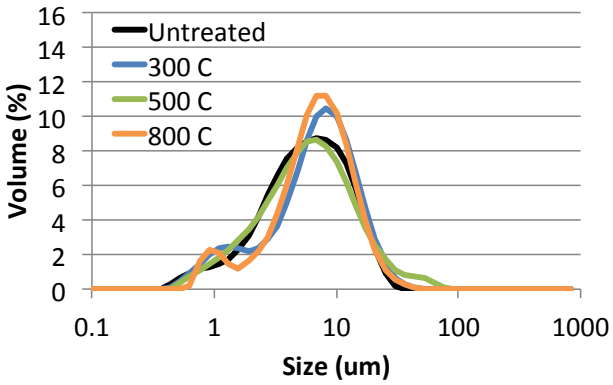

(b)

Figure 4.19 - Particle size distribution of untreated and calcined zeolite Z (a) cumulative particle size distribution, (b) volumetric particle size distribution

Table 4.3 - Particle sizes of zeolite B before and after calcination

Calcination Temperature (°C)	Particle Sizes (µm)		
	d_{10}	d_{50}	d_{90}
0	3.0	34.3	129.6
300	7.1	33.4	105.0
500	7.8	34.5	88.0
800	9.2	41.1	124.4
965	9.3	38.4	100.9

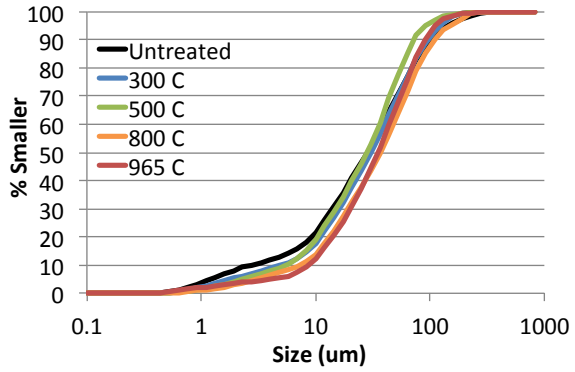

(a)

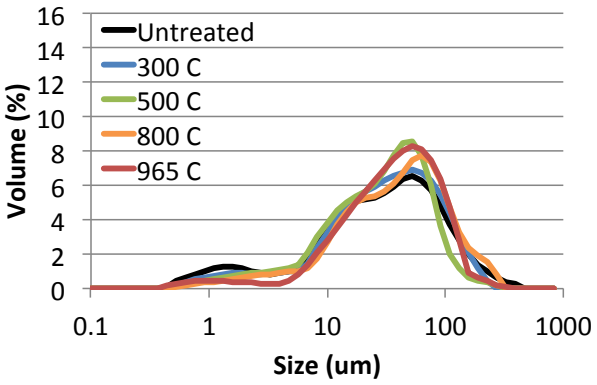

(b)

Figure 4.20 - Particle size distribution of untreated and calcined zeolite B, (a) cumulative particle size distribution, (b) volumetric particle size distribution

Table 4.4 - Particle sizes of zeolite L before and after calcination

Calcination Temperature (°C)	Particle Sizes (µm)		
	d_{10}	d_{50}	d_{90}
0	222.2	802.1	1388.3
300	310.3	859.0	1377.1
500	256.9	771.7	1405.9
800	246.7	727.5	1263.2
965	117.8	596.9	1147.4

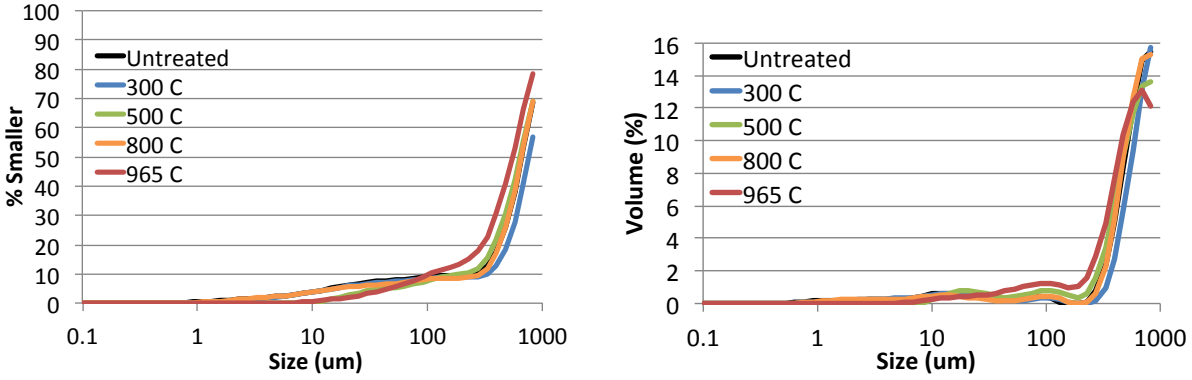

(a) (b)

Figure 4.21 - Particle size distribution of untreated and calcined zeolite L, (a) cumulative particle size distribution, (b) volumetric particle size distribution

Table 4.5 - Particle sizes of zeolite T before and after calcination

Calcination Temperature (°C)	Particle Sizes (µm)		
	d_{10}	d_{50}	d_{90}
0	12.8	77.4	408.6
300	6.6	66.0	442.2
500	10.1	83.7	293.7
800	24.2	178.9	496.5
965	34.9	205.5	551.8

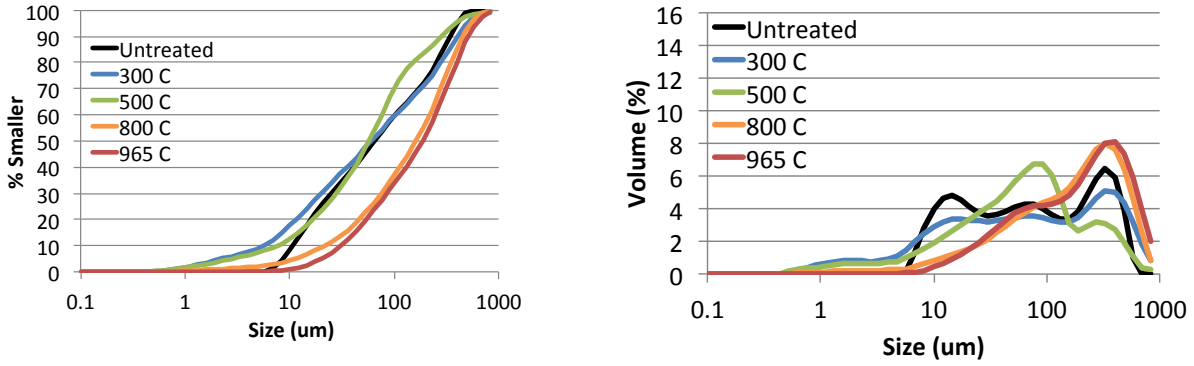

(a) (b)

Figure 4.22 - Particle size distribution of untreated and calcined zeolite T, (a) cumulative particle size distribution, (b) volumetric particle size distribution

Table 4.6 - Particle sizes of zeolite C before and after calcination

Calcination Temperature (°C)	Particle Sizes (µm)		
	d_{10}	d_{50}	d_{90}
0	4.0	45.9	167.4
300	4.3	43.2	189.2
500	13.5	77.3	201.6
800	22.8	107.8	284.4
965	43.7	127.4	331.8

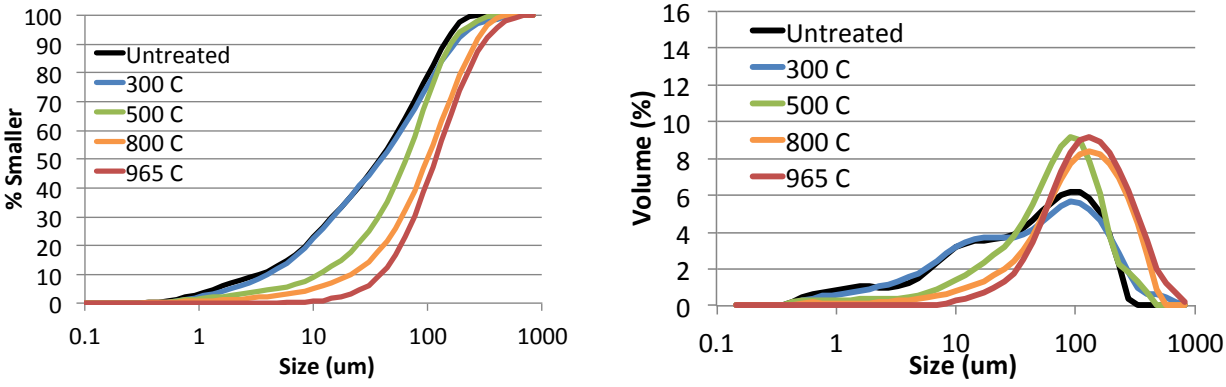

(a) (b)

Figure 4.23 - Particle size distribution of untreated and calcined zeolite C, (a) cumulative particle size distribution, (b) volumetric particle size distribution

Table 4.7 - Particle sizes of zeolite A before and after calcination

Calcination Temperature (°C)	Particle Sizes (µm)		
	d_{10}	d_{50}	d_{90}
0	9.8	220.6	509.6
300	4.4	47.0	222.6
500	7.7	99.9	334.8
800	24.5	125.0	348.8
965	45.8	154.2	449.4

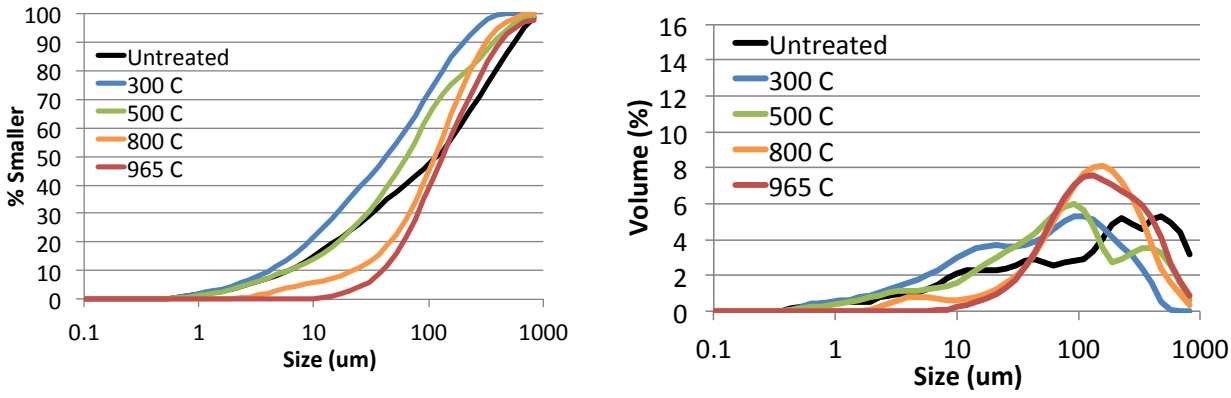

(a) (b)

Figure 4.24 - Particle size distribution of untreated and calcined zeolite A, (a) cumulative particle size distribution, (b) volumetric particle size distribution

4.3.1.4 Material Topography from SEM

The topography of zeolite Z, obtained using SEM, is shown in Figure 4.25. Particle surfaces appear smoother after calcination, but otherwise very little change can be seen between the untreated sample and the sample calcined at 965°C. The topography of zeolite B is shown in Figure 4.26. Particle size appears slightly larger for the calcined sample. One particularly noticeable change is the appearance of small particles adhered to the surface of the larger particles in the calcined zeolite, whereas the surfaces of the uncalcined zeolites appear smooth. The appearance of small, adhered particles on the surface of larger zeolite particles were also seen in zeolites L, T, C, and A, shown in

Figure 4.25 to 4.30. Zeolite L, unlike the other samples, also appears to have either a much higher degree of agglomeration occurring or generation of porosity within the zeolite structure. As the pore size distribution and reaction area both decreased with calcination of this sample, as shown in Figure 4.11 and 4.21, the 'holes' in the sample surface are most likely just spaces between densified solid particles. SEM images of the sample after calcination at 500°C are included in Figure 4.30 and may help explain the large increase in porosity indicated in the pore size distribution data in section 4.3.1.2. After calcination at 500°C, the sample surface does not appear to have yet acquired attached smaller particles visible in images of the zeolite calcined at 965°C. Additionally, the sintering process may contribute to the creation of larger, heterogenous pores on the surface of the zeolites as the solid materials densify. However, the surface of the zeolite shown in Figure 4.30 does appear to have a noticeably greater amount of approximately 10 μm pores compared to the uncalcined sample. In general, it appears from SEM images that calcination resulted in agglomerations of particles, with many of the finer particles becoming adhered to the surfaces of larger particles.

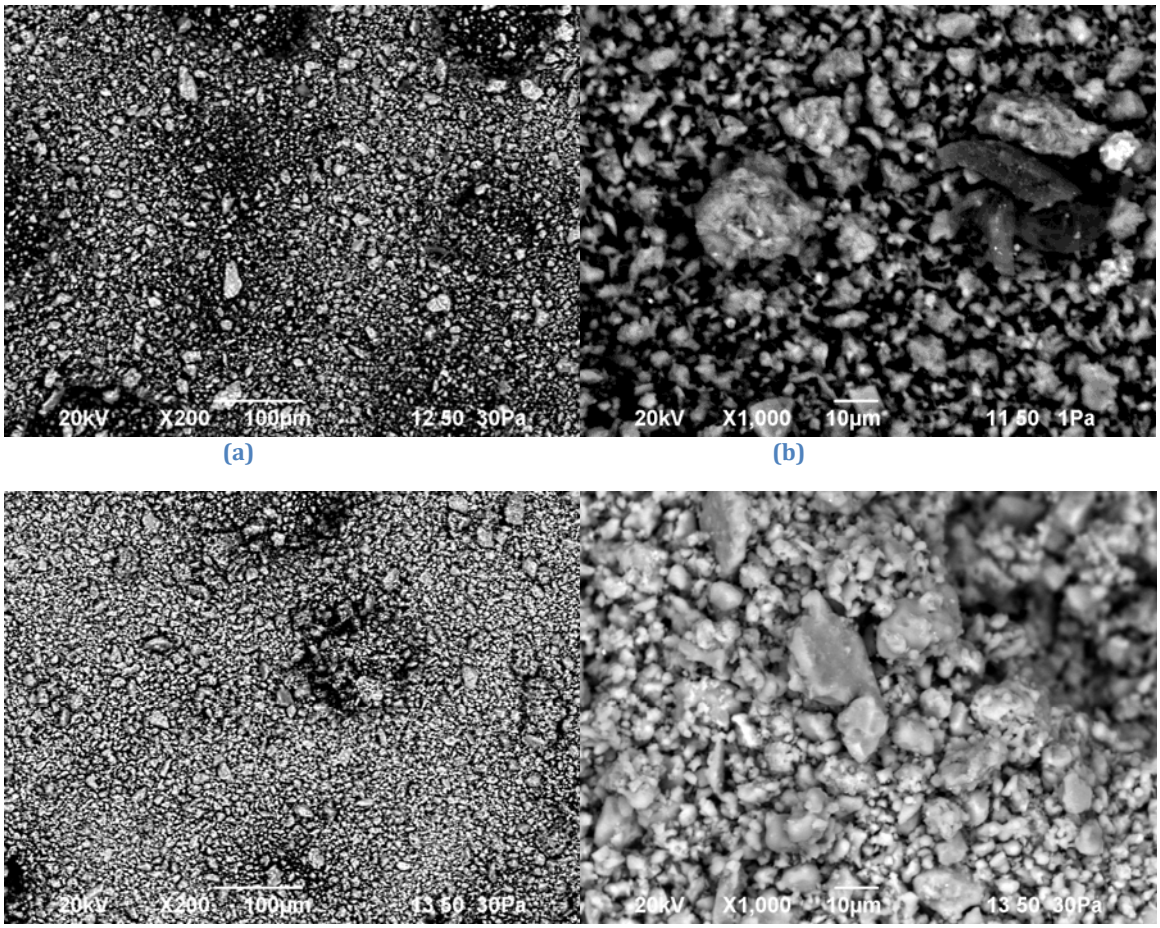

(a) (b)

(c) (d)

Figure 4.25 - SEM images of zeolite Z – (a) – uncalcined, (a) uncalcined at higher magnification, (c) calcined at 965°C and (d) calcined at 965°C at higher magnification

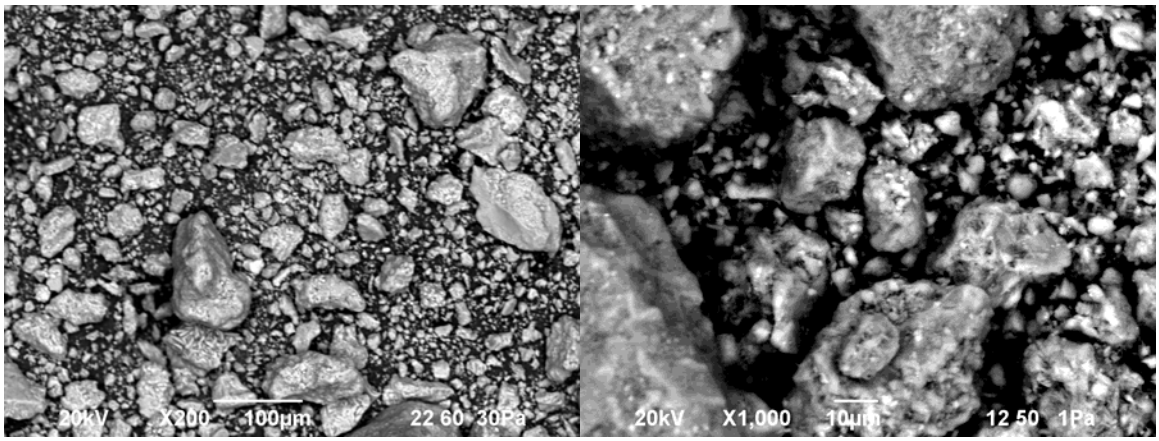

(a) (b)

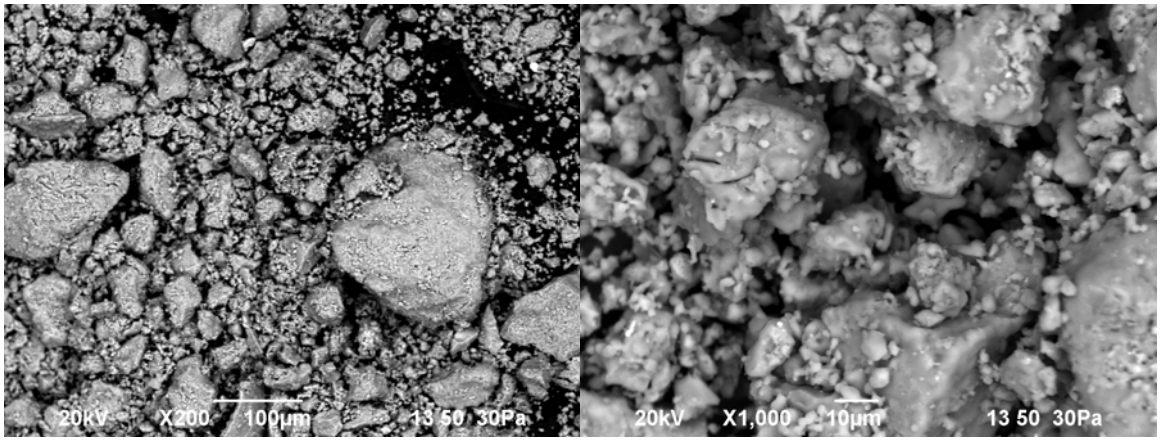

(c) (d)

Figure 4.26 - SEM images of zeolite B – (a) – uncalcined, (b) uncalcined at higher magnification, (c) calcined at 965°C and (d) calcined at 965°C at higher magnification

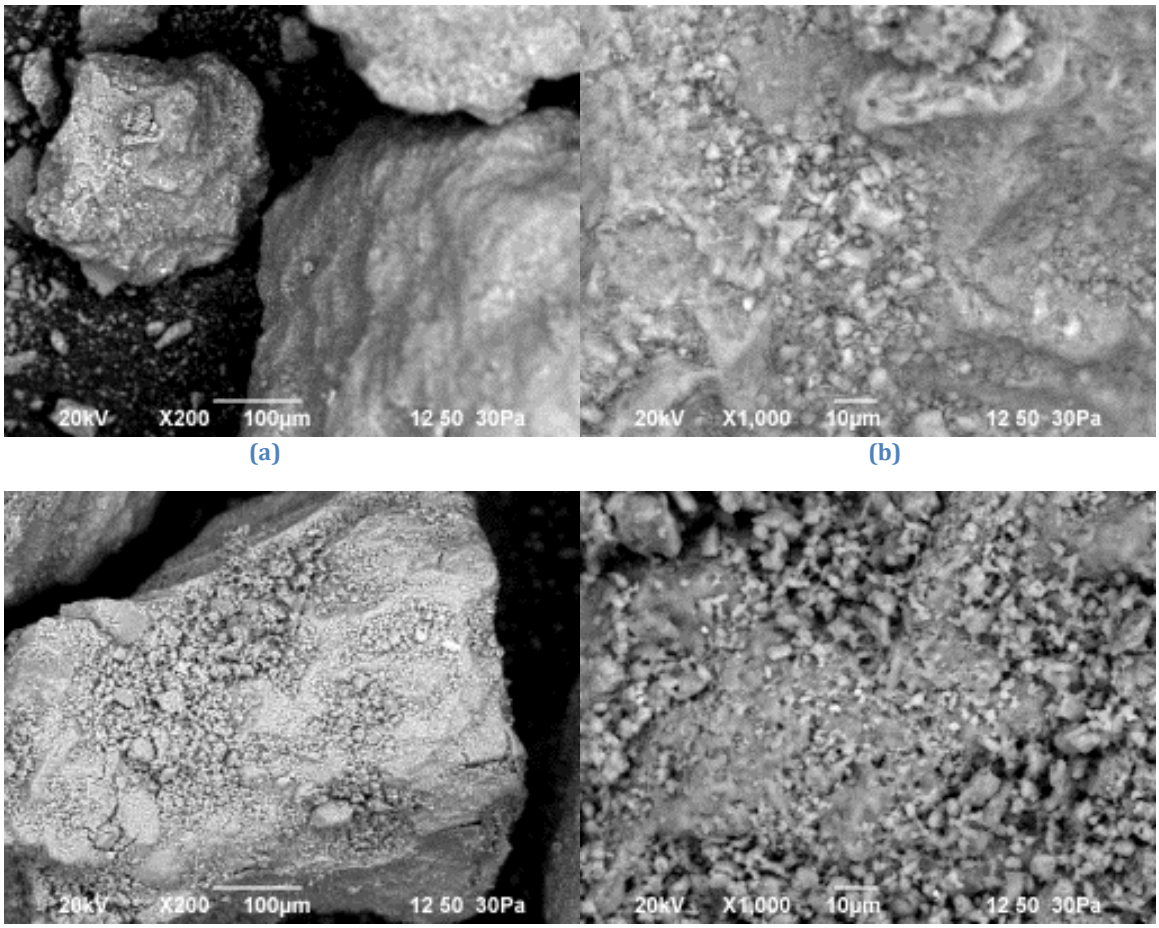

(a) (b)

(c) (d)

Figure 4.27 - SEM images of zeolite L - (a) – uncalcined, (b) uncalcined at higher magnification, (c) calcined at 965°C and (d) calcined at 965°C at higher magnification

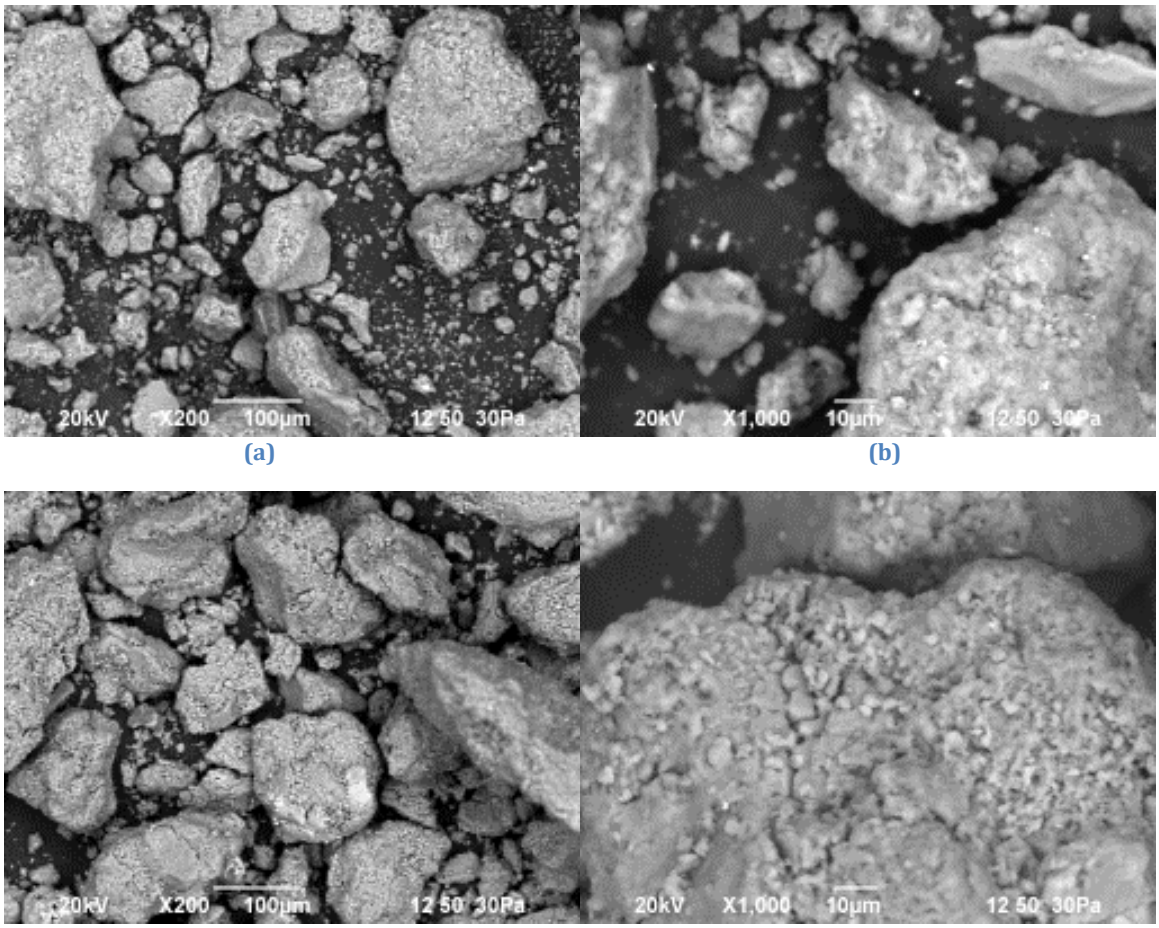

(a) (b)

(c) (d)

Figure 4.28 - SEM images of zeolite T – (a) – uncalcined, (b) uncalcined at higher magnification, (c) calcined at 965°C and (d) calcined at 965°C at higher magnification

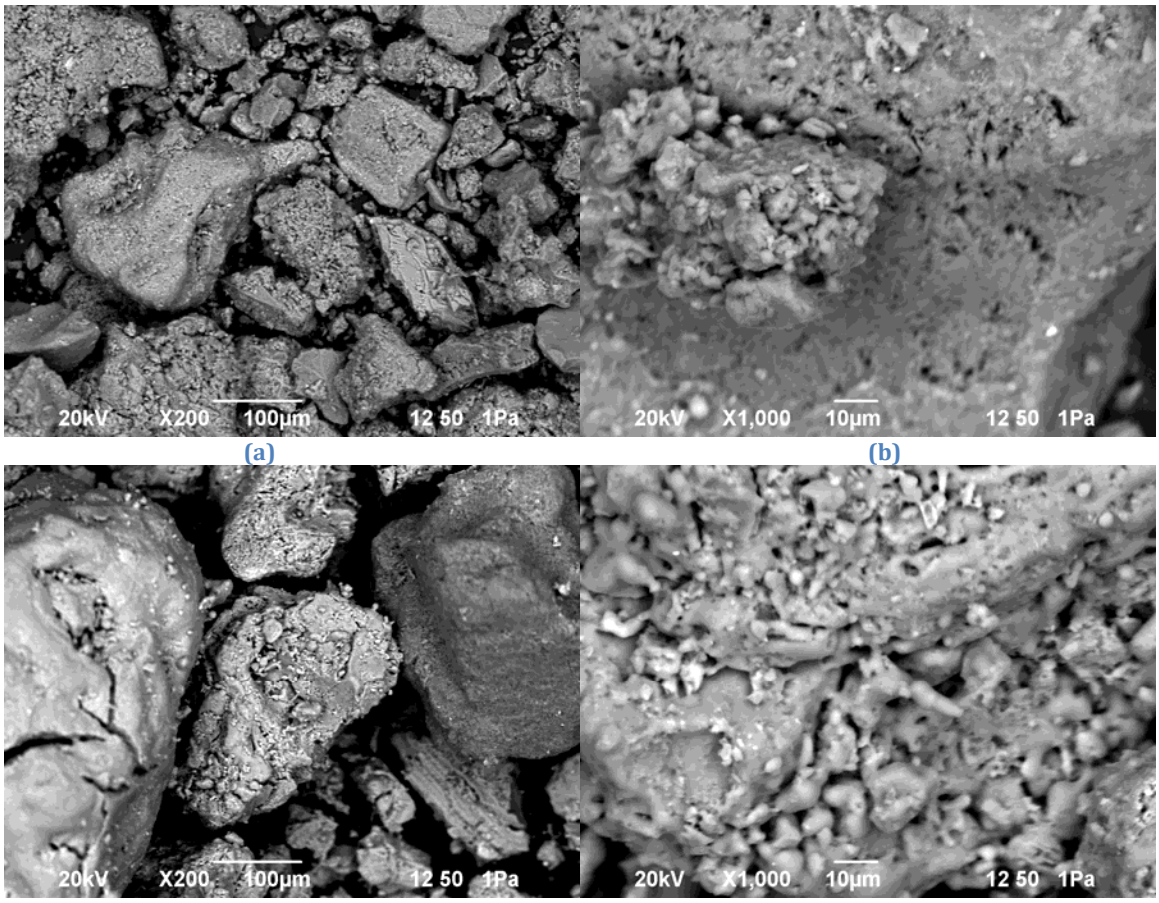

(a) (b)

(c) (d)

Figure 4.29 - SEM images of zeolite C – (a) – uncalcined, (b) uncalcined at higher magnification, (c) calcined at 965°C and (d) calcined at 965°C at higher magnification

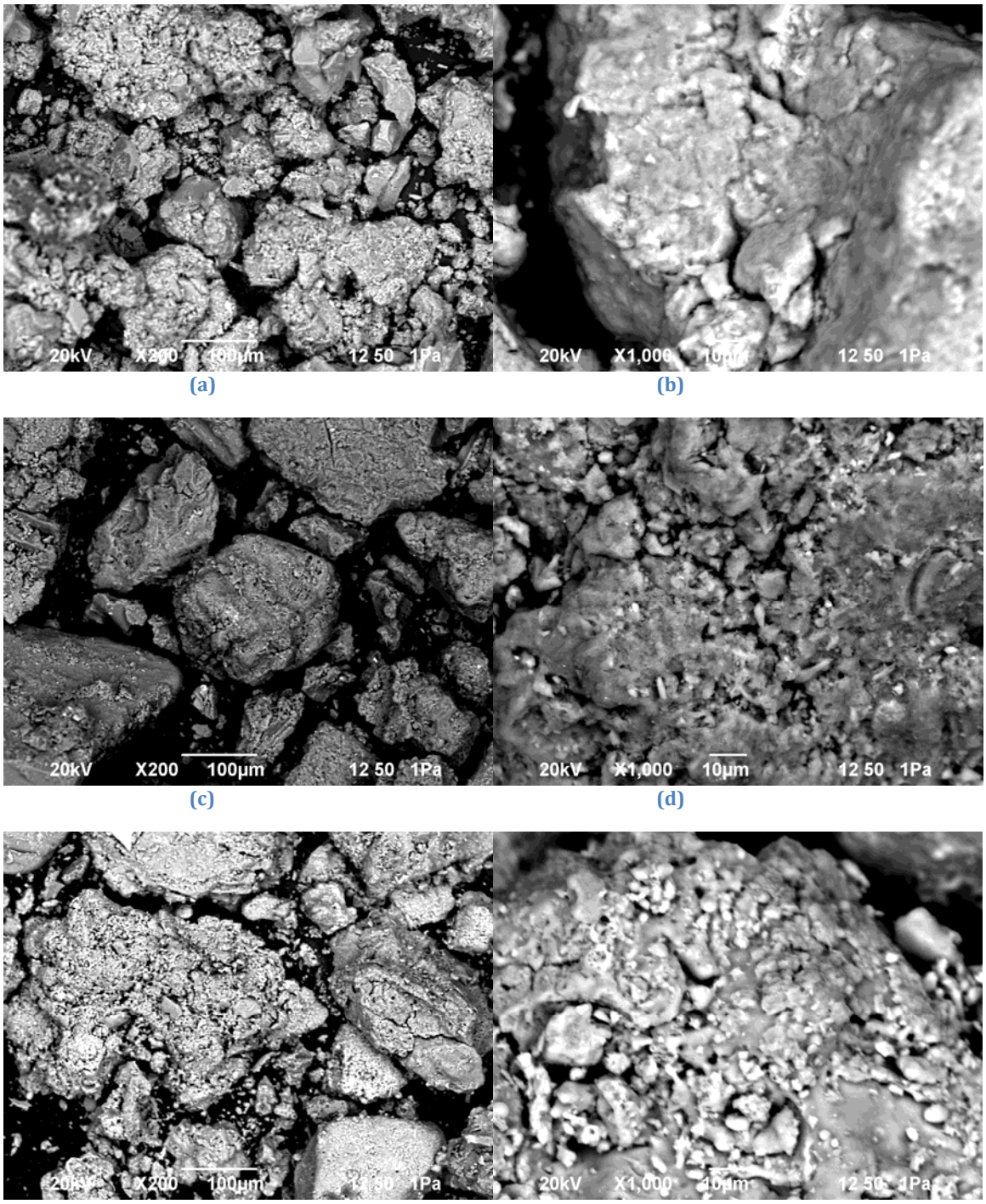

Figure 4.30 - SEM images of zeolite A – (a) – uncalcined, (b) uncalcined at higher magnification, (c) calcined at 500°C and (d) calcined at 500°C at higher magnification (e) calcined at 965°C and (f) calcined at 965°C at higher magnification

4.3.2 Zeolite Reactivity Characterization

4.3.2.1 Calcium Hydroxide Measurements of Calcined Zeolite-Cement Pastes to Determine Pozzolanic Reactivity

The calcium hydroxide contents of pastes containing raw and calcined zeolites are shown in Figure 4.31 to 4.36. All untreated systems showed evidence of pozzolanic reaction after 28 and 90 days, having lower calcium hydroxide contents than both the sample using inert quartz filler and the cement-only paste. As discussed in Chapter 2, Antoni et al. (2012) showed that a quartz filler slightly increased the amount of $Ca(OH)_2$ produced compared to a cement-only paste because it allowed more space for hydration product growth. The same effect is shown in Figure 4.31 to 4.36. Reduction in $Ca(OH)_2$ content compared to the quartz filler sample is due to the pozzolanic reaction of the added zeolite. Overall, calcination at temperatures of 800°C or lower had a very small effect on the pozzolanicity of the zeolites, while calcination of the zeolite at 965°C nearly eliminated the pozzolanic effect of the zeolite. However, zeolite samples calcined at 965°C were not completely inert, as all 965°C zeolite-cement pastes resulted in reduced calcium hydroxide contents compared to those using non-pozzolanic quartz filler.

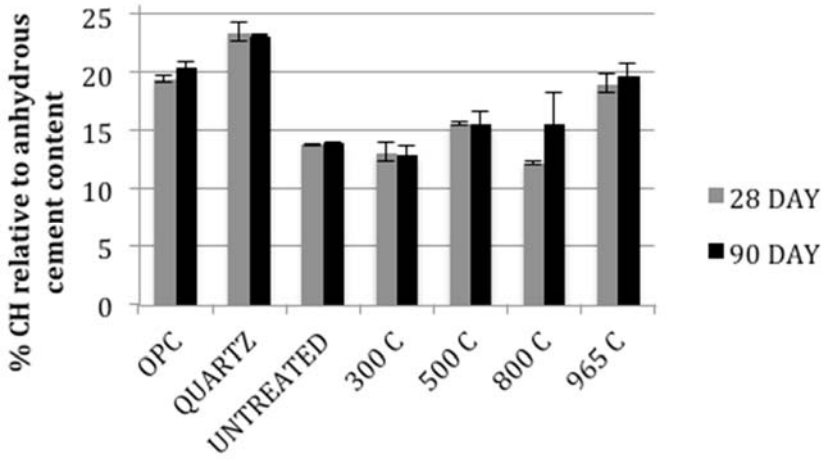

Figure 4.31 - $Ca(OH)_2$ content by weight of hydrated cement pastes containing 80-100% cement and 0-20% untreated zeolite Z, calcined zeolite Z or quartz filler, (w/cm = 0.4)

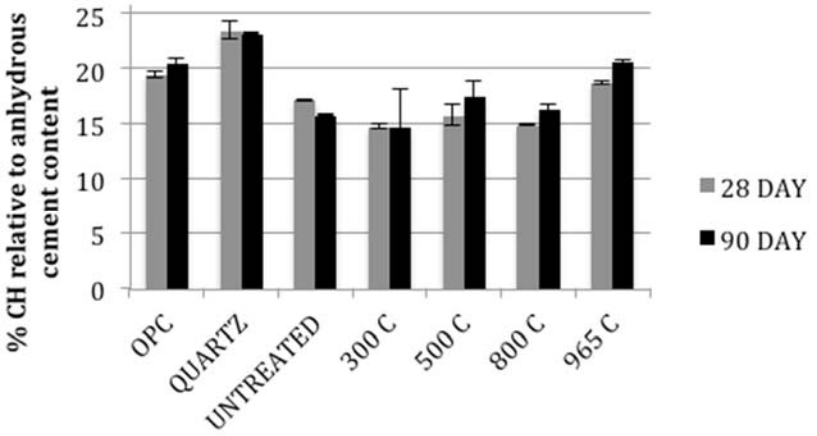

Figure 4.32 - $Ca(OH)_2$ content by weight of hydrated cement pastes containing 80-100% cement and 0-20% untreated zeolite B, calcined zeolite B or quartz filler, (w/cm = 0.4)

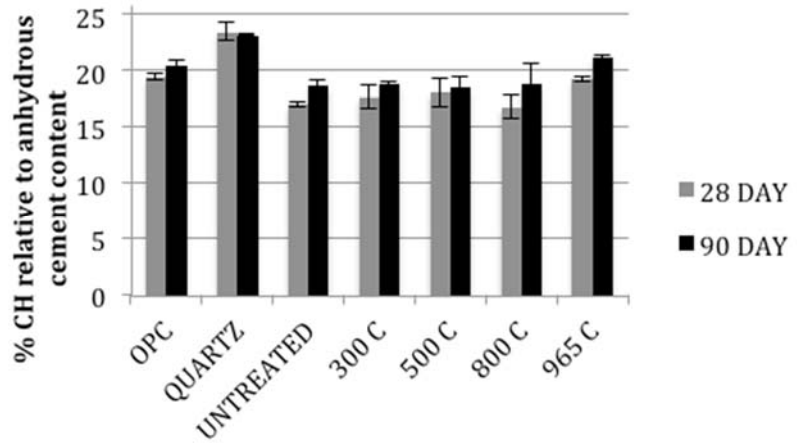

Figure 4.33 - $Ca(OH)_2$ content by weight of hydrated cement pastes containing 80-100% cement and 0-20% untreated zeolite L, calcined zeolite L or quartz filler, (w/cm = 0.4)

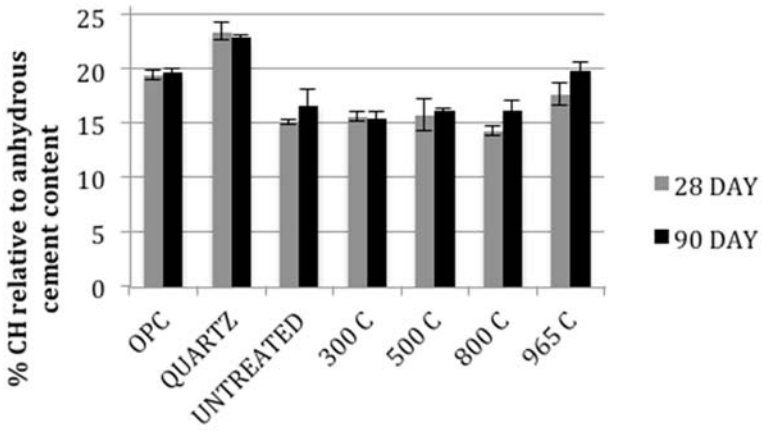

Figure 4.34 - $Ca(OH)_2$ content by weight of hydrated cement pastes containing 80-100% cement and 0-20% untreated zeolite T, calcined zeolite T or quartz filler, (w/cm = 0.4)

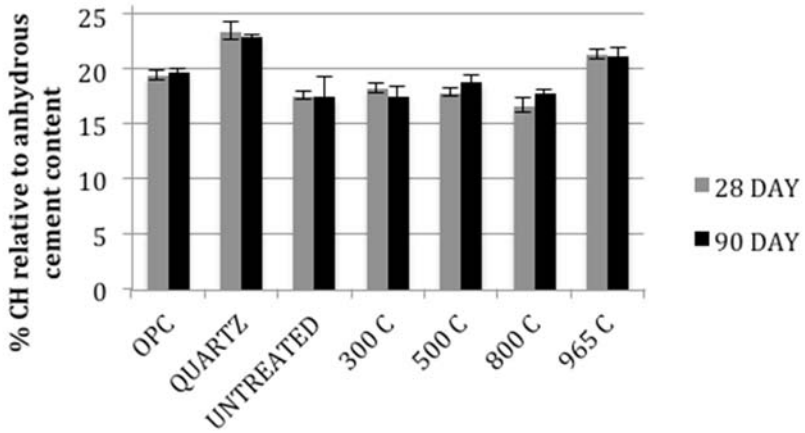

Figure 4.35 - $Ca(OH)_2$ content by weight of hydrated cement pastes containing 80-100% cement and 0-20% untreated zeolite C, calcined zeolite C or quartz filler, (w/cm = 0.4)

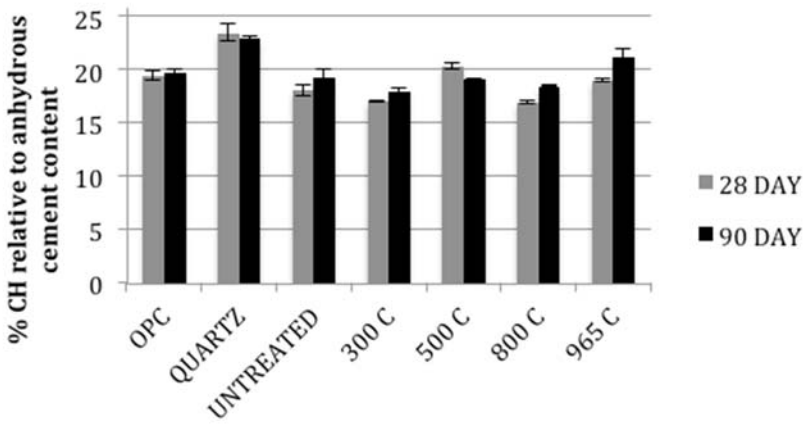

Figure 4.36 - $Ca(OH)_2$ content by weight of hydrated cement pastes containing 80-100% cement and 0-20% untreated zeolite A, calcined zeolite A or quartz filler, (w/cm = 0.4)

4.3.2.2 Chapelle Test of Calcined Zeolites to Determine Pozzolanic Potential

The results of the Chapelle test for pozzolanicity are shown in Figure 4.37 to 4.42. The results of the Chapelle test were varied and lacked discernable trends for most of the materials calcined at 800°C or lower. One discernable trend in the Chapelle test results, however, was the reduced reactivity of the samples calcined at 965°C. In most cases, the 965°C sample consumed the least calcium from solution, and in the cases of zeolites L, T, and A, may not have consumed any, suggesting that the material is unable to remove calcium from solution. In the case of zeolites Z and B, size effects may have helped overcome changes in reactivity due to calcination at 965°C, with the small particle sizes of zeolites Z and B, shown in Table 4.2 and Table 4.3, even after calcination at 965°C, removing calcium from the system simply through adsorption to particle surfaces. Additional discussion of the accuracy of the Chapelle test for the prediction of pozzolanic potential is presented in Appendix A.

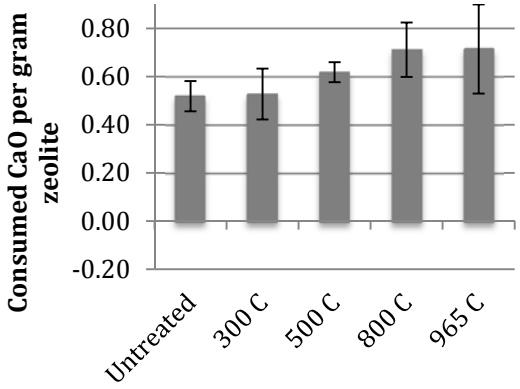

Figure 4.37 - Chapelle test results for raw and calcined zeolite Z

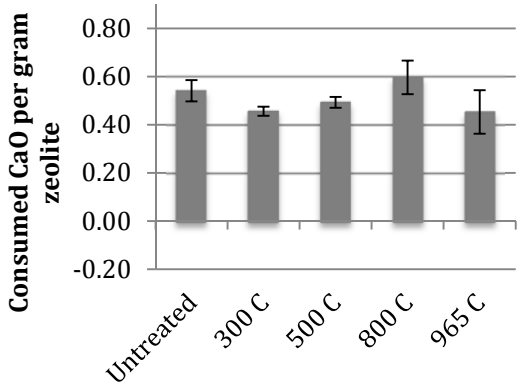

Figure 4.38 - Chapelle test results for raw and calcined zeolite B

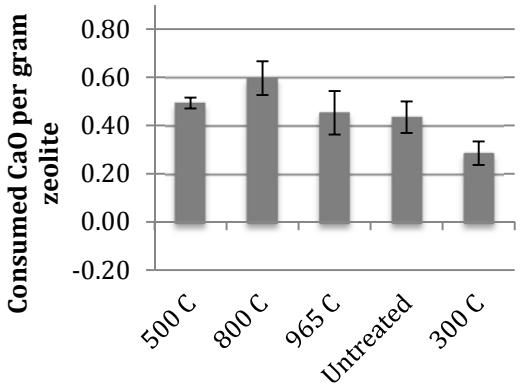

Figure 4.39 - Chapelle test results for raw and calcined zeolite L

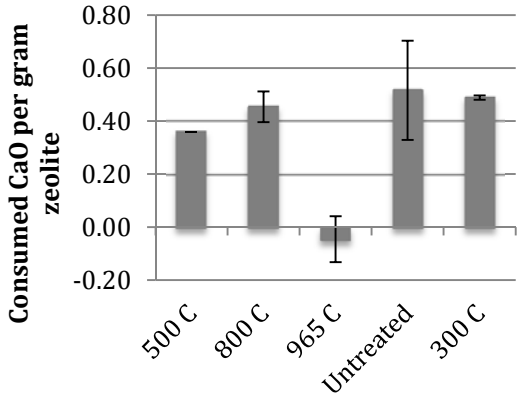

Figure 4.40 - Chapelle test results for raw and calcined zeolite T

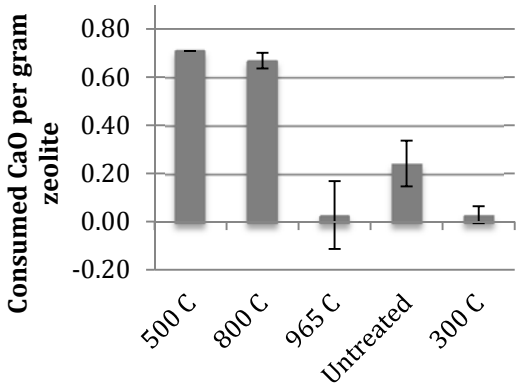

Figure 4.41 - Chapelle test results for raw and calcined zeolite C

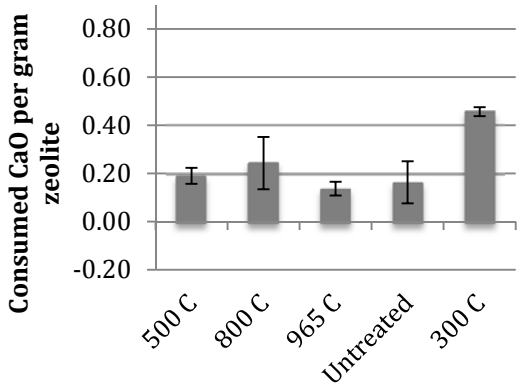

Figure 4.42 - Chapelle test results for raw and calcined zeolite A

4.3.2.3 Compressive Strengths of Cement-Calcined Zeolite Mortars

The effect of calcination on compressive strength is shown in Figure 4.43 to 4.48. Mortars containing zeolites calcined at 300°C had greater strengths at 28 and 90 days than mortars using untreated zeolite, with the exception of mortars containing zeolites L and T, which had strengths equal to the strength of the untreated zeolite-cement mortar, within error. An approximately 10% increase in strength compared to the cement-only mortar was seen at 90 days for mortars containing zeolites Z, B and A. Calcination of zeolites Z and B also resulted in significant strength gains at 90 days compared to the uncalcined zeolite mortar.

In many of the mortars, calcination at 500°C and 965°C reduced compressive strengths compared to mortars containing the untreated zeolite. The strengths of these mortars often coincided with the strengths of the mortar containing quartz filler, especially when taking into account differences due to particle size. For example, the strength resulting from use of zeolite L calcined at 500°C was much lower than that of the quartz sample, but the d_{50} of the quartz sample was approximately 80 μm, whereas the d_{50} of zeolite L was 700 μm. Similarly, the strength of the sample containing zeolite Z calcined at 500°C was considerably greater than the quartz sample, while the zeolite Z d_{50} was much smaller, at 6.5 μm. All of the other zeolite samples, with the exception of the large-size zeolite L, outperformed the mortars containing quartz filler.

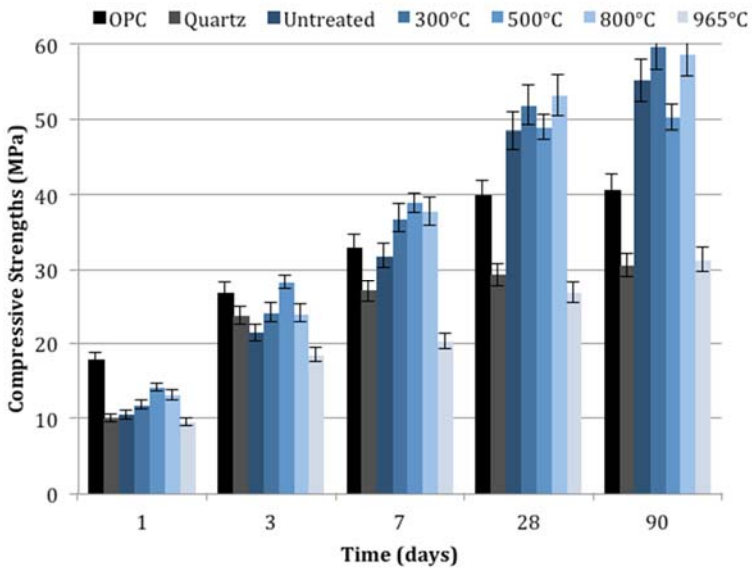

Figure 4.43 - Compressive strengths of untreated and calcined zeolite Z

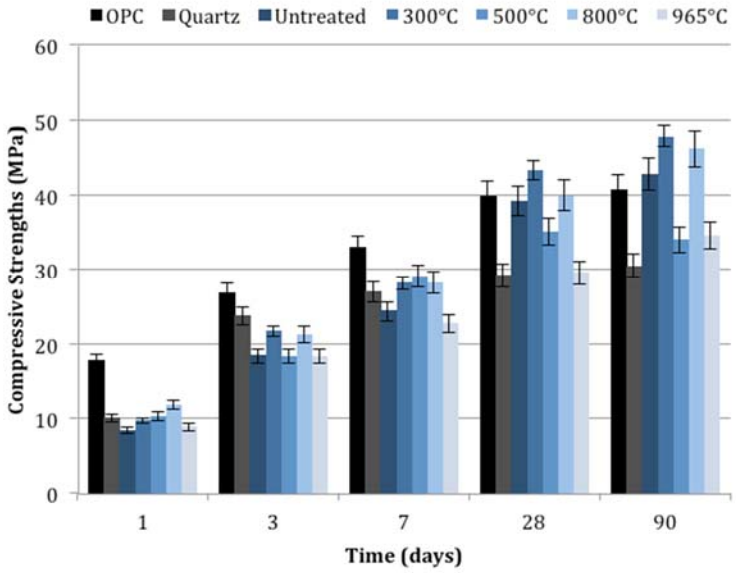

Figure 4.44 - Compressive strengths of untreated and calcined zeolite B

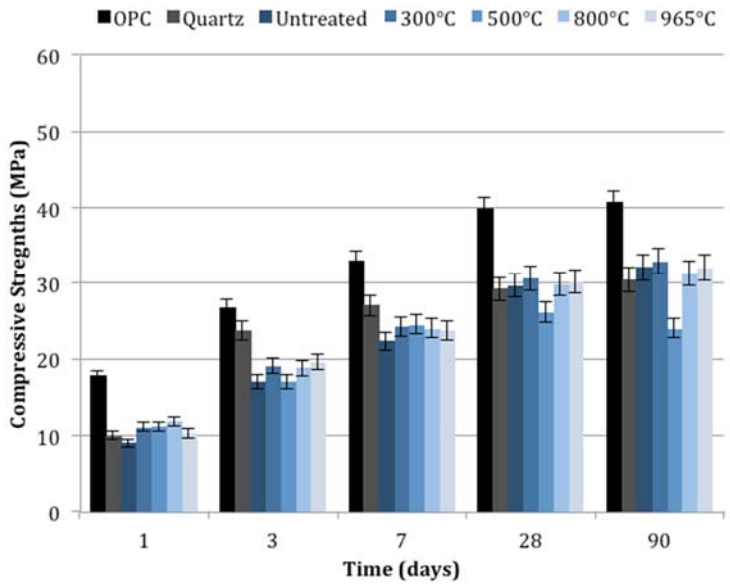

Figure 4.45 - Compressive strengths of untreated and calcined zeolite L

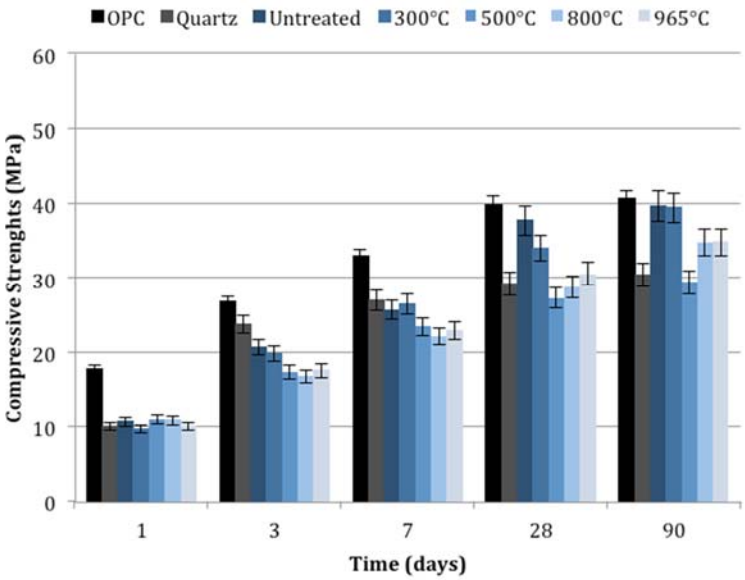

Figure 4.46 - Compressive strengths of untreated and calcined zeolite T

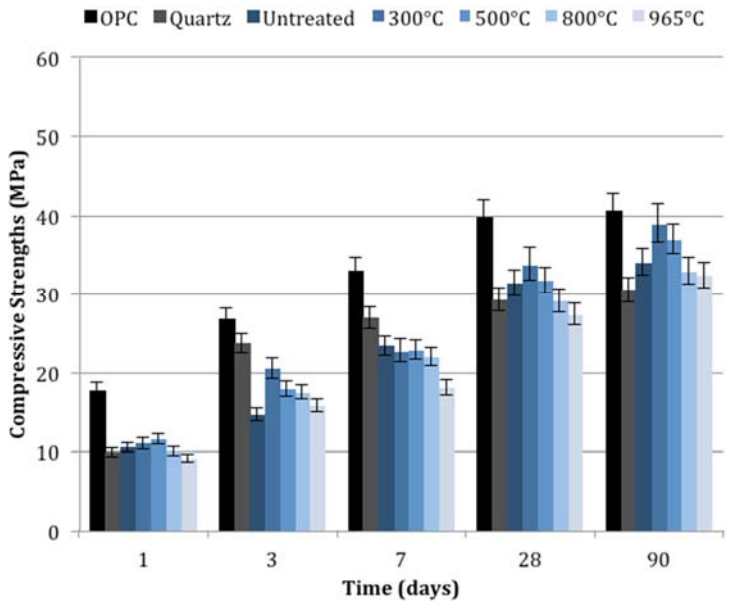

Figure 4.47 - Compressive strengths of untreated and calcined zeolite C

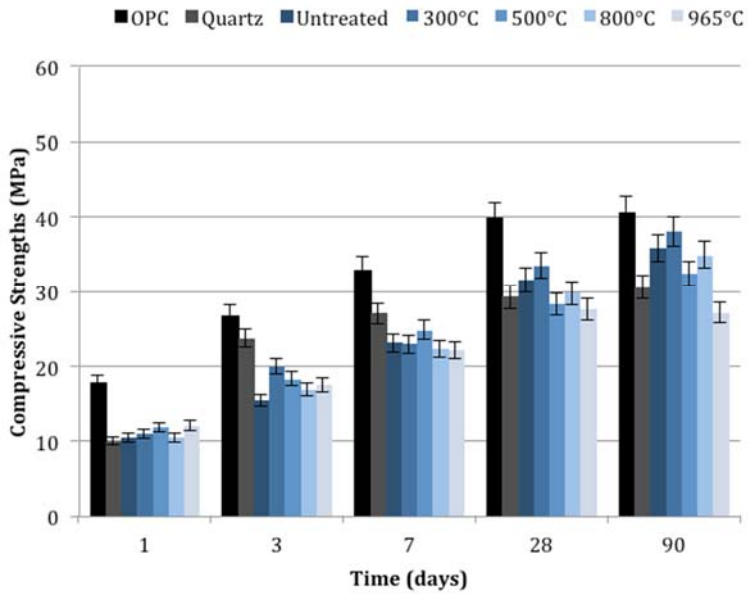

Figure 4.48 - Compressive strengths of untreated and calcined zeolite A

4.3.3 Influence of Calcined Zeolites on Cement Hydration

The effects of calcined zeolites on the early age hydration behavior of cement paste are shown in Figure 4.49 to 4.72. The results varied considerably between the different zeolites. Use of untreated zeolite Z and zeolite Z calcined to 300°C, 500°C, and

800°C, shown in Figure 4.49 to 4.52 and Table 4.8, drastically reduced the time to the start of the acceleration period as well as the time to the maximum rate of heat evolution compared to the cement-only paste, likely because the very fine zeolite particles served as nucleation sites for C-S-H precipitation. Zeolite Z calcined to 965°C did not show this effect, however, with this sample having a time to the start of acceleration similar to the cement-only paste. Use of untreated zeolite Z and zeolite Z calcined to 300°C, 500°C, and 800°C in the cement paste also resulted in greater magnitude, and earlier, heat releases from calcium aluminate hydration than in the cement-only paste, as evidenced by the increasing second peak heights of Figure 4.49. Use of zeolite Z calcined to 300°C lowered the maximum rate of heat evolution, but use of zeolite Z calcined at 500 and 800°C did not seem to affect the maximum rate of heat evolution in the system compared to the cement-only paste. Despite the initially lower time to the start of the acceleration period in the mixtures containing untreated zeolite Z or zeolite Z calcined to 300, 500 or 800°C, the rate of reaction during the acceleration period, described by the slope during that period, was lower for all of the untreated and calcined mixtures, with the exception of the 965°C zeolite paste. The earlier start of the acceleration compensated for lower reaction rates during the acceleration period and total heat released at 72 hours was similar for the cement-only paste and pastes using untreated zeolite Z and zeolite Z calcined to 500°C and 800°C. Only mixtures using zeolite Z calcined to 300°C evolved less total heat over 72 hours. Calcination of zeolite Z at 965°C eliminated the accelerating effects seen with zeolite Z calcined to 300°C, 500°C, and 800°C; however, it resulted in an increased maximum rate of heat release for that sample. In addition, use of zeolite Z calcined at 965°C lengthened the total time of the deceleration period of the zeolite-

cement paste relative to the cement-only paste and the other zeolite Z-cement pastes, an effect similar to the quartz filler-cement paste and other pastes containing filler materials due to the dilution effect demonstrated by other researchers (Lothenbach et al. 2011; Oey et al. 2013a).

Figure 4.52 to 4.56 and Table 4.9 illustrate the effect of zeolite B on early age cement hydration. Although none of the zeolite B mixtures affected the timing of the start of the acceleration period and the time to the peak rate of heat release, use of untreated zeolite B and zeolite B calcined at 300°C and 500°C reduced the maximum rate of heat release of the pastes and, additionally, decreased the rate of reaction during the acceleration period compared to the cement-only paste. Calcination at temperatures of 800 and 965°C moderated the reductions in the magnitude of the maximum rate of heat release seen with the untreated zeolite B and zeolite B calcined at 300°C and 500°, resulting in cement hydration curves similar to the cement-only paste. Similar to zeolite Z, calcination of zeolite B increased the magnitude and decreased the time to the start of the calcium aluminate reactions, although this effect was much less pronounced for zeolite B compared to zeolite Z. The total heat evolved for all of the zeolite B mixtures was greater at 72 days than for the reference cement-only paste, although lower than the total cumulative heat evolved by the quartz filler paste.

The effect of calcination on zeolite L is shown in Figure 4.57 to 4.60 and Table 4.10. Calcination of zeolite L at temperatures of 300 to 800°C did not change the time to the start of the acceleration, nor the time to the maximum rate of heat release by the pastes, although all pastes containing untreated or zeolite L calcined to 800°C or less significantly reduced the maximum rate of heat evolution at the peak compared to the

OPC paste and reduced the rate of reaction during the acceleration period. Both effects are likely the result of the much greater particle size of the zeolite L compared to the cement (Table 4.4). Calcination at 965°C greatly increased the maximum rate of heat release of the zeolite L-cement paste, generating more heat at its peak than the cement-only paste. Additionally, the 965°C zeolite-cement paste mixture sustained greater rates of heat evolution than the cement-only paste for approximately 30 hours after mixing. The cumulative heat evolved for the untreated zeolite L and zeolite L mixtures calcined at 300, 500 or 800°C was less at 72 hours than the amount of heat evolved for the cement-only paste, while the heat evolved by the 965°C zeolite L mixture mimicked very closely the amount of heat evolved for the quartz filler mixture.

Use of uncalcined zeolite T, shown in Figure 4.61 to 4.64 and Table 4.11, resulted in a slightly reduced maximum rate of heat release compared to the cement-only paste, although untreated zeolite T did also slightly reduce the time to the start of acceleration as well as the time to the maximum rate of heat release. Calcination of zeolite T at 300°C increased maximum rate of heat release to a slightly higher magnitude than that of the cement-only paste. Mixtures using untreated zeolite T and zeolite T calcined to 300°C also had similar reaction rates during the acceleration period to the cement-only paste. However, higher calcination temperatures reduced the rate of reaction in the acceleration period as well as the maximum rate of heat release, with the maximum rate of heat release for the paste using zeolite T calcined at 800°C being 25% lower than both the paste using zeolite T calcined at 300°C and the cement-only paste. The total amount of heat evolved over 72 hours was also lower for all of the zeolite mixtures except the 965°C zeolite. Similar to the zeolite Z and B systems, heating the zeolite to 965°C

increased the maximum rate of heat evolved by the system to levels greater than the cement-only paste. This reaction was also sustained longer than in the cement-only pastes, with increased rates of heat release continuing until approximately 22 hours after mixing and resulting in greater total heat evolved over the 72 hour testing period compared to the cement-only paste, although the amount of heat evolved was significantly lower than for the quartz filler mixture.

Zeolite C accelerated the hydration of all zeolite-cement mixtures, shown in Figure 4.65 to 4.68 and Table 4.12**,** regardless of the temperature of calcination. Use of the untreated zeolite C and zeolite C calcined at 300 and 500°C reduced the time to maximum rate of heat release of the paste. The 300, 800 and 965°C zeolite C samples increased the rate of reactions during the acceleration period and slightly increased the maximum rate of heat release. The total amount of heat evolved for the zeolite C mixtures was greater at 72 hours than the amount of heat evolved by the cement-only pastes, although less than the quartz filler mixture. Unlike previous samples, calcination did not appear to increase the magnitude of the C_3A peak for zeolite C pastes.

Zeolite-cement systems using zeolite A, shown in Figure 4.69 to 4.72 and Table 4.13, had reduced maximum rates of heat release compared to the cement-only paste, a condition which was only exacerbated by calcination. Maximum rate of heat release of the mixtures was inversely correlated with higher calcination temperatures, with the uncalcined zeolite system releasing the greatest amount of heat and the zeolite calcined at 965°C releasing the least. Similarly, the rate of reaction during the acceleration period was reduced for all zeolite A-cement pastes compared to the cement-only paste. Calcination also retarded both the time to the start of the acceleration period and the time

to the maximum rate of heat release. The cumulative heat evolution of the untreated and calcined zeolite-A-cement pastes at 72 hours was similar to that of the cement-only paste and significantly lower than that of the quartz filler paste.

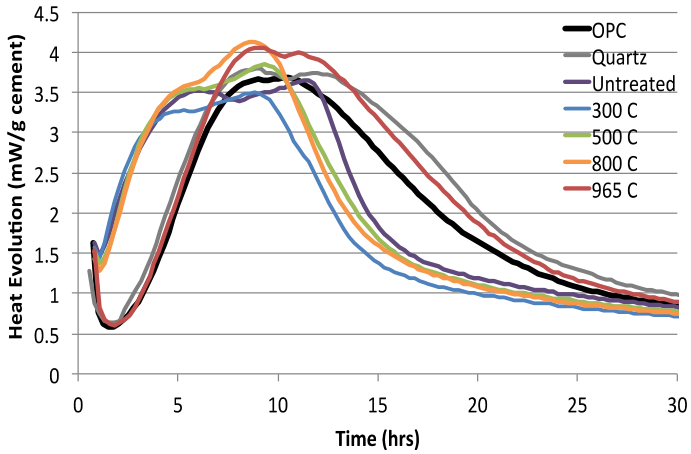

Figure 4.49 – Isothermal calorimetry (23°C) results of pastes with 80-100% cement and 0-20% untreated or calcined zeolite Z (w/cm = 0.4)

Table 4.8 - Acceleration period slope in isothermal calorimetry (23°C) of pastes with 80-100% cement and 0-20%untreated or calcined zeolite Z or quartz filler (w/cm = 0.4)

SCM/Filler	Acceleration Period Slope (mW/g/hr)
None	0.69±0.05
Quartz filler	0.64±0.03
Untreated zeolite Z	0.44±0.03
300°C zeolite Z	0.48±0.09
500°C zeolite Z	0.60±0.04
800°C zeolite Z	0.52±0.11
965°C zeolite Z	0.73±0.21

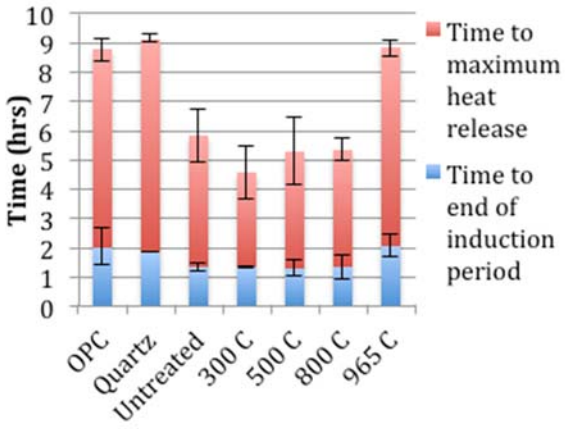

Figure 4.50 - Time to the end of the induction period and time to the maximum value of heat flow in isothermal calorimetry (23°C) of pastes with 90-100% cement and 0-20% untreated or calcined zeolite Z or quartz filler (w/cm = 0.4)

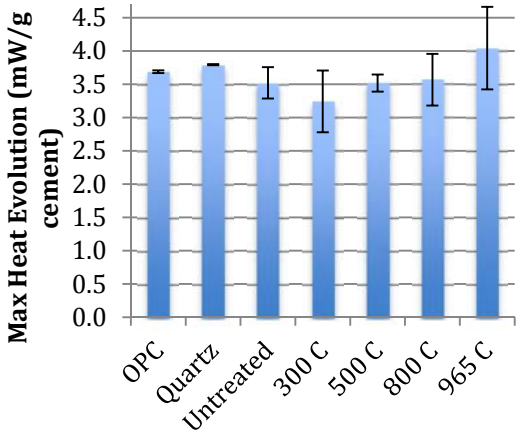

Figure 4.51 - Value of the maximum heat flow in isothermal calorimetry (23°C) of pastes with 80-100% cement and 0-20% untreated or calcined zeolite Z or quartz (w/cm = 0.4)

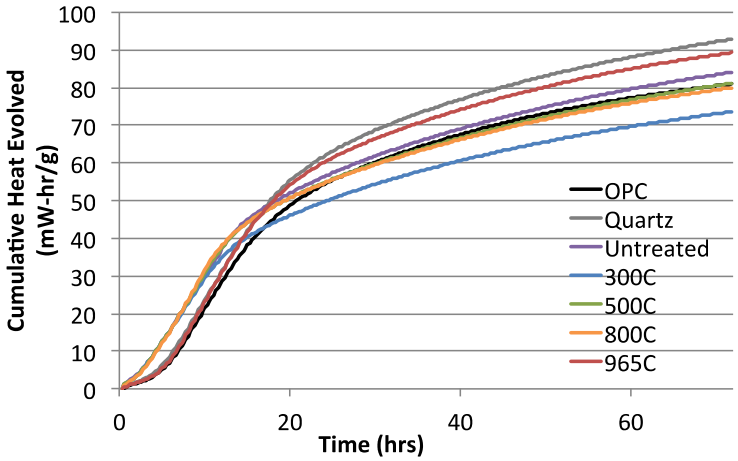

Figure 4.52 - Cumulative heat evolved over 72 hours during isothermal calorimetry (23°C) of 80-100% cement and 0-20% untreated or calcined zeolite Z or quartz filler pastes (w/cm = 0.4)

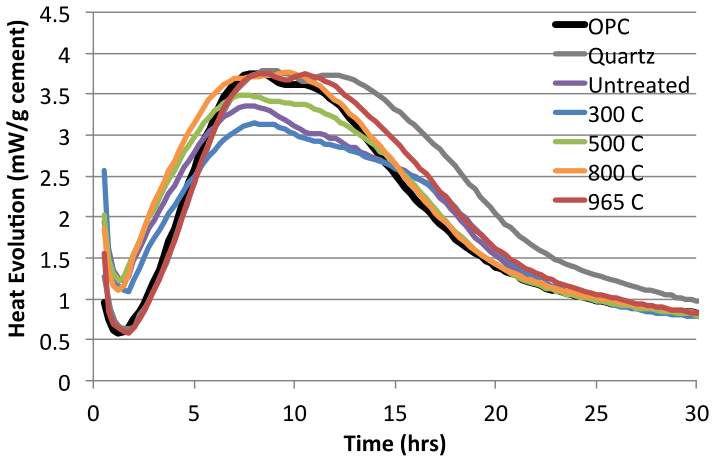

Figure 4.53 - Isothermal calorimetry (23°C) results of pastes with 80-100% cement and 0-20% untreated or calcined zeolite B (w/cm = 0.4)

Table 4.9 - Acceleration period slope in isothermal calorimetry (23°C) of pastes with 80-100% cement and 0-20%untreated or calcined zeolite B or quartz filler (w/cm = 0.4)

SCM/Filler	Acceleration period slope (mW/g/hr)
None	0.71±0.05
Quartz filler	0.58±0.03
Untreated zeolite	0.38±0.01
300°C zeolite B	0.31±0.06
500°C zeolite B	0.38±0.01
800°C zeolite B	0.48±0.04
965°C zeolite B	0.72±0.01

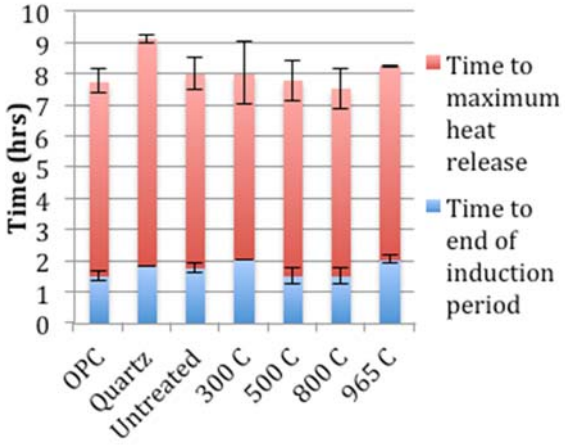

Figure 4.54 - Time to the end of the induction period and time to the maximum value of heat flow in isothermal calorimetry (23°C) of pastes with 80-100% cement and 0-20% untreated or calcined zeolite B or quartz (w/cm = 0.4)

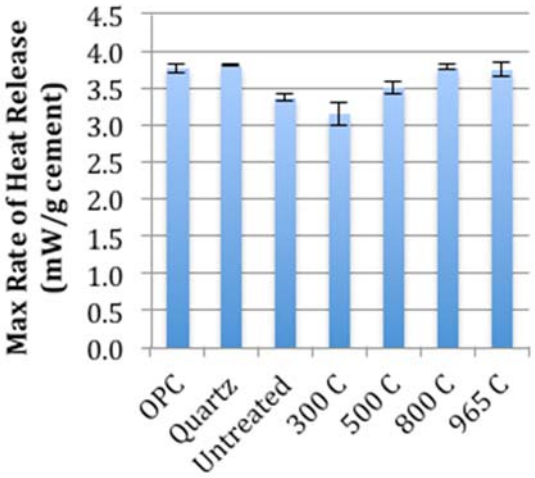

Figure 4.55 - Value of the maximum heat flow in isothermal calorimetry (23°C) of pastes with 80-100% cement and 0-20% untreated or calcined zeolite B or quartz (w/cm = 0.4)

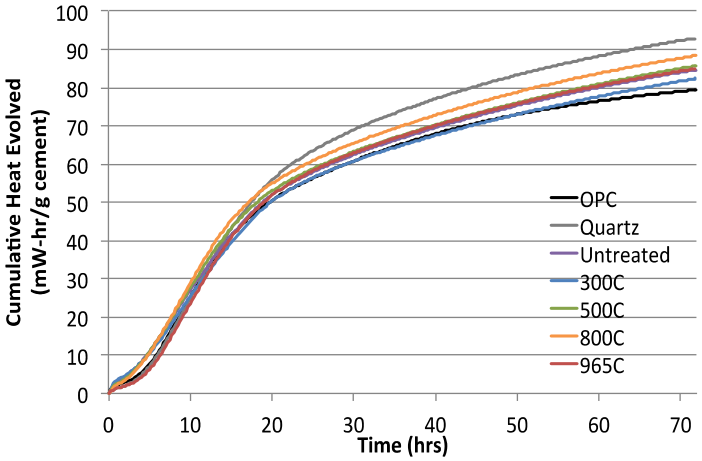

Figure 4.56 - Cumulative heat evolved over 72 hours during isothermal calorimetry (23°C) of 80-100% cement and 0-20% untreated or calcined zeolite B or quartz filler pastes (w/cm = 0.4)

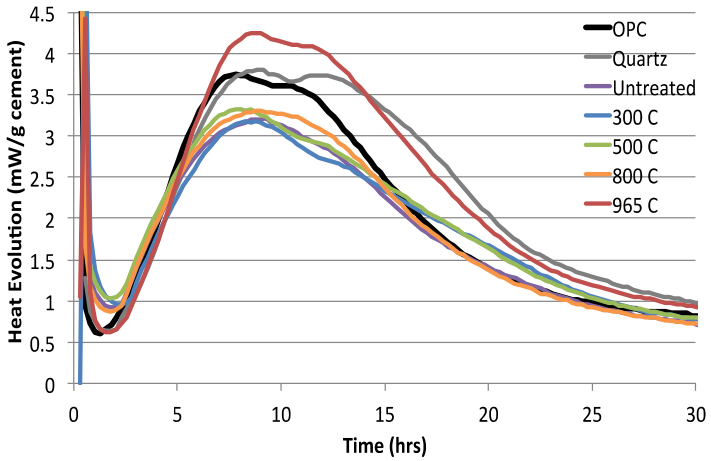

Figure 4.57 - Isothermal calorimetry (23°C) results of pastes with 80-100% cement and 0-20% untreated or calcined zeolite L or quartz filler (w/cm = 0.4)

Table 4.10 - Acceleration period slope in isothermal calorimetry (23°C) of pastes with 80-100% cement and 0-20%untreated or calcined zeolite L or quartz filler (w/cm = 0.4)

SCM/Filler	Acceleration period slope (mW/g/hr)
None	0.74±0.05
Quartz filler	0.64±0.03
Untreated zeolite L	0.36±0.01
300°C zeolite L	0.45±0.01
500°C zeolite L	0.42±0.03
800°C zeolite L	0.44±0.08
965°C zeolite L	0.79±0.14

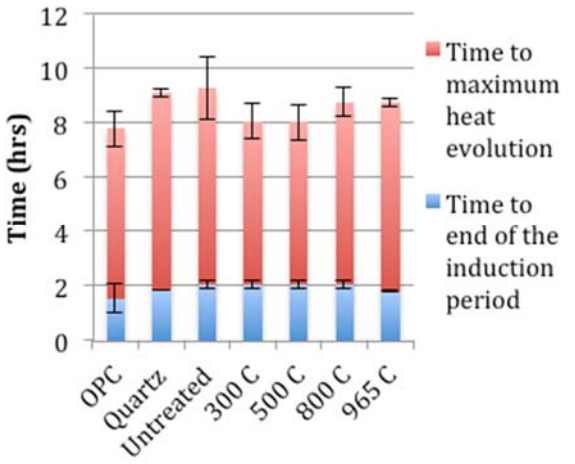

Figure 4.58 - Time to the end of the induction period and time to the maximum value of heat flow in isothermal calorimetry (23°C) of pastes with 80-100% cement and 0-20% untreated or calcined zeolite L or quartz (w/cm = 0.4)

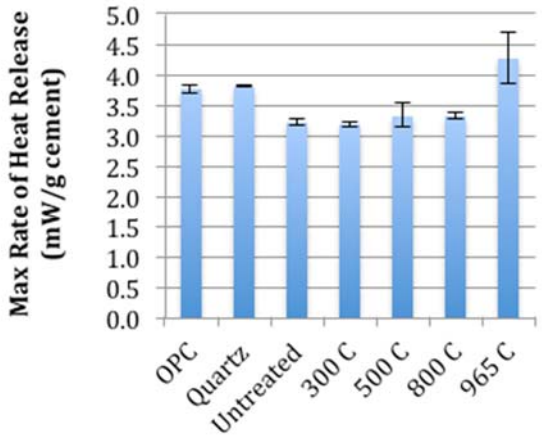

Figure 4.59 - Value of the maximum heat flow in isothermal calorimetry (23°C) of pastes with 80-100% cement and 0-20% untreated or calcined zeolite L or quart filler (w/cm = 0.4)

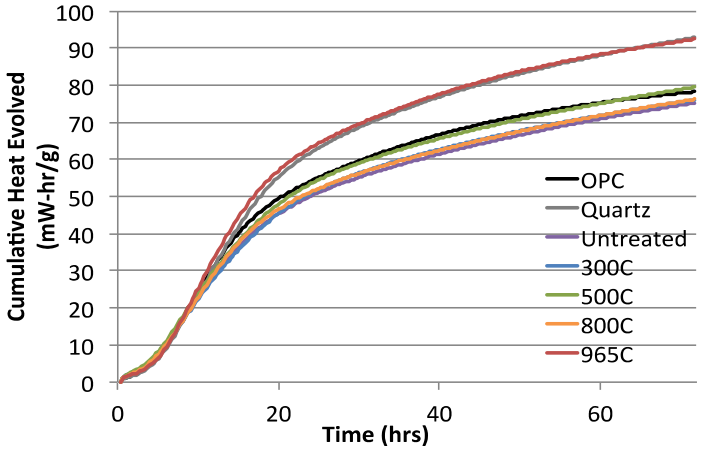

Figure 4.60 - Cumulative heat evolved over 72 hours during isothermal calorimetry (23°C) of 80-100% cement and 0-20% untreated or calcined zeolite L or quartz filler pastes (w/cm = 0.4)

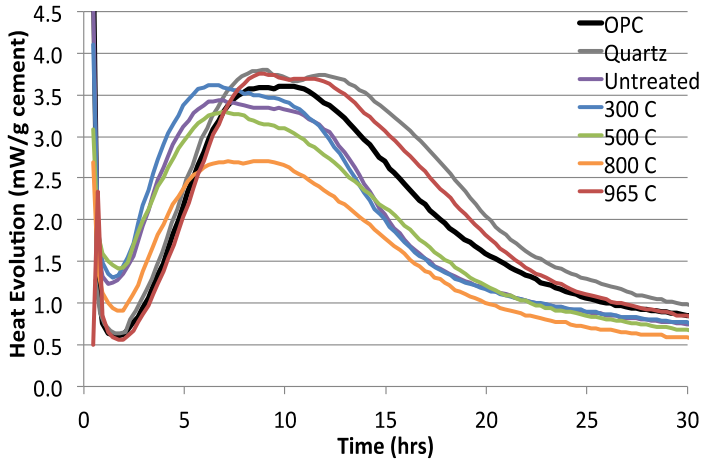

Figure 4.61 - Isothermal calorimetry (23°C) results of pastes with 80-100% cement and 0-20% untreated or calcined zeolite T (w/cm = 0.4)

Table 4.11 – Acceleration period slope in isothermal calorimetry (23°C) of pastes with 80-100% cement and 0-20%untreated or calcined zeolite T or quartz filler (w/cm = 0.4)

SCM/Filler	Acceleration period slope (mW/g/hr)
None	0.68±0.05
Quartz filler	0.64±0.03
Untreated zeolite T	0.60±0.11
300°C zeolite T	0.63±0.05
500°C zeolite T	0.48±0.05
800°C zeolite T	0.45±0.03
965°C zeolite T	0.68±0.03

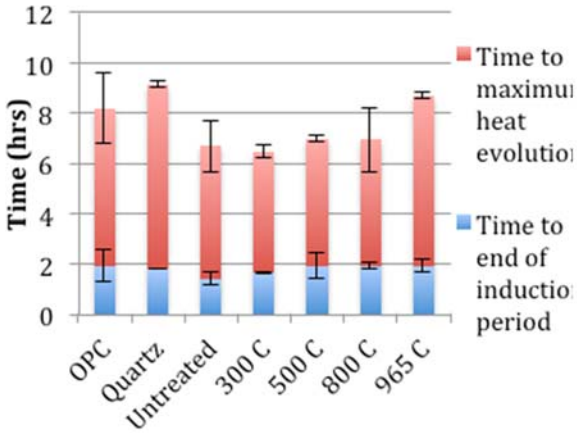

Figure 4.62 - Time to the end of the induction period and time to the maximum value of heat flow in isothermal calorimetry (23°C) of pastes with 80-100% cement and 0-20% untreated or calcined zeolite T or quartz (w/cm = 0.4)

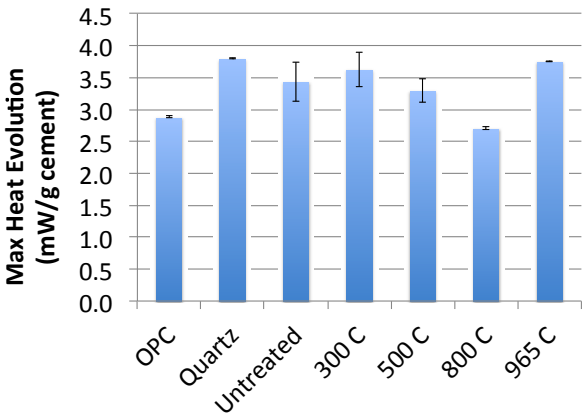

Figure 4.63 - Value of the maximum heat flow in isothermal calorimetry (23°C) of pastes with 80-100% cement and 0-20% untreated or calcined zeolite T or quartz filler (w/cm = 0.4)

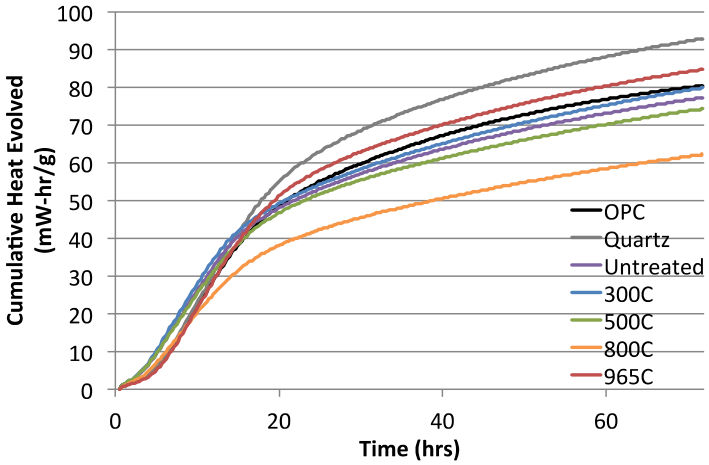

Figure 4.64 - Cumulative heat evolved over 72 hours during isothermal calorimetry (23°C) of 80-100% cement and 0-20% untreated or calcined zeolite T or quartz filler pastes (w/cm = 0.4)

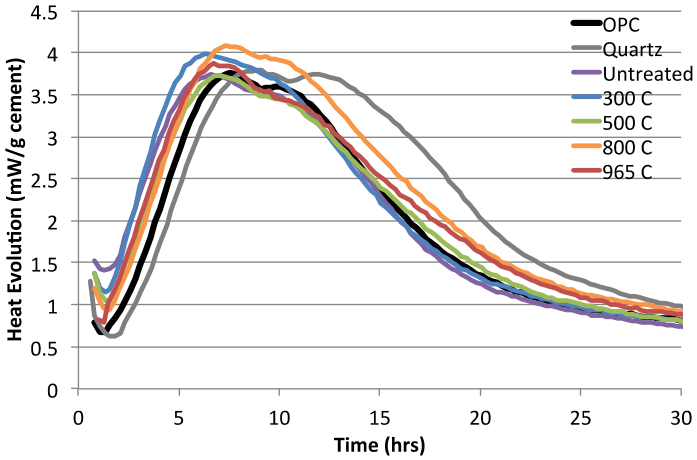

Figure 4.65 - Isothermal calorimetry (23°C) results of pastes with 80-100% cement and 0-20% untreated or calcined zeolite C (w/cm = 0.4)

Table 4.12 - Heat evolution data for the cement, untreated and calcined zeolite C-cement pastes

SCM/Filler	Acceleration period slope (mW/g/hr)
None	0.70±0.05
Quartz filler	0.64±0.03
Untreated zeolite C	0.61±0.01
300°C zeolite C	0.88±0.11
500°C zeolite C	0.68±0.04
800°C zeolite C	0.75±0.03
965°C zeolite C	0.75±0.01

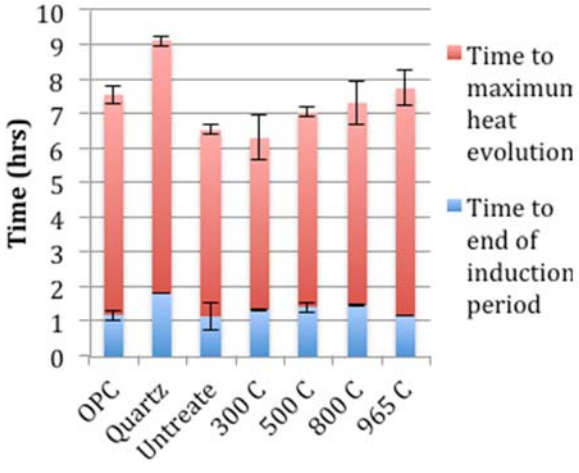

Figure 4.66 - Time to the end of the induction period and time to maximum value of heat flow in isothermal calorimetry (23°C) of pastes with 80-100% cement and 0-20% untreated or calcined zeolite C or quartz filler (w/cm = 0.4)

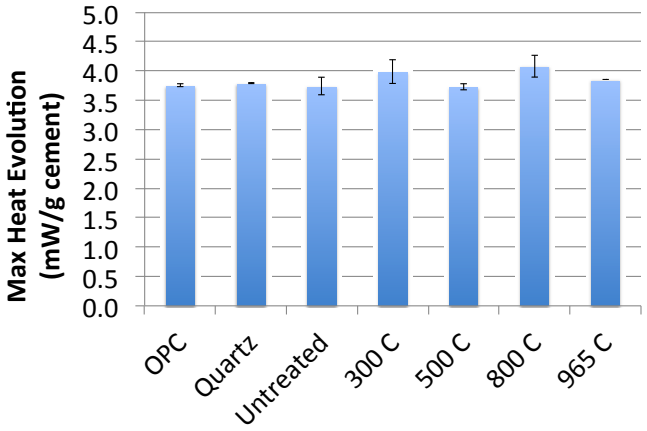

Figure 4.67 - Value of the maximum heat flow in isothermal calorimetry (23°C) of pastes with 80-100% cement and 0-20% untreated or calcined zeolite C (w/cm = 0.4)

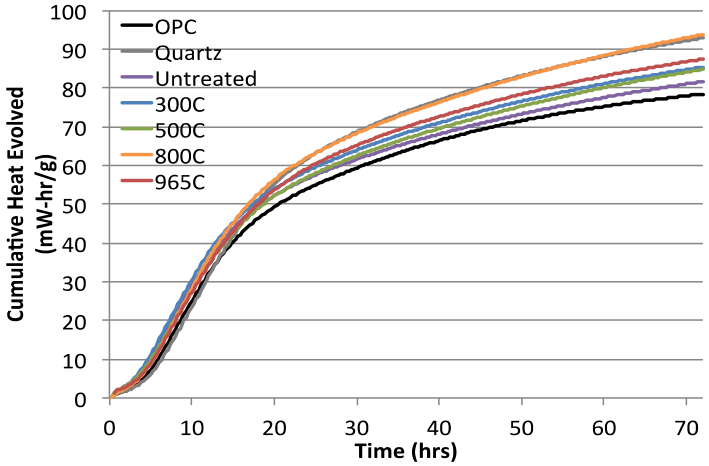

Figure 4.68 - Cumulative heat evolved over 72 hours during isothermal calorimetry (23°C) of 80-100% cement and 0-20% untreated or calcined zeolite C or quartz filler pastes (w/cm = 0.4)

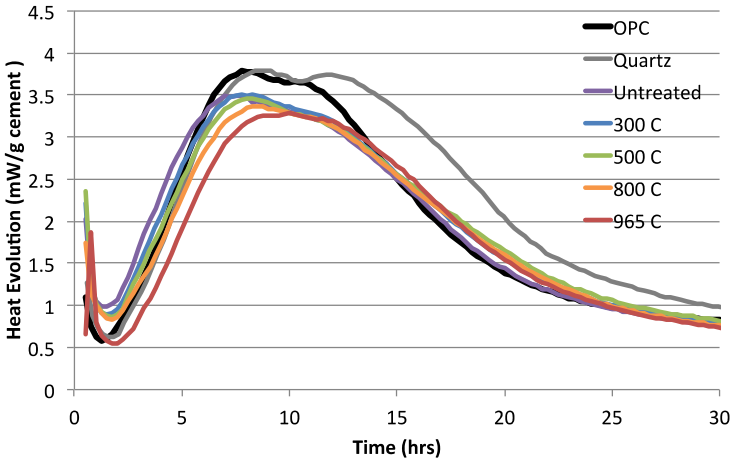

Figure 4.69 - Isothermal calorimetry results (23°C) of pastes with 80-100% cement and 0-20% untreated or calcined zeolite A (w/cm = 0.4)

Table 4.13 - Heat evolution data for the cement, untreated and calcined zeolite A-cement pastes

SCM/Filler	Acceleration period slope (mW/g/hr)
None	0.73±0.05
Quartz filler	0.64±0.03
Untreated zeolite A	0.62±0.05
300°C zeolite A	0.56±0.02
500°C zeolite A	0.58±0.02
800°C zeolite A	0.57±0.08
965°C zeolite A	0.47±0.04

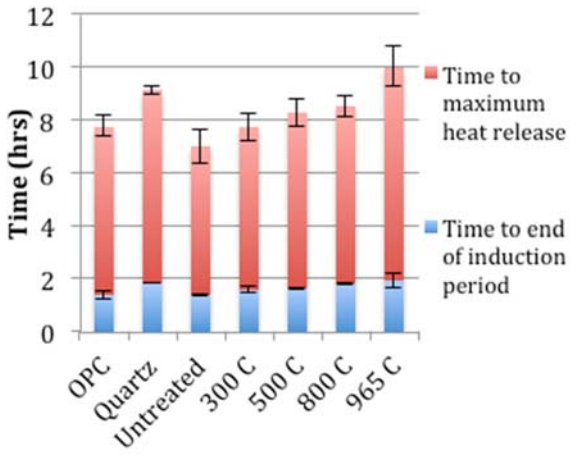

Figure 4.70 - Time to the end of the induction period and time to the maximum value of heat flow in isothermal calorimetry (23°C) of pastes with 80-100% cement and 0-20% untreated of calcined zeolite A or quartz filler (w/cm = 0.4)

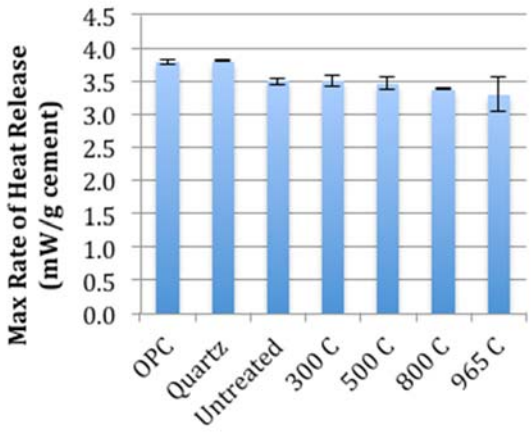

Figure 4.71 – Value of the maximum heat flow in isothermal calorimetry (23°C) of pastes with 80-100% cement and 0-20% untreated or calcined zeolite A or quartz filler (w/cm = 0.4)

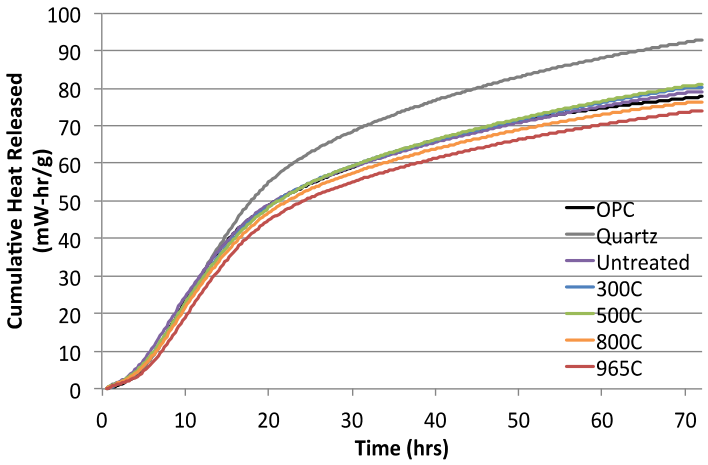

Figure 4.72 - Cumulative heat evolved over 72 hours during isothermal calorimetry (23°C) of 80-100% cement and 0-20% untreated or calcined zeolite A or quartz filler pastes (w/cm = 0.4)

4.4 Discussion of the Effects of Calcination on Pozzolanic Reactivity of Zeolites

The goal of the calcination pretreatment was to improve the physical and compositional properties of the zeolite to allow it to react faster or more completely as a pozzolan, resulting in improved performance in cementitious systems. It was hoped that calcination would result in a loss of zeolite crystallinity, creating a greater quantity of more reactive amorphous material and eliminating crystalline impurities. The literature suggests that the zeolite crystal structure becomes destabilized after calcination at 300°C (Perraki et al. 2005; Fernández, Vigil de la Villa, Garcia et al. 2011). While XRD analysis did show a reduction in both the zeolite crystallinity and in some crystalline impurities, these reductions did not begin until temperatures greater than 300°C, and some impurities, for example cristobalite, were never eliminated at the calcination temperatures used in this study. It can be concluded that temperatures higher than 300°C are needed to reduce crystallinity in zeolites. However, interestingly, almost complete

elimination of crystalline phases, such as occurred in some samples after heating to 965°C, did not necessarily result in a more reactive zeolite.

In addition to changing the structure of the crystalline phases in the material, calcination also impacted zeolite surface area and porosity. Four of the six zeolites showed an inverse correlation between temperature and surface area, with calcination at higher temperatures resulting in significant reductions in nitrogen-available specific surface area. Similar phenomena were reported by Ates and Hardacre (2012). The pore size distribution data in Figure 4.7 to 4.18 show that calcination initially resulted in the filling, closing, or elimination of the small, ~2-7 nm, pores with little effect on pores greater than 7 nm in size. Elimination of the smallest pores occurred at temperatures lower than 500°C for some zeolites, including zeolites L and A, while others required higher calcination temperatures to eliminate small porosity. All zeolites, except zeolite Z, had significantly fewer 7-50 nm pores after calcination at 800°C compared to the uncalcined material. After elimination of the small pores, the majority of pore volume for all of the zeolites hovered around 10 nm, and did not seem to be affected by calcination up to 800°C. After calcination at 965°C the total pore volume of all the zeolites was significantly reduced, explaining the significant drop in nitrogen-available specific surface areas from the 800°C samples to the 965°C samples for zeolites Z, B, L and T. Two zeolites, zeolites C and A, had large drops in surface area after calcination at 800°C. These zeolites also showed a significant reduction in overall pore volume between 500 and 800°C. As these two zeolites also showed reductions in internal surface area with calcination, it is likely that the solid material in the zeolites densified with exposure to

increased temperatures, resulting in closing the smallest nitrogen-accessible pores, and reductions in nitrogen available specific surface area.

The reduction in surface area with calcination was coupled with an increase in particle size, as shown in Figure 4.7 to Figure 4.24. This is likely due to agglomeration of particles through sintering at higher temperatures (Elaipolous et al. 2010, Ates and Hardacre 2012), an effect that also occurs in clay samples (Fernández, Vigil de la Villa, Garcia et al. 2011). This effect is confirmed qualitatively in the SEM images of the untreated and calcined zeolites in Figure 4.25 to 4.30. Images of all zeolites calcined at 965°C show a proliferation of small particles on the surface of larger zeolite particles. The only exception to the general particle size increase with increasing temperature was for the zeolite with the largest particle sizes, zeolite L. For zeolite L, particles became smaller with calcination, likely due to internal pressures from moisture attempting to quickly diffuse through the zeolite to evaporate. Other researchers have shown that zeolitic water loss, such as this, can occur up to 750°C (Duvarcı et al. 2007).

Several conclusions can be drawn from the tests on pozzolanic reactivity through measurement of hydrated paste calcium hydroxide content. First, the zeolite is reacting pozzolanically in the zeolite-cementitious systems, as the calcium hydroxide content of each system is reduced compared to the cement-only pastes and the cement-quartz pastes, although the magnitude of the reduction varies considerably depending on the zeolite used. Secondly, the pozzolanic reaction appears to have been completed before 28 days. Few instances were observed where the 90-day paste calcium hydroxide content was less than that of the 28-day paste and also outside of the error range for that sample. Third,

calcination up to 800°C does not seem to significantly affect the consumption of calcium hydroxide by the zeolite. Variations do occur from sample to sample; however, in most cases all the results for each zeolite set are within the error limits of one another. Therefore, it can be concluded that reductions in crystallinity resulting from calcination at 800°C do not result in increased pozzolanicity. Lastly, calcination at 965°C resulted in smaller reductions in the calcium hydroxide content of all pastes relative to the pastes containing untreated zeolites or zeolites calcined at lower temperatures. In many cases the calcium hydroxide contents of the pastes containing zeolites calcined at 965°C were higher than the calcium hydroxide contents of the cement-only pastes. This effect is likely an amalgamation of several factors. First, the surface area of the 965°C particles was significantly reduced and the particle size increased as particles agglomerated and became sintered together at high temperatures. Second, other tests, including compressive strength tests discussed in section 4.3.2.3 and isothermal calorimetry testing discussed in section 4.3.3 shown evidence that the zeolite calcined to 965°C may be acting similarly to an inert filler. Fillers promote increased formation of calcium hydroxide because of increased free space available in the mixture (Lothenbach et al. 2011). The calcium hydroxide pastes using zeolites calcined to 965°C showed similarly increased calcium hydroxide content, shown in Figure 4.31 to 4.36. However, the calcium hydroxide content of the 965°C zeolites was less than the magnitude of calcium hydroxide present in the quartz filler pastes, suggesting that the zeolite calcined to 965°C was not completely inert.

The majority of the results of reactivity testing using the Chapelle test were inconclusive due to the large error ranges experienced with many of the zeolite samples. Even for samples showing results that were not equal, within error, the differences between the quantity of CaO consumed for each uncalcined and calcined zeolite set were extremely small. The quantity of CaO consumed by the zeolites was, however, similar to results shown by other researchers, who also had difficulties relating the results of the Chapelle test to other methods of determining pozzolanic reactivity of zeolites (Perraki et al. 2005). The exception to this is the results of the Chapelle test for the zeolites calcined to 965°C. A large difference was seen, in Figure 4.37 to 4.42, between the untreated zeolites and zeolites calcined to ≤800°C and the zeolites calcined to 965°C. For the 965°C samples the Chapelle test did an excellent result predicting the reduced pozzolanic reactivity of the zeolite, confirmed by compressive strength and isothermal calorimetry testing, discussed in sections 4.3.2.3 and 4.3.3.

Results of the compressive strength testing were extremely varied, but despite this, several trends were apparent. First, particle size plays a significant role in the compressive strength results, with the smaller particle size zeolites, Z and B, generating samples with much higher average strengths. However, increasing particle size does not seem to have an effect once particles are larger than 45 μm, as the strengths of mortars containing zeolite L were similar to those of zeolites T, C and A, despite that zeolite L has a much larger particle size. Second, in all cases, calcination at 965°C was unsuccessful in increasing compressive strengths. The samples containing zeolites calcined at 965°C performed very similarly to the samples containing the quartz filler,

likely because these materials have become inert, a fact also supported by the calcium hydroxide and Chapelle testing as well as the effect of the 965°C zeolites on heat evolution in isothermal calorimetry testing. It is interesting to note that several of the zeolites calcined at 500°C performed very similarly to the 965°C samples. Based on their crystalline phase composition, surface area and particle size, samples using 500°C zeolites should have performed similar to the 300°C or 800°C samples. It is unclear why the zeolites calcined to 500°C had such poor performance and this could be the subject of future research. It can be seen from the compressive strength results that, although increases in particle size and decreases in surface area of most of the zeolites would suggest that calcination would be unsuccessful as a pretreatment method, many of the samples calcined to 300°C achieved greater strengths than their untreated counterparts, perhaps due to destabilization of the crystal structure postulated by other researchers (Perraki et al. 2005; Fernández, Vigil de la Villa, Garcia et al. 2011).

In general, incorporation of zeolite resulted in acceleration of hydration reactions, but also often resulted, after initial nucleation of the precipitation of hydration products, in interference in the cement hydration process, evidenced by often lower peak magnitudes of heat release. Despite this, most mixtures containing both untreated zeolite and zeolites calcined up to 800°C resulted in similar cumulative heat released at 72 hours to the cement-only paste. Total heat evolution of mixtures incorporating zeolites calcined to 965°C was often significantly greater than both the cement-only paste and mixtures containing the same form of zeolite treated at different temperatures, or not at all. This is a trend also exhibited by filler materials, which provide more space for the growth of

hydration products and so tend to extend the magnitude of hydration during the first 72 hours (Cyr et al. 2006; Oey et al. 2013a; Rus et al. 2000). However, many of the 965°C mixtures produced less cumulative heat than the quartz filler mixture, which may suggest that the increased hydration due to the filler effect was offset by the hindrance of cement hydration reactions by the zeolite.

4.5 CONCLUSIONS

Natural zeolites were calcined to 300, 500, 800 and 965°C and were characterized to determine the changes to zeolite crystallinity, particle size, surface area and porosity with calcination. Performance was measured by tracking reductions in calcium hydroxide in zeolite-cement pastes and the compressive strengths of zeolite-cement mortars. The effect of calcination on early age cement hydration was also investigated using isothermal calorimetry.

In general, calcination of zeolites increased particle size, eliminated fine materials, filled porosity, and decreased surface area. All of these effects correlate to lower reactivity of materials used in cementitious systems (Costa and Massazza 1974; Cyr et al. 2005; Lawrence et al. 2003). However, calcination did reduce zeolite crystallinity and eliminated most system impurities, although a pozzolanically inert form of SiO_2 – cristobalite, was not eliminated by calcination. Zeolites effectively reduced calcium hydroxide in cementitious systems. However, calcination did not improve zeolite pozzolanic potential and, in the case of calcination at 965°C, it reduced the material's ability to participate in the pozzolanic reaction. Calcination of zeolites at 300°C increased the compressive strength of zeolite-cement mortars, but calcination at 500°C or 965°C

led to lower strengths relative to cement-only and untreated zeolite mortars. Overall calcination was an ineffective measure for increasing the reactivity of zeolites for use as supplementary cementitious materials.

Chapter 5: Zeolite Pretreatment Methods to Increase the Reactivity of Zeolites for Use as SCMs – Acid Treatment

5.1 INTRODUCTION

No work has been published in the literature to determine the effect of acid pretreatment on the reactivity of zeolites used as SCMs. However, previous studies have shown that acid treatment improves some zeolite properties that can be linked to better SCM performance, especially increases in the SiO_2/Al_2O_3 ratio (Elaiopoulos et al. 2010; Matias et al. 2009; Salvestrini et al. 2010; Unveren et al. 2005; Wang and Peng 2010), reductions in zeolite crystallinity (Cakicioglu-Ozkan and Ulku 2005; Elaiopoulos et al. 2010; Unveren et al. 2005), removal of system impurities (Ates and Hardacre 2012) and increases in specific surface area (Salvestrini et al. 2010).

Many studies have investigated the effects of acid on the physical and chemical properties of zeolites. Treatment with 0.1-6M HCl and 4M HNO_3 resulted in changes to the structure of zeolites, increasing the SiO_2/Al_2O_3 ratio of the zeolites (Elaiopoulos et al. 2010, Matias et al. 2009, Salvestrini et al. 2010, Wang and Peng 2010). Higher SiO_2/Al_2O_3 ratio could increase the pozzolanic reactivity of the zeolites (Blanco Varela et al. 2006; Snellings et al. 2010). Increase in the SiO_2/Al_2O_3 ratio of the zeolite is accomplished through removal of the aluminum ions from the structure as they complex strongly with the acid's conjugate base ion (Beers et al. 2003). Greater dealumination occurs with greater concentrations of acid and longer treatment times (Matias et al. 2009). Increases in the SiO_2/Al_2O_3 ratio with acid treatment can be very significant, with Beers et al. (2003) observing increases of nearly 400% (13 to 51) after treatment for 2

hours with oxalic acid. However, these large increases may not be applicable for all types of acids used in treatments, as they are linked to the complexation ability of each acid's conjugate base.

Several studies have found that acid treatment with 1-4M HNO_3 and 0.1-6M HCl resulted in structural degradation, dissolution and phase transformations of the zeolite (Klieve and Semmens 1980; Matias et al. 2009; Salvestrini et al. 2010), with higher acid concentrations resulting in more severe decomposition. Similarly, other researchers observed either an increase in amorphous content or a reduction in crystallinity of the zeolites (based on zeolite XRD peak heights) with treatment with HCl concentrations as low as 1M (Elaiopoulos et al. 2010, Unvernen et al. 2005, Cakiciogly-Ozkan and Ulku 2005). However, scanning electron microscopy and transmission electron microscopy imaging did not show evidence of crystalline structural collapse, even after treatment with very highly concentrated 6N HCl (Elaiopoulos et al. 2010, Beers et al. 2003).

Acid treatment has also been shown to reduce the presence of non-zeolitic phases in the samples, including dolomite, quartz, and feldspar phases (Ates and Hardacre 2012). Further, researchers demonstrated the effectiveness of removing Ca^{2+}, Mg^{2+}, Na^{+}, K^{+} and Fe^{3+} cations from the system through exchange with protons from the acid solution (Ates and Hardacre 2012, Wang and Peng 2010, Klieve and Semmens 1980). In these studies acid treatment was most effective in removing Ca^{2+} and Na^{+} from the system, but less effective in removing Fe^{3+} and K^{+} ions, which were hypothesized to be more strongly bound within the zeolite crystal structure (Ates and Hardacre 2012).

Increased specific surface area, greater micro- and mesoporosity of zeolites, and decreased average pore diameter were also all found to be linked to structural degradation due to removal of aluminum from the structure (Elaiopoulos et al. 2010, Ates and Hardacre 2012, Cakiciogly-Ozkan and Ulku 2005, Unvernen et al. 2005). One study even demonstrated the creation of new, larger, micropores after acid treatment with 1M HCl up to 6M HCl (Allen et al. 2009). Specific surface area was increased by up to 500% in some zeolite samples treated with 0.5M hydrochloric acid (Salvestrini 2010). Removal of amorphous phases and hydrated cations with acid treatment increased pore volume due to a reduction in the occurrence of blocked micropores (Elaiopoulos et al. 2010, Unvernen et al. 2005). Unfortunately, these increases also resulted in a reduced propensity for cation exchange, as acid treatment has also been found to partially dissolve silica tetrahedra and free linkages, destroying exchange sites (Cakiciogly-Ozkan and Ulku 2005).

The results of studies examining the effects of acid treatment on zeolite properties suggest that acid treatment can increase zeolite SiO_2/Al_2O_3 ratio and amorphous content, remove non-zeolite phases and cations from the sample, and significantly increase zeolite surface area and porosity. Such changes should produce increased pozzolanic reactivity of the zeolite and improve the performance of zeolite-cement mixtures using acid-treated zeolites (Ates and Hardacre 2012; Duvarcı et al. 2007; Johnson et al. 2003). However, none of the studies in the literature examining acid treatment on zeolites actually tested treated zeolites in cementitious systems. Therefore, the study presented in this chapter examined the effects of acid treatment on zeolite physical and chemical properties and

investigated the correlation between these properties and zeolite-cement mixture performance to determine whether acid treatment could be an effective process for increasing the reactivity of zeolites used as SCMs.

5.2 EXPERIMENTAL METHODS AND MATERIALS

5.2.1 Zeolite Sample Preparation

5.2.1.1 Acid Treatment Solutions

Three treatment solutions were chosen to test the effect of acid treatment on zeolite reactivity: hydrochloric acid (HCl), nitric acid (HNO_3), and acetic acid (HAc). ACS grade HCl was initially used for preliminary testing, and then the matrix was expanded to include nitric and acetic acid to study the effect of different acids and also to attempt to increase the feasibility of using acid treatment in the field. ACS grade nitric acid was chosen as an alternative strong acid to HCl, in order to avoid using an acid that could potentially leave behind Cl^- ions, which can contribute to corrosion of reinforcing steel in concrete (Ann and Song 2007; Glass and Buenfeld 1997; Hussain et al. 1995). A household grade acetic acid, Heinz All Natural Distilled White Vinegar, was used to determine if a weak acid could obtain similar effects seen with strong acids. The use of household vinegar was chosen because this acid would pose far fewer environmental and worker safety concerns than would the use of the other two strong acids, and if all three successfully increased zeolite reactivity, would be preferable and easier to use in the field.

Each acid treatment solution was prepared with three concentrations 0.1M, 0.5M, and 1M for the HCl and HNO_3 solution, and 0.1M, 0.5M and 0.87M (molarity of the

stock solution) for the acetic acid solution. The molar solutions for each acid were prepared from stock acid solutions (12.1M HCl, 15.8M HNO3, and 50 grain (0.87M) HAc), using ultrapure water (resistivity of 18 MΩ-cm) for dilution, in order to determine the effect of acid strength on zeolite changes. Exact molarities of each solution may have varied slightly from intended values due to impurities and in the stock acid solutions, but for the purposes of this research variations were assumed to be negligible.

5.2.1.2 Acid Treated Sample Preparation

To prepare acid-treated samples, 15g of zeolite T was ground to pass the #100 sieve and dried for at least 24 hours in a low vacuum desiccator. The zeolite was then added to a 0.1M, 0.5M or 1M solution of hydrochloric, nitric or acetic acid with 1g zeolite to 25mL of solution. The samples were continuously mixed on a U.S. Stoneware rotary mill for 24 hours. At 24 hours from sample-solution contact time the samples were centrifuged in a Beckman Coulter Avanti J-E centrifuge at 7500 rpm for 5 minutes. The liquid was decanted and saved for analysis. Each sample was washed with deionized water, centrifuged and decanted four additional times in order to prevent remove the acids' conjugate base ions and prevent their interference in future test results. The zeolites were dried for 24 hours at 60°C and then lightly ground to return the sample to powder form.

5.2.2 Zeolite Physical and Chemical Characterization Testing

Characterization testing was completed in order to determine what primary factors contributed to changes in zeolite reactivity in cementitious systems. Characterization

testing tracked changes from acid treatment in the phases present in the zeolite samples, as well as particle size, surface area and pore sizes, as discussed in Chapter 3.

Inductively coupled plasma spectrometry (ICP) was used to measure aluminum remaining in the acid solutions after treatment of the zeolite in order to help gauge the effectiveness of acid at dealumination of the zeolite structure. Iron remaining in solution after zeolite acid treatment was also measured using ICP to determine if changes in the zeolite's surface area with acid treatment could be due to removal of an iron oxide surface layer from the zeolite. Element concentrations present in the decant solutions reserved from zeolite acid treatment were analyzed using a Varian 710-ES Inductively Coupled Plasma-Optical Emission Spectrometer. The spectrometer was calibrated using seven standard solutions of 10 μg/L, 40 μg/L, 100 μg/L, 500 μg/L, 1 mg/L, 10 mg/L, 100 mg/L Fluka Analytical TraceCert aluminum and iron standards. A blank sample was created by soaking 0.5g of zeolite in 14ml of deionized water for 24 hours. After 24 hours the sample was filtered using P5 Qualitative grade Fisherbrand filter paper.

5.2.3 Acid Treatment Testing Methods: Reactivity Testing

Changes to zeolite pozzolanic reactivity after acid treatment were tracked through two methods of measuring the pozzolanic reaction: (1) measurement of the calcium hydroxide content of zeolite-cement pastes; and (2) through the Chapelle test, which measures the amount of calcium consumed by a sample in aqueous solution, as described in Chapter 3. All paste samples used the cement described in section 3.2.1. The calcium hydroxide content of hydrated cement-zeolite pastes was determined for pastes using untreated zeolites and zeolites treated with 0.1M, 0.5M, or 1M HCl, 0.1M, 0.5M, or 1M

HNO_3 or 0.1M, 0.5M or 0.87M HAc. The sample preparation and data analysis procedure for these tests are described in Chapter 3, section 3.1.2.1. The Chappelle test for pozzolanic reactivity, based on the French standard NF P 18-513 (2010) measures the amount of $Ca(OH)_2$ consumed by a pozzolan in a saturated calcium hydroxide solution and was used to evaluate the pozzolanicity of the zeolites before and after acid treatment. The testing procedure is described in Chapter 3, section 3.1.2.2. Results are given in grams of $Ca(OH)_2$ consumed per gram of zeolite initially added to the solution.

5.2.4 Influence of Acid Treated Zeolite on Cement Hydration Testing

Isothermal calorimetry was used to compare the initial rate of hydration of cement pastes with zeolite replacement of cement. Testing was done on cement pastes with 0% or 20% zeolite replacement for zeolites treated with 0.1M, 0.5M, or 1M HCl, 0.1M, 0.5M, or 1M HNO_3 or 0.1M, 0.5M or 0.87M HAc. Testing methods are described in Chapter 3, section 3.1.3.1.

5.3 RESULTS

5.3.1 Physical and Chemical Characterization Testing Results

The crystalline phases present in each zeolite sample before and after acid treatment are shown in Figure 5.1 to 5.3. No significant changes were observed after acid treatment.

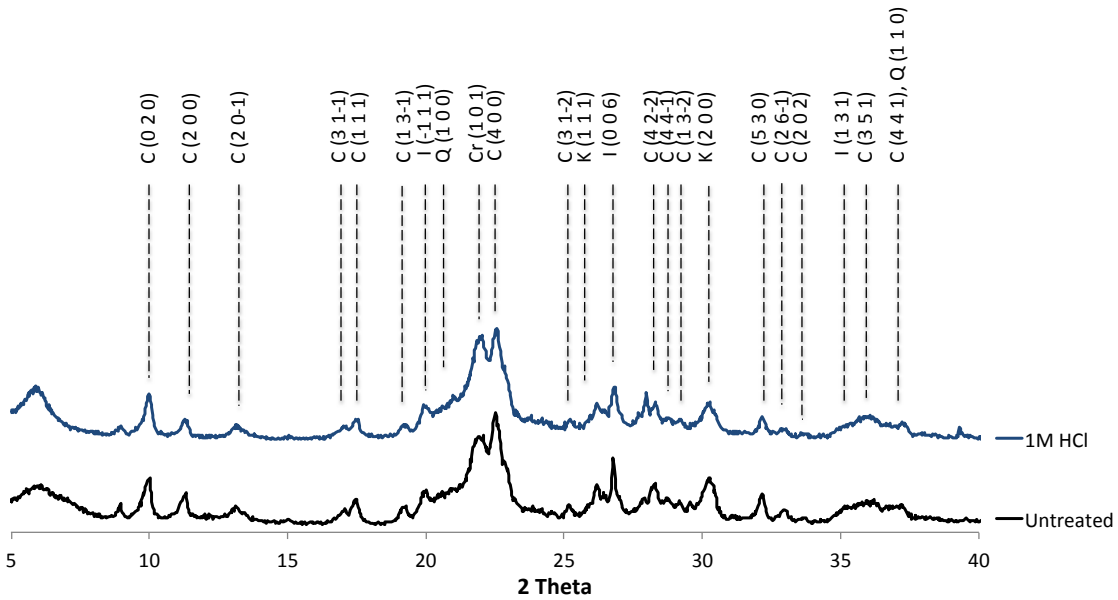

Figure 5.1 - Phases present in the zeolite T sample before and after treatment with hydrochloric acid. C = clinoptilolite, I = illite, Q = quartz, K = potassian halite. Numbers in parenthesis indicate the d-spacing of the reflection.

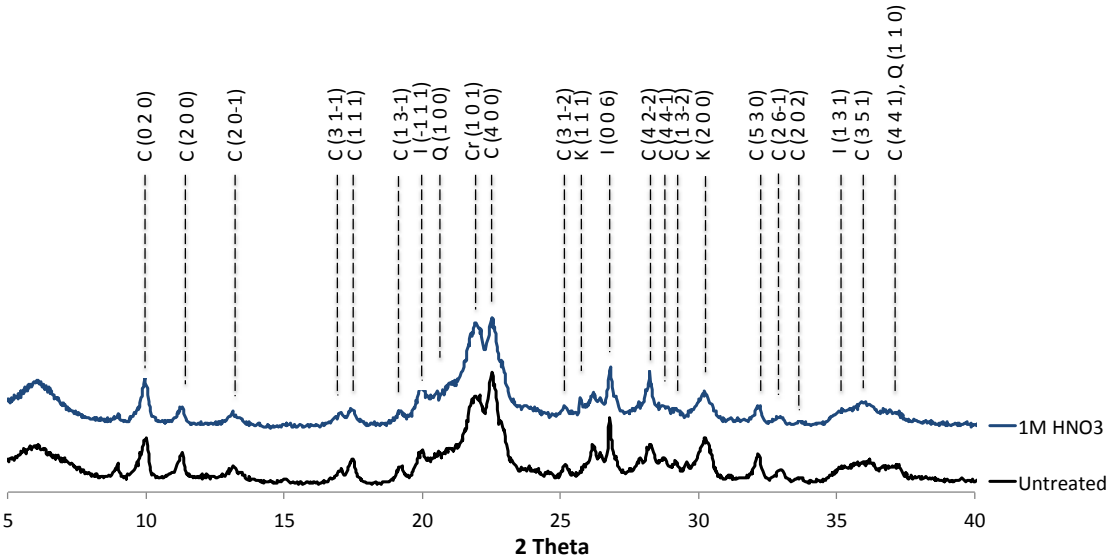

Figure 5.2 - Phases present in the zeolite T sample before and after treatment with nitric acid. C = clinoptilolite, I = illite, Q = quartz, K = potassian halite. Numbers in parenthesis indicate the d-spacing of the reflection.

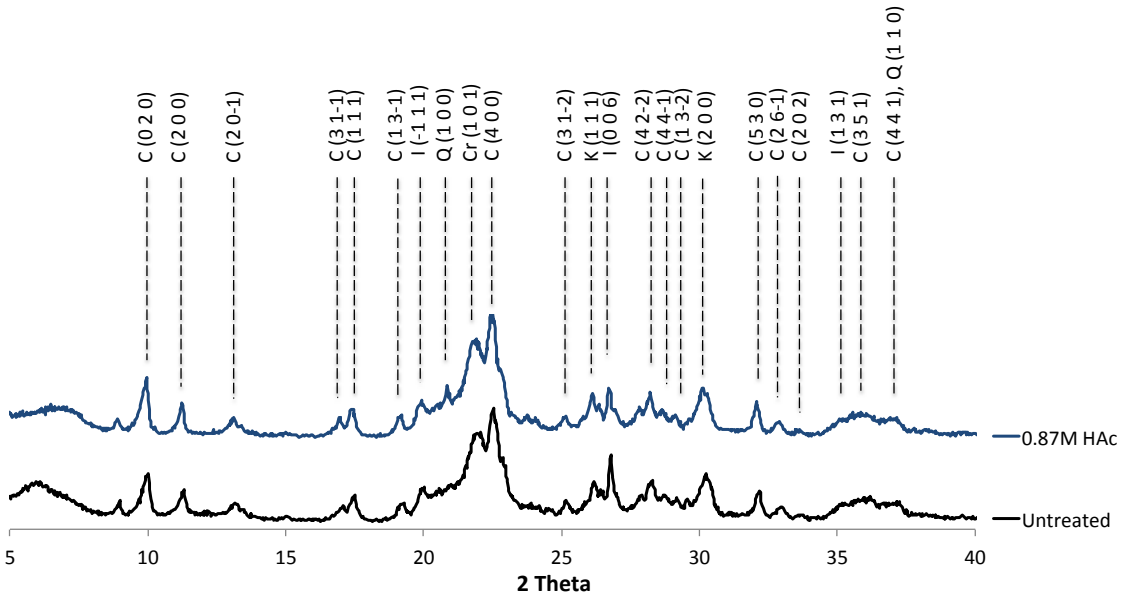

Figure 5.3 - Phases present in the zeolite T sample before and after treatment with acetic acid. C = clinoptilolite, I = illite, Q = quartz, K = potassian halite. Numbers in parenthesis indicate the d-spacing of the reflection.

The changes to the nitrogen available specific surface area (henceforth, surface area, see section 4.3.1.2) and the pore sizes of the zeolites after acid treatment are shown in Figure 5.4 to 5.9. Figure 5.4 shows the effect of hydrochloric acid on the zeolite surface area. Treatment with 0.1M, 0.5M and 1M HCl resulted in increases in the nitrogen-available surface area relative to the nitrogen-available surface area of the untreated zeolite. However, treatment with the 1M acid concentration increased the surface area less than the 0.1M and 0.5M concentrations. Figure 5.4 also shows that the increase in surface area was primarily a result of increased internal surface area, as external surface areas remained constant regardless of the concentration of the acid treatment solution. The pore size distribution data in Figure 5.5 also reveals that the increase in the surface area of the 0.5M HCl treated zeolite may be due to an increase in porosity.

Treating the zeolite with nitric acid resulted in large increases in surface area proportional to the strength of the acid, as shown in Figure 5.6, which, similar to the hydrochloric acid treated samples, appear to result due to increases in internal surface area. Treatment with 0.1M HNO_3 more than doubled the nitrogen-available surface area of the zeolite, and after treatment with 1M HNO_3, the nitrogen-available surface area was nearly triple the surface area of the untreated sample. The pore size distribution data in Figure 5.7 show that treatment with 0.5M or 1M HNO_3 resulted in increases in the volume of ~2-7 nm pores present on the sample surface.

Similar to the zeolites treated with hydrochloric and nitric acid, treatment with acetic acid increased the surface area of the zeolite compared to the untreated sample, as

shown in Figure 5.8. However, the magnitude of the increase in surface area of the zeolite after treatment with acetic acid was much less than for the other acids and did not significantly affect the pore size distribution of the zeolite, as shown in Figure 5.9. Further, treatment with different concentrations of acetic acid did not produce differences in surface area or porosity.

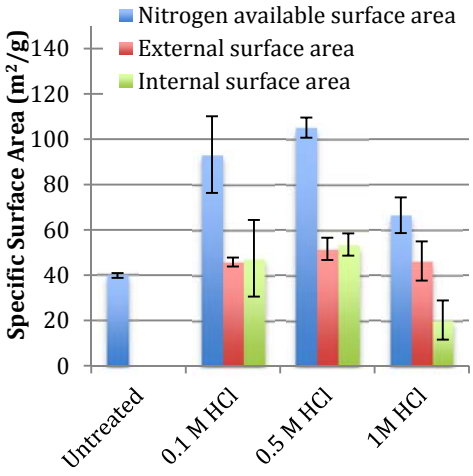

Figure 5.4 - Nitrogen-available specific surface area of untreated zeolite and zeolite treated with hydrochloric acid

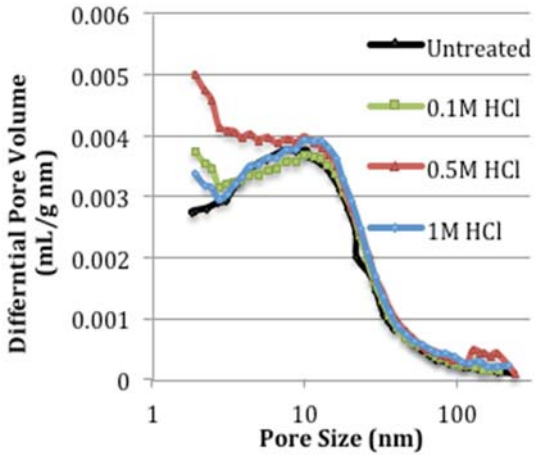

Figure 5.5 - Pore size distribution of untreated zeolite and zeolite treated with hydrochloric acid

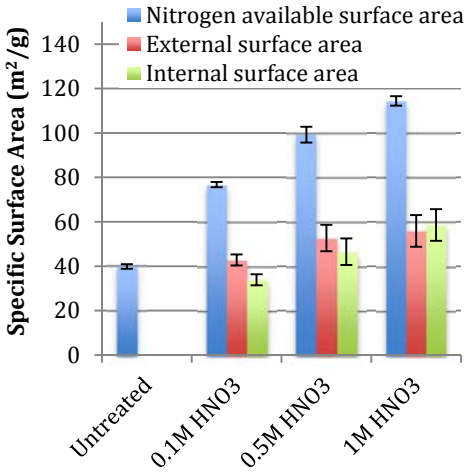

Figure 5.6 - Nitrogen-available specific surface area of untreated zeolite and zeolite treated with nitric acid

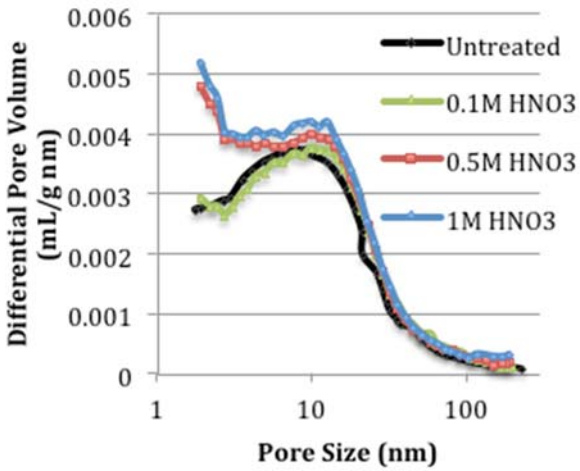

Figure 5.7 - Pore size distribution of untreated zeolite and zeolite treated with nitric acid

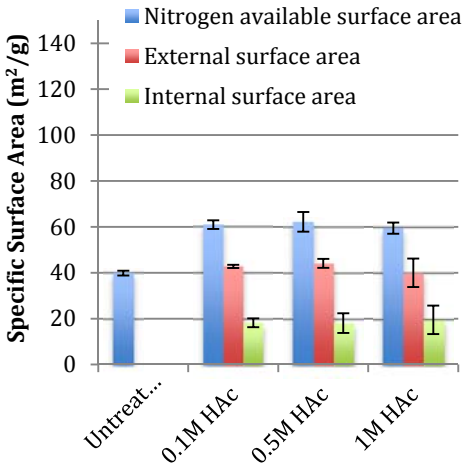

Figure 5.8 - Nitrogen-available specific surface area of untreated zeolite and zeolite treated with acetic acid

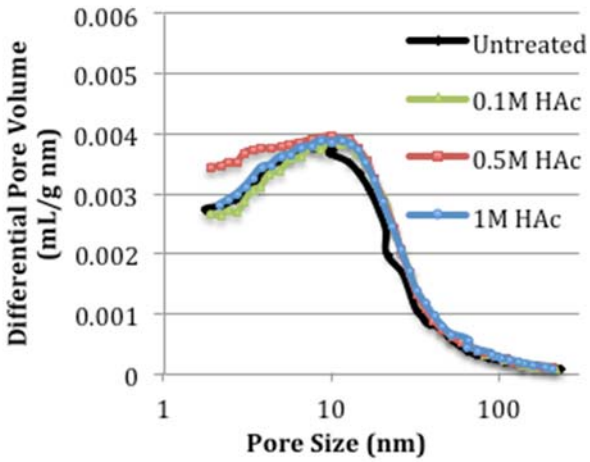

Figure 5.9 - Pore size distribution of untreated zeolite and zeolite treated with acetic acid

Changes to the zeolite particle size after acid treatment are shown in Table 5.1 to 5.3 and Figure 5.10 to 5.12. Treatment with all acid types and concentrations reduced the coarsest fraction, the d_{90}, of the zeolite, shown in Table 5.1 to 5.3. The volume percent particle size distribution (PSD) charts, Figures 5.10b, 5.11b, and 5.12b, show that, for all samples, the volume of material greater than 500µm was eliminated from the sample during acid treatment. Also apparent from Table 5.1 to 5.3 is that, in addition to the effect of the acids on the coarsest material fraction, the nitric acid and acetic acid also reduced the mean particle size, the d_{50}, of the zeolite by about 50%. Acid concentration, however, did not seem to have a significant effect on the zeolite particle size after treatment with any of the acids.

Table 5.1 – Summary of zeolite T particle size distribution before and after treatment with hydrochloric acid

Acid Treatment	Particle Sizes (μm)		
	d_{10}	d_{50}	d_{90}
Untreated	2.62	33.29	142.29
0.1M HCl	4.02	31.72	100.96
0.5M HCl	3.80	29.46	100.90
1M HCl	3.91	32.20	105.83

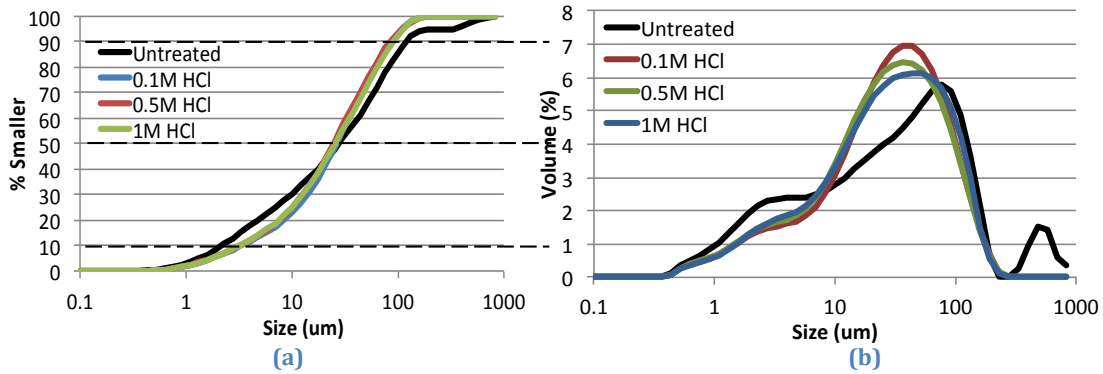

(a) (b)

Figure 5.10 - Particle size distributions of untreated and hydrochloric acid-treated zeolite T, (a) Cumulative particle size distribution, (b) volumetric size fraction distribution

Table 5.2 - Summary of zeolite T particle size distribution before and after treatment with nitric acid

Acid Treatment	Particle Sizes (μm)		
	d_{10}	d_{50}	d_{90}
Untreated	2.62	33.29	142.29
0.1M HNO_3	3.38	23.19	95.48
0.5M HNO_3	3.13	22.55	90.80
1M HNO_3	3.19	20.75	80.09

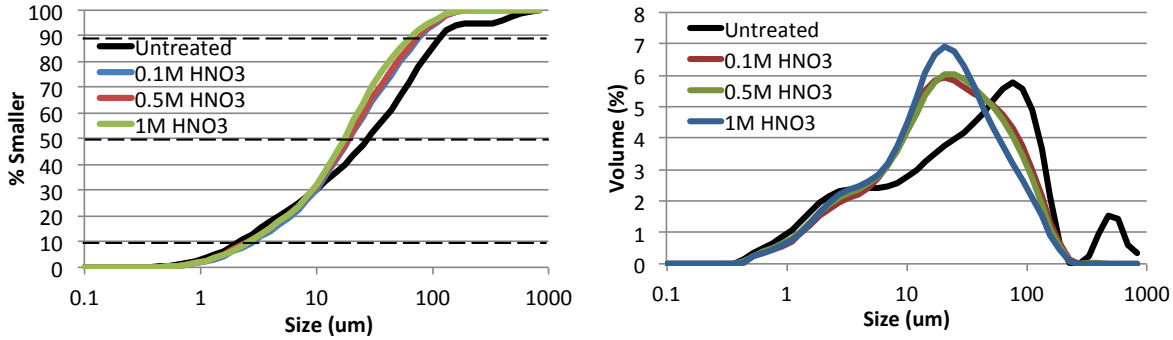

(a) (b)

Figure 5.11 - Particle size distribution of untreated and nitric acid-treated zeolite

Table 5.3 - Summary of zeolite T particle size distribution before and after treatment with acetic acid

Acid Treatment	Particle Sizes (μm)		
	d_{10}	d_{50}	d_{90}
Untreated	2.62	33.29	142.29
0.1M HAc	2.27	16.72	86.88
0.5M HAc	2.83	23.40	97.31
1M HAc	2.72	18.45	93.42

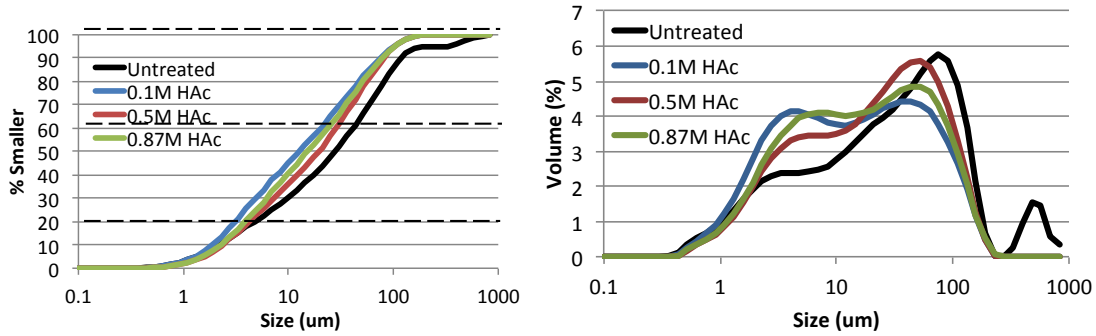

(a) (b)

Figure 5.12 - Particle size distribution of untreated and acetic acid-treated zeolite T

5.3.1.1 Changes to SiO_2/Al_2O_3 ratio and Fe^{3+} content

The Al^{3+} ion concentrations present in the decants reserved from acid treatment of the zeolites were measured in order to gauge the relative amount of dealumination occurring in the zeolite with acid treatment and are shown in Figure 5.12. The quantity of aluminum present in each sample was normalized by the sample's external surface area.

Significantly higher concentrations of Al^{3+} were present in the HCl and HNO_3 solutions compared to the aluminum present in the blank sample. The quantity of aluminum present in the decant from both strong acids (HCl and HNO_3) was equal, indicating that acid strength contributes more significantly to zeolite dealumination than does anion type. In contrast to the hydrochloric and nitric acid decant solutions, the acetic acid decant had virtually no Al^{3+} present in solution, less even than the blank solution. It is not clear exactly why lower quantities of aluminum were present in the acetic acid sample decant compared to the blank sample, however the is apparent from the results shown in Figure 5.13 that use of hydrochloric and nitric acid result in structural dealumination of the zeolite while acetic acid does not.

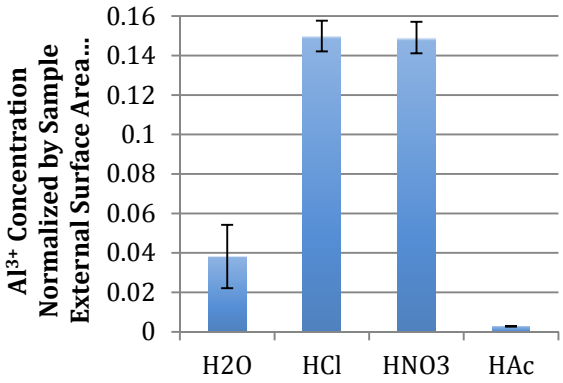

Figure 5.13 - Aluminum concentration of acid treatment decants

The elemental iron concentrations present in the decants reserved from acid treatment of the zeolites were measured to determine if removal of framework iron by acid treatment contributed to changes in the reactivity of acid-treated zeolites. Iron has been directly linked to the performance of zeolites for other processes such as adsorption of pollutants or catalytic activity and so it was theorized that it could affect pozzolanic reactivity as well (Perez-Ramirez et al. 2003). Higher concentrations of iron present in

solution would indicate that iron was removed from the zeolite samples with acid treatment. However, the results, shown in Figure 5.14, and normalized to account for differences in sample external surface area, show that less iron was present in the acid decant solutions than in the blank solution. It is hypothesized that iron hydroxide solubility in the differing pH conditions of each solution may have affected the quantity of iron present in each sample. However, more work is needed, both to understand the results shown in Figure 5.14 and to understand the contribution of iron species to zeolite reactivity.

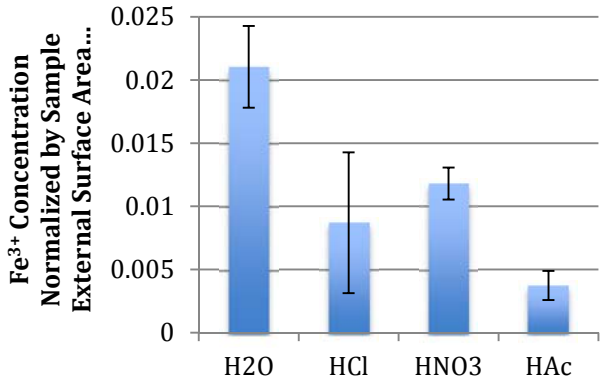

Figure 5.14 - Iron concentration of acid treatment decant

5.3.2 Zeolite Reactivity Characterization

The calcium hydroxide contents of pastes containing untreated zeolite and zeolite treated with hydrochloric, nitric or acetic acid are shown in Figure 5.15 to 5.17. In Figure 5.15 and 5.16, for both the 28 day and 90 day hydrated paste samples, the hydrochloric acid and nitric acid-treated zeolite-cement pastes had lower amounts of calcium hydroxide present relative not only to the cement-only and quartz-cement samples, but also to the untreated zeolite-cement pastes, indicating that the hydrochloric and nitric acid

treatments increased pozzolanic reactivity of the zeolite. The calcium hydroxide content of acetic acid-treated zeolite-cement paste, shown in Figure 5.17, was approximately equal to the untreated zeolite-cement paste at 28 days, but was significantly lower at 90 days. The zeolites treated with the strong acids, hydrochloric and nitric, reduced the paste's calcium hydroxide content more than the zeolite treated with acetic acid did for the 28-day samples. However, use of the stronger acids seemed only to have slowed the reaction rate, as the amount of calcium hydroxide in the acid-treated zeolite-cement pastes was similar for all three types of acid shown in Figure 5.15 to 5.17 after 90 days. Acid concentration had very little effect on the magnitude of the calcium hydroxide reduction.

Interestingly, acid treatment seemed to delay the pozzolanic reaction for all acid types, as the calcium hydroxide contents of the 90-day pastes were lower than in the 28-day pastes regardless of acid type. For the pastes using untreated zeolite, as well as pastes that used zeolites treated using other methods, such as calcination shown in Figures 4.31 to 4.36, ball milling, shown in Figure 6.5, and cation exchange, shown in Figure 7.5, the pozzolanic reaction appeared to have been finished before 28 days, evidenced by the similar or greater quantities of calcium hydroxide present in pastes at 90 days compared to 28 days.

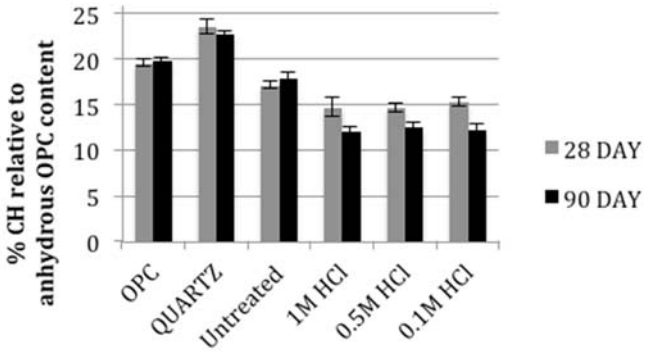

Figure 5.15 - $Ca(OH)_2$ content by weight of hydrated cement pastes containing 80-100% cement and 0-20% untreated Zeolite T, hydrochloric acid-treated Zeolite T or quartz filler, (w/cm = 0.4)

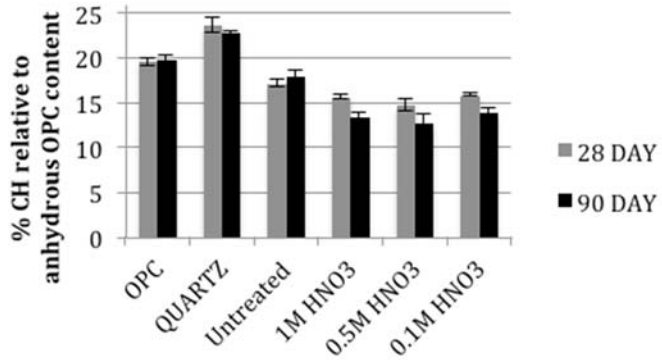

Figure 5.16 - $Ca(OH)_2$ content by weight of hydrated cement pastes containing 80-100% cement and 0-20% untreated zeolite T, nitric acid-treated zeolite T or quartz filler, (w/cm = 0.4)

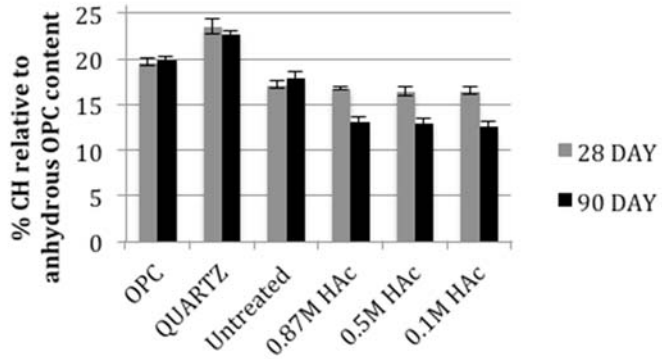

Figure 5.17 - $Ca(OH)_2$ content by weight of hydrated cement pastes containing 80-100% cement and 0-20% untreated zeolite T, acetic acid-treated zeolite T or quartz filler, (w/cm = 0.4)

The results of the Chapelle test for the acid-treated zeolites are shown in Figure 5.18 to 5.20. The Chapelle test results do not indicate a difference in pozzolanic reactivity

after acid treatment as the results for all tested acid-treated samples, are the same, within error as the untreated samples. Further discussion on the ability of the Chapelle test to predict pozzolanic potential of natural zeolites is provided in Appendix A.

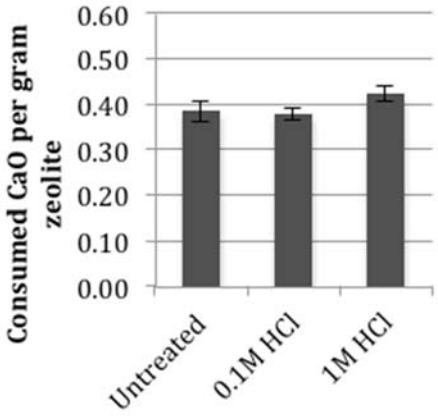

Figure 5.18 - Chapelle test results for untreated zeolites and zeolites treated with hydrochloric acid

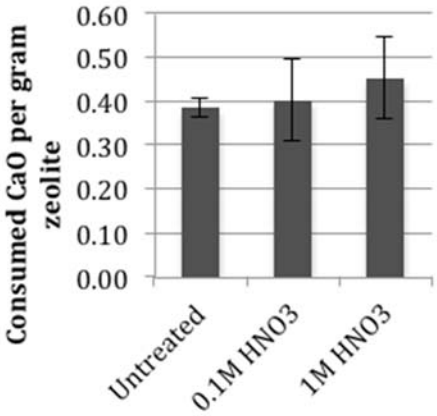

Figure 5.19 - Chapelle test results for untreated zeolites and zeolites treated with nitric acid

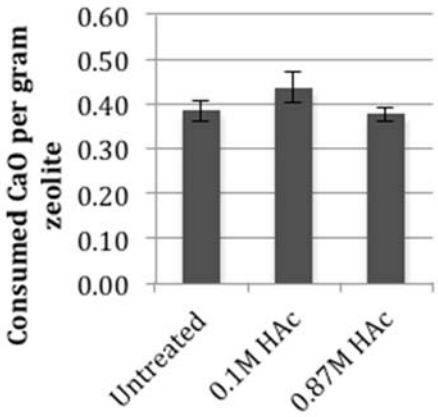

Figure 5.20 - Chapelle test results for untreated zeolites and zeolites treated with acetic acid

5.3.3 Influence of Acid Treated Zeolite on Cement Hydration Testing Results

The effects of acid-treated zeolites on cement hydration, measured through isothermal calorimetry, are shown in Figure 5.21 to 5.31 and Table 5.4 to 5.6. While the

time to the start of the acceleration period and time to the maximum rate of heat release were not significantly different in the acid-treated zeolite T-cement pastes compared to the untreated zeolite T-cement pastes, the rate of reaction in the acceleration period and the maximum rate of heat release were increased for all acid-treated zeolite T-cement pastes. The slope for hydrochloric and nitric acid-treated zeolite-cement pastes, shown in Table 5.4 and 5.5, are considerably higher than for the cement-only, quartz filler and untreated zeolite pastes, whereas for the acetic acid-treated zeolite, shown in Table 5.6, the slope is increased much less.

Differences in the maximum heat evolved for each zeolite-cement pastes are shown in Figure 5.23, 5.27 and 5.31. Using acid-treated zeolites generally resulted in increases to the maximum heat of hydration of zeolite-cement pastes relative to the cement-only, quartz filler and untreated zeolite-cement pastes for all types and concentrations of acids treatments tested. One exception to this results was the 1M hydrochloric acid-treated sample, which may have increased the maximum heat released, but had very large error. The total cumulative heat evolved by 72 hours was greater, for all acid-treated zeolite-cement pastes, than the cement-only paste, but less than for the quartz filler paste, regardless of the type or concentration or acid used in treatment.

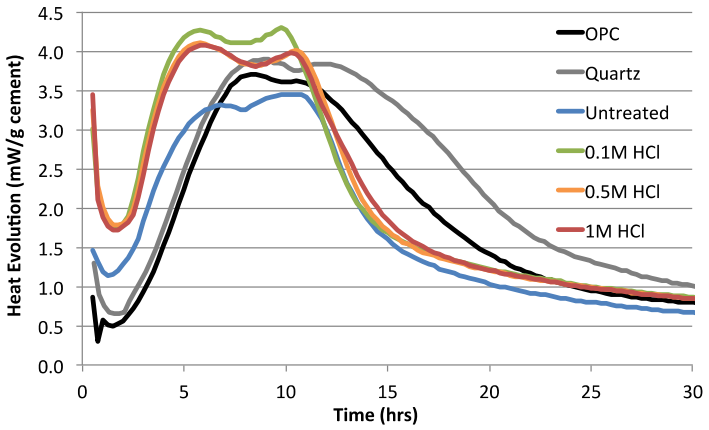

Figure 5.21 – Isothermal calorimetry (23°C) results of pastes with 80-100% cement and 0-20% untreated or hydrochloric acid-treated Zeolite T (w/cm = 0.4)

Table 5.4 - Acceleration period slope in isothermal calorimetry (23°C) of pastes with 80-100% cement and 0-20% untreated or hydrochloric acid-treated zeolite T or quartz filler (w/cm = 0.4)

SCM/filler	Acceleration Period Slope (mW/g/hr)
None	0.66±0.05
Quartz	0.64±0.03
Untreated Zeolite T	0.61±0.11
0.1M HCl Treated ZeoliteT	0.89±0.01
0.5M HCl Treated Zeolite T	0.87±0.05
1M HCl Treated Zeolite T	0.87±0.05

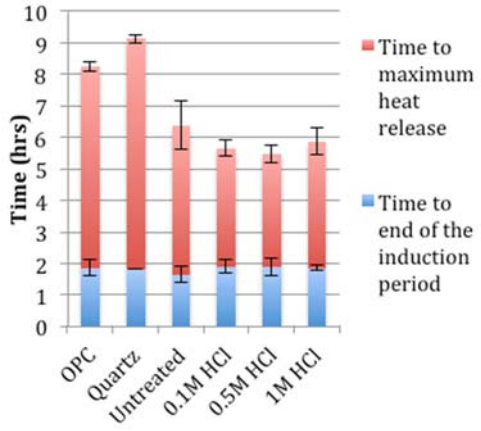

Figure 5.22 - Time to the end of the induction period and time to the maximum value of heat flow in isothermal calorimetry (23°C) of pastes with 80-100% cement and 0-20% untreated or hydrochloric acid-treated Zeolite T (w/cm = 0.4)

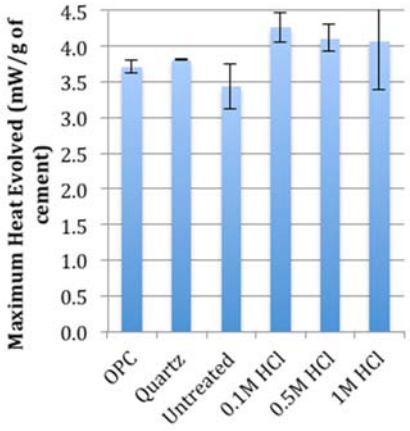

Figure 5.23 - Value of the maximum heat flow in isothermal calorimetry (23°C) of pastes with 80-100% cement and 0-20% untreated or hydrochloric acid-treated Zeolite T (w/cm = 0.4)

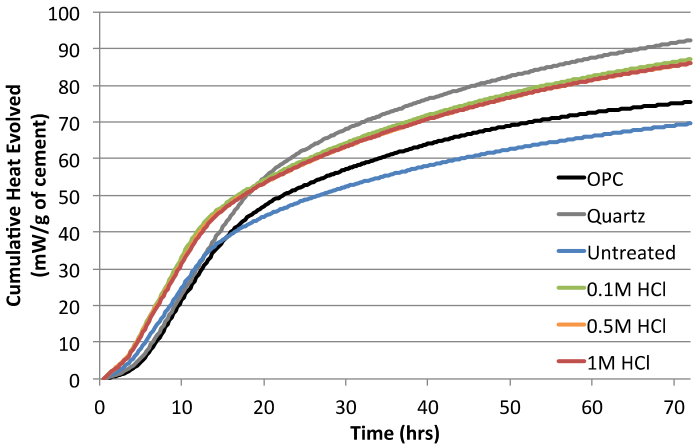

Figure 5.24 - Cumulative heat evolved over 72 hours during isothermal calorimetry (23°C) of 80-100% cement and 0-20% untreated or HCl acid-treated Zeolite T or quartz filler pastes (w/cm = 0.4)

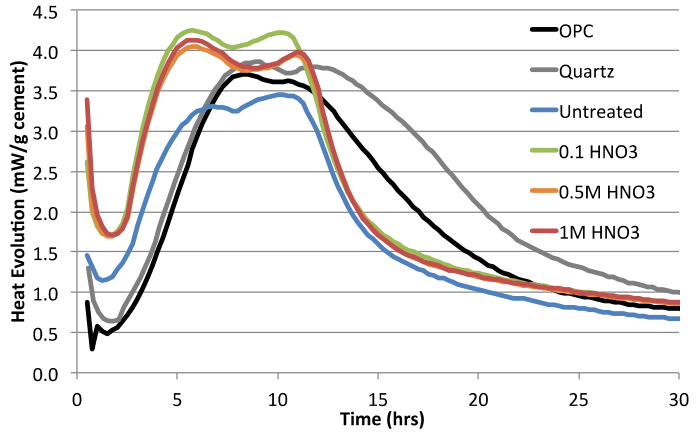

Figure 5.25 - Isothermal calorimetry (23°C) results of pastes with 80-100% cement and 0-20% untreated or nitric acid-treated Zeolite T (w/cm = 0.4)

Table 5.5 - Acceleration period slope in isothermal calorimetry (23°C) of pastes with 80-100% cement and 0-20% untreated or nitric acid-treated Zeolite T or quartz filler (w/cm = 0.4)

SCM/filler	Acceleration Period Slope (mW/g/hr)
None	0.66±0.05
Quartz	0.64±0.03
Untreated Zeolite T	0.61±0.011
0.1M HNO_3 Treated ZeoliteT	0.90±0.04
0.5M HNO_3 Treated Zeolite T	0.82±0.02
1M HNO_3 Treated Zeolite T	0.85±0.01

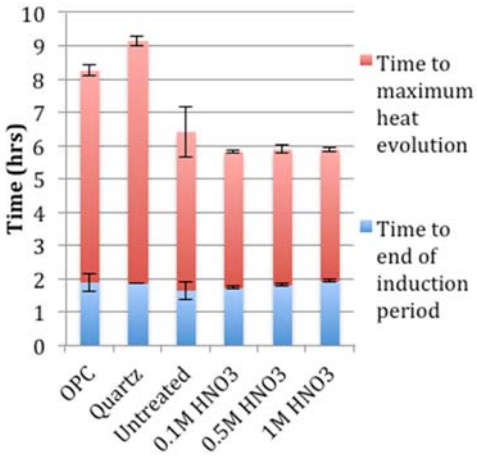

Figure 5.26 - Time to the end of the induction period and time to the maximum value of heat flow in isothermal calorimetry (23°C) of pastes with 80-100% cement and 0-20% untreated or nitric acid-treated Zeolite T (w/cm = 0.4)

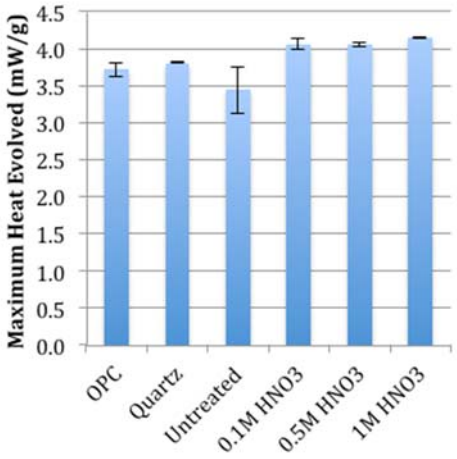

Figure 5.27 - Value of the maximum heat flow in isothermal calorimetry (23°C) of pastes with 80-100% cement and 0-20% untreated or nitric acid-treated Zeolite T (w/cm = 0.4)

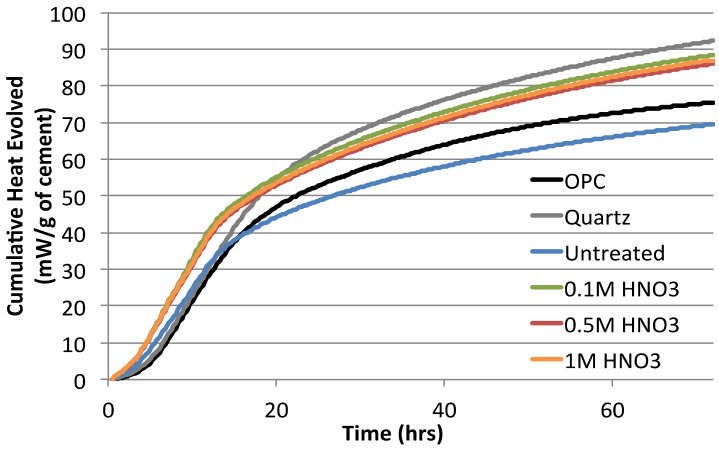

Figure 5.28 - Cumulative heat evolved over 72 hours during isothermal calorimetry (23°C) of 80-100% cement and 0-20% untreated or nitric acid-treated Zeolite T or quartz filler pastes (w/cm = 0.4)

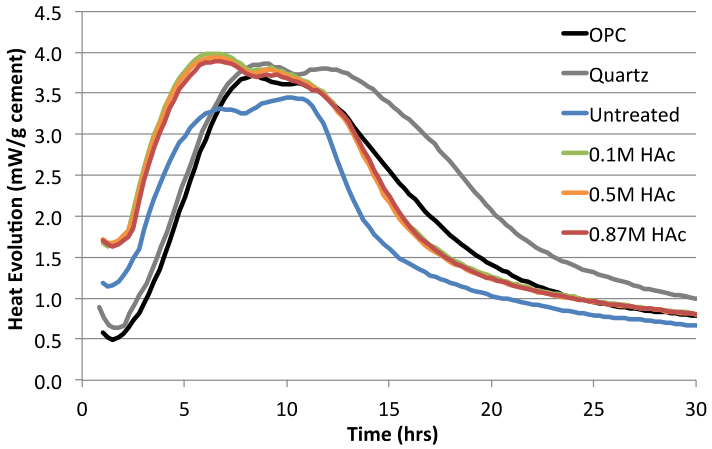

Figure 5.29 - Isothermal calorimetry (23°C) results of pastes with 80-100% cement and 0-20% untreated or acetic acid-treated Zeolite T (w/cm = 0.4)

Table 5.6 - Acceleration period slope in isothermal calorimetry (23°C) of pastes with 80-100% cement and 0-20% untreated or acetic acid-treated zeolite T or quartz filler (w/cm = 0.4)

SCM/filler	Acceleration Period Slope (mW/g/hr)
None	0.66±0.05
Quartz	0.64±0.03
Untreated Zeolite T	0.61±0.11
0.1M HAc Treated ZeoliteT	0.70±0.01
0.5M HAc Treated Zeolite T	0.71±0.02
1M HAc Treated Zeolite T	0.70±0.01

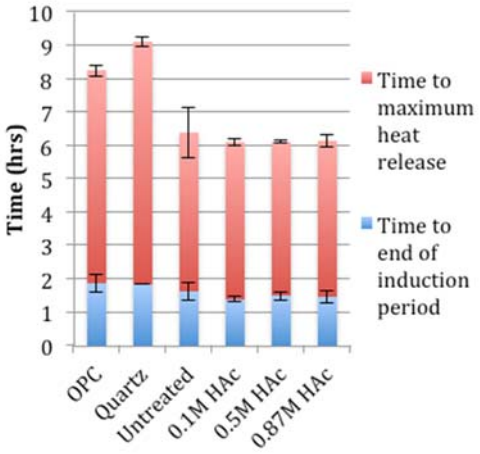

Figure 5.30 - Time to the end of the induction period and time to the maximum value of heat flow in isothermal calorimetry (23°C) of pastes with 80-100% cement and 0-20% untreated or acetic acid-treated Zeolite T (w/cm = 0.4)

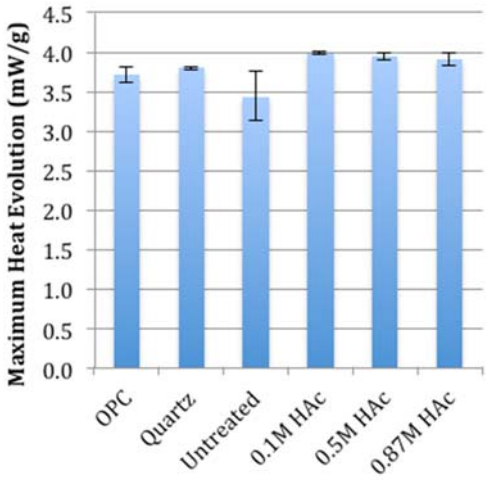

Figure 5.31 - Value of the maximum heat flow in isothermal calorimetry (23°C) of pastes with 80-100% cement and 0-20% untreated or acetic acid-treated Zeolite T (w/cm = 0.4)

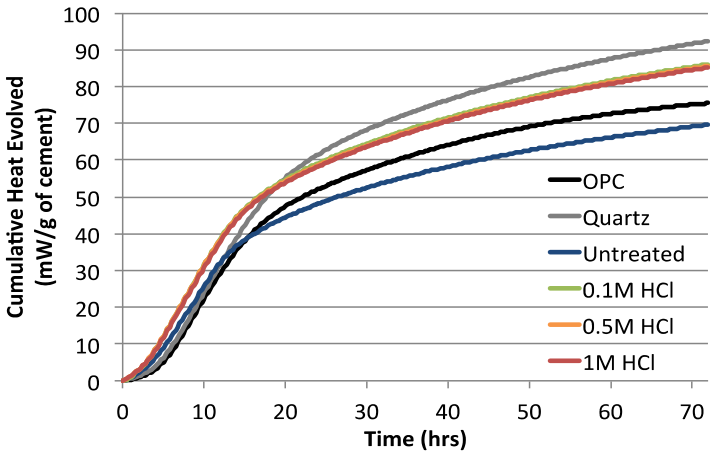

Figure 5.32 - Cumulative heat evolved over 72 hours during isothermal calorimetry (23°C) of 80-100% cement and 0-20% untreated or acetic acid-treated zeolite T or quartz filler pastes (w/cm = 0.4)

5.4 Discussion of the Effects of Acid Treatment on Zeolite Pozzolanic Reactivity

In general, the results of the physical characterization testing and pozzolanic reactivity testing of the acid-treated zeolites were encouraging. Although acid treatment did not result in changes to crystallinity or reductions in system impurities, it did result in substantial increases in surface area and reductions in particle size of the zeolite. Acid treated zeolites also showed evidence of increased pozzolanic reactivity compared to the untreated zeolites through reduced calcium hydroxide contents measured from zeolite-cement pastes.

Previous research suggested that acid treatment could reduce the crystallinity of zeolites (Elaiopoulos et al. 2010, Unvernen et al. 2005, Cakiciogly-Ozkan and Ulku 2005) and reduce system impurities such as dolomite, quartz and feldspar phases, which are inert with respect to the hydration reactions occurring in cementitious systems (Ates and Hardacre 2012). This was not found to be true for the samples tested in this study, as XRD phase analysis results, shown in Figure 5.1 to 5.3, did not reveal any changes in the

phases present in the zeolite samples after treatment with acid. It was also suggested that acid treatment of zeolites could improve the abilities of zeolites to remove system cations through exchange with cations such as Ca^{2+}, Mg^{2+}, Na^{+}, K^{+} and Fe^{3+} (Ates and Hardacre 2012, Wang and Peng 2010, Klieve and Semmens 1980). In many cases the error ranges of acid-treated zeolite samples were considerably smaller compared to those of the untreated zeolite, especially for isothermal calorimetry testing, shown in Figure 5.21 to 5.31, which is perhaps a consequence of the removal of variability resulting from cations present in the untreated zeolite.

Acid treatment was generally successful at increasing the nitrogen-available specific surface area, shown in Figure 5.4, 5.6, and 5.8, and decreasing the particle size of the zeolite, shown in Figure 5.10 to 5.12 and Table 5.1 to 5.3, similar to the results shown in literature (Elaiopoulos et al. 2010, Ates and Hardacre 2012, Cakiciogly-Ozkan and Ulku 2005). However, the response of the zeolite differed with acid type and concentration. Changes in zeolite surface area are likely primarily effects of cation exchange and structural dealumination, a conclusion which is supported by the increases in internal surface area versus external surface area of the zeolite with acid treatment.

Treatment of zeolite with hydrochloric acid increased the zeolite surface area relative to the untreated zeolite for all concentrations tested, shown in Figure 5.4. The surface area was increased considerably more for the 0.1M and 0.5M concentrations compared to the 1M HCl treatment. Some of the increases in surface area are likely due to exchange of larger cations (Ca^{2+}, Mg^{2+}, K^{+}, Na^{+}) for H^{+} protons, which allows nitrogen molecules to more easily penetrate the interior of the zeolite structure. Further changes

may be a result of increasing porosity. The pore size distribution data shown in Figure 5.5 suggest that treatment with 0.5M HCl resulted in an increase in small mesopore volume, which may be a result of the removal of Al^{3+} from the structure (Beers et al. 2003, Elaiopoulos et al. 2010, Ates and Hardacre 2012, Cakiciogly-Ozkan and Ulku 2005). The subsequent decrease in surface area after treatment with 1M HCl could be a result of structural collapse from further structural dealumination, as observed by Rivera et al. (2000) and Salvestrini (2010). The slight increase in particle size after treatment with 1M HCl compared to the 0.5M HCl-treated sample seems to support this theory.

Treatment of the zeolite with nitric acid was the most successful of the acid treatments attempted in this study, resulting in increases to surface area proportional to the concentration of acid used. Shown in Figure 5.6, zeolite treated with 1M HNO_3 had 300% greater surface area than the untreated zeolite. The pore size distribution data from Figure 5.7 show that the volume of ~2-7 nm pores was increased after treatment with 0.5M and 1M HNO_3. Therefore, it is again likely that increases in surface area occurred as a result of cation exchange of larger cations with protons from the acid, followed by increases in surface area due to increased zeolite porosity. The increase in surface area after treatment with 1M HNO_3 could be a result of continued cation exchange, slightly increased porosity, reduced particle size and further structural dealumination that did not, in this case, result in structural collapse. However, experimental verification of this theory was outside the scope of this work.

Overall, treatment with acetic acid, shown in Figure 5.8, was less successful than with nitric and hydrochloric acid, although it did increase the zeolite specific surface area

compared to the control. Reduced improvements to surface area relative to the other acids are likely a result of the strength of the acid, with the stronger acids able to exchange greater quantities of cations for protons. Additionally, use of acetic acid resulted in less structural dealumination, shown by considerably lower amount of Al^{3+} in solution in the ion analysis results in Figure 5.12. Further, treatment with acetic acid resulted in very little change in pore size distribution of the zeolite, although it was still effective at reducing zeolite particle size.

The amount of aluminum in solution after treatment, shown in Figure 5.12, was similar for the HCl and HNO_3 solutions, although slightly higher in the HNO_3 solution, and may indicate that the zeolite sample underwent significant dealumination during acid treatment. The decrease in aluminum concentration with acetic acid treatment may indicate that the acetic acid was not a strong enough acid to induce dealumination of the zeolite structure. However, the reduced aluminum concentrations could also simply indicate that a complexation reaction occurred between the acetic acid conjugate base and the Al^{3+} in solution.

Acid treatment was effective in improving the performance of the zeolite as an SCM, with calcium hydroxide content of all pastes using acid-treated zeolites reduced compared to the untreated zeolite-cement pastes, , shown in Figure 5.14 to 5.16. Treatment with the strong acids, hydrochloric and nitric, seemed to be more effective at increasing the calcium hydroxide consumption ability of the zeolite, with pastes using strong-acid-treated-zeolites yielding lower calcium hydroxide contents at 28 days. However, the calcium hydroxide contents of pastes using acid-treated zeolites were very

similar at 90 days regardless of the type of acid used to treat the zeolite. It is interesting to note the extension of the time for the pozzolanic reaction of the zeolite after acid treatment. All of the other testing of paste calcium hydroxide contents completed for this dissertation yielded samples that appear to have completed the extent of their pozzolanic reaction before 28 days, as calcium hydroxide contents for all 28 and 90 day pastes were similar, or sometimes slightly higher for the 90 day samples. However, using acid-treated zeolites, the calcium hydroxide content of all of the pastes was reduced at 90 days from the 28-day level by around 3-4% of the total paste content. This effect is likely a result of the dealumination occurring in the sample during acid treatment, increasing the amount of silica available to participate in the pozzolanic reaction and affecting zeolite long-term pozzolanicity, an effect that is supported by the findings of Snellings et al. (2010).

The results of the Chapelle test on the acid-treated zeolites, shown in Figure 5.17 to 5.19, were inconclusive, as all of the results for all of the acid types and concentrations were within error of each other, suggesting that acid treatment has no effect on zeolite reactivity. It is more likely, however, that the Chapelle test is simply not a precise enough measurement of the pozzolanicity for zeolites used as SCMs.

In addition to improvements in the calcium hydroxide consumption of acid-treated zeolites, use of acid-treated zeolites also increased the maximum heat of hydration of zeolite-cement pastes, shown in Figure 5.22, 5.26 and 5.30, and slightly accelerated hydration for the hydrochloric and nitric acid-treated samples, shown in Figure 5.21 and 5.25. These increases could be due, at least partially, to a filler effect, as these effects are similar to those seen with the use of inert quartz fillers (Rahhal and Talero 2005).

However, the cumulative heat evolved at 72 hours for all of the acid-treated zeolite-cement pastes, although greater than for the cement-only paste, was substantially less than for the quartz filler paste. These results are shown in Figure 5.23, 5.27 and 5.31 and may indicate that the zeolite particles initially act as nucleating agents, speeding up the timing and rate of reactions, but dissolve soon after the peak of heat evolution, preventing the extension of the reaction seen with the use of filler materials, which provide more space for the growth of hydration products and so tend to extend the magnitude of hydration during the first 72 hours.

5.5 CONCLUSIONS

Natural zeolite was treated for 24 hours with one of three types of acid, hydrochloric, nitric, or acetic, at three different concentration levels, 0.1M, 0.5M or 1M for hydrochloric and nitric acid samples, or 0.1M, 0.5M or 0.87M for acetic acid samples. The physical and chemical characteristics of the material was then determined using XRD, nitrogen adsorption, laser particle size analysis, and atomic emission spectrometry in order to determine what changes the material underwent with acid treatment. These results were then compared to the results of performance testing, comparing the calcium hydroxide contents of pastes using untreated and acid-treated zeolites as well as looking at the results of the Chapelle test for pozzolanicity. The effect of acid-treated zeolites on early age hydration of cement was also tested using isothermal calorimetry.

Acid treatment was found to improve the pozzolanicity of the zeolite through removal of Al^{3+} from the zeolite crystal structure. In addition, it is hypothesized that cation exchange played a role in standardizing zeolite performance due to removal of

non-structural cations from the system and replacement with protons. This cation exchange may also resulted in the significant increase in the nitrogen available specific surface area of the material, while structural dealumination may have resulted in decreased particle sizes, due to the breaking of material bonds. Overall, acid treatment appeared to be successful at improving the performance of zeolites as SCMs.

Chapter 6: Zeolite Pretreatment Methods to Increase the Reactivity of Zeolites for Use as SCMs – Milling

6.1 INTRODUCTION

Milling, the process of reducing a material's particle size, is a common process in the manufacture of cement, and has also been used to prepare other materials, such ground granulated blast furnace slag, for use as SCMs (Kumar et al. 2008; Snellings et al. 2012; Wan et al. 2004). Many studies have shown that milling can improve the performance of SCMs (Kumar et al. 2008; Lawrence et al. 2005; Paya et al. 1997; Vizcayno et al. 2010; Wan et al. 2004), therefore it is hypothesized that milling will also be successful in improving the performance of zeolites as SCMs. Several studies have already explored the idea of increasing zeolite reactivity through milling. However, these studies primarily employed high-energy ball mills operating at speeds in excess of 500 rpm (Charkhi et al. 2010; Kosanovic et al. 1995; Xie and Kaliaguine 1997; Zielinski et al. 1995), conditions that are not feasible for use with the large quantities of used in the construction industry. Large-scale milling operations in the construction industry typically consist of large rotary ball mills operating at relatively slow rotational speeds (Cleary 2009; Ene 2007). The work presented in this chapter explores whether conditions similar to those found in industrial cement mills can generate improvements in zeolite performance similar to those seen with the use of high-energy planetary mills.

The influence of particle size on the performance of zeolites used as SCMs has not been comprehensively characterized, although several studies' findings point towards increased reactivity of zeolites after a reduction in particle size (Charkhi et al. 2010; Kosanovic et al. 1995, 1997; Ortega et al. 2000; Snellings et al. 2010; Zielinski et al.

1995). Charkhi et al. (2010) noted that, "reduction of particle size causes larger external surface areas available for interaction shorter diffusion path lengths reducing mass and heat transfer resistances in catalytic and sorption applications, decreasing of side reactions, [and] enhancing selectivity." Snellings et al. (2010) showed that in paste mixtures of clinoptilolite zeolites and calcium hydroxide in a 1:1 ratio, smaller grain size and higher external surface area increased both the early heat evolution and the rate of heat release during the pozzolanic reaction. In addition, in the zeolite-calcium hydroxide pastes, more calcium hydroxide was consumed by the finer-zeolite mixtures when tested at 6, 24, and 72 hours. Similarly, using 20 mm x 20 mm cubes made of a hydrated clinoptilolite zeolite and calcium hydroxide, Ortega et al. (2000) demonstrated that unconfined compressive strength and zeolite particle size are almost inversely linearly related, with lower particle sizes yielding higher compressive strengths.

Interestingly, the researchers that have investigated the effect of zeolite milling have found that milling can not only decrease zeolite particle size, but that long milling time and high rotational speed result in a reduction of crystallinity and increase in the quantity of amorphous material (Charkhi et al. 2010, Kosanovic et al. 1995a,b,c, Zielinski et al. 1995). Kosanovic et al. (1995) milled a 1g zeolite T sample using 10 mm Wolfram carbide balls in a planetary ball mill operated at 3000 rpm. During the first 15-20 minutes of milling they found that 75% of the crystalline phase was converted to amorphous material in addition to reduced particle sizes (Kosanovic et al. 1995). Zielinski et al. (1995) saw similar results after milling six types of artificially-synthesized zeolites in a high-energy ball mill using a set of three 6/16" steel balls and a speed of 1010 rpm. The crystallinity of all six types of zeolite was significantly reduced after only

ten minutes of milling and eliminated in nearly all of the samples by 60 minutes. Charkhi et al. (2010) also saw nearly complete elimination of clinoptilolite zeolite crystallinity after milling for only 20 minutes at 600 rpm using 20 mm zirconium oxide balls and a high-energy planetary ball mill. Similarly, Xie and Kaliaguine (1997) found that KNaX zeolites milled at 1010 rpm became amorphous after 120 minutes of milling. The amorphization of zeolite crystals with milling was suggested by several researchers to occur as a result of breakage of the Si-O-Si and Si-O-Al bonds on the external surface of the zeolite leading to structural collapse (Charkhi et al. 2010, Kosanovic et al. 1995a). However, Kosanovic et al. (1995) also investigated the influence of cations on the amorphization of zeolites during ball milling. They found that the interstitial cations of a zeolite do not affect the mechanism of amorphization through ball milling, but they do change the rate of the process. Filled interstitial spaces in the zeolite generate greater repulsive forces, counteracting the impact forces in the ball mill. Thus the rate of amorphization is linearly related to the volume of space occupied by cations. This theory was confirmed when the study showed that Na-exchanged zeolites decomposed more quickly than those exchanged with larger cations of Ca^{2+}, K^{+} or NH^{4+} (Kosanovic et al. 1995).

In addition to reductions in particle size and crystallinity, other researchers saw observed changes in the zeolite pore structure and surface area after milling. Xie and Kaliaguine (1997) found that milling their KNaX zeolites at 1010 rpm progressively reduced the surface area and micropore volume with increasing milling time. The work of Zielinski et al. (1995) suggested that ball milling initially opened macropores. However, additional milling time caused these pores to gradually disappear. They linked the rate of

surface area loss resulting from the destruction of the macropores to the SiO_2/AlO_3 content of the zeolites, with high silica materials decomposing more slowly.

The results of studies examining the effects of ball milling on zeolite properties suggest that milling can increase zeolite amorphous content, decrease particle size, and increase accessible porosity. Such changes should produce increased pozzolanic reactivity of the zeolite and improve the performance of zeolite-cement mixtures using milled zeolites (Ates and Hardacre 2012; Duvarcı et al. 2007; Johnson et al. 2003). However none of the studies in the literature examining milled zeolites actually tested milled zeolites in cementitious systems. Therefore, the study presented in this chapter examined the effects of ball milling on zeolite properties, including external surface area, particle size, and crystallinity, and investigated the correlation between these properties and zeolite-cement mixture performance using milling techniques closer to those currently in use by the construction industry.

6.2 EXPERIMENTAL METHODS AND MATERIALS

6.2.1 Raw Zeolite and Milled Zeolite Sample Preparation

6.2.1.1 Raw Zeolite

Unground zeolite T was used as the starting material for ball milling treatment testing. Zeolite T was chosen because it was one of the poorer performing of the six zeolite sources shown in Chapter 3, and thus had room for improvement. The zeolite was dried at 105°C for 12 hours before milling.

6.2.1.2 Ball Milled Sample Preparation

Ball milled samples were prepared using a U.S. Stoneware laboratory ceramic mill of 14 cm internal diameter and ball load of 30% of the mill volume filled with the ball bed. Alumina grinding media were used, consisting of a mixture of 2 mm, 10 mm and 25 mm balls. Although several of the literature studies investigated the effect of milling on zeolites milled in high energy planetary mills, a simple rotational mill was chosen to mimic the conditions present in mills currently used to grind cement clinker or other SCMs such as metakaolin, since this type of milling would be easier to industrially implement. A low powder load corresponding to a formal interstitial filling of the void spaces of the ball bed was chosen to attempt to mimic the conditions present in industrial cement grinding mills (Ene 2007). Prior to milling, samples were dried at 105°C for 12 hours in a ceramic crucible.

Ball mills grind samples through the impact of grinding media on the particle surface as the media falls as a result of rotation of the mill. In order for this to be possible, the mill must rotate at a fast enough speed to prevent the balls from sliding along the mill sides, but slowly enough that the balls do not become "pinned" to the side of the mill by the centrifugal forces. The critical speed of the mill (n_{cr}), or the speed at which centrifugal force is greater than gravitational force on the grinding media, was calculated by equation 6.1:

$$n_{cr} = \frac{30\sqrt{2}}{\sqrt{D}} \tag{6.1}$$

where D is the mill diameter. The mill was operated at 85 rpm, or 75% of the critical speed, similar to industrial cement ball mills. The zeolite was then milled for 1, 2, 4, 6, or 8 hours. In preliminary testing it was noticed that samples ground for longer than 2

hours became caked against the sides of the mill. This was believed to be a result of moisture released from the zeolite as particle size was reduced, so samples ground for longer than 2 hours were stopped at 2 hours of milling and dried for an additional 8 hours at 105°C to remove excess moisture from the system, then returned to the ball mill to continue milling.

6.2.2 Zeolite Physical and Chemical Characterization Testing

The zeolite physical and chemical properties were characterized in order to determine the changes resulting from milling and which of these factors contributed to changes in zeolite reactivity in cementitious systems. Characterization testing tracked changes from milling in particle size, surface area and crystalline phases present in the zeolites. X-ray diffraction (XRD) was used to determine what phases were present in each sample and to gauge the effectiveness of reducing crystallinity by milling. The procedure used for x-ray diffraction testing of powdered samples is described in Chapter 3, section 3.1.1.1. Specific surface area was measured on zeolite samples before and after milling by nitrogen sorption using a Micromeretics ASAP 2020. Surface area was determined using the BET model and pore size distribution with the BJH model, as described in Chapter 3, section 3.1.1.2. Particle size distribution of the zeolites was measured before and after milling using a Malvern 2000 Laser Particle Size Analyzer as described in Chapter 3, section 3.1.1.3.

6.2.3 Zeolite Reactivity Testing

Changes to zeolite pozzolanic reactivity after milling were tracked through three methods: the Chapelle test, which measures the amount of calcium consumed by a

sample in aqueous solution; the calcium hydroxide content of hydrated zeolite-cement pastes; and the compressive strengths developed by zeolite-cement mortars. All pastes and mortar mixtures used a 20% replacement by mass of cement with zeolite T. All paste and mortar samples used the cement described in section 3.2.1. All mortar samples used the sand described in section 3.2.2. The calcium hydroxide content of hydrated cement-zeolite pastes was determined for pastes using unmilled zeolite T and zeolite T milled for 0, 2, 4, 6 or 8 hours. The sample preparation procedure is described in Chapter 3, section 3.1.2.1. Samples were tested after 28 and 90 days of curing. The amount of calcium hydroxide present in the sample was calculated from the amount of mass lost from 450°C to 550°C, which corresponds to the dehydration of $Ca(OH)_2$, as described in Chapter 3. The Chappelle test for pozzolanic reactivity, based on the French standard NF P 18-513 (2011) measures the amount of $Ca(OH)_2$ consumed by a pozzolan in a saturated calcium hydroxide solution and was used to evaluate the pozzolanicity of zeolite T before and after milling for 1 or 8 hours. The testing procedure is described in Chapter 3, section 3.1.2.2. Results are given in grams of $Ca(OH)_2$ consumed per gram of zeolite initially added to the solution. The influence of milling on compressive strength was tested on mortars of cement and either unmilled zeolite or zeolites milled for 0, 2 or 8 hours. Experimental details are provided in Chapter 3, section 3.1.2.3.

6.2.4 Effects of Zeolite on Cement Hydration

Isothermal calorimetry was used to examine the effects of the milled zeolites on cement hydration kinetics. Testing was done on cement pastes with 0% or 20% zeolite T mass replacement of cement for zeolite T milled for 0, 2, 4, 6, or 8 hours. Testing methods are described in Chapter 3, section 3.1.3.1.

6.3 RESULTS

6.3.1 Physical and Chemical Characterization Testing Results

The crystalline phases present in zeolite T after milling are shown in Figure 6.1. Even after 8 hours of milling, crystalline phases in the zeolite appear unchanged.

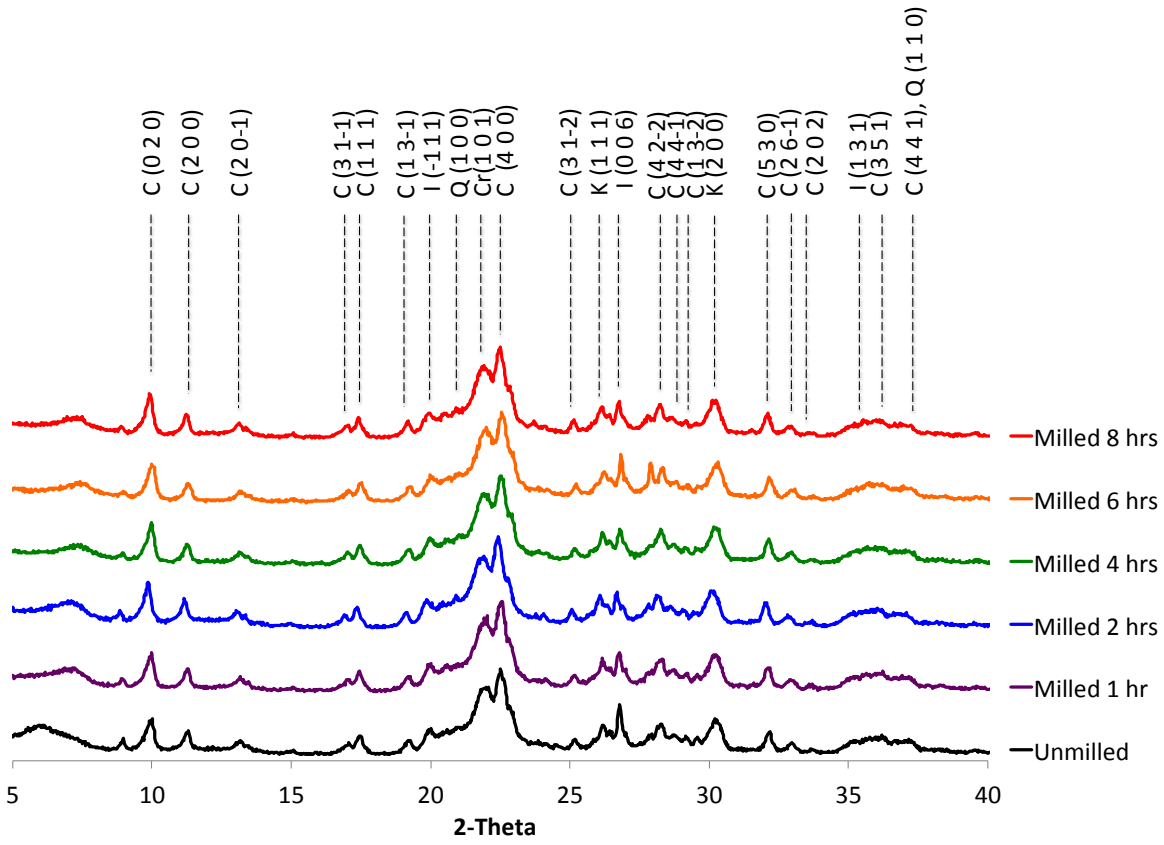

Figure 6.1 - Crystalline phases in zeolite T before and after milling. C = clinoptilolite, I = illite, Q = quartz, Cr = cristobalite, K = potassian halite. Numbers in parenthesis indicate the d-spacing of the reflection.

Zeolite T particle size distributions before and after milling are shown in Table 6.1 and Figure 6.2. Particle sizes were reduced progressively over 8 hours of milling with the most significant reduction taking place in the first 4 hours. From Figure 6.2b it can be seen that milling completely eliminated the coarsest fraction of the original zeolite material (> 500 μm) and increased the volume of material approximately 2 nm and 20 nm in diameter. Although particle sizes continued to decline slightly from 4 to 8 hours of

milling, overall the particle size distribution stabilized after 4 hours of milling, with only slight increases in the volume of fines present in the system after 4 hours of milling.

Table 6.1 – Summary of zeolite T particle size distributions before and after milling

Mill Time (hrs)	Particle Sizes (µm)		
	d_{10}	d_{50}	d_{90}
Unmilled	12.8	77.4	408.6
1	2.6	25.1	111.7
2	2.0	13.9	42.3
4	1.7	9.0	29.5
6	1.7	7.8	25.7
8	1.6	6.9	24.3

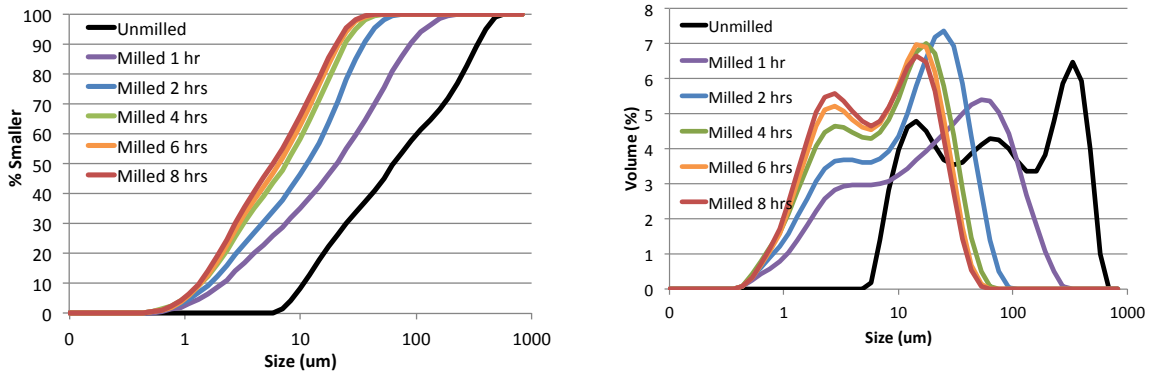

(a) (b)

Figure 6.2 - Particle size distribution of unmilled and milled zeolite T, (a) cumulative particle size distribution, (b) volumetric particle size distribution.

The effect of milling on the nitrogen-accessible surface area of the zeolite T is shown in Figure 6.3 and the materials' pore size distributions are shown in Figure 6.4. It is evident from Figure 6.3, that the surface area of the material is inversely correlated with particle size, as it trends upward until 2 hours of milling, at which time there are no further increases in surface area. Figure 6.4 confirms this hypothesis, as milling had little effect on the pore size distribution of the material.

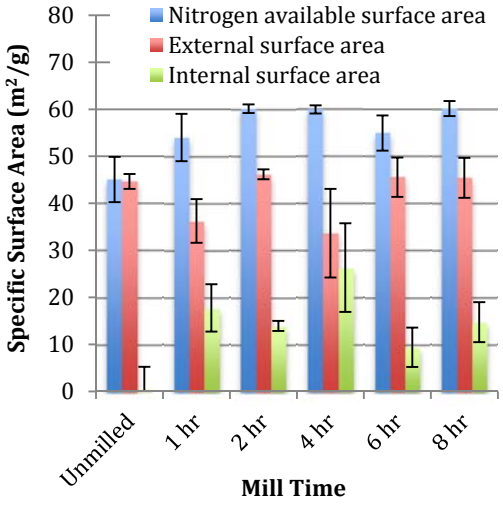

Figure 6.3 – Nitrogen available surface area of zeolite T before and after milling

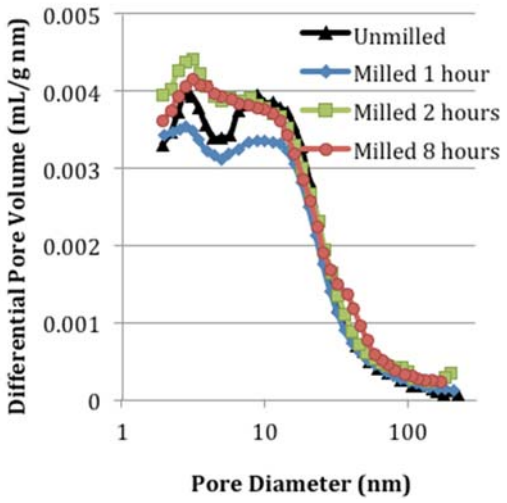

Figure 6.4 - Pore size distribution of milled and unmilled zeolite T

6.3.2 Zeolite Reactivity Characterization Results

The calcium hydroxide contents of hydrated pastes containing unmilled and milled zeolite T are shown in Figure 6.5. The pastes containing unmilled zeolite T showed evidence of the pozzolanic reaction, having lower calcium hydroxide contents than both the sample using inert quartz filler and the cement-only paste. As discussed in Chapter 2, Antoni et al. (2012) showed that a quartz filler slightly increased the amount of $Ca(OH)_2$ produced compared to a cement-only paste because it allows more space for hydration product growth. The same effect is shown in Figure 6.5. Reduction in $Ca(OH)_2$ content compared to the quartz filler sample is due to the pozzolanic reaction of the added zeolite. Additional work included in Appendix B investigated calcium hydroxide reducing ability of natural zeolites compared to another common type of filler, limestone, used in high limestone cements. Synergistic effects of using the two

types of materials used together were also investigated as part of that study. Refer to Appendix B for more information.

As far as the relationship between mill time and pozzolanicity of the zeolite is concerned, milling the zeolite for 1 hour did not change the zeolite pozzolanicity relative to the unmilled zeolite. The zeolite milled for 1 hour showed the same magnitude of reduction of calcium hydroxide as the unmilled sample. Milling times greater than 1 hour were successful in improving the calcium hydroxide consumption of the zeolite, with $Ca(OH)_2$ contents of the 28-day samples lower than for the paste with unmilled zeolite. Milling for 4 hours further increased the calcium hydroxide consumption, however further improvements were not seen with mill times greater than 4 hours.

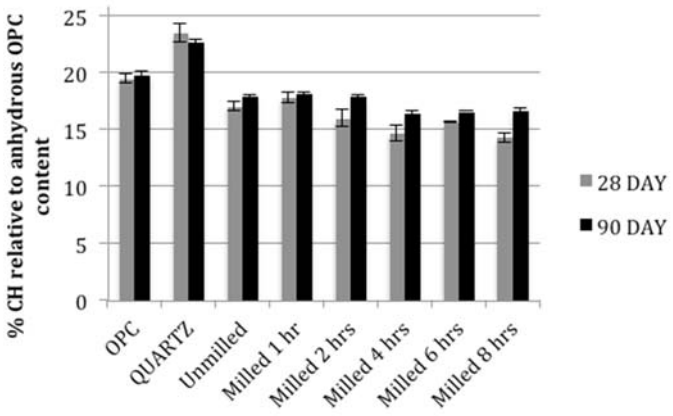

Figure 6.5 - $Ca(OH)_2$ content by weight of hydrated cement pastes containing 80-100% cement and 0-20% unmilled or milled zeolite T or quartz filler (w/cm = 0.4)

The results of the Chapelle test for unmilled zeolite T and zeolite T milled for 1 and 8 hours are shown in Figure 6.6. As the calcium oxide consumed by all samples is

the same, within error, to the unmilled sample, the results suggest that no change in zeolite pozzolanic potential occurred as a result of milling.

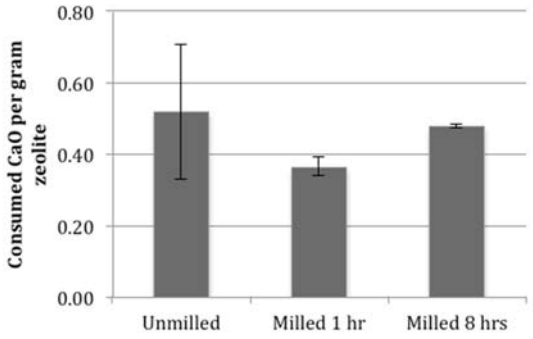

Figure 6.6 - Chapelle test results for unmilled and milled zeolite T

The effect of milling on the compressive strengths of the zeolite-cement mortars is shown in Figure 6.7. Milling the zeolite increased the compressive strengths of the mortars at all ages compared to the unmilled zeolite mortar. However, the zeolite milled for 8 hours generated significantly more compressive strength in a mortar than the zeolite milled for 2 hours. Strengths of the zeolite-cement mortars were initially lower than or equal to strengths generated by mortars containing a similar replacement level of a quartz filler, but the strengths of all zeolite-cement mortars exceeded that of the quartz filler mortars after 28 days. Strengths of mortars using the milled zeolites exceeded the quartz filler mortars after only 7 days and exceeded the strength of the cement mortar at 28 days.

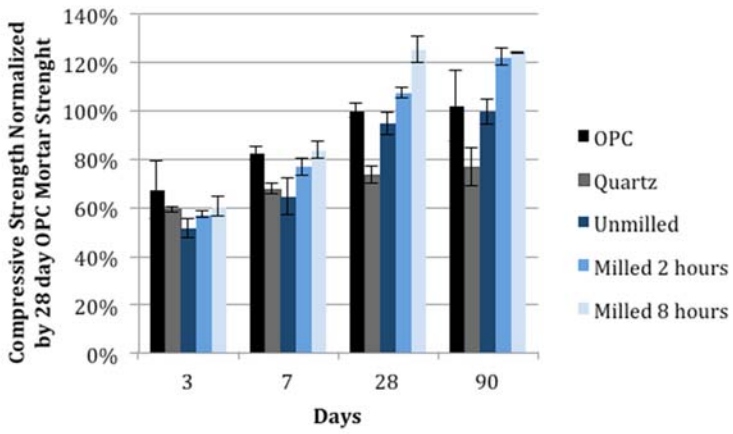

Figure 6.7 - Compressive strengths of cement mortars containing 80-100% cement and 0-20% of unmilled zeolite T, milled zeolite T, or an inert quartz filler (w/cm = 0.51)

6.3.3 Influence of Milled Zeolites on Cement Hydration Testing Results

The effects of milled Zeolite T on cement hydration kinetics are shown in Figure 6.8 to 6.11. Both the unmilled and milled zeolites decreased the time to the start of the acceleration period and also decreased the time to the maximum rate of heat release compared to the cement-only paste (Figure 6.9). Longer milling times correlated with greater reductions in times to the end of induction and the peak of heat release. Milled zeolites also increased the rate of reaction during the acceleration period compared to the cement-only, quartz and unmilled zeolite-cement pastes (Table 6.2). Similar to the results seen with the calcium hydroxide testing, initial milling for one and two hours resulted in increases in the rate of reaction during the acceleration period, shown in Table 6.2. Additional milling, for 4 hours, further increased the slope of the acceleration period but the rates of reaction during the acceleration period of the 4, 6 and 8 hour milled zeolite-cement pastes were equivalent. In addition, whereas the unmilled zeolite may have hindered cement hydration, evidenced by the lower maximum rate of heat released by the

cement compared to the cement-only paste (Figure 6.10), the pastes using milled zeolites generated greater rates of heat release per gram of cement than the cement-only paste as well as the quartz filler paste. Time of milling did not seem to make a significant difference in the magnitude of the maximum rate of heat release, shown in Figure 6.8 and 6.10, as all milled samples had similar maximum rates. Similarly, Figure 6.11 shows that, except for the paste using zeolite milled for 1 hour, all milled zeolite-cement pastes evolved similar amounts of heat over 72 hours.

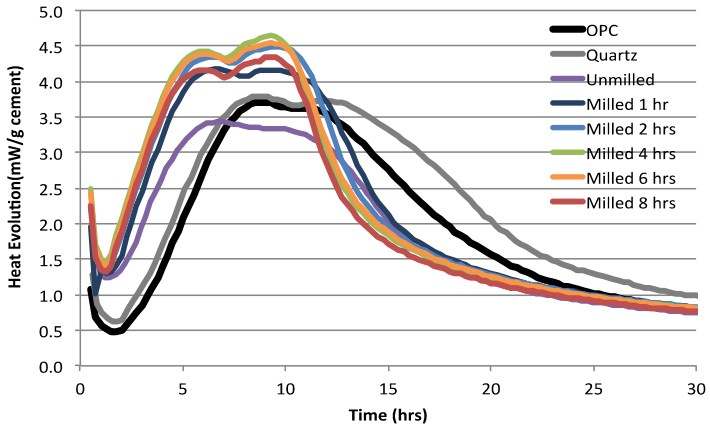

Figure 6.8 - Isothermal calorimetry (23°C) results of pastes with 80-100% cement and 0-20% unmilled or milled zeolite T or quartz filler (w/cm = 0.4)

Table 6.2 - Acceleration period slope in isothermal calorimetry (23°C) of pastes with 80-100% cement and 0-20% unmilled or milled zeolite T or quartz filler (w/cm = 0.4)

SCM/filler	Acceleration Period Slope (mW/g/hr)
None	0.66±0.05
Quartz	0.64±0.03
Unmilled zeolite T	0.60±0.11
Milled 1 hr zeolite T	0.76±0.06
Milled 2 hrs zeolite T	0.77±0.10
Milled 4 hrs zeolite T	0.83±0.08
Milled 6 hrs zeolite T	0.85±0.12
Milled 8 hrs zeolite T	0.83±0.07

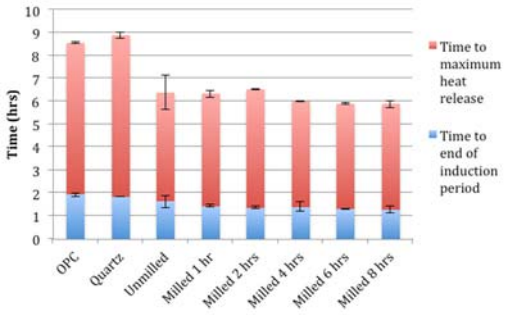

Figure 6.9 - Time to the end of the induction period and time to the maximum value of heat flow in isothermal calorimetry (23°C) of pastes with 80-100% cement and 0-20% unmilled or milled zeolite T (w/cm = X)

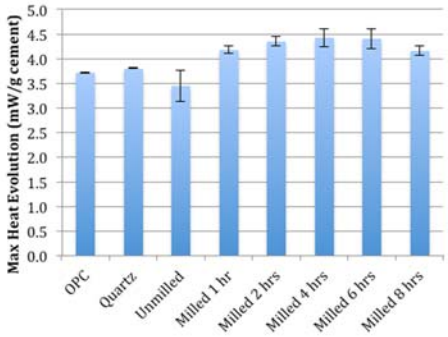

Figure 6.10 – Value of the maximum heat flow in isothermal calorimetry (23°C) of pastes with 80-100% cement and 0-20% unmilled or milled zeolite T (w/cm = 0.4)

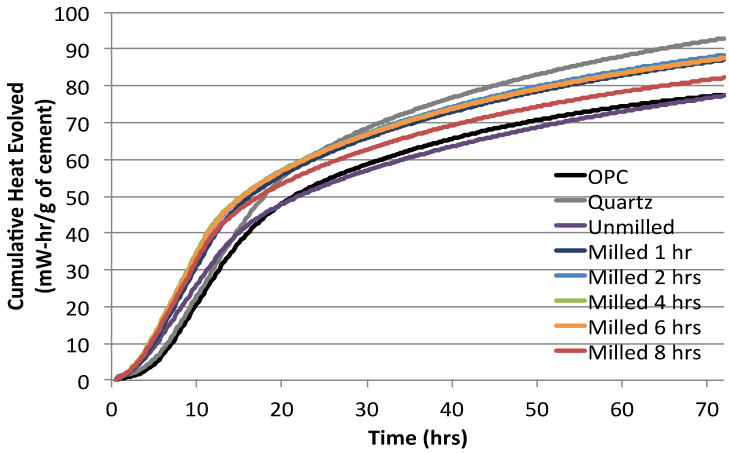

Figure 6.11 - Cumulative heat evolved over 72 hours during isothermal calorimetry (23°C) of 80-100% cement and 0-20% unmilled or milled zeolite T or quartz filler pastes (w/cm = 0.4)

6.4 Discussion of the Effects of Milling on Zeolite Pozzolanic Reactivity

The goal of the ball milling pretreatment was to improve the properties of the zeolite to allow it to react faster or more completely as a pozzolan, resulting in improved performance in cementitious systems. It was hoped that milling would result in reduced particle sizes, increased porosity, and a loss of zeolite crystallinity, creating a more

reactive material. The literature suggests that milling substantially reduces zeolite crystallinity with very short durations of milling (Charkhi et al. 2010, Kosanovic et al. 1995a,b,c, Zielinski et al. 1995, Ene 2007). However, nearly all of the studies of milled zeolites to date employed planetary ball mills capable of much greater forces than cylindrical ball mills with only a single axis of rotation, such as the mill used in this work and by the cement industry. It is evident from the XRD results shown in Figure 6.1 that the forces imposed on the zeolites in a horizontal rotary ball mill were not high enough to cause a reduction in zeolite crystallinity as in the studies using high energy planetary ball mills.

Although milling did not reduce the zeolite crystallinity, it did significantly reduce particle size and increase surface area of the zeolite, as shown in Figure 6.2 and 6.3. Contrary to previous work that showed that milling increased porosity through the creation of macropores (Zielinski et al. 1995), very little change occurred in the pore sizes of the material, shown in Figure 6.4, and it can be assumed that the increases in surface area in this work occurred only as a result of the reductions in particle size.

Performance tests on the milled zeolite showed that the pozzolanicity of the zeolite was increased by milling. Shown in Figure 6.5, zeolite milled for 2 hours or more reduced paste calcium hydroxide content relative to unmilled zeolite. However, milling for greater than 4 hours generated no additional calcium hydroxide reduction as pastes using the zeolites milled for 4, 6 and 8 hours all reduced the calcium hydroxide content by similar amounts. Evidence of increased pozzolanicity with milling was also shown in the increased compressive strengths of the zeolite-cement mortars. Milled zeolite-cement

mortars, shown in Figure 6.7, yielded significant increases in compressive strengths compared to the unmilled zeolite. Chapelle results, shown in Figure 6.6, indicated that milling did not affect the zeolite's pozzolanic potential, likely because this test is not sensitive to particle size effects since it is an accelerated test at elevated temperatures. Additional information concerning the ability of the Chapelle test to accurately gauge pozzolanic potential is given in Appendix A.

Particle size seems to play a large role in the pozzolanicity of the milled zeolites. However, particle size and filler effects (Antoni et al. 2012) do not entirely explain zeolite performance. For example, milling for 1 hour resulted in a 67% reduction in median particle size with no corresponding decrease in calcium hydroxide content. Additionally, although the particle size reductions slowed after 4 hours of milling, a substantial increase in compressive strengths was generated for mortars using zeolites milled for 8 hours versus those milled for 2 hours. Therefore, while performance improvements are definitely linked, they are not completely explained by the decreased particle size of the zeolites used in the compressive strength mortars. Other researchers have concluded that milling can result in breakage of the surface Si-O-Si and Si-O-Al bonds of the zeolite structure (Charkhi et al. 2010, Kosanovic et al. 1995a) and this may have played a role in the unexpected performance results. Longer milling times may have generated greater quantities of broken Si-O and Al-O bonds, enabling the zeolite crystal structure to more easily dissolve and react than unmilled zeolites and zeolites milled for shorter times which may lack, or have fewer broken chemical bonds. However, testing the surface characteristics of the zeolites after milling is beyond the scope of the work

presented here. The relationship between zeolite physical and chemical properties and performance is further explored in Chapter 8.

In addition to increased pozzolanicity, milled zeolites also contributed an accelerating effect to cement hydration reactions, decreasing both the time to the start of the acceleration period as well as the time of the maximum C_3S reaction peak, shown in Figure 6.8 to 6.10. These times decreased corresponding to the particle size, with the largest reductions in time seen in the 8 hour milled zeolite. The rate of nucleation and growth, expressed by the slope of the acceleration period and peak rate of heat release values shown in Table 6.2 and Figure 6.10, were also increased for all milled zeolites relative to both the cement-only, quartz filler and the unmilled zeolite-cement pastes. Both of these effects are similar to effects seen in the literature with the use of very fine inert quartz fillers (Oey et al. 2013, Rahhal and Talero 2005), finer than the one used in this study. However, the length of the hydration reactions during the deceleratory period until reaching steady-state conditions, evidenced by the rate of heat release during the deceleratory period compared to the cement-only paste and quartz filler paste, was much shorter for the milled-zeolite pastes compared to the quartz filler-paste. This may indicate that the zeolite particles initially act as nucleating agents, speeding up the timing and rate of reactions, but are not contributing to the dilution effect often seen with fillers which tend to extend the magnitude of hydration during the first 72 hours (Lothenbach et al. 2011).

6.5 CONCLUSIONS

Zeolite T was milled using a ball mill in order to mimic a pretreatment that could be implemented in the field using existing industrial SCM and cement clinker ball mills (Ene 2007; Jankovic et al. 2004). Zeolite T was milled for 1, 2, 4, 6, or 8 hours and characterized to determine the changes with ball milling to zeolite crystallinity, particle size, surface area, porosity. Performance was determined by measuring the calcium consumption in a calcium hydroxide solution, tracking reductions in calcium hydroxide in zeolite-cement pastes due to the pozzolanic reaction, and testing the compressive strengths of zeolite-cement mortars. The effect of milling on early age cement hydration was also investigated.

Ball milling of zeolites significantly improved the performance of the zeolite used in cementious mixtures, increasing the pozzolanicity of the zeolites as well as increasing compressive strengths of mortars containing milled zeolites. Milled zeolites also accelerated cement hydration reactions seen in isothermal calorimetry and increased the maximum rate of heat release of the milled zeolite-cement mixtures. Milling zeolites for four hours or longer, corresponding to an average particle size (d_{50}) of 9 μm or less, yielded the greatest gains in reactivity. These improvements were primarily due to decreased particle sizes with milling, but undetected chemical changes to the zeolites with increased mill times may have also contributed to the enhanced performance seen in ball milled zeolite-cement mixtures.

Chapter 7: Zeolite Pretreatment Methods to Increase the Reactivity of Zeolites for Use as SCMs – Cation Exchange

7.1 INTRODUCTION

The basic structure of zeolites is a three-dimensional framework of silicate tetrahedra. Substitutions of aluminum within the crystal structure of the zeolite result in a net negative charge throughout the structure, which is balanced by cations such as Na^+, K^+ and Ca^{2+} (Pabalan and Bertetti 2001). The cations sit within the holes formed by the aluminosilicate tetrahedra, and are only loosely bound to the structure, making it possible for the cations to be replaced with other cations of similar size and charge, a process known as cation exchange.

It has been suggested that the type of exchangeable cations present in a zeolite influences pore solution chemistry and both short- and long-term pozzolanic reactivity, although these studies have primarily investigated zeolite reactions in calcium hydroxide solutions, not in mixtures of zeolites and cement (Lilkov et al. 2011a; Mertens et al. 2009; Snellings et al. 2010). In determining how cation type affects pozzolanic reactivity, Mertens et al. (2009) and Snellings et al. (2010) found that after 28 days, clinoptilolite exchanged to K^+ form reacted with a greater quantity of lime in solution than did clinoptilolite exchanged with Ca^{2+} or Na^+ ions, suggesting that K^+ rich zeolites have greater pozzolanic reactivity versus Ca^{2+}or Na^+ rich zeolites. It was suggested that the pozzolanicity of the zeolites was increased due to increased hydroxyl contents that are associated with K^+-exchanged zeolite, resulting in higher pH, which increases silica solubility and leads to greater zeolite pozzolanicity (Mertens et al. 2009). Snellings et al.

(2010) observed similar trends in cementitious mixtures, with higher calcium content zeolites showing lower rates of pozzolanic reaction.

The results of previous studies are very limited, but point towards cation exchange being a good treatment to increase the pozzolanic reactivity of zeolites used as SCMs. However, none of the previous studies examined the effect of different cations on zeolite reactivity in actual cementitious systems. Therefore, the study presented here examined the effects of K^+, Na^+ or Ca^{2+} homoionic forms on the properties of natural clinoptilolite zeolite and gauged their effects on calcium hydroxide content in cement-zeolite pastes, an indicator of pozzolanicity.

7.2 EXPERIMENTAL METHODS AND MATERIALS

7.2.1 Zeolite Sample Preparation

7.2.1.1 Cation Exchange Solutions

A single exchange method, described by other researchers (Inglezakis 2005) and in more detail in section 7.2.1.2, was used to quantify the total cation exchange capacity of the zeolite. This procedure involved two solutions, shown in Table 7.1. In addition to cation exchange capacity testing, three solutions were used to create homoionic forms of zeolite T, used for testing the effect of different cationic forms of zeolite on pozzolanic reactivity. The three solutions used are shown in Table 7.2.

Table 7.1 – Solutions for cation exchange capacity testing

Exchange Step	Solution Used	Chemical Formula
Na^+-exchange	1M Sodium Chloride	NaCl
NH_4^+-exchange	2M Ammonium Acetate	$NH_4C_2H_3O_2$

Table 7.2 – Solutions used to create homoionic cation forms

Zeolite Homoionic Form	Solution Used	Chemical Formula
K^+	1M Potassium Acetate	$C_2H_3KO_2$
Na^+	1M Sodium Acetate	$C_2H_3NaO_2$
Ca^{2+}	1M Calcium Acetate	$C_4H_6CaO_4 \cdot H_2O$

7.2.1.2 Cation Exchange Capacity Sample Preparation

The cation exchange capacity of the zeolite was determined using a two step exchange procedure in order to determine the total amount of cations in meq/g the zeolite was capable of uptaking from solution. The cation exchange procedure was similar to procedures used by other researchers (Inglezakis 2005; Kitsopoulos 1999). General cation exchange capacities are available in literature, but vary for each zeolite source, depending upon the amount of aluminum ions substituted into the zeolite crystal structure. Therefore, it was decided to test the zeolites used in this study experimentally. The single exchange procedure used involved two steps: (1) preparation of a homoionic zeolite form using 1M sodium chloride (NaCl) and (2) re-exchange of the intralayer sodium cations using a 2 equivalent/L ammonium acetate ($NH_4C_2H_3O_2$).

In the first step, in order to determine the cation exchange capacity, 10 g of zeolite was first converted to its sodium homoionic form by soaking the zeolite in a100 mL 1M NaCl solution for 10 days. The NaCl solution was decanted and replaced 7 times during the 10 days in order to maintain a large diffusion potential between the solution and the

cations present in the zeolite. The zeolite and exchange solution were combined and sealed in a 125mL Nalgene polyethelene bottle in a nitrogen environment in order to prevent undesirable complexation reactions occurring between the zeolite, NaCl solution and the air. In order to prevent settlement and maintain constant contact between the zeolite and the solution, the sample container was continuously rotated on a U.S. Stoneware rotary mill for 24 hours at 20 rpm. The sample was filtered before each replacement of the solution using a 5 cm Buchner funnel and Fisherbrand P5 Qualitative filter paper with 10 μm pore size.

In the second step, exchange of the Na^+ cations with NH_4^+ was accomplished by exposing the zeolite to a 100 mL 2N NH_4Ac solution for ten days, separating the solution and zeolite through filtration and replacing the solution eight times. The solution from each decant was reserved for testing to determine the total exchanged sodium content (i.e. the amount of sodium replaced by ammonia) using a Varian 710-ES Inductively Coupled Plasma-Optical Emission Spectrometer. The spectrometer was calibrated using seven standard solutions of 30 μg/L, 100 μg/L, 500 μg/L, 1 mg/L, 10 mg/L, 100 mg/L sodium (Fluka Analytical TraceCert). The total concentration of sodium ions in solution was determined to be the cation exchange capacity of the zeolite.

7.2.1.3 Cation Exchanged Zeolite Sample Preparation

To prepare homoionic natural zeolite forms, 50 g of zeolite T was ground to pass the #100 sieve and dried for at least 24 hours in a low vacuum desiccator. The zeolite was then combined with 1M solutions of potassium acetate, sodium acetate or calcium acetate with of 1g zeolite to 10 mL of solution in polyethylene bottles. The samples were

continuously mixed at 20 rpm on a U.S. Stoneware rotary mill for 20 days. In order to maintain a high concentration gradient between the solution and the cations present in the zeolite, the sample was centrifuged and the solution was refreshed after 3 and 12 days. After 20 days the sample was centrifuged, and the solution was decanted and discarded. Each sample was washed with deionized water, centrifuged and decanted four times in order to remove acetate ions from the sample. Samples were then dried in a 60°C oven for 24 hours, lightly ground to return them to powder form and stored in a vacuum desiccator for at least 24 hours before testing.

Figure 7.1 - Cation exchange treatment setup

7.2.2 Zeolite Physical and Chemical Characterization Testing

Characterization testing was completed in order to determine what factors resulting from cation exchange contributed to changes in zeolite reactivity in

cementitious systems. Characterization testing tracked changes in the phases present in the zeolite samples, as well as particle size, surface area and pore size, as discussed in Chapter 3.

7.2.2.1 Zeolite Reactivity Testing

Changes to zeolite pozzolanic reactivity after cation exchange were tracked through two methods of measuring the pozzolanic reaction: measurement of the calcium hydroxide content of hydrated zeolite-cement pastes; and through the Chapelle test, which measures the amount of calcium consumed by a sample in aqueous solution, as described in Chapter 3.

7.2.2.2 Effects of Zeolite Ionic Form on Cement Hydration

Isothermal calorimetry was used to examine the effect of cation-exchanged zeolite on the rate of hydration of cement pastes according to the procedures outlined in section 3.1.3.1. In order to help understand the effect of possible charge balancing cation releases into the cement paste on the cement hydration using cation-exchanged zeolite-cement pastes, cement pastes were also studied that included an addition of Ca^{2+}-, Na^{+}- or K^{+}-acetate, with and without untreated zeolite. Results of the cation addition testing are shown in Appendix C.

7.3 RESULTS

7.3.1 Physical and Chemical Characterization Testing Results

The results of the cation exchange capacity testing described in section 7.2.1.2 are shown in Table 7.3. Values shown are the quantity of sodium in the solution separated from the zeolite by filtration. The sodium in the solution was assumed to be present as a result of exchanging NH_4^+ ions from the exchange solution into the zeolite crystal structure, replacing Na^+ present from the first step of the exchange process. The results are an average of two duplicate samples.

As is clear from Table 7.3, the exchange of Na^+ cations from the zeolite occurred rapidly, with most of the cations having been released by exchange number three. The total cation exchange capacity, equal to the cumulative amount of cations in solution at the end of the exchange period, was found to be 1.36 meq/g of zeolite. This is less than the cation exchange capacity of 2.22 meq/g calculated for clinoptilolite based on the idealized unit cell formula for clinoptilolite (Colella 1996; Pabalan and Bertetti 2001), but well within the range of 1.09-2.25 meq/g that has been experimentally determined for impure natural clinoptilolite samples (Kitsopoulos 1999, Mertens et al. 2009).

Table 7.3 - Quantity of Na^+ cations present in solution filtered from the zeolite sample before each solution refresh during the second step of the cation exchange capacity testing

Solution Refresh Number		Quantity of Na+ in solution (meq/g zeolite)
	1	1.2070 ± 0.0266
	2	0.1006 ± 0.0046
	3	0.0287 ± 0.0008
	4	0.0054 ± 0.0016
	5	0.0059 ± 0.0003
	6	0.0031 ± 0.0008
	7	0.0033 ± 0.0001
	8	0.0094 ± 0.0009
Total Quantity of Na^+ Cations Released from the Zeolite		1.3634 ± 0.0357

The crystalline phases present in each zeolite sample before and after cation exchange are shown in Figure 7.2. Very few differences occurred in the samples with the exception of the broad humps from 5-7° 2θ, which are assumed to be artifacts of testing. The lack of differences in the XRD reflections of the different cation form materials has been noted by other researchers for clays, which show only sight differences in peak intensities depending on cation type (Bookin and Drits 1993).

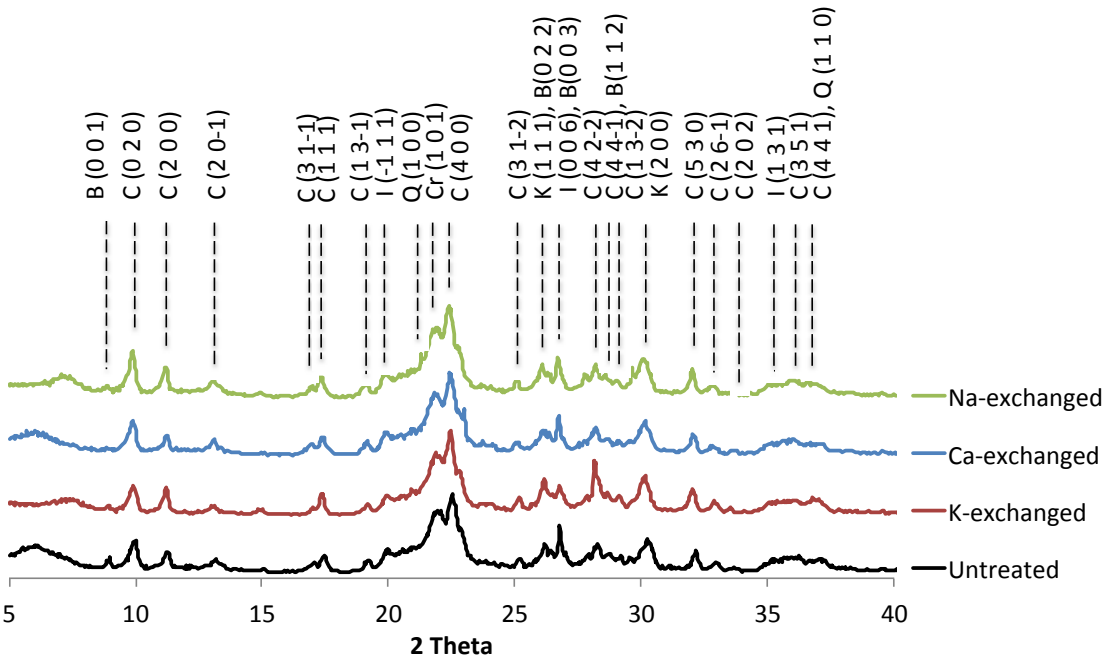

Figure 7.2 - Phases present in the zeolite T before and after cation exchange. Phases and their designations are: B-bentonite, C-clinoptilolite, I-illite, Q-quartz, Cr-cristobalite, K-potassium halite. Numbers in parenthesis indicate the d-spacing of the reflection.

The nitrogen available specific surface areas of the untreated and cation exchanged zeolites are shown in Figure 7.3. Replicate tests were not performed and the error shown is the representative error obtained from replicate testing of the untreated zeolite. The surface area of the zeolite was increased after the cation exchange treatments, with the K^+-exchanged zeolite showing the greatest gain in surface area. This is likely a result of differences in the hydrated radii of the cations. The hydrated radii of cations present in the zeolite structure are shown in Table 7.4. The increase in surface area seen after cation exchange treatment may be due to the removal of magnesium cations, which have a large hydrated radius compared to the potassium, sodium, and calcium cations (Khaleghian-Moghadam and Seyedeyn-Azad 2009, Erdogan et al. 2010). However, testing for magnesium removal was beyond the scope of this research. By the same logic, the greater increase in surface area resulting from cation exchange treatment

with potassium acetate relative to the sodium or calcium solutions may be due to the smaller size of the hydrated potassium cations, which could allow more nitrogen to fill the zeolite pore structure and increase the nitrogen available specific surface area of the zeolite. However, increased zeolite surface area could also simply be a result of the removal of soluble pore-blocking matter during the cation-exchange process.

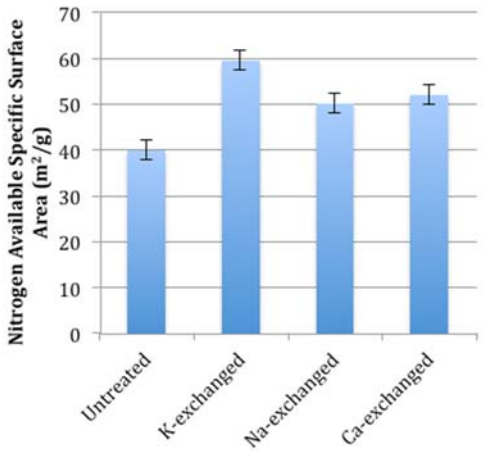

Figure 7.3 - Nitrogen-available specific surface area of untreated zeolite and zeolite exchanged with potassium-acetate, sodium-acetate or calcium-acetate

Table 7.4 - Radii of hydrated cations present in the zeolite crystal structure (Kielland 1937)

Cations	Hydrated Ionic Radius (pm)
K^+	150
Na^+	225
Ca^{2+}	300
Fe^{2+}	300
Mg^{2+}	400

Cation exchange of the zeolites with sodium or potassium acetate resulted in very little change to the zeolite particle size distribution, aside from elimination of the largest particle size material, likely as a result of material handling and processing during cation-exchange treatment. Exchange with the calcium acetate, however, resulted in a shift in

the volume of material in the range of approximately 100 µm to approximately 30 µm. Reduction in the zeolite particle size may have occurred as a result of breakdown of the zeolite crystal structure bonds due to induced structural distortions from the large calcium cations (Khaleghian-Moghadam and Seyedeyn-Azad 2009).

Table 7.5 - Particle size changes of the zeolite exchanged with potassium-acetate, sodium-acetate or calcium-acetate

Zeolite ionic form	Particle sizes		
	d_{10}	d_{50}	d_{90}
Untreated	2.62	33.3	142.3
Ca^{2+} exchanged	3.1	24.5	107.7
K^{+} exchanged	2.5	30.9	131.7
Na^{+} exchanged	2.2	27.6	114.1

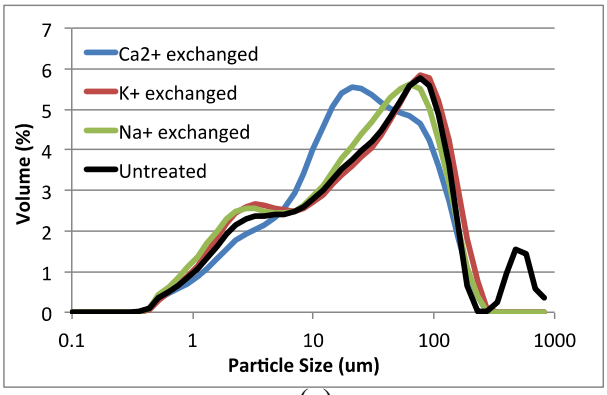

(a)

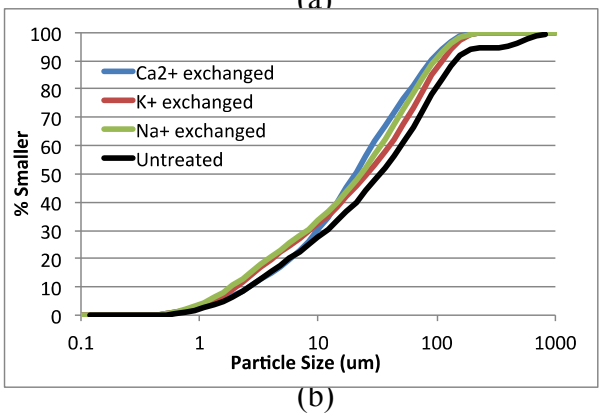

(b)

Figure 7.4 - Particle size distribution of untreated zeolite and zeolite T exchanged with potassium-acetate, sodium-acetate or calcium-acetate, (a) cumulative pore size distribution, (b) volumetric pore size distribution.

7.3.2 Zeolite Reactivity Characterization Results

Figure 7.5 shows the effect of the different cation forms of the zeolite on calcium hydroxide in cement pastes. Calcium hydroxide contents of pastes made using homoionic zeolite forms were reduced compared to the calcium hydroxide content of the untreated form. The reductions did not appear to be dependent on the cationic form of the zeolite, however, as the calcium hydroxide content of pastes using K-exchanged, Ca-exchanged and Na-exchanged zeolites were the same, within error, at both 28 and 90 days of hydration.

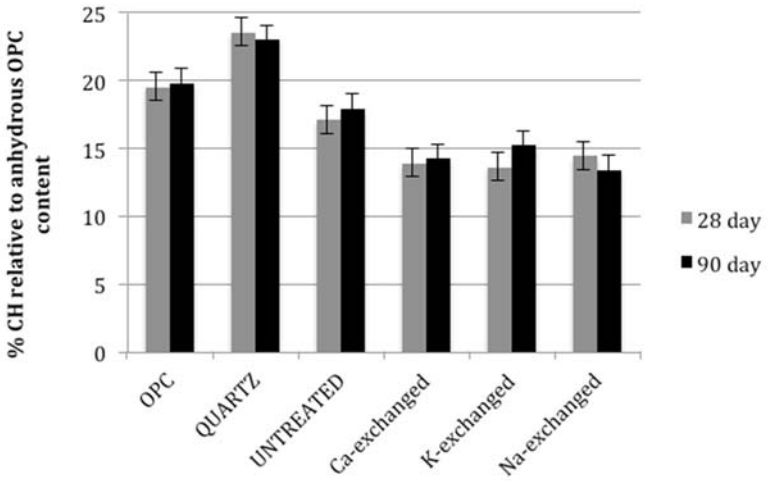

Figure 7.5 - $Ca(OH)_2$ content by weight of hydrated cement pastes containing 80-100% cement and 0-20% untreated zeolite T and zeolite T cation-exchanged with Ca^{2+}, K^+ or Na^+ or quartz filler, (w/cm = 0.4)

The results of the Chapelle test shown in Figure 7.6 may indicate that zeolite cationic form affects the pozzolanicity of the zeolite as measured by this test. The K-exchanged zeolite consumed more calcium oxide in solution than the untreated zeolite. The Na- and Ca-exchanged zeolites also appear to have consumed a greater quantity of

calcium oxide than the untreated zeolite, however, due to the large error for the untreated sample, this difference is not definitive.

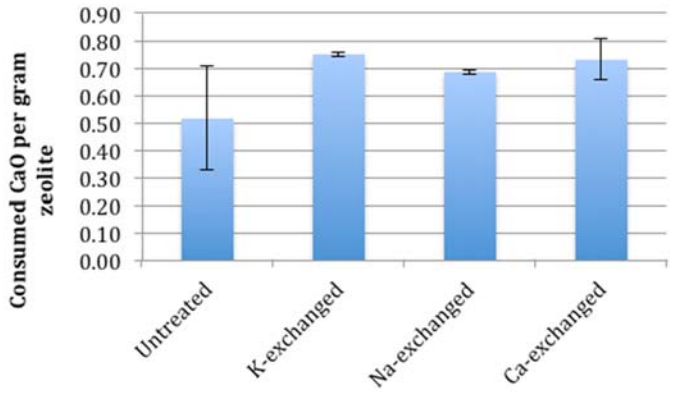

Figure 7.6 - Chapelle test results for untreated zeolites and zeolites treated with hydrochloric acid

7.3.3 Influence of Cation Exchanged Zeolite on Cement Hydration Testing Results

Figure 7.7 to 7.10 shows the effect of cation exchange on the hydration kinetics of the zeolite-cement pastes in comparison to a cement-only paste, a paste with quartz filler and an untreated zeolite-cement paste. It is evident from Figure 7.7 and 7.8, that use of untreated or cation-exchanged zeolites resulted in a significant acceleration of hydration compared to the cement-only and quartz filler pastes with significantly reduced time to the start of the acceleration period and time to the maximum rate of heat release. However, the pastes using cation-exchanged zeolite were slightly retarded compared to the untreated zeolite-cement paste. Additionally, shown in Figure 7.7, the homoionic zeolite forms each had a very different effect on early age heat evolution of the cement paste, impacting the rate of reaction during the acceleration period, the time to the peak rate of heat release and the magnitude of the maximum rate of heat release. Shown in

Figure 7.8, use of the Na-zeolite resulted in the greatest acceleration of the paste's heat release, resulting in the least time to the maximum rate of heat release. The Na-zeolite also had the greatest rate of reaction during the acceleration period, evidenced by the slope of the curve during that period shown in Table 7.6, as well as the highest peak rate of heat release, shown in Figure 7.7 and 7.9. Table 7.6 also shows that the Ca- and K-exchanged zeolites reduced the rate of heat release compared to pastes with untreated zeolite, but had rates of reaction during the acceleration period release similar to the cement only paste. The maximum rate of heat release of the Ca-exchanged zeolite paste, shown in Figure 7.9, was also comparable to that of the cement-only and quartz filler pastes, while the K-exchanged zeolite paste had a greater maximum rate of heat release compared to the cement only and quart filler pastes. In addition, use of Na- and K-exchanged zeolites increased the magnitude of, and decreased the time required for, the C_3A peak, evidenced by larger second heat peaks for these two samples. See Appendix C for more information about the effects of cations present in the zeolite-cement system on cement hydration reactions.

The graph of the cumulative heat evolution over the first 72 hours after mixing, shown in Figure 7.10, shows that the untreated zeolite and Na- and K-exchanged zeolite-cement pastes evolved greater cumulative quantities of heat during the first 18 hours of hydration compared to the cement-only and quartz filler pastes. Similarly, the Ca-exchanged zeolite-cement paste evolved a greater quantity of heat over the first 15 hours. However, after 18 hours (15 for the Ca-exchanged zeolite paste) the quantity of heat

evolved by the zeolite pastes was greater than for the cement-only paste but less than for the quartz filler paste.

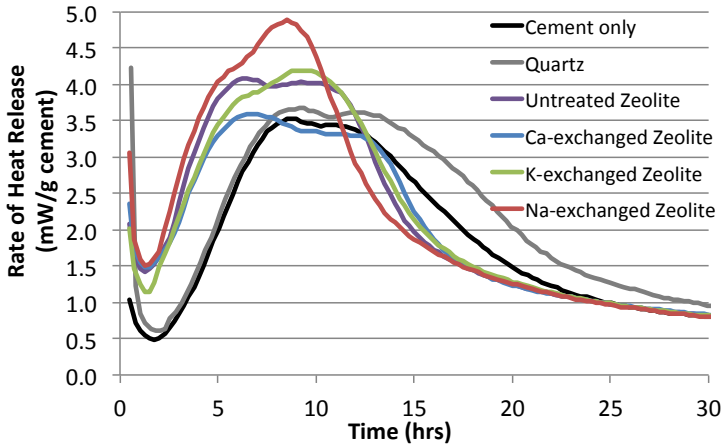

Figure 7.7 – Isothermal calorimetry (23°C) results of pastes with 80-100% cement and 0-20% untreated or cation-exchanged zeolite T (w/cm = 0.4)

Table 7.6 – Acceleration period slope in isothermal calorimetry (23°C) of pastes with 80-100% cement and 0-20% untreated or cation-exchanged zeolite T or quartz filler (w/cm = 0.4)

SCM/filler addition	Acceleration Period Slope (mW/g/hr)
None	0.69±0.05
Quartz	0.62±0.03
Untreated zeolite T	0.76±0.11
Ca-exchanged zeolite T	0.66±0.05
K-exchanged zeolite T	0.70±0.05
Na-exchanged zeolite T	0.74±0.05

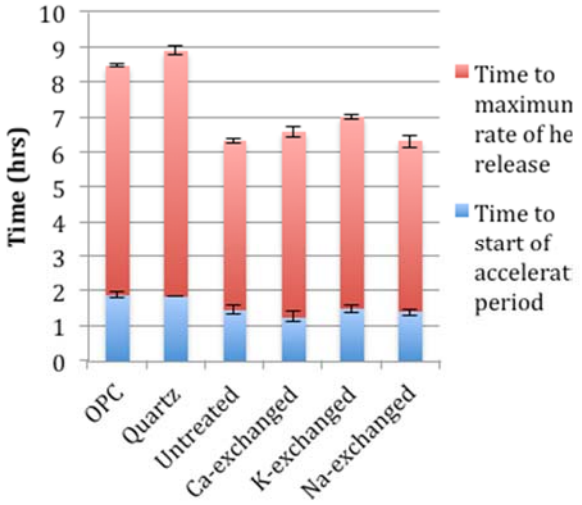

Figure 7.8 - Time to the end of the induction period and time to the maximum value of heat flow in isothermal calorimetry (23°C) of pastes

with 80-100% cement and 0-20% untreated or cation-exchanged zeolite T (w/cm = 0.4)

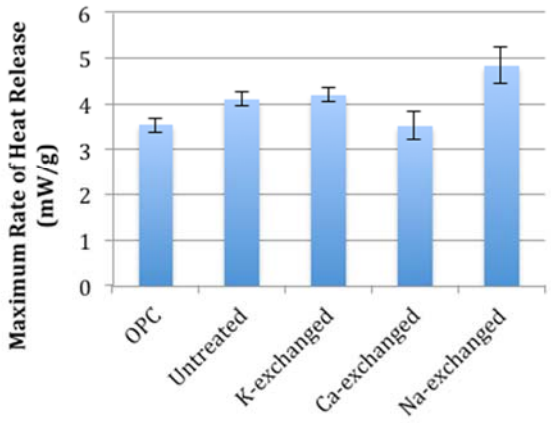

Figure 7.9 - Value of the maximum heat flow in isothermal calorimetry (23°C) of pastes with 80-100% cement and 0-20% untreated or cation-exchanged zeolite T (w/cm = 0.4)

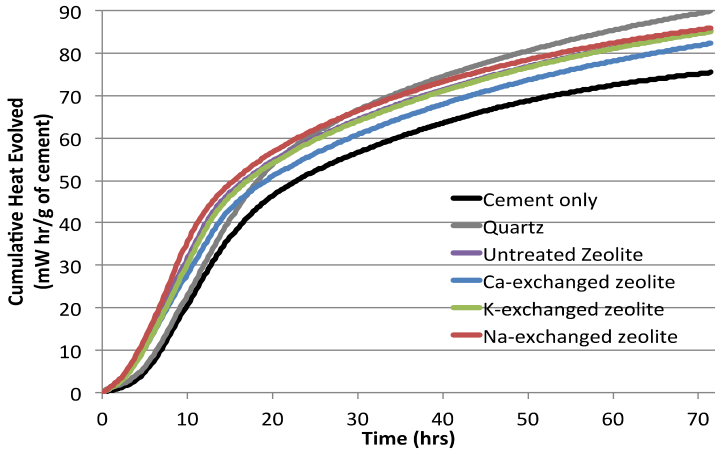

Figure 7.10 - Cumulative heat evolved in isothermal calorimetry (23°C) over 72 hrs by 80-100% cement and 0-20% untreated or cation-exchanged zeolite T or quartz filler (w/cm = 0.4)

7.4 Discussion of the Effects of Cation Exchange on Zeolite Pozzolanic Reactivity

Phases present in the zeolite sample and the relative crystallinity of the sample remained unchanged after cation exchange, shown in Figure 7.2. The nitrogen surface area, shown in Figure 7.3 was increased through cation-exchange treatment and the

particle size of the material, shown in Figure 7.4, was also slightly reduced. However, it is not known whether these changes were a result of exchanging the cations of the material, due to dissolution of soluble phases upon exposure of the zeolite to the exchange solutions or as a result of handling and processing of the material during treatment.

Regardless of the reason for the differences in surface area and particle size, cation exchange treatment did seem to result in increases to the pozzolanic reactivity of the zeolite. In Figure 7.5, cation exchange treatment reduced the calcium hydroxide content of the pastes relative to the untreated zeolite paste. Similarly, the Chapelle test results in Figure 7.6 show that the potassium form, and perhaps also the sodium and calcium forms of the zeolite can consume greater quantities of CaO from solution than the untreated zeolite. It is not clear why cation exchange treatment resulted in an increase in the zeolite's pozzolanicity, although other studies have similarly shown that conversion to a homoionic form also significantly increases cation exchange capacity (Kesraoul-oukl et al. 1993). It is theorized that these results could be due to increased access to the zeolite channels due to unblocking of the pores, which occurs during acid treatment and may also be applicable for the environment the zeolite is exposed to for cation exchange (Ates and Hardacre 2012). The increase in pozzolanicity of the zeolite after cation exchange treatment could also be a result of changes in the ionic charge of the material with cation exchange treatment, as cation content can affect material acidity (Ates and Hardacre 2012; Matias et al. 2009; Ward 1968).

The type of cation present, however, did not appear to have a significant effect on the performance of the zeolite, an effect that contrasted with previous published results (Mertens et al. 2009). Mertens et al. (2009) found that potassium exchanged zeolites reacted with greater quantities of lime in a $Ca(OH)_2$ solution compared with the other cation forms. Although these results were confirmed in this study by the Chapelle test results shown in Figure 7.6, the effect did not translate to the cement-zeolite pastes, as all exchanged forms had similar quantities of $Ca(OH)_2$ remaining in the paste, shown in Figure 7.5.

It is interesting to note that the Ca-exchanged zeolite did not remove lower quantities of calcium from the system compared to the Na- and K-exchanged zeolites. If cation exchange isotherms dominated the reactions in the Chapelle test's solution, it would be expected that the Ca-exchanged zeolite already contained the maximum amount of calcium cations it is capable of carrying, and should be unable to remove further calcium cations from the system. That the Ca-exchanged zeolite continued to remove CaO from the system gives evidence of chemical reaction occurring between the zeolite and calcium as opposed to removal of calcium solely through exchange of cations. The results of the calorimetry testing support the conclusions of previous research indicating first day reaction rates of homoionic cation-exchanged zeolites, evidenced by acceleration of the heat evolution, greater slope of the rates of heat evolution during the acceleration period and larger peak rates of heat evolution shown in Figure 7.7 to 7.10 and Table 7.6, follow the order of: $Na^+ > K^+ > Ca^{2+}$ (Snellings et al. 2010). This order is interesting, as prior research has indicated that the effectiveness of cations at accelerating

cement hydration follows the order: $Ca^{2+}>K^{+}>Na^{+}$ (Kantro 1974), which is opposite the effect shown in this study. The greater reaction rate of Na- and K-exchanged zeolites has been attributed by other researchers to increased pore solution pH with the presence of Na^{+} and K^{+} ions, which also leads to greater solubility of silica (Mertens et al. 2009). Accelerated reaction rates for the cation-exchanged zeolites, in general, may also be due to effects of residual anions from the cation exchange procedure. Inconsistencies between the cation reactivity order found by this study and previous work on materials used to accelerate hydration reactions may be related to the anions studied, as acetate anions have been shown to have essentially no affect on hydration rates, (Edwards and Angstadt 1966) compared to the high accelerating potential of the Cl^{-} ions investigated in conjunction with the cations used by Kantro (1974). Accelerations of the cation-exchanged zeolite-cement pastes may also be due to destabilization of the zeolite crystal structure due to increased cation content and changes in zeolite surface charge. As Allen et al. (2009) showed, the type of cations in zeolite pores changes the ionic density of the lattice and thus strongly influences the adsorption of polar molecules. This may affect the interactions between the zeolite and other constituents of the cementitious mixture and result in the increases in heat evolution seen with the cation-exchanged zeolites.

7.5 CONCLUSIONS

Natural zeolite was treated with Na-, K-, or Ca-acetate salt solutions in order to create a homoionic form of zeolite T. The total cation exchange capacity of zeolite T was tested and found to be 1.36 meq/g of zeolite, which was low compared to the theoretical clinoptilolite cation exchange capacity (2.22 meq/g), but within the range of 1.09-2.25

meq/g that has been experimentally determined by other researchers for impure natural clinoptilolite samples (Kitsopoulos 1999, Mertens et al. 2009). The homoionic zeolite forms were characterized using XRD, laser particle size analysis, and nitrogen adsorption, and the effect of the zeolite on the performance of the zeolite was tested through the determination of calcium hydroxide contents of cement pastes containing the exchanged zeolites as well as by measurement of the amount of calcium removed by the zeolite from solution in the Chapelle test.

Cation exchange treatment resulted in increases in zeolite nitrogen surface area and reductions in particle size that led to small improvements to zeolite pozzolanicity, as evidenced by lower calcium hydroxide contents present in zeolite-cement pastes, compared to pastes using the untreated zeolite, as well as increased calcium consumption during the Chapelle test. Cation exchanged zeolites also changed cement hydration kinetics, accelerating the hydration of pastes in which they were included, dependent upon the cation form of the zeolite. The Na-exchanged zeolite was most effective in increasing hydration rates out of the zeolite-cement pastes tested, although the cumulative heat evolved at 72 hours was not increased for the Na-exchanged zeolite-cement paste compared to the untreated zeolite. In general, cation exchange treatment does not appear to be an effective method for treating natural zeolites to improve their properties and performance for use as a supplementary cementitious material.

Chapter 8: Discussion of Factors Affecting Natural Zeolite Reactivity in Cementitious Systems

8.1 INTRODUCTION

In order to effectively engineer good systems of any type, it is essential to understand the mechanisms through which system components interact. For zeolite-cement systems such mechanisms are poorly understood, with studies describing a large variety of factors that control the development of properties of zeolite-cement systems without converging on accepted mechanisms. For example, several studies have suggested that framework SiO_2/Al_2O_3 ratio has an influence on both short and long-term reactivity of zeolites with higher silica content resulting in greater pozzolanic activity (Snellings et al. 2010, Martinez-Ramirez et al. 2006), and reactive silica content has also been shown to play a role in pozzolanic reactivity and in the development of mechanical properties of the zeolite-cement system (Yilmaz et al. 2009). However, another study found early reactivity to be linked to external surface area, while only long-term reactivity was based on SiO_2/Al_2O_3 ratio (Lilkov et al. 2011). Zeolite cation content has also been shown to affect reactivity, with Na^+- and K^+- zeolites reacting with a greater quantity of lime in solution than Ca^{2+}- zeolites (Mertens et al. 2009, Snellings et al. 2010). Fineness and percent crystallinity also play important roles in zeolite interactions with cementitious system components, with finer zeolite powders resulting in greater reduction in pore solution pH (Naiqian and Tingyu 1998). More highly crystalline materials were shown by Naiqian and Tingyu (1998) to have a greater propensity for reducing calcium hydroxide, an indication of pozzolanic reactivity.

The research highlighted in the previous paragraph suggests that zeolites used as SCMs can generate adequate or improved properties in cementitious systems; however, these studies have not defined which parameters actually govern the development of material properties in a zeolite-cement system or quantified what zeolite properties are necessary to produce a desired level of performance. This study used data from material and reactivity testing discussed in this dissertation in chapters 4-7 to establish these relationships.

8.2 TESTING AND ANALYSIS METHODOLOGY

Significance testing and single or multivariable regression analysis were performed in order to determine the strength of relationships between zeolite material properties (average particle size, nitrogen available specific surface area, SiO_2/Al_2O_3 ratio, cation content) and performance parameters (compressive strength, calcium hydroxide content, rate of reaction during the cement hydration acceleration period, time to the start of the acceleration period, time to the maximum rate of heat release, magnitude of the maximum rate of heat release). All statistical analyses were performed using the Analysis Toolpack available in Microsoft Excel.

The set of values used to statistically test property-performance relationships was chosen from the data gathered from pretreatment testing. The data used throughout this study are compiled in Table 8.1 and 8.2. The methods used to obtain the data can be found in Chapter 3. The samples used for each analysis varied depending on the data available for the particular property/parameter under investigation. The number of samples used in an analysis depended on how many samples were available for each

property and parameter. For example, when the relationship between SiO_2/Al_2O_3 ratio and compressive strength was examined only 8 samples were available for which both the SiO_2/Al_2O_3 ratio was known and compressive strength testing was also performed. Additionally some samples were excluded from these investigations because it was believed that the zeolite pretreatment resulted in a significant change to the nature of the material. For example, the zeolites calcined to 965°C were not used during this study due to the elimination of their zeolitic crystal structure during calcination. Also, SiO_2/Al_2O_3 ratios of untreated zeolites could not be assumed to be unchanged in calcined or acid treated zeolites as both of these processes are reported to result in dealumination of the zeolite crystal structure (Ates and Hardacre 2012; Beers 2003; Triantafillidis et al. 2001), and so these materials were excluded from analyses examining SiO_2/Al_2O_3 ratio as a factor. On the other hand, the SiO_2/Al_2O_3 ratio of the milled zeolite was assumed to be equal to the SiO_2/Al_2O_3 ratio of the untreated zeolite, as the milling process did not result in structural or chemical changes to the zeolite, only reduction in particle size. So, milled zeolites were included in analyses examining SiO_2/Al_2O_3 ratio as a variable.

In order to determine if a zeolite property and performance parameter had a strong relationship, individual significance testing was performed. In statistical significance testing, the P-value is used to describe the possibility of obtaining a null hypothesis, thus a P-value of 0.05 represents a 5% chance that the null hypothesis could be true (Thompson 2013). For this study an example hypothesis would be, “a zeolite’s particle size affects the compressive strength of a zeolite-cement mortar.” Therefore, the null hypothesis in this example would be, “a zeolite’s particle size *does not* affect the

compressive strength of the zeolite-cement mortar." In this case, a low P-value would indicate a very low chance that zeolite particle size was not related to compressive strength of the zeolite-cement mortar, and inversely, a high P-value would indicate a high chance that zeolite particle size and zeolite-cement mortar compressive strength were not related. In order to avoid excessive analysis and discussion of variables with limited connections to each other, only relationships having a very low chance of not being related were considered. For this study, a 95% confidence interval was used, meaning that only relationships with P-values less than 0.05 were considered 'statistically significant.'

Following significance testing, regression was performed to develop relationships between the zeolite properties and performance parameters for all variables determined to be statistically significant by significance testing. If only one property was found to be significant single variable analysis was used, if multiple properties were significant multivariable regression was performed. The correlation coefficient, R^2, was shown for each data set. The correlation coefficient, the value of which can range from 0-1, represents the percentage of the data that can be explained by the relationship presented. Values close to 1 show that the zeolite properties included in the relationship closely control the development of the particular performance parameter investigated, whereas low R^2 values suggest that other factors, may significantly contribute to the development of that performance parameter, or that the sample error is large.

Table 8.1 - Zeolite sample properties and performance parameters

Sample Set	Zeolite	Treatment	Zeolite Physical and Chemical Properties				Compressive Strengths (MPa)					Calcium Hydroxide Content (%)		Hydration Kinetics		
			Avg. Particle Size (d_{50})	Nitrogen Available Specific Surface Area (m^2/g)	SiO_2/Al_2O_3	Cation Content (%)	1 day	3 day	7 day	28-day	90	28-day	90	Slope of the Accel. Period (mW/g/hr)	Time to Max Heat Release Rate (hrs)	Max Heat Release Rate (mW/g)
Raw Zeolites	Z	None	6	37	5.96	8.55	10	21	32	48	55	14	14	0.44	1.31	5.81
	B	None	31	30	5.84	8.25	8	18	24	39	43	17	16	0.38	1.76	8.01
	L	None	785	29	6.00	7.94	9	17	22	30	32	17	19	0.36	2.04	9.29
	T	None	77	53	5.24	5.52	11	21	26	38	40	15	17	0.60	1.44	6.69
	C	None	46	36	4.89	12.60	10	15	23	31	34	18	18	0.61	1.14	6.56
	A	None	51	25	5.01	13.82	10	15	23	31	36	18	19	0.62	1.41	7.01
Milled Zeolites	T	Milled to pass #100 sieve	33	40	5.24	5.52	-	-	-	-	-	-	-	0.66	1.63	6.38
	T	Milled 1 hr	25	54	5.24	5.52	-	-	-	-	-	18	18	0.76	1.43	6.32
	T	Milled 2 hrs	14	60	5.24	5.52	14	24	33	50	49	16	18	0.77	1.35	6.50
	T	Milled 4 hrs	9	60	5.24	5.52	-	-	-	-	-	15	17	0.83	1.39	5.99
	T	Milled 6 hrs	8	55	5.24	5.52	-	-	-	-	-	16	17	0.85	1.30	5.89
	T	Milled 8 hrs	7	60	5.24	5.52	13	23	31	43	49	14	17	0.83	1.26	5.87

Table 8.2 - Zeolite sample properties and performance, continued

Sample Set	Zeolite	Treatment	Zeolite Physical and Chemical Properties				Compressive Strengths (MPa)					Calcium Hydroxide Content (%)		Hydration Kinetics		
			Average Particle Size (d_{50})	Nitrogen Available Specific Surface Area (m^2/g)	SiO_2/Al_2O_3	Cation Content (%)	1 day	3 day	7 day	28-day	90	28-day	90	Slope of the Accel. Period (mW/g/hr)	Time to Max Heat Release Rate (hrs)	Max Heat Release Rate (mW/g)
Calcined Zeolites	Z	Calcined at 300C	7	34	-	-	12	24	37	52	60	13	13	0.48	1.32	4.57
	Z	Calcined at 500C	6	29	-	-	14	28	39	49	50	16	16	0.60	1.30	5.30
	Z	Calcined at 800C	7	24	-	-	13	24	38	53	59	12	16	0.52	1.31	5.31
	B	Calcined at 300C	33	25	-	-	10	22	28	43	48	15	15	0.31	2.00	8.00
	B	Calcined at 500C	35	22	-	-	10	18	29	35	34	16	18	0.38	1.51	7.76
	B	Calcined at 800C	41	18	-	-	12	21	28	40	46	15	16	0.48	1.50	7.50
	L	Calcined at 300C	859	28	-	-	11	19	24	31	33	18	19	0.45	2.05	8.05
	L	Calcined at 500C	772	24	-	-	11	17	24	26	24	18	19	0.42	2.04	8.04
	L	Calcined at 800C	728	20	-	-	12	19	24	30	31	17	19	0.44	2.04	8.79
	T	Calcined at 300C	66	52	-	-	10	20	26	34	39	16	16	0.63	1.70	6.45
	T	Calcined at 500C	84	45	-	-	11	17	23	27	29	16	16	0.48	1.95	6.95
	T	Calcined at 800C	179	35	-	-	11	17	22	29	35	14	16	0.45	1.94	6.94
	C	Calcined at 300C	43	22	-	-	11	20	23	34	39	18	18	0.88	1.33	6.31
	C	Calcined at 500C	77	17	-	-	12	18	23	32	37	18	19	0.68	1.42	7.07
	C	Calcined at 800C	108	6	-	-	10	17	22	29	33	17	18	0.75	1.49	7.31
	A	Calcined at 300C	47	18	-	-	11	20	23	33	38	17	18	0.56	1.55	7.75
	A	Calcined at 500C	100	48	-	-	12	18	25	28	32	20	19	0.58	1.66	8.26
	A	Calcined at 800C	125	6	-	-	11	17	22	30	35	17	18	0.57	1.81	8.51

8.3 Relationship between Zeolite Physical and Chemical Properties and Compressive Strength

The influence of one physical or chemical zeolite property compared to another property on the development of compressive strengths has not been quantified in the literature. However many studies have shown that compressive strengths of SCM-cement mortars are related to particle size (Chindaprasirt et al. 2005; Ortega et al. 2000), surface area (Esping 2008; Lawrence et al. 2005), or composition (Caputo et al. 2008; Huizhen 1992; Rodriguez-Camacho and Uribe-Afif 2002). This section looks at the correlation between four material properties, median particle size, nitrogen-available specific surface area, the ratio of silica to alumina and total cation content, determined from composition data from XRF testing, and the relationship between these properties and the development of compressive strength in zeolite-cement mortars using the methods described in section 8.2.

Compressive strengths of mortars using untreated zeolites, zeolites milled for 2 or 8 hours, and calcined zeolites, except for samples calcined at 965°C, were used to correlate zeolite particle size and strengths. Strengths of the zeolites calcined at 965°C were not used because calcination was shown to have nearly eliminated their zeolitic crystal structure, discussed in Chapter 4. Strengths for acid treated zeolites, zeolites milled for 1, 4, or 6 hours and cation exchanged zeolites were not available, and so were not used in this correlation.

Before performing the significance testing, the relationship between each of the zeolite properties and compressive strengths was preliminarily examined to determine the

nature of their relationship. The relationship between most of the properties and compressive strength seemed to be linear. However, this was not the case for the relationship between zeolite particle size and compressive strengths. Figure 8.1 shows the evolution of the particle size-compressive strength relationship over time. At earlier ages (1-3 days), particle size does not appear to have an effect on compressive strength of zeolite-cement mortars as the strengths of all samples were approximately equal at about 10 MPa, independent of particle size. However, over time differences in strength development between samples using zeolites with different particles sizes became more pronounced, with smaller particle sizes generating much higher strengths. However, for zeolite particle size, the relationships were best represented as a logarithmic function, especially for later age compressive strengths.

Additionally, most properties were directly correlated to compressive strengths, with higher property values correlated with higher compressive strengths. The relationship between zeolite particle size and compressive strength was found to be inversely related. Therefore, throughout this work the inverse log of the average particle size was used to correlate particle size to compressive strengths. Figure 8.1 illustrates the relationship between average particle size and compressive strength while Figure 8.2 shows the relationship between the inverse log of average particle size and compressive strength.

Further, for many materials surface area is often strongly linked to particle size, so these properties would not be considered as independent variables. This is not the case for natural zeolites, which have larger internal surface areas as a result of their open

crystal structure. The relationship between surface area and particle size does trend in the expected direction, with larger particle size materials tending to have lower surface area, but the trend is weak and the data are not well correlated. Therefore, for the remainder of this discussion these two parameters are treated as being independent of one another.

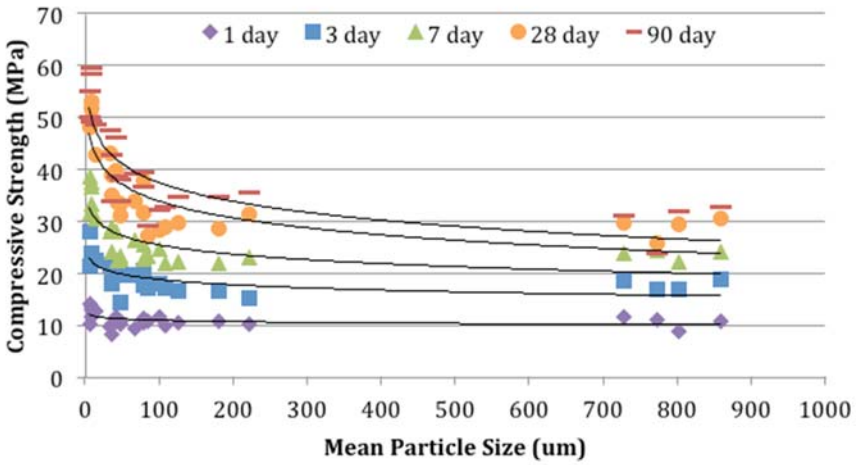

Figure 8.1 – Relationship between average particle size and compressive strengths of zeolite-cement mortars (w/cm = 0.51)

Table 8.1 shows the results of the significance testing for the zeolite physical and chemical properties and compressive strengths of mortars made with those zeolites. The significance testing indicates that for strengths tested at 1, 7, 28 and 90 days after casting the only significant variable is average particle size. For compressive strengths at 3 days, initial zeolite cation content was also shown to be significant. Plots of the correlation between particle size and compressive strength and cation content and strength are shown in Figures 8.2 and 8.3. Plots for the other testing times were very similar to Figure 8.2 and so were omitted.

The correlation coefficients, which measure the proportion of variation in the outcome that is accounted for by the predictors (Thompson 2013), are shown in Table 8.4

for all relationships determined to be significant by significance testing. Equations describing the relationships between zeolite particle size, cation content and compressive strength of mortars are shown in Equations 8.1-8.5. For the 3-day compressive strength, the correlation coefficient found for the relationship between zeolite particle size and compressive strength and zeolite initial cation content and compressive strengths were examined together using multivariable regression. The results shown in Table 8.4 show that, although it was considered a significant variable, zeolite particle size is a poor predictor of mortar compressive strengths at 1-day. The relationships between zeolite particle size and compressive strengths are considerably better at ages later than 1 day, and particle size becomes an increasingly accurate predictor of compressive strength as time progresses. Some of the spread of the data may be a result of variability inherent in the zeolite, cement or sand used to make mortar cubes or slight differences in casting, curing and testing the mortar cubes and indeed, the ASTM specification covering the making of compressive strength mortar cubes, ASTM C 109 (2011), allows a range of test results for mortar cube strengths using blended cements of up to 9.6% at 28 days.

Table 8.3 - P-values describing whether the correlation between compressive strengths and zeolite physical and chemical properties is significant. Gray cells indicate the relationships considered "not significant" (P>0.05)

Compressive Strength Samples	Zeolite Physical and Chemical Properties			
	Particle Size ($1/\log d_{50}$)	Nitrogen Available Surface Area (m^2/g)	SiO_2/Al_2O_3 ratio	Initial Zeolite Cation Content (%)
1-day	0.0065	0.207	0.179	0.330
3-day	3.34E-06	0.108	0.691	0.007
7-day	4.42E-09	0.118	0.899	0.127
28-day	7.43E-10	0.148	0.661	0.110
90-day	8.92E-10	0.321	0.457	0.272

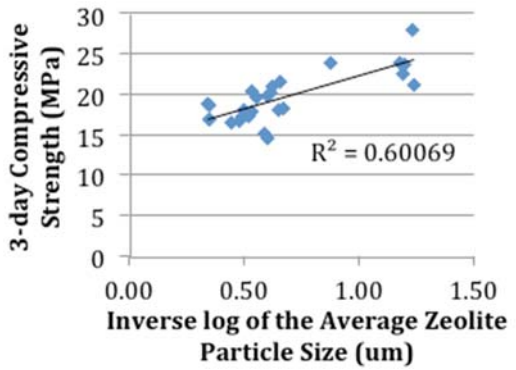

Figure 8.2 - Correlation between zeolite particle size and mortar compressive strengths at 3 days

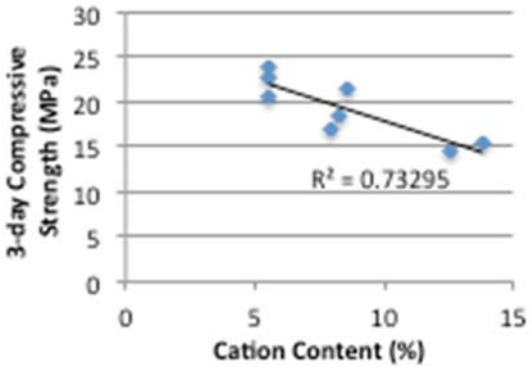

Figure 8.3 - Correlation between initial cation content of the zeolite and compressive strengths at 3 days

Table 8.4 - Correlation coefficients (R^2) for the relationships between zeolite average particle size, zeolite initial cation content and the compressive strengths of mortars for a given testing age

Compressive Strength Samples	Zeolite Properties		
	Average Particle Size	Cation Content	Average Particle Size and Cation Content considered together
1-day	0.270	-	-
3-day	0.601	0.733	0.914
7-day	0.768	-	-
28-day	0.800	-	-
90-day	0.797	-	-

$$f'c_{1-day} = 2.378 \cdot \frac{1}{\log(d_{50})} + 9.493 \quad (8.1)$$

$$f'c_{3-day} = 4.822 \cdot \frac{1}{\log(d_{50})} - 0.769 \cdot CC + 22.116 \quad (8.2)$$

$$f'c_{7-day} = 15.283 \cdot \frac{1}{\log(d_{50})} + 16.571 \quad (8.3)$$

$$f'c_{28-day} = 25.444 \cdot \frac{1}{\log(d_{50})} + 19.417 \quad (8.4)$$

$$f'c_{90-day} = 28.308 \cdot \frac{1}{\log(d_{50})} + 21.153 \quad (8.5)$$

8.4 Relationship Between Zeolite Characteristics and Calcium Hydroxide Consumption

There is little agreement among researchers about the zeolite properties that control the zeolites propensity for participating in the pozzolanic reaction in the cementitious system (Lilkov et al. 2011; Martinez-Ramirez et al. 2006; Mertens et al. 2009; Snellings et al. 2010). For example, several studies have suggested that framework SiO_2/Al_2O_3 ratio has an influence on both short and long-term reactivity of zeolites with higher silica content resulting in greater pozzolanic activity (Snellings et al. 2010,

Martinez-Ramirez et al. 2006). However, another study found early reactivity to be linked to external surface area, while only long-term reactivity was based on SiO_2/Al_2O_3 ratio (Lilkov et al. 2011), and Mertens et al. (2009) found that the reactivity of natural zeolite was strongly correlated with the quantity and type of cation present in the zeolite crystal structure. This section looks at the correlation between seven material properties, average particle size, nitrogen-available specific surface area, the ratio of silica to alumina, total cation content, and contents of Ca^{2+}, Na^{+}, or K^{+}, and the calcium hydroxide contents in zeolite-cement mortars using the methods described in section 8.2.

Untreated and milled zeolites were used to correlate zeolite particle size, surface area, SiO_2/Al_2O_3 ratio, total initial cation content, and Ca^{2+}, Na^{+}, or K^{+} content with calcium hydroxide content of zeolite-cement pastes in order to determine what zeolite physical and chemical properties correlate most strongly with zeolite pozzolanicity. Similar to the reasoning behind the sample set chosen for compressive strength correlations in section 8.2, data on the cation content and SiO_2/Al_2O_3 ratio were not available for the acid treated zeolites and cation exchanged zeolites, so these samples were not used in this correlation.

Table 8.5 shows the results of the significance testing for the zeolite physical and chemical properties and calcium hydroxide (CH) contents of pastes made with those zeolites. The procedure for significance testing is detailed in section 8.2. The significance testing indicates that for CH contents tested at 28 days, the only significant variable ($P<0.05$) is average particle size. However, the P-values for nitrogen available specific surface area and Ca^{2+} content, 0.055 and 0.058, respectively, were very close to the 0.05

value and so were included in developing a relationship to determine CH content of zeolite-cement pastes at 28 days, shown in Equation 8.6 and Equation 8.7. Plots of the correlation between particle size, surface area and Ca^{2+} content and 28-day CH content are shown in Figure 8.4 to 8.6. For 90 CH pastes, significance testing identified both average particle size and nitrogen available specific surface area as significant variables. The correlation between particle size and surface area and 90-day CH content are shown in Figure 8.4 and 8.5. The correlation coefficients of the relationships developed for particle size, surface area and Ca^{2+} content and 28-day and 90-day CH content are shown in Table 8.6 for all relationships determined to be significant by significance testing. Equations describing the relationships between zeolite particle size, cation content and CH content of mortars are shown in Equations 8.6-8.7. These equations show that, for CH content at 28 days, greater surface area, lower particle size and lower calcium cation content correlates with lower CH content and increased zeolite pozzolanicity. For 90-day pastes, smaller particle size and lower surface area correlate with decreased CH content and, therefore, increased zeolite pozzolanicity. The results in Table 8.6 also show that, although none of the 'significant' variables examined correlated well with 28-day CH content when examined individually, they produced a much better correlated relationship when considered together. However, for 90-day CH content, neither average particle size nor nitrogen available specific surface area correlate well with CH content regardless of whether they were used individually or together. Thus it appears that factors other than average zeolite particle size, nitrogen available specific surface area, SiO_2/Al_2O_3 ratio, contents of Ca^{2+}, Na^+ or K^+, and total cation content must play a large role in governing

the pozzolanicity of zeolites used in cementitious mixtures, especially for mixtures hydrated for 90 days or greater.

Table 8.5 - P-values describing whether the correlation between calcium hydroxide content and zeolite physical and chemical properties is significant. Gray cells indicate the relationships considered "not significant" (P>0.05)

$Ca(OH)_2$ Content Samples	Zeolite Physical and Chemical Properties						
	Particle Size ($1/logd_{50}$)	Nitrogen Available Surface Area (m^2/g)	SiO_2/Al_2O_3 ratio	Total Initial Zeolite Cation Content (%)	Initial Zeolite Ca^{2+} Content (%)	Initial Zeolite Na^+ Content (%)	Initial Zeolite K^+ Content (%)
28-day	1.35E-04	0.055	0.511	0.075	0.058	0.104	0.902
90-day	0.009	7.09E-07	0.178	0.389	0.184	0.133	0.270

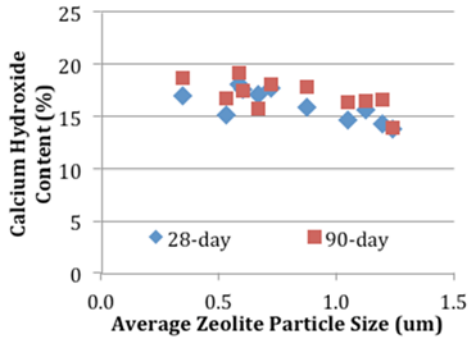

Figure 8.4 - Relationship between average particle size and 28 or 90 calcium hydroxide content of 80% cement, 20% zeolite pastes (w/cm = 0.4)

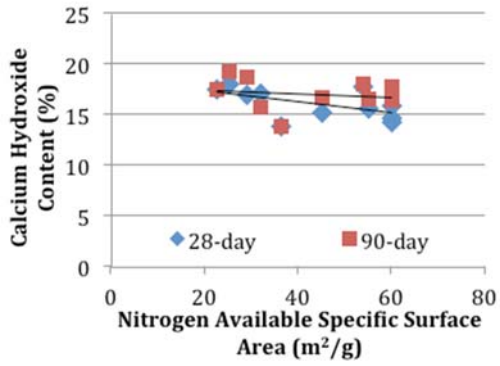

Figure 8.5 - Relationship between nitrogen available specific surface area and 28 or 90 day calcium hydroxide content of 80% cement, 20% zeolite pastes (w/cm = 0.4)

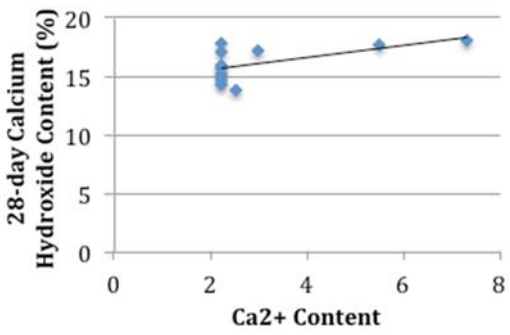

Figure 8.6 - Relationship between Ca^{2+} content and 28-day calcium hydroxide content of 80% cement, 20% zeolite pastes (w/cm = 0.4)

Table 8.6 - Correlation coefficients (R^2) for the relationships between zeolite average particle size, nitrogen available surface area, zeolite Ca^{2+} content and CH content of pastes for given testing ages

$Ca(OH)_2$ Content (CH) (%)	Zeolite Properties				
	Average Particle Size	Nitrogen Available Surface Area	Initial Zeolite Ca^{2+} Content	Average Particle Size, Surface Area and Ca^{2+} Content Considered Together	Average Particle Size and Surface Area Considered Together
28-day	0.315	0.091	0.343	0.703	-
90	0.164	0.472	-	-	0.518

$$CH_{28day}\,(\%) = -0.0216 \cdot SSA - 3.546 \cdot \frac{1}{logd_{50}} + 0.4146 \cdot Ca^{2+} + 16.872 \qquad (8.6)$$

$$CH_{90day}\,(\%) = 0.037 \cdot SSA - 4.330 \cdot \frac{1}{logd_{50}} + 19.004 \qquad (8.7)$$

8.5 Relationship between Zeolite Physical Properties and Hydration Kinetics

Hydration kinetics of SCM-cement pastes area often assumed to be primarily affected by the SCM's particle size and surface area (Kadri and Duval 2009; Oey et al. 2013a; Snellings et al. 2010a; Tuan et al. 2011). However, it has been suggested that cation content also plays a role with the use of zeolites, with zeolites having greater K^+ contents having lower rates of heat release compared to those with greater Na^+ or Ca^{2+}

content (Snellings et al. 2009). This section looks at the correlation between seven material properties, average particle size, nitrogen-available specific surface area, the ratio of silica to alumina, total cation content, and contents of Ca^{2+}, Na^{+}, or K^{+}, and four parameters that can be used to describe the kinetics of the early age hydration of cementitious pastes: the rate of reaction in the acceleration period; the time to the beginning of the acceleration period, the time to reach the maximum rate of heat release by the paste and the magnitude of the maximum rate of heat release from the paste. For discussion of the significance of each of these parameters see Chapter 3. Relationships between zeolite properties and the aforementioned parameters were developed using the methods described in section 8.2 and used data gathered from isothermal calorimetry testing presented and discussed in Chapters 4-7.

The result of significance testing for the hydration kinetics parameters is shown in Table 8.7. Surface area, SiO_2/Al_2O_3 ratio and K^{+} content were shown to be significant with respect to the rate of reactions occurring in the zeolite-cement pastes during the acceleration period. In addition to particle size, the time to the start of the acceleration period was also found to be affected by SiO_2/Al_2O_3 ratio, presumably due to the relationship between the start of precipitation of C-S-H and silica content, shown by other researchers to contribute to early age hydration behavior (Snellings et al. 2012). Zeolite particle surface area was found to be significant with respect to the time to the maximum rate of heat release of the paste, in addition to zeolite particle size. Finally, particle size, surface area and K^{+} content were found to be significant in their relationship with the maximum rate of heat release from the pastes.

The correlation coefficients for the relationship between each of the previously mentioned zeolite properties and the parameters used to describe hydration kinetics are shown in Table 8.7. These results show that surface area, SiO_2/Al_2O_3 ratio and the K^+ content of the zeolite are very closely correlated with the rate of reaction during the acceleration period. Considering the error associated with the use of any natural material, along with typical error from isothermal calorimetry testing, including differences in mixing, starting material temperatures and possible issues with adequately dispersing the materials within the paste, the relationship shown in Equation 8.8, fits the experimental data very closely. The developed relationship, shown in Equation 8.8, shows that the rate of reaction is greater with zeolites that have greater surface area, lower SiO_2/Al_2O_3 ratio and greater K^+ content.

Equation 8.9 closely describes the impact of particle size and SiO_2/Al_2O_3 ratio on the time to the start of the acceleration period. Other researchers have shown that small particles can have an accelerating effect on cement hydration reactions (Esping 2008; Isaia et al. 2003; Paya et al. 1997; Snellings et al. 2009), so it was not unexpected to see that particle size was significant for both the time to the start of the acceleration period and the time to the maximum rate of heat release. The relationship shown in Equation 8.9 shows that lower particle size, higher SiO_2/Al_2O_3 ratio zeolites result in accelerated reactions in zeolite-cement pastes.

The relationship describing the time to the maximum rate of heat release using particle size and surface area, shown in Equation 8.10, with $R^2 = 0.704$, was somewhat correlated to the experimental data. However, lower R^2 values indicate that zeolite

particle size and surface area do not fully explain the behavior of the zeolite-cement paste with respect to the time to the maximum rate of heat release and other zeolite properties not considered by this study, likely also affect the time to the maximum rate of heat release. Still, Equation 8.10 showed that greater surface area and smaller particle size zeolites correlate with reduced time to the peak of heat release.

Finally, the maximum rate of heat release was described by the zeolite particle size, surface area and K^+ content by Equation 8.11. Equation 8.11 shows that the maximum rate of heat release is increased when using zeolites with lower particle size, greater surface area and lower K^+ content. The closeness of fit of the relationship, shown in Equation 8.11, to the experimental data was similar to that of the relationship developed to describe the time to the start of the acceleration period based on particle size and SiO_2/Al_2O_3 ratio and does a good job describing the relationship between particle size, surface area and K^+ content. One interesting note, however, is the poor relationship between particle size and the maximum rate of heat release, which may imply that, although particle size affects the maximum rate of heat evolution, its role in determining the magnitude of the maximum rate of heat release is small compared to the effect of zeolite surface area and K^+ content on the maximum rate of heat release.

In summary, the results shown in Table 8.7 and 8.8 support the conclusions of other researchers who hypothesized that particle size, surface area and zeolite composition, primarily with respect to SiO_2/Al_2O_3 ratio and cation content significantly contribute to the hydration kinetics of zeolite-cement pastes, although in this study, only the K^+ cation content, and not the total content or Ca^{2+} or Na^+ contents, were significant.

Table 8.7 - P-values describing whether the correlation between hydration parameters and zeolite physical and chemical properties is significant. Gray cells indicate the relationships considered "not significant" (P>0.05)

Mixture Heat Evolution Parameters	Zeolite Physical and Chemical Properties						
	Particle Size ($1/logd_{50}$)	Nitrogen Available Surface Area (m^2/g)	SiO_2/Al_2O_3 ratio	Cation Content (%)	Initial Zeolite Ca^{2+} Content (%)	Initial Zeolite Na^+ Content (%)	Initial Zeolite K^+ Content (%)
Reaction rate during the acceleration period	0.081	3.00E-06	0.012	0.224	0.656	0.745	1.40E-4
Time to the start of the acceleration period	9.07E-06	0.416	0.016	0.836	0.530	0.164	0.103
Time to the maximum rate of heat release	2.04E-08	1.16E-04	0.108	0.491	0.788	0.781	0.097
Magnitude of the maximum rate of heat release	0.049	2.50E-04	0.112	0.121	0.326	0.833	0.010

Table 8.8 - Correlation coefficients (R^2) for the relationships between zeolite average particle size, nitrogen available surface area, zeolite Ca^{2+} content and CH content of pastes for given testing ages

Mixture Heat Evolution Parameters	Zeolite Physical and Chemical Properties							
	Particle Size	Nitrogen Available Surface Area	SiO_2/Al_2O_3 ratio	Initial Zeolite K^+ Content	Particle Size and Surface Area	Particle Size, Surface Area, and K+ Content	Particle Size and SiO_2/Al_2O_3 ratio	Surface Area, SiO_2/Al_2O_3 ratio and K+ content
Reaction rate during the acceleration period	-	0.424	0.521	0.816	-	-	-	0.949
Time to the start of the acceleration period	0.392	-	0.493	-	-	-	0.826	-
Time to the maximum rate of heat release	0.548	0.313	-	-	0.704	-	-	-
Magnitude of the maximum rate of heat release	0.093	0.288	-	0.537	-	0.831	-	-

$$Rxn\ Rate\ in\ the\ Accel.Period\left(\frac{mW/g}{hr}\right)=$$

$$0.01 \cdot SSA - 0.394 \cdot \frac{Si}{Al} + 0.047 \cdot K^{+} + 2.194 \quad (8.8)$$

$$Time\ to\ Start\ of\ Accel.\ (hrs) = -0.482 \cdot \frac{1}{log d_{50}} + 0.466 \cdot \frac{Si}{Al} - 0.675 \quad (8.9)$$

$$Time\ to\ Max\ Heat\ Release\ (hrs) = -0.017 \cdot SSA - 2.758 \cdot \frac{1}{log d_{50}} + 9.375 \quad (8.10)$$

$$Max\ Rate\ of\ Heat\ Release\ \left(\frac{mW}{g}\right) = 0.009 \cdot SSA + 0.594 \cdot \frac{1}{log d_{50}} - 0.185 \cdot K^{+} + 3.458 \quad (8.11)$$

8.6 DISCUSSION

8.6.1 Discussion of the Relationship between Zeolite Physical and Chemical Properties and Compressive Strengths of Zeolite-Cement Mortars

Examining the relationship between compressive strengths and particle size, shown in section 8.3, two interesting trends emerge. First, the early age strengths of all the mixtures are the same regardless of particle size. This indicates that the zeolites are likely not serving as nucleation sites for C-S-H hydration, otherwise using smaller particle size zeolites should result in greater strengths compared to the strengths of the mixtures using larger particle size materials (Chindaprasirt et al. 2005; Shao et al. 2000). This effect has been observed for other materials, including quartz, limestone and fly ash (Lawrence et al. 2005), but may also be a function of the zeolite material. Secondly, particle size is not at first influential relative to compressive strengths, but begins to have a greater impact on strengths of the mixtures as time progresses. This could be an indication that a greater percentage of the material is able to dissolve and react in the system, compared to the larger materials, which have less external surface area. This

effect was also shown by Lawrence et al. (2005) to be of importance in pozzolanic materials, whereas 'inert' materials, such as limestone filler and quartz do not demonstrate such large increases in strength for fine materials compared to their coarser counterparts.

That the relationships developed between zeolite particle size and compressive strengths correlate very well indicates that pretreatments resulting in changes to the zeolite that effect anything other than particle size would have little effect on the reactivity of the material. While other studies have suggested that destabilization of the zeolite crystal structure or phase composition drove the differences seen in mixtures using calcined zeolites compared to mixtures using the untreated zeolite (Caputo et al. 2008; Cheng-yi and Feldman 1985; Lilkov et al. 2011b; Snellings et al. 2010), the work presented in this dissertation indicates that particle size is the predominant predictor of compressive strength of zeolite-mortars after pretreatments.

8.6.2 Discussion of the Relationship between Zeolite Physical and Chemical Properties and Calcium Hydroxide Consumption in Zeolite-Cement Pastes

Examining the relationships investigated for the zeolite characteristics and 28-day calcium hydroxide content of zeolite-cement pastes presented in section 8.4, it can be concluded that that particle size, nitrogen available surface area and Ca^{2+} content are the only variables examined by this study that contribute to zeolite pozzolanicity. The influence of particle size and surface area were expected, as smaller particle size and greater surface area result in increased contact between the zeolite and cement pore solution, facilitating dissolution of the zeolite in solution. The correlation between lower

calcium cation content and increased pozzolanicity is likely merely a correlation and not causation, as lower paste calcium content of pastes corresponds to lower CH content, independent of the presence of zeolite.

Several previous studies have purported that SiO_2/Al_2O_3 ratio factors significantly into the pozzolanicity of zeolites (Martinez-Ramirez et al. 2006; Mertens et al. 2009; Snellings et al. 2009), however the results of this study, discussed in section 8.4, do not support this assertion. This result is counterintuitive, as it is generally known that the availability of silica dominates the effectiveness of many materials used as SCMs (Snellings et al. 2012). It could be that the differences in the SiO_2/Al_2O_3 ratio of the zeolites used in this study was simply not large enough to reveal a significant relationship between SiO_2/Al_2O_3 ratio and pozzolanic reactivity, although it may be a factor in a sample set involving multiple types of zeolite with significantly differing SiO_2/Al_2O_3 ratios. Research presented in Appendix D investigated the dissolution of zeolites in a simulated pore solution and found that the magnitude of dissolution was directly correlated with SiO_2/Al_2O_3 ratio. It is currently unclear why, in this testing, SiO_2/Al_2O_3 ratio did not play a larger role in the pozzolanicity reactivity of natural zeolites.

8.6.3 Discussion of the Relationships between Zeolite Physical and Chemical Properties and Early Age Hydration Kinetics of Zeolite-Cement Pastes

Increases in the rate of hydration are generally expected to correlate with greater surface area and smaller particle size, both of which result in greater amounts of free energy and inherent instability, increasing dissolution rates of the zeolites (Morel and Herring 1993). Additionally, increased surface area and smaller particle sizes allow for

greater interaction between cement hydration products and the zeolite particles as well as increased numbers of nucleation sites in the solution to instigate precipitation of C-S-H (Cyr et al. 2005). Decreases in time to the start of acceleration and to the maximum rate of heat release peak for mixtures containing high surface area or low particle size zeolites are in agreement with general knowledge of hydration kinetics of systems with added mineral fillers (Lawrence et al. 2003; Princigallo et al. 2003). In general, the results shown in section 8.5 support these conclusions. The correlation between greater potassium content and increased rate of reaction during the acceleration period, shown in Equation 8.8, may not be quite as obvious, but may be linked to the zeolite cation exchange capacity (Snellings et al. 2009). K^+ ions in the zeolite crystal structure may exchange with Ca^{2+} in the pore solution, removing from the solution and resulting in a rise in pH. Greater pH corresponds to increased silica solubility (Mertens et al. 2009; Snellings et al. 2009), which is initially the rate controlling step in the cement hydration process before C-S-H nucleation and growth accelerates (Snellings et al. 2012). However, if this is the mechanism resulting in greater reaction rates during the acceleration period with greater K^+ it is unclear why Na^+ content was also not significant, as Na^+ exchanges more easily from the zeolite crystal structure due to its smaller size (Mertens et al. 2009; Snellings et al. 2009).

8.7 CONCLUSIONS

This chapter explored the relationships between zeolite physical and chemical properties and performance of zeolite-cement mixtures. It was found that at early ages compressive strengths of zeolite-cement mortars are independent of zeolite physical and

chemical properties. As time progressed, however, average particle size became the determinant factor in strength development, with smaller particle sizes leading to greater gains in compressive strengths. Particle size was not, however, the only factor determining the pozzolanicity of zeolite mixtures evidenced by lower CH content of zeolite-cement pastes as surface area was also found to contribute significantly to the differences in CH content. Rates of reaction during the acceleration period were found to be most affected by surface area, SiO_2/Al_2O_3 ratio and K^+ content, while time to the start of the acceleration period was influenced by particle size, presumably due to nucleation effects, and SiO_2/Al_2O_3 ratio. Time to the maximum rate of heat evolution was partially determined by zeolite average particle size and surface area, but these relationships were not strongly correlated and suggest that other factors beyond this scope of this work significantly influence the time to the maximum rate of heat release. The maximum rate of heat release was found to be subject to zeolite particle size and surface area, as well as the initial K^+ content of the zeolite.

Overall, based on the results shown in this chapter, average particle size plays the largest role in determining the behavior of zeolite-cement pastes and mortars. Nitrogen surface area was also found to significantly influence the pozzolanic reactivity of the zeolite as well as the hydration kinetics of zeolite-cement pastes, although it had little contribution to compressive strengths. Ca^{2+} content was shown to affect 3-day compressive strengths and K^+ cation concentration was shown to play a role in the kinetics of the zeolite-cement hydration reactions. However, for the most part, cation content was not an important factor in the performance of the zeolite cement pastes and

mortars. As the different performance parameters were each affected by different zeolite properties, future zeolite treatment work should therefore, first determine which properties are most important for the intended purpose of the cement mixture. The information provided in this study can then be used to focus on alterations of specific properties depending on the desired performance parameters. Additionally, further work should be done to determine the influence of other parameters, such as zeolite crystallinity, amorphous content and surface charge on the development of properties of zeolite-cement mixtures.

Chapter 9: Summary, Conclusions, and Suggested Future Work

9.1 Summary of Experimental Program

Use of natural zeolites as SCMs can have many benefits for cementitious systems. Previous research has shown that natural zeolites are pozzolanic, reacting with calcium hydroxide and water to create more C-S-H binding phase, and can improve many of the properties of concrete including resistance to alkali silica reaction, sulfate attack and penetration by chlorides, in addition to reducing the environmental impact of concrete by offsetting the quantity of cement required for each volume of concrete used. However, understanding of the zeolite properties governing zeolite reactions in concrete is limited and several disadvantages are associated with the use of natural zeolites in cementious mixtures including significant variability in properties depending on zeolite source, lower compressive strengths and increased costs compared to other SCMs such as fly ash.

The goals of this work were to provide a deeper and more thorough understanding of the way zeolites interact with the components of cementitious systems, determine the factors that control the performance of zeolites in cementitious mixtures and determine if pretreatments such as calcination, acid treatment, milling and cation exchange could be used to improve zeolites for use as SCMs by increasing their reactivity.

In the research presented in this dissertation, the chemical and physical properties of six sources of natural zeolite were characterized, and their effects on the chemical and mechanical performance of cementitious mixtures using natural zeolites as SCMs were determined. Pretreatments, including calcination, soaking in acid, ball milling and exchanging the zeolite's cations to create a homoionic zeolite form, were then employed

in an attempt to increase the reactivity of the zeolite. In order to determine if pretreatment techniques were successful, the relative reactivities of the untreated and treated materials were tracked by three methods: (1) measuring the amount of calcium hydroxide converted to calcium silicate hydrate (C-S-H) in zeolite-cement pastes relative to the calcium hydroxide present in cement-only pastes; (2) measuring the amount of calcium hydroxide consumed by the untreated and treated zeolites in a heated calcium hydroxide aqueous solution (the Chapelle test); and (3) comparing the compressive strengths developed in mortar cubes composed of sand and cement with and without treated or untreated zeolites. Changes in reactivity were then linked to changes induced by the pretreatments in: material phases, relative crystallinity, particle size, and surface area or pore size distribution. The effect of untreated and calcined, acid treated, milled or cation-exchanged zeolites on the kinetics of the cement hydration reacts were also investigated using isothermal calorimetry. Lastly, data from pretreatment testing were evaluated using statistical significance testing and multivariate regression in order to determine which zeolite properties, including average particle size, nitrogen available specific surface area, Si/Al ratio, overall initial zeolite cation content and content of K^+, Na^+ and Ca^{2+}, played significant roles in governing the compressive strengths or zeolite-cement mortars, pozzolanic reactivity as measured using the calcium hydroxide content of zeolite-cement pastes, and hydration kinetics of zeolite-cement pastes.

9.2 SUMMARY OF RESULTS AND CONCLUSIONS

In general, calcination of zeolites increased particle size, eliminated fine materials, filled porosities, and decreased surface area, effects which correlate to lower

reactivity of materials used in cementitious systems (Lawrence et al. 2005, Kraiwood et al. 2001). However, calcination also reduced zeolite crystallinity and eliminated most system impurities, although a pozzolanically inert form of SiO_2, cristobalite, was not eliminated by calcination. The natural zeolites tested effectively reduced calcium hydroxide content in cementitious systems. However, calcination did not improve zeolite pozzolanic potential and, in the case of calcination at 965°C, it reduced the material's ability to participate in the pozzolanic reaction. Calcination of zeolites at 300°C increased the compressive strength of zeolite-cement mortars, but calcination at other temperatures generally resulted in lower strengths relative to OPC and untreated zeolite mortars. Overall calcination was an ineffective process for increasing the reactivity of zeolites for use as supplementary cementitious materials.

Acid treatment was found to improve the pozzolanicity of the zeolite as a result of dealumination with the removal of Al^{3+} from the zeolite crystal structure. The cation exchange of hydrated Ca^{2+}, Na^{+} and K^{+} cations with H^{+} from the acid solutions resulted in a significant increase in the nitrogen available specific surface area of the material, and structural dealumination may have resulted in decreased particle sizes, due to the breaking of material bonds. Acid treated zeolites removed greater quantities of calcium hydroxide in zeolite-cement pastes than their untreated counterparts and also accelerated the rates and magnitudes of early age cement hydration reactions. Of the three types of acid used, treatment with hydrochloric and nitric acid resulted in similarly good improvements in surface area, pozzolanic reactivity and increases in hydration kinetics. However, use of a weak acid, household grade acetic acid, also yielded improvements to

surface area and pozzolanicity and also accelerated cement hydration reactions. Use of 0.1M versus 1M concentrations of the acids did not seem to affect the results. Overall, acid treatment appeared to be successful at improving the performance of zeolites as SCMs.

Ball milling of zeolites significantly improved the performance of the zeolite used in cementious mixtures, increasing the pozzolanicity of the zeolites as well as increasing compressive strengths of mortars containing milled zeolites. With respect to cement hydration, milling the zeolite resulted in significant accelerations in the rate of hydration reactions in addition to increasing the magnitude of the peak rate of heat release, similar to the behavior of a filler material. Improvements in compressive strengths and pozzolanicity were hypothesized to be primarily a result of decreased particle size, but particle size could not completely account for all changes in the material, especially changes from 2 to 8 hours of milling, when the magnitude of decrease of average particle size was small. Overall, milling was very effective as a pretreatment to improve the reactivity of zeolites for use as SCMs.

Cation exchange treatment resulted in increases in zeolite nitrogen surface area and reductions in particle size that led to small improvements to zeolite pozzolanicity, as evidenced by lower calcium hydroxide contents present in zeolite-cement pastes, compared to pastes using the untreated zeolite, as well as increased calcium consumption during the Chapelle test. Cation exchanged zeolites also changed cement hydration kinetics, accelerating the hydration of pastes in which they were included, dependent upon the cation form of the zeolite. The Na-exchanged zeolite was most effective in

increasing hydration rates out of the zeolite-cement pastes tested, although the cumulative heat evolved at 72 hours was not increased for the Na-exchanged zeolite-cement paste compared to the untreated zeolite. In general, cation exchange treatment does not appear to be an effective method for treating natural zeolites to improve their properties and performance for use as a supplementary cementitious material.

Compressive strengths at 1 day for zeolite-cement mortars were found to be independent of zeolite physical and chemical properties. Increased hydration time, however, revealed that average particle size was the determinant factor in strength development, with smaller particle sizes leading to greater gains in compressive strengths. Particle size was not, however, the only factor determining the pozzolanicity of zeolite mixtures as surface area was also found to contribute significantly to the differences in CH content. With respect to hydration kinetics, rates of reaction during the acceleration period were found to be most affected by surface area, Si/Al ratio and K^+ content, while time to the start of the acceleration period was influenced by particle size, presumably due to nucleation effects, and Si/Al ratio. Time to the maximum rate of heat evolution was partially determined by zeolite average particle size and surface area, but these relationships were not strongly correlated and suggest that other factors beyond this scope of this work significantly influence the time to the maximum rate of heat release. The maximum rate of heat release was found to be subject to zeolite particle size and surface area, as well as the initial K^+ content of the zeolite.

Pretreatment testing revealed that the largest gains in reactivity come from decreasing zeolite particle size through milling. Increases in the rate of reaction and

magnitude of the maximum heat release seen using acid-treated zeolites and tested in isothermal calorimetry also showed promise for increasing the performance of zeolite-cement mixtures, but adapting this procedure to industrial volumes could prove expensive.

Overall this research contributed several key new findings concerning the use of natural zeolites as SCMs to the field of concrete materials. First, this work showed that research performed in lime-zeolite systems (Mertens et al. 2009; Snellings et al. 2010a) may not correlate with the behavior demonstrated when the zeolite is used with cement. Second, this work disproved theories implying that cation exchange properties of the zeolite and cation content of the zeolite contributed significantly to the performance of the zeolite in cementitious systems (Mertens et al. 2009; Snellings et al. 2010a). Third, highly crystalline materials, such as natural zeolites, are not necessarily less reactive, slower to react than highly amorphous materials such as fly ash. Fourth, this research showed that calcination, a pretreatment method suggested by other researchers to improve natural zeolite reactivity, was not a reliable method for improving zeolite, and also showed that much greater gains can be obtained simply through milling. Lastly, this work showed that particle size is the predominant factor that determines the compressive strengths of zeolite-cement mixtures, while both zeolite particle size and nitrogen surface area contribute to the pozzolanic reactivity of the zeolites. This information has not been previously quantified by other researchers for natural zeolites.

9.3 SUGGESTIONS FOR FUTURE WORK

The current research investigated several methods of increasing the reactivity of natural zeolites used as SCMs. However, many unanswered questions remain that could help improve understanding of this material and improve it for use in concrete. Suggestions for future work are provided here:

First and foremost, it is essential to develop a simple method to quantify the phases present in the natural zeolites. Natural zeolites are known to be roughly 70% pure in nature and it is believed that composition and amorphous content play a significant role in the performance of the material. However, quantification of materials was found to be very difficult, especially due to the inconsistencies of results when using Rietveld analysis (Fernandez, personal communication, May 2014). Future work to investigate alternative pretreatment methods should seek to track the evolution of phases and use more quantitative methods to determine their success based on changes to material properties. These data will also enable refinement of the relationships presented in Chapter 8, and increase the accuracy of predictive equations.

Second, isothermal calorimetry testing revealed significant undersulfation issues associated with zeolite use in cement pastes. Zeolite-cement paste undesrsulfation can be seen in the increased rates of heat release of the second rate of heat release peak in isothermal calorimetry results presented for the calcined zeolites, in section 4.3.3 and for the acid-treated zeolites, discussed in section 5.5.3. Other researchers have also noticed this issue with SCMs such as metakaolin (Antoni et al. 2012) and fly ash (Niemuth et al. 2012), particularly when the material is used in high volumes. One benefit of conducting

research with a highly crystalline material is that reactions and reaction mechanisms are more easily understood than with a highly amorphous material such as fly ash. Research into the mechanism behind changes to sulfate requirements with the addition of SCMs could help identify the mechanism behind the interactions of C_3A and gypsum, which is currently not well understood (Bullard et al. 2011), as well as increasing the feasibility and success association with using SCMs at very high replacement rates.

Third, only four methods of pretreating zeolites were explored in this study, and work investigating the effect of these pretreatments focused on determining the effect of pretreatments only on calcium hydroxide content of pastes and, in some cases, compressive strengths. However, many other opportunities for pretreatments exist including multi-step treatments, for example, calcination followed by milling, or the use of polymeric additives. Use of zeolites in ternary blends has not been explored. Mixtures using zeolites in conjunction with other SCMs could result in synergistic improvements. Further, it is possible that the pretreatments, especially acid treatment, which increases the cation exchange ability of the zeolite, could be useful for mitigating pH dependent durability issues such as alkali silica reactions, and should be investigated in more depth.

Lastly, one of the goals of this testing was standardization of the natural zeolite and removal of some of the variability inherent in natural materials using the pretreatment methods. Some evidence of success with this was seen in the acid treatment of the zeolites, but future testing should consider a larger zeolite sample set and evaluate the ability with which pretreatments can produce materials that generate consistent properties independent of source location and exposure.

Appendix A: Does the Chapelle Test Accurately Predict Zeolite Pozzolanicity?

A.1 Introduction

The Chapelle test for pozzolanic reactivity, based on the French standard NF P 18-513 (2010), measures the amount of $Ca(OH)_2$ consumed by an SCM in a saturated lime solution, and was used in this study to evaluate the pozzolanicity of the materials before and after pretreatment by calcination, acid treatment, milling or cation exchange. This test attempts to measure the relative capacity for the pozzolanic reaction in 16 hours, as opposed to the 56 to 90 days required to measure pozzolanicity through calcium hydroxide contents of pastes. This is done through increased temperature and contact between dissolved Ca^{2+} and the pozzolan in solution. However, the test was designed to be used with metakaolin and has not been proven as an effective predictor of zeolite reactivity. This study investigates the ability of the Chapelle test to predict the pozzolanic reactivity of untreated and pretreated zeolites.

A.2 Experimental Methods and Materials

For the Chapelle tests, a 1g sample of the pozzolan was combined with 2g CaO and 250 mL distilled water and heated at 85°C for 16 hours with continuous stirring. The solution was then cooled to room temperature and combined with 60g of sucrose and an additional 250 mL of distilled water for 15 minutes in order to stop the reaction between the calcium and pozzolan. Finally, the mixtures was filtered using a Buchner funnel and titrated with 0.1M hydrochloric acid to determine the amount of $Ca(OH)_2$ remaining in solution. Results are given in grams of $Ca(OH)_2$ consumed per gram of sample initially

added to the solution. In order to gain the best picture of the relationship between zeolite pozzolanic reactivity and the Chapelle test, the correlations presented in this study utilized all zeolites for which both the calcium hydroxide content of zeolite-cement paste was measured and the Chapelle test was performed. Additionally the Chapelle test was examined as an indicator of compressive strength using all the zeolites for which both mortar cube compressive strength and Chapelle test results were available.

A.3 RESULTS

Figure A.1 shows the correlation between the calcium hydroxide content of zeolite-cement pastes and the results of the Chapelle test. The results of the Chapelle test do not show an absolute correlation but they do show the general trend expected for the materials, especially for the calcium hydroxide contents at 90 days. The Chapelle test does not, however, correlate with the magnitude of compressive strengths developed in the zeolite-cement mortars, shown in Figure A.2. This suggests that the Chapelle test is not a good predictor of compressive strength development.

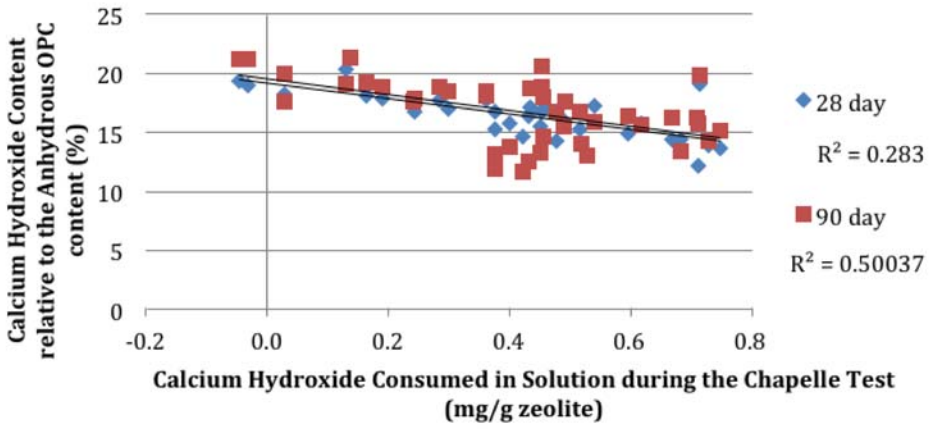

Figure A.1 - Relationship between the results of the Chapelle test and paste calcium hydroxide content

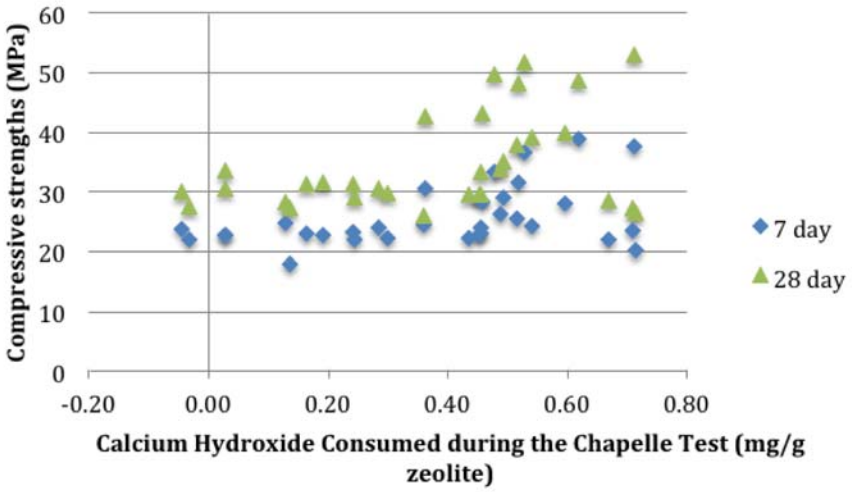

Figure A.2 - Relationship between the Chapelle test and compressive strengths

A.4 DISCUSSION

Agreement between the results of the Chapelle test and the ability of the zeolites to consume calcium hydroxide from pastes hydrated for 28 days, shown in Figure A.1 is good, especially considering the large error of 10% inherent in the Chapelle test (NF P 18-513-2010). The correlation of these two methods also suggests that the pozzolanic reaction of zeolites in cementitious systems can be predicted using the Chapelle test.

A.5 CONCLUSIONS

In addition to the investigation of the influence of zeolite properties on strength and pozzolanicity, the Chapelle test was confirmed as an adequate indicator of long-term zeolite pozzolanicity.

Appendix B: High Limestone Cements and Natural Zeolites

B.1 INTRODUCTION

Additions of fine limestone powder have been shown to increase the rate and magnitude of cement hydration reactions when used as a filler material (Oey et al. 2013a; Ramezanianpour et al. 2009). In addition, limestone has been shown to interact synergistically when used in ternary blends with SCMs such as fly ash metakaolin and blast furnace slag (Antoni et al. 2012; Menendez et al. 2003; De Weerdt, Kjellsen, et al. 2011), improving the properties of pastes, mortars and concretes through the filler effect (Esping 2008; Lawrence et al. 2005; Oey et al. 2013b), as well as through the formation of new hydration products such as calcium hemicarboaluminate hydrate, monocarboaluminate, and calcium carboaluminate hydrate, which bind calcium hydroxide and remove it from the cementitious system (Antoni et al. 2012; Ramezanianpour et al. 2009; De Weerdt et al. 2011a). Limestone has even been shown to decrease the time to the onset of the pozzolanic reaction when used in a ternary blend with metakaolin (Antoni et al. 2012). It is hypothesized that use of limestone cements with natural zeolite will result in similar increases in strength and pozzolanicity compared to zeolite-cement pastes and mortars.

B.2 EXPERIMENTAL METHODS AND MATERIALS

B.2.1 High Limestone Cements and Zeolite

Two cements were used for high limestone cement testing, and are designated cements A and B. The cements were Type I white cements from Lehigh White Cement Company. The oxide composition of each cement is shown in Table B.1. The quantity of

limestone in each cement was determined using thermogravimetric analysis (TGA), calculating the $CaCO_3$ content based on the mass loss between 650 -750°C in TGA, and is shown in Table B.2. Based on these data, cement A was designated as ordinary white portland cement, with cement B being the high limestone cement. Zeolite B was the only zeolite used throughout this study.

Table B.1 - Oxide compositions of the cement, in percent, determined using XRF

Cement	Elements present (%)							
	SiO_2	Al_2O_3	Fe_2O_3	CaO	MgO	SO_3	Na_2O	K_2O
A	22.17	4.12	0.28	65.30	1.70	2.80	0.04	0.02
B	20.56	3.68	0.21	64.33	1.99	2.63	0.03	0.02

Table B.2 - Quantity of limestone in the cements determined using the mass loss found in TGA from 650-750°C

Cement	Limestone (%)
A	3.48
B	10.20

B.2.2 XRD Testing

XRD was used to determine if additional phases were formed when high limestone cements and natural zeolites were used together, similar to the monocarboaluminate phases seen in metakaolin-high limestone mixtures (Antoni et al. 2012). Sample preparation was similar to the preparation of calcium hydroxide test specimens and testing parameters was completed using the same procedure as described for XRD testing of untreated and pretreated zeolites. Both sets of procedures are described in Chapter 3, section 3.1.1.1.

B.2.3 Reactivity Testing

Pozzolanic reactivity was studied for the high limestone cement and high limestone cement-zeolite pastes through measurement of the calcium hydroxide content of zeolite-cement pastes. The sample preparation and data analysis procedures for these tests are described in Chapter 3, section 3.1.2.1. Mortar cubes were cast to test the effect of limestone on compressive strength. The procedure was the same as for the zeolite-cement mortars described in section 3.1.2.3.

B.2.4 Cement Hydration Testing

Isothermal calorimetry was used to compare the rate of hydration of high limestone cement pastes with the rate of hydration of high limestone-zeolite pastes. Testing was done on cement pastes with 80-100% of cement A or B and 0-20% untreated zeolite B. Testing methods are described in Chapter 3, section 3.1.3.1.

B.3 Results and Discussion

B.3.1 Physical and Chemical Characterization Testing

Some of the crystalline phases present in each sample are shown in Figure B.1. Only a very small range of 2θ was studied in order to facilitate close examination of the formation of a monocarboaluminate phase in the hydrated cement paste. The monocarboaluminate phase, shown at approximately 11.5° 2θ, is present in the ordinary white cement-only paste, the high limestone white cement-only paste and the pastes with natural zeolite.

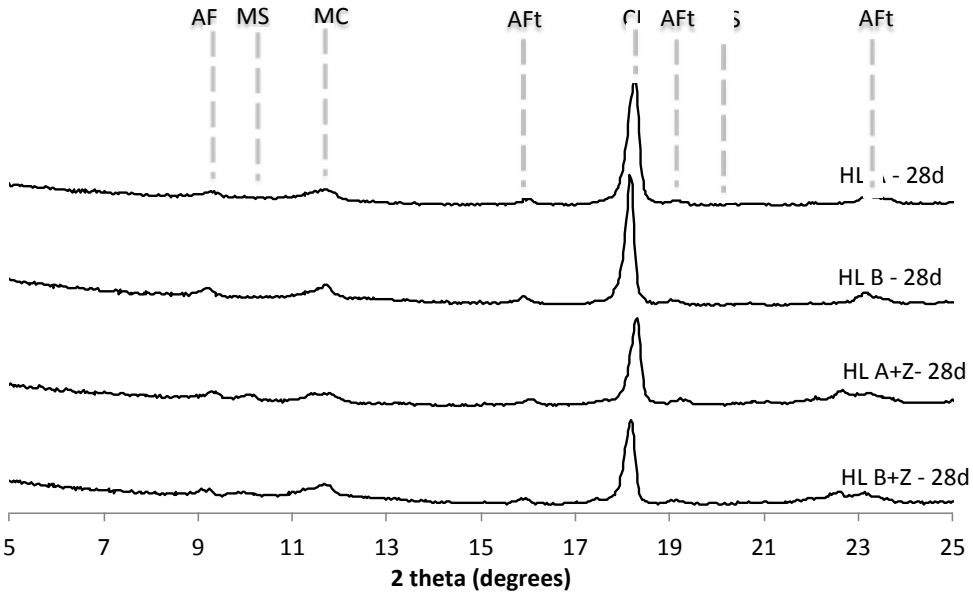

Figure B.1 - Evidence of the formation of a monocarboaluminate (MC) phase in the 28-day pastes made using 80-100% white limestone cement and 0-20% zeolite B (w/cm = 0.5). (HLA = high limestone cement A, HLA+Z = high limestone cement A and zeolite B, HLB = high limestone cement B, HLB+Z = high limestone cement B and zeolite B, AFt = ettringite, MS = monosulfoaluminate, CH = calcium hydroxide, MC = monocarboaluminate).

B.3.2 Pozzolanic Reactivity Testing

Results of calcium hydroxide (CH) content testing are shown in Figure B.2. Figure B.2 reveals several trends. First, the high limestone cement had lower CH content than the 3.5% limestone cement at both 28 and 90 days. Second, the incorporation of natural zeolite significantly reduced the CH content of the pastes, evidencing their pozzolanic reactivity. Third, the CH content of the cement-only mixtures increased from 28 to 90 days, suggesting that the limestone in the cements is not pozzolanic and also does not reduce a significant quantity of CH through the transformation of other hydration products into hemicarboaluminate, calcium carboaluminate, or monocarboaluminate phases, despite that monocarboaluminate was shown to be present in section B.3.1.. Lastly, when compared to the prior CH content testing of zeolite B

shown in section 4.3.2, the zeolite consumed a greater quantity of CH from the limestone cement pastes compared to the OPC used for the other studies in this dissertation. When used with the OPC in Chapter 4, the zeolite reduced the calcium hydroxide content at 28 days from 19.5% in the OPC paste to 17.2% in the zeolite-cement. In comparison, the CH content of the white cements was reduced from 25.7% and 24.2% for the 3.5% limestone white cement and the 10.2% limestone white cement, respectively, to 20.2% and 18.8% with the substitution of zeolite. This may evidence enhanced pozzolanic reactivity of the natural zeolite when used in conjunction with limestone cements.

The results of compressive strength testing of white limestone cement mortars and white limestone cement-zeolite mortars are shown in Figure B.3. Although compressive strength at most times for all of the mixtures are equal, within error, the trend appears to suggest that replacement of white limestone cement with zeolite resulted in a decrease in compressive strengths that is still evident after 90 days. Figure B.3 also shows that, for the cement-only mortars, high limestone content resulted in an increase in compressive strength compared to the lower limestone content white cement at day three. However the strength of the 3.5% limestone content mortar had caught up to the 10.2% limestone content mortar by 7 days and surpassed it's strength by 28 days.

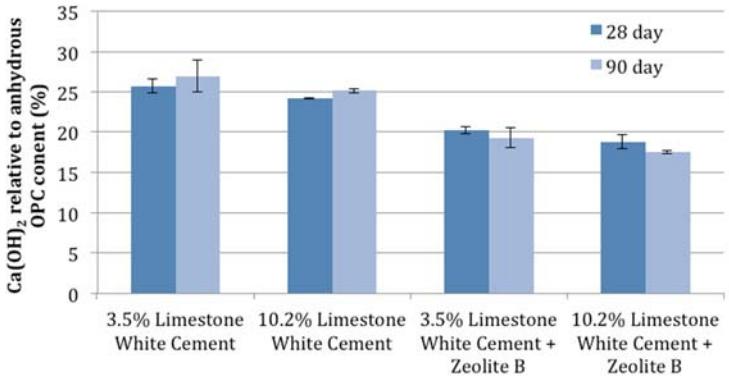

Figure B.2 - Calcium hydroxide content of 80-100% white limestone cement and 0-20% natural zeolite pastes (w/cm = 0.4)

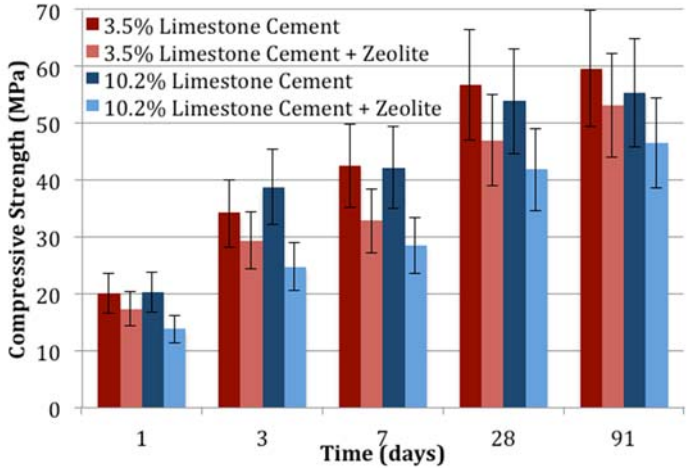

Figure B.3 - Compressive strengths of mortar cubes with 80-100% white limestone cements and 0-20% natural zeolite (w/cm = 0.5)

B.3.3 Cement Hydration Testing

Due to sulfation issues, the limestone cements were not tested using isothermal calorimetry with natural zeolite. The hydration kinetics of the two types of white limestone cements were compared to each other, however, and are shown in Figure B.4, which shows that greater limestone content resulted in a decrease in the magnitude of the maximum rate of heat release and a retardation of the time to the maximum rate of heat release compared to the lower limestone content white cement.

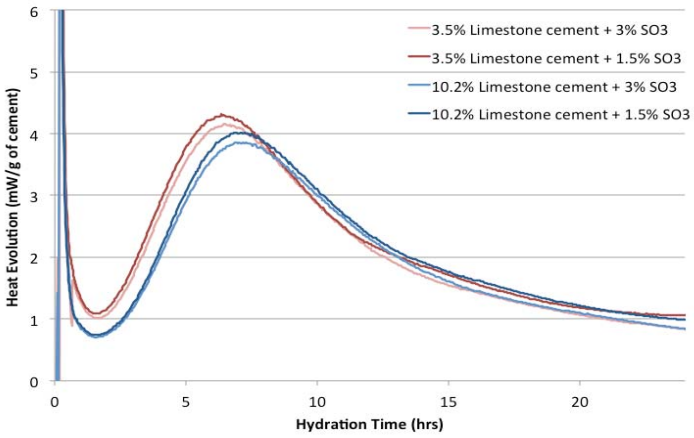

Figure B.4 - Isothermal calorimetry (23°C) results of white cement and white limestone cement pastes with $CaSO_4$ added to correct for sulfate imbalances

B.4 CONCLUSIONS

Two white limestone cements with differing quantities of limestone were mixed with zeolite to evaluate: the development of carboaluminate phases in pastes with XRD; the effect of limestone on zeolite pozzolanic reactivity through CH content of pastes; compressive strength of mortars; and cement hydration reactions in pastes through isothermal calorimetry. XRD analysis revealed that a monocarboaluminate phase was present in both the high and low limestone content cements, with and without zeolites. However, this did not seem to significantly contribute to the reduction of CH content, as was suggested by previous research (De Weerdt et al. 2011b). The zeolite significantly reduced the CH content of pastes, evidence of its pozzolanic activity, and the high quantity of CH removed from the system compared to the amount removed when zeolite B was used with an OPC may suggest that the limestone increased the pozzolanic reactivity of the zeolite. Higher limestone content increased the compressive strength of the mortar at 3 days, but the lower limestone content mortar had greater strength than the

10.2% limestone content mortar by 28 days, a result similar to some researchers (Thongsanitgarn et al. 2011), but in contrast with the findings of others (Tsivilis et al. 2002). Lastly, using high limestone content was found to reduce the maximum rate of heat release and retard cement pastes.

Appendix C: Isothermal Calorimetry Testing of Cation Influence on Cement Hydration Kinetics

C.1 INTRODUCTION

The goal of this study was to determine if the differences between the hydration kinetics of the untreated zeolite-cement pastes and cation-exchanged zeolite-cement pastes was due to the presence of extra cations in the solution, released from the cation-exchanged zeolite. Several researchers have investigated the effect of cations and anions on cement hydration reactions. Murakami and Tanaka (1969) tested the effect of accelerators on the rate of heat evolution of pastes, tracked with adiabatic calorimetry and found that, when used in the same quantity (3%), both $CaCl_2$ and NaCl accelerated the time to the maximum rate of heat release and the maximum rate of heat release of a cement-only paste. Of the two accelerators, $CaCl_2$ accelerated the mixture more and resulted in a great maximum rate of heat release (Murakami and Tanaka 1969). Since the anion was similar for both materials, this suggests that Ca^{2+} decreases the time to the maximum rate of heat release and increases the maximum rate of heat release more effectively than Na^{+}. Murakami and Tanaka (1969) also discussed the effectiveness of anions as accelerators, but showed that the acetate anion does not accelerate cement hydration reactions. Similarly Kantro (1974) showed, using isothermal calorimetry, that a C_3S mixture with $CaCl_2$ reached nearly double the maximum rate of heat release as a C_3S mixture with KCl. With further testing, the accelerating effect of various cations was shown to be: $Ca^{2+}>K^{+}>Na^{+}$ (Kantro 1974). Thus, if the cations of the cation-exchanged zeolites are affecting the rates of cement hydration, it should be expected that the

mixtures should be accelerated, reaching the maximum rate of heat evolution in less time and generating greater maximum rates of heat release than the corresponding untreated zeolite-cement pastes.

C.2 EXPERIMENTAL METHODS AND MATERIALS

In order to help understand the effect of the charge balancing cation on the changes seen when using cation-exchanged zeolites in cement pastes, cement pastes were studied that included an addition of Ca^{2+}-, Na^{+}- or K^{+}-acetate, without zeolite and with untreated zeolite. The amount of acetate added corresponded to 2.2 meq/g, the theoretical quantity of cations that could be exchanged into a zeolite structure (Colella et al. 1996, Pabalan and Bertetti 2001). The effect of the acetate added to a zeolite-cement mixture was also tested and compared to a cation-exchanged zeolite substituted for 20% of the cement. The materials used in each mixture and the name by which the mixtures are referred to in this chapter are shown in Table C.1.

Table C.1 - Cation exchange testing material proportions

Sample Name	Cement (g)	Type of Zeolite	Zeolite (g)	Type of Acetate	Acetate (g)
Ca	10	-	-	Calcium	0.341
Ca&Z	8	Untreated	2	Calcium	0.341
Ca-EZ	8	Ca-exchanged	2	-	-
Na	10	-	-	Sodium	0.424
Na&Z	8	Untreated	2	Sodium	0.424
Na-EZ	8	Na-exchanged	2	-	-
K	10	-	-	Potassium	0.354
K&Z	8	Untreated	2	Potassium	0.354
K-EZ	8	K-exchanged	2	-	-

C.2.1 Cement Hydration Testing

Isothermal calorimetry was used to compare the rate of hydration of high limestone cement pastes with the rate of hydration of high limestone-zeolite pastes. Testing was done on cement pastes with 0% or 20% zeolite replacement for zeolites. Testing methods are described in Chapter 3, section 3.1.3.1.

C.3 RESULTS AND DISCUSSION

The addition of calcium acetate to a cement paste resulted in negligible changes in the amount of time to both the start of the acceleration period and to the maximum rate of heat release, compared to the cement-only pastes, so it seems that this amount of calcium acetate added to a cement paste does not affect the rate of the reaction during the acceleration period or the maximum rate of heat release. However, the time to the start of the acceleration period and time to the maximum rate of heat release was significantly reduced for all mixtures that included zeolite, whether untreated or cation-exchanged, compared to the cement-only and Ca paste. Addition of calcium acetate did not affect the peak rate of heat release compared to the peak rates of heat evolved for both the cement-only and untreated zeolite pastes, although the shape of the curve is significantly different and points to undersulfation of the system. Addition of the calcium acetate in conjunction with untreated zeolite (Ca&Z) delayed the start of the acceleration period, but decreased the time to the maximum heat release and resulted in a very narrow, high peak curve, evidencing a severely undersufated system. Substitution of cement with Ca-EZ, however, did not produce a similar curve to the Ca&Z curve, as was expected if the differences in the Ca-EZ hydration curves were a result of cations released from the zeolite into the pore solution. The Ca-zeolite did not produce a significant change in the rate of heat

evolution compared to the untreated zeolite-cement paste and merely evolved slightly less heat at its peak compared to the untreated zeolite paste.

The addition of sodium acetate to a cement mixture resulted in a substantial delay in the time to the maximum rate of heat release relative to the zeolite-cement pastes and the cement-only paste, although it did not affect the time to the start of the acceleration period. The maximum rate of heat release from the Na paste was equal to that evolved from the cement-only paste and slightly less than the heat evolved from the untreated zeolite paste. Addition of zeolite tempered the retardation caused by the sodium addition, reducing the delay from the sodium cations, although the mixture was still significantly delayed compared to both the cement-only and untreated zeolite pastes. The Na-EZ-cement paste accelerated the onset of the acceleration period, compared to the cement-only paste and reached its peak of heat release at a similar time compared to the cement only paste. The reactions of the Na-EZ-cement paste were slower than the untreated zeolite cement paste, however. Use of the Na-EZ also resulted in a very large increase in the maximum rate of heat released, with a significantly greater rate of heat release at its peak than either the untreated zeolite or cement-only pastes.

Addition of the potassium acetate to the cement-only mixture resulted in a significant delay in the time to the start of the acceleration period as well as to the time to the maximum rate of heat release, compared to the cement-only and the untreated zeolite pastes. The rate of reaction in the acceleration period was also reduced compared to both the cement-only and untreated zeolite pastes. The K&Z paste reduced the delay from the level seen with the K paste, reaching the start of the acceleration period and maximum

rate of heat release at times similar to the cement-only paste, although the mixture was still delayed relative to the untreated zeolite. The maximum rate of heat evolution was not increased for the K&Z paste from the level generated by the K paste. Incorporation of the K-EZ resulted in an increase in the rate of reaction during the acceleration period compared to the cement-only paste. The times to the start of the acceleration period and to the maximum rate of heat release were similar for the untreated zeolite and K-EZ pastes. In addition to an acceleration of the mixture, use of the K-EZ increased the maximum rate of heat release from the mixture relative to the K and K&Z pastes, although the maximum rate of heat evolution for the K-EZ paste was similar to both the cement-only and untreated zeolite pastes.

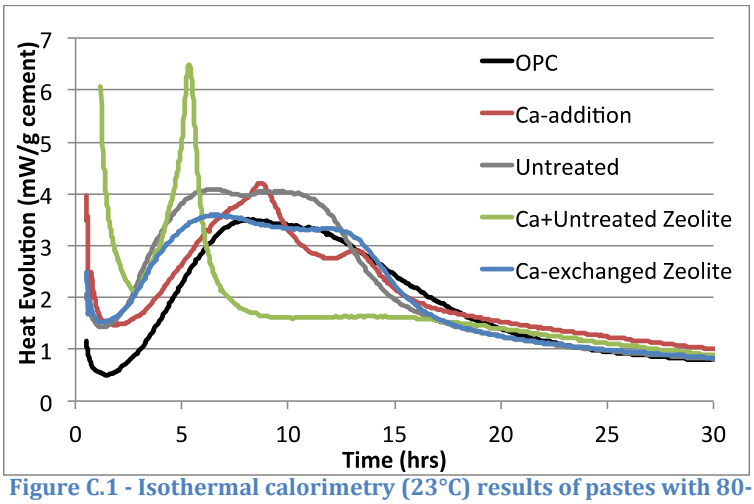

Figure C.1 - Isothermal calorimetry (23°C) results of pastes with 80-100% cement, additions of calcium acetate, and 0-20% untreated or Zeolite T cation exchanged with calcium acetate (w/cm = 0.4)

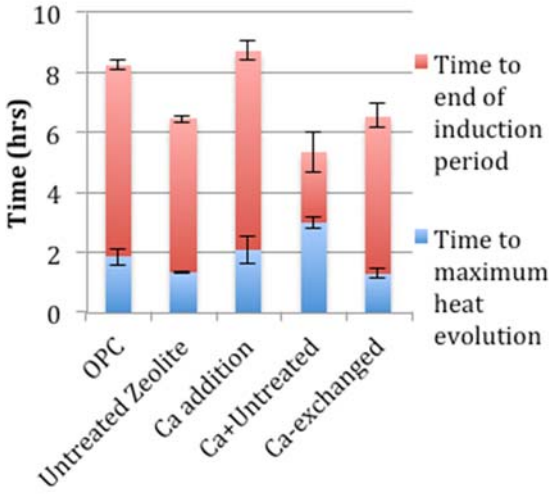

Figure C.2 - Time to the start of the acceleration period and time to the maximum value of heat flow in isothermal calorimetry (23°C) of pastes with 80-100% cement and 0-20% untreated or Zeolite T cation exchanged with calcium acetate (w/cm = 0.4)

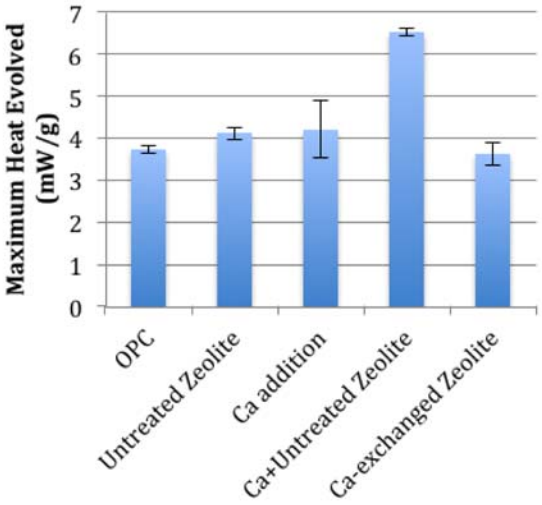

Figure C.3 - Value of the maximum heat flow in isothermal calorimetry (23°C) of pastes with 80-100% cement and 0-20% untreated or Zeolite T cation exchanged with calcium acetate (w/cm = 0.4)

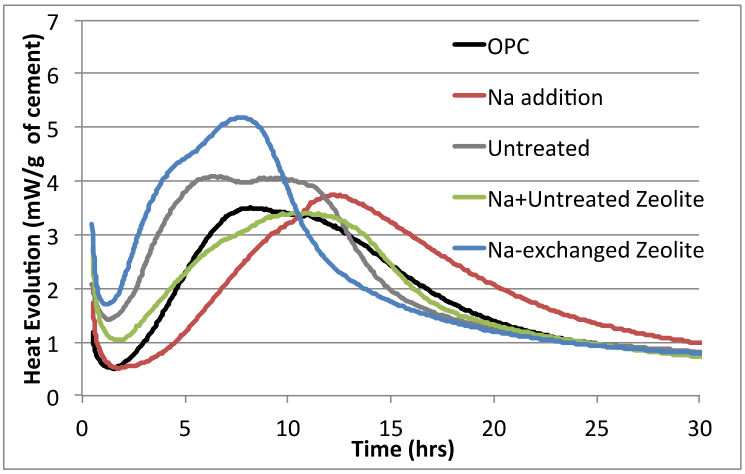

Figure C.4 - Isothermal calorimetry (23°C) results of pastes with 80-100% cement, additions of sodium acetate, and 0-20% untreated or Zeolite T cation exchanged with sodium acetate (w/cm = 0.4)

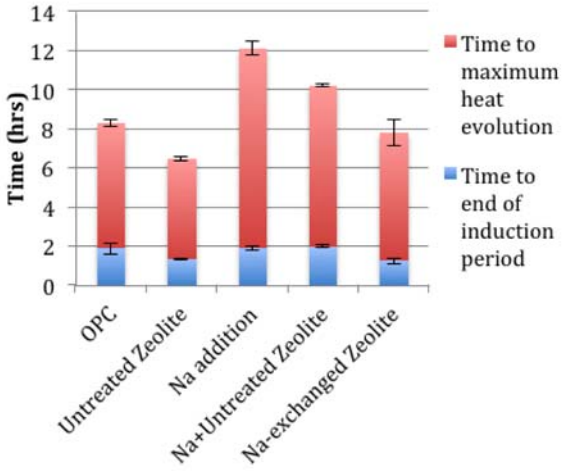

Figure C.5 - Time to the start of the acceleration period and time to the maximum value of heat flow in isothermal calorimetry (23°C) of pastes with 80-100% cement and 0-20% untreated or Zeolite T cation exchanged with sodium acetate (w/cm = 0.4)

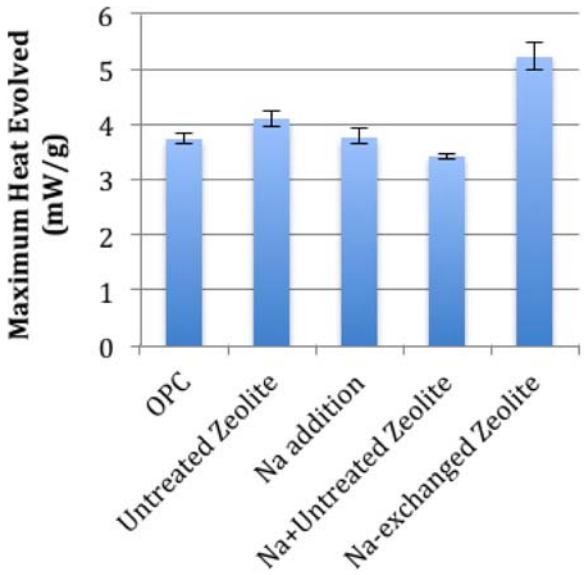

Figure C.6 - Value of the maximum heat flow in isothermal calorimetry (23°C) of pastes with 80-100% cement and 0-20% untreated or Zeolite T cation exchanged with sodium acetate (w/cm = 0.4)

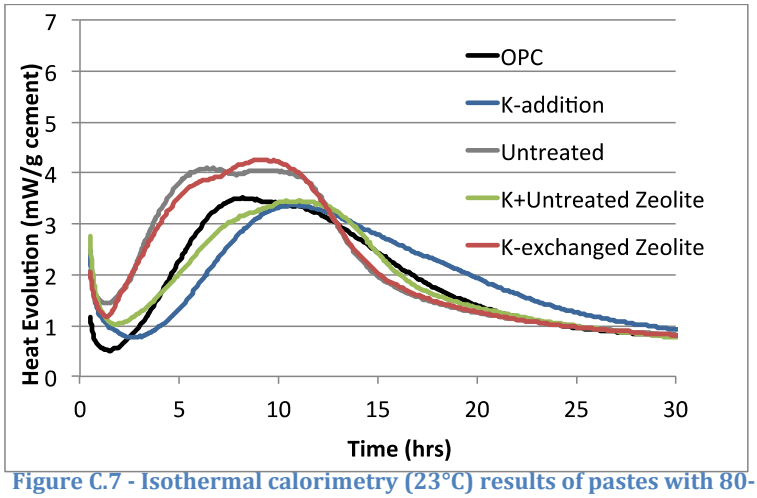

Figure C.7 - Isothermal calorimetry (23°C) results of pastes with 80-100% cement, additions of potassium acetate, and 0-20% untreated or Zeolite T cation exchanged with potassium acetate (w/cm = 0.4)

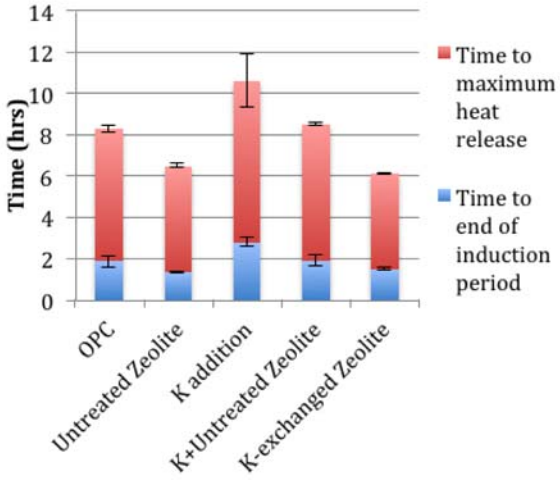

Figure C.8 - Time to the start of the acceleration period and time to the maximum value of heat flow in isothermal calorimetry (23°C) of pastes with 80-100% cement and 0-20% untreated or Zeolite T cation exchanged with potassium acetate (w/cm = 0.4)

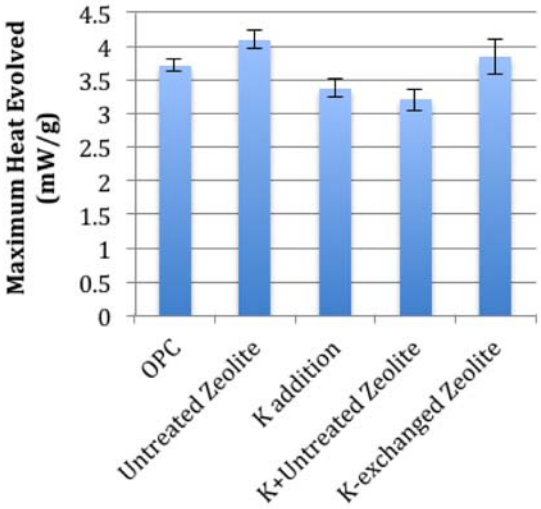

Figure C.9 - Value of the maximum heat flow in isothermal calorimetry (23°C) of pastes with 80-100% cement and 0-20% untreated or Zeolite T cation exchanged with potassium acetate (w/cm = 0.4)

C.4 CONCLUSIONS

The results of the calorimetry testing do not seem to indicate that the changes in heat evolution are as a result of cations being released from the zeolite structure into the pore solution. If the changes in heat evolution were due to cations being released from zeolite structure it would be expected that the heat evolution of the cation exchanged zeolite-cement paste would resemble the heat evolution curve of the cation + untreated zeolite-cement paste. However, none of the cation exchanged zeolite-cement pastes have similar peak rates of heat release or rates of reaction in the acceleration period. The differences between the cation-exchanged zeolite-cement pastes and the untreated zeolite-cement paste may instead be due to destabilization of the zeolite crystal structure due to increased cation content and changes in zeolite surface charge. As Allen et al. (2009) showed, the type of cations in zeolite pores changes the ionic density of the lattice

and thus strongly influences the adsorption of polar molecules. This may affect the interactions between the zeolite and other constituents of the cementitious mixture and result in the increases in heat evolution seen with the cation-exchanged zeolites.

Appendix D: Zeolite Dissolution Testing

D.1 INTRODUCTION

There is little agreement about what zeolite properties determine zeolite reactivity in cementitious mixtures. For example, several studies have suggested that framework SiO_2/Al_2O_3 ratio has an influence on zeolite reactivity (Snellings et al. 2010, Martinez-Ramirez et al. 2006, Lilkov et al. 2011). One study also found reactivity to be also linked to external surface area (Lilkov et al. 2011) and cation content, with Na^+- and K^+- zeolites reacting with a greater quantity of lime in solution than Ca^{2+}- zeolites (Mertens et al. 2009, Snellings et al. 2010). Fineness and percent crystallinity also play important roles in zeolite interactions with cementitious system components, with finer zeolite powders resulting in greater reduction in pore solution pH (Naiqian and Tingyu 1998).

A significant contributor to reactivity is dissolution rate. Thus, in order to understand what affects reactivity, the dissolution behavior must also be understood. With that in mind, this study was developed to increase understanding of the effect of the pore solution on the zeolite.

D.2 EXPERIMENTAL METHODS AND MATERIALS

Zeolite dissolution was studied using a simulated pore solution similar to the one created by Chancey (2008) and shown in Table D.1. 0.8 gram samples of zeolites L, T or C were combined with 15mL of simulated pore solution in 15mL polyethylene centrifuge tubes and rotated continuously end-over-end at 8 rpm until testing. At the specified time, the solutions were filtered using a Buchner funnel setup with a Fisherbrand P5 qualitative

filter paper. The filter paper was weighed prior to filtration in order to ensure that differences in filter paper mass did not contribute to test error. The sample was washed several times before the filtrate was removed from the Buchner funnel and placed in a covered ceramic crucible and dried for 12 hours at 105°C. At the end of drying cycle, the filter papers and dried filtrate were carefully weighed to determine the change in mass for each sample.

Table D.1 – Simulated pore solution recipe used for zeolite dissolution testing

Ion	Concentration (mmol)	Chemical	Quantity in 100mL (g)
K^+	440	KOH	5.61
Na^+	150	NaOH	4.00
Ca^{2+}	40	K_2SO_4	17.42
SO_4^{2-}	180	$Ca(OH)_2$	7.41

D.3 RESULTS

Figure D.1 shows the change in mass over time of a sample of zeolite after exposure to a simulated pore solution. The surface area, cation content, and SiO_2/Al_2O_3 ratio of the zeolite samples are shown in Table D.2 to help understand Figure D.1. All of the zeolites were ground to pass the #100 sieve to remove the effects of differences in particle sizes. Each of the three zeolites exhibited the same trend, initially a gain in mass from the first day until day seven, followed by a continuous loss in mass until the test was truncated at 28 days. XRD scans of the filtered solids, separated from the zeolite T solutions each day, are shown in Figure D.2. No changes in the crystallinity of the sample or phases present are evident in the scans.

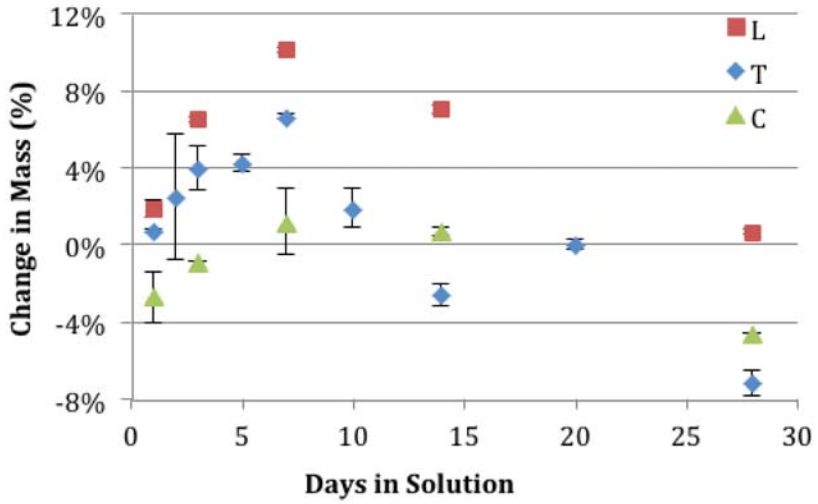

Figure D.1 - Change in mass of zeolite L, C and T after exposure to a simulated pore solution

Table D.2 - Physical and chemical properties of zeolites used in the simulated pore solution study

Zeolite Sample	SSA (m^2/g)	SiO_2/Al_2O_3 (%/%)	CaO (%)	MgO (%)	Na_2O (%)	K_2O (%)	Total Cation Content (%)
L	29.07	5.99	2.2	0.8	0.7	4.2	7.9
T	45.08	5.24	2.2	0.6	1.0	1.7	5.5
C	22.70	4.89	5.5	0.9	3.6	2.6	12.6

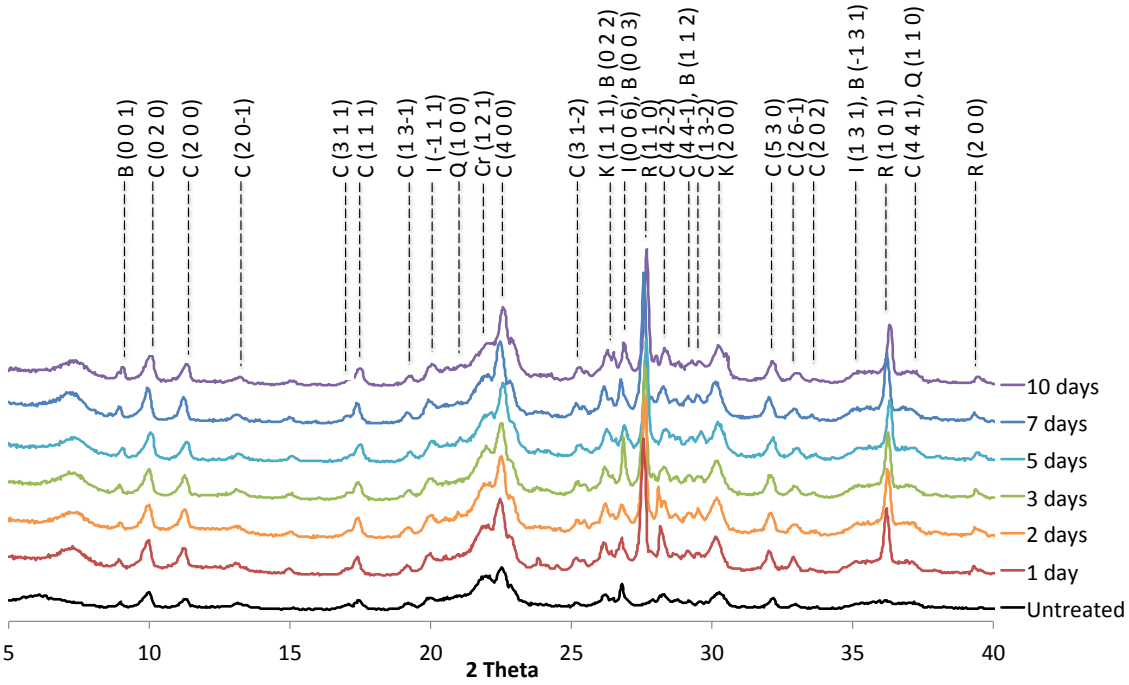

Figure D.2 - Phases present after treatment in simulated pore solution. Rutile was used as a reference material to facilitate quantification of phase changes and is not present in the original sample. (B = biotite, C = clinoptilolite, Q = quartz, K = potassian halite, R = rutile)

D.4 Discussion of the Changes to Zeolites Exposed to Simulated Pore Solutions

The distinct changes in the mass of the zeolite samples exposed to simulated pore solutions, paired with the lack of any change in crystallinity shown in Figure D.2 indicate that the changes due are due to: (1) from days 1-7, uptake of chemically bound water to the zeolite crystal structure; and (2) after day 7, dissolution of the zeolite and removal of dissolved ions during filtration. Increasing the quantity of adsorbed water in the zeolite crystal structure would not result in changes to the crystal structure seen by XRD scans (Kesraoul-Ouki 1993), and similarly, removal of dissolved substances from the zeolite would sustain the proportion of crystalline material present in the zeolite sample, resulting in unchanged XRD scans. Therefore, this test indicates that dissolution, and the pozzolanic reaction, of the zeolite occurred in this sample beginning as early as 7 days after exposure to the simulated pore solution.

Other researchers have found that the pozzolanic reaction begins for zeolites used in cementitious systems between day 3 (Snellings 2010) and day 7 (Cornejo 2014). The findings shown in Figure D.1 support that conclusion because the pore solutions used in this study were not refreshed, so, as cations bonded with zeolite ionic species, they were removed from the system. In a cementitious system, the level of cations in the pore solution would be relatively stable, as hydration continuously released additional cations into solution. The effect of lower concentrations of cations in solution would be to slow the dissolution of the zeolite. Therefore the beginning of dissolution witnessed after 7

days in the simulated pore solution could correspond with an earlier onset of zeolite dissolution and pozzolanic reaction in a true cementitious system.

The magnitudes of the gain or loss in mass of the samples are an indication of the factors responsible for relative zeolite reactivity. It is likely that dissolution is associated with the SiO_2/Al_2O_3 ratio of the zeolites as the sample with the largest gain in mass, zeolite C, was also the sample with the highest SiO_2/Al_2O_3 ratio. Similarly, the sample with the largest mass loss, zeolite C, was the zeolite with the lowest SiO_2/Al_2O_3 ratio. Additionally, shown in Table D.2, surface area and cation contents do not correspond with the results shown in Figure D.1. However, it is possible that the amount of mass loss could also be due to the percentage of impurities in the system or the percent crystallinity of the zeolite, which are not known for these samples. That the SiO_2/Al_2O_3 ratio controls the rate of dissolution, and consequently, the magnitude of pozzolanicity of the material is supported by the results shown in Figure D.1 indicating the increasing influence of SiO_2/Al_2O_3 ratio in determining CH content of pastes.

D.5 CONCLUSIONS

Using simulated pore solutions, zeolites were shown to dissolve starting around day 7, with their magnitude of dissolution related closely to SiO_2/Al_2O_3 ratio.

References

18-513, N. (2010). “NF P 18-513: Metakaolin, addition pouzzolanique pour betons.”

Ahmadi, B., and Shekarchi, M. (2010). “Use of natural zeolite as a supplementary cementitious material.” *Cement and Concrete Composites*, 32, 134–141.

Aini, N. S., Amsyar Haniff, M. H. M., Fadzil, M. a., Ridzuan, a. R. M., and Abdul Halim, a. G. (2013). “Effect of WPSA particle size to the morphology and compressive strength properties of hydrated cement paste contain WPSA as SCM.” *2013 IEEE Business Engineering and Industrial Applications Colloquium (BEIAC)*, 301–305.

Allen, S. J., Ivanova, E., and Koumanova, B. (2009). “Adsorption of sulfur dioxide on chemically modified natural clinoptilolite. Acid modification.” *Chemical Engineering Journal*, 152(2-3), 389–395.

Alver, B. E., Sakizci, M., and Yörükoğullari, E. (2009). “Investigation of clinoptilolite rich natural zeolites from Turkey: a combined XRF, TG/DTG, DTA and DSC study.” *Journal of Thermal Analysis and Calorimetry*, 100(1), 19–26.

Ann, K. Y., and Song, H.-W. (2007). “Chloride threshold level for corrosion of steel in concrete.” *Corrosion Science*, 49(11), 4113–4133.

Antoni, M., Rossen, J., Martirena, F., and Scrivener, K. (2012). “Cement substitution by a combination of metakaolin and limestone.” *Cement and Concrete Research*, 42, 1579–1589.

“ASTM C109: Standard Test Method for Compressive Strength of Hydraulic Cement Mortars (Using 2-in . or [50-mm] Cube Specimens).” (2011). *ASTM International*, West Conshohocken, PA, 2005.

“ASTM C305: Standard Practice for Mechanical Mixing of Hydraulic Cement Pastes and Mortars.” (2011). *ASTM International,* West Conshohocken, PA, 2005.

"ASTM C1157: Standard Performance Specification for Hydraulic Cement.” (2011). *ASTM International*, West Conshokocken, PA, 2005.

"ASTM C1567: Standard Test Method for Determining the Potential Alkali-Silica Reactivity of Combinations of Cementitious Materials and Aggregate (Accelerated Mortar-Bar Method).” (2011). *ASTM International,* West Conshokocken, PA, 2005.

"ASTM C1679: Standard Practice for Measuring the Hydration Kinetics of Hydraulic Cementitious Mixtures Using Isothermal Calorimetry." (2009). *ASTM International*, West Conshohocken, PA, 2005.

Ates, A., and Hardacre, C. (2012). "The effect of various treatment conditions on natural zeolites: ion exchange, acidic, thermal and steam treatments." *Journal of colloid and interface science*, 372(1), 130–40.

Aumento, F. (1966). "Thermal Transformations of Stilbite." *Canadian Journal of Earth Sciences*, 3(3), 351–366.

Bae, Y.-S., Yazaydin, a O., and Snurr, R. Q. (2010). "Evaluation of the BET method for determining surface areas of MOFs and zeolites that contain ultra-micropores." *Langmuir : the ACS journal of surfaces and colloids*, 26(8), 5475–83.

Beers, a. (2003). "Optimization of zeolite Beta by steaming and acid leaching for the acylation of anisole with octanoic acid: a structure–activity relation." *Journal of Catalysis*, 218(2), 239–248.

Bergerhoff, G., and Brown, I. D. (1987). "Crystallographic Databases." *International Union of Crystallography*.

Bilim, C. (2011). "Properties of cement mortars containing clinoptilolite as a supplementary cementitious material." *Construction and Building Materials*, 25(8), 3175–3180.

Blanco Varela, M. T., Martinez Ramirez, S., Erena, I., Gener, M., and Carmona, P. (2006). "Characterization and pozzolanicity of zeolitic rocks from two Cuban deposits." *Applied Clay Science*, 33(2), 149–159.

Bongdanov, B., Georgiev, D., Krasimira, A., and Yaneva, K. (2009). "Natural Zeolites: Clinoptilolite Review." *International Science Conference: Economics and Society development on the Base of Knowledge*, Stara Zagora, Bulgaria, 6–11.

Bookin, A. S., and Drits, V. A. (1993). "Polytype diversity of the hydrotalcite-like minerals. I. Possible polytupes and their diffraction features" *Clays and Clay Minerals*, 41(5), 551–557.

Borrachero, M. V., Payá, J., Bonilla, M., and Monzó, J. (2008). "The use of thermogravimetric analysis technique for the characterization of construction materials." *Journal of Thermal Analysis and Calorimetry*, 91(2), 503–509.

Branco, F. A., Mendes, P., and Mirambell, E. (1992). "Heat of Hydration Effects in Concrete Structures." *ACI Materials Journal*, 89(2), 139–145.

Bullard, J. W., Jennings, H. M., Livingston, R. a., Nonat, A., Scherer, G. W., Schweitzer, J. S., Scrivener, K. L., and Thomas, J. J. (2011). "Mechanisms of cement hydration." *Cement and Concrete Research*, 41(12), 1208–1223.

Cakicioglu-Ozkan, F., and Ulku, S. (2005). "The effect of HCl treatment on water vapor adsorption characteristics of clinoptilolite rich natural zeolite." *Microporous and Mesoporous Materials*, 77(1), 47–53.

Caputo, D., Liguori, B., and Colella, C. (2008). "Some advances in understanding the pozzolanic activity of zeolites: The effect of zeolite structure." *Cement and Concrete Composites*, 30(5), 455–462.

Chancey, R. T. (2008). "Characterization of Crystalline and Amorphous Phases and Respective Reactivities in a Class F Fly Ash." University of Texas at Austin.

Charkhi, A., Kazemian, H., and Kazemeini, M. (2010). "Optimized experimental design for natural clinoptilolite zeolite ball milling to produce nano powders." *Powder Technology*, 203(2), 389–396.

Cheng-yi, H., and Feldman, R. F. (1985). "Hydration reactions in portland cement-silica fume blends." *Cement and Concrete Research*, 15, 585–592.

Cheung, J., Jeknavorian, a., Roberts, L., and Silva, D. (2011). "Impact of admixtures on the hydration kinetics of Portland cement." *Cement and Concrete Research*, 41(12), 1289–1309.

Chindaprasirt, P., Jaturapitakkul, C., and Sinsiri, T. (2005). "Effect of fly ash fineness on compressive strength and pore size of blended cement paste." *Cement and Concrete Composites*, 27(4), 425–428.

Cleary, P. W. (2009). "Ball motion, axial segregation and power consumption in a full scale two chamber cement mill." *Minerals Engineering*, 22(9-10), 809–820.

Colella, C. (1996). "Ion exchange equilibria in zeolite minerals." *Mineral Deposita*, 31, 554–562.

Colella, C., Gennaro, M. D., and Aiello, R. (2001). "Use of Zeolitic Tuff in the Building Industry." *Reviews in Mineralogy and Geochemistry*, 45(1), 551–587.

Cornejo, M. H., Elsen, J., Paredes, C., and Baykara, H. (2013). "Thermomechanical treatment of two Ecuadorian zeolite-rich tuffs and their potential usage as supplementary cementitious materials." *Journal of Thermal Analysis and Calorimetry*, 115(1), 309–321.

Costa, U., and Massazza, F. (1974). “Costa - 1974 - Factors affecting the reaction with lime of Italian pozzolanas.pdf.” *Pozzolane Italiane*, 3, 131–140.

Cyr, M., Lawrence, P., and Ringot, E. (2005). “Mineral admixtures in mortars, Quantificantion of the physical effects of inert materials on short-term hydration.” *Cement and Concrete Research*, 35(4), 719–730.

Cyr, M., Lawrence, P., and Ringot, E. (2006). “Efficiency of mineral admixtures in mortars: Quantification of the physical and chemical effects of fine admixtures in relation with compressive strength.” *Cement and Concrete Research*, 36(2), 264–277.

Day, R. L., and Shi, C. (1994). “Influence of the fineness of pozzolan on the strength of lime natural-pozzolan cement pastes.” *Cement and Concrete Research*, 24(8), 1485–1491.

Downs, R. T., and Hall-Wallace, M. (2003). “The American Mineralogist crystal structure database.” *American Mineralogist*, 88, 247–250.

Duvarcı, Ö. Ç., Akdeniz, Y., Özmıhçı, F., Ülkü, S., Balköse, D., and Çiftçioğlu, M. (2007). “Thermal behaviour of a zeolitic tuff.” *Ceramics International*, 33(5), 795–801.

Edwards, G. C., and Angstadt, R. L. (1966). “The effect of some soluble inorganic admixtures on the early hydration of portland cement.” *Journal of Applied Chemistry*, 16, 166–168.

Elaiopoulos, K., Perraki, T., and Grigoropoulou, E. (2010). “Monitoring the effect of hydrothermal treatments on the structure of a natural zeolite through a combined XRD, FTIR, XRF, SEM and N2-porosimetry analysis.” *Microporous and Mesoporous Materials*, 134(1-3), 29–43.

Ene, G. (2007). “The Grinding Charge of Rotary.” *The Annals of “Dunarea de Jos” University of Galati*, 35–41.

Esping, O. (2008). “Effect of limestone filler BET(H_2O)-area on the fresh and hardened properties of self-compacting concrete.” *Cement and Concrete Research*, 38(7), 938–944.

Fernández, R., Vigil de la Villa, R Garcia, E. V.-C., Fernández, R., Villa, R. V. de la, Garcia, R., and Villar-Cociña, E. (2011). “Characterization and pozzolanic activity of a calcined natural zeolite.” *13th International Congress on the Chemistry of Cement*, 1–7.

Glass, G. K., and Buenfeld, N. R. (1997). "The presentation of the chloride threshold level for corrosion of steel in concrete." *Corrosion Science*, 39(5), 1001–1013.

Gordon, L. E., Milestone, N. B., and Angus, M. J. (2011). "The Immobilisation of Clinoptilolite Within Cementitious Systems." *MRS Proceedings*, 1107(0), 135.

Habert, G., Choupay, N., Montel, J. M., Guillaume, D., and Escadeillas, G. (2008). "Effects of the secondary minerals of the natural pozzolans on their pozzolanic activity." *Cement and Concrete Research*, 38(7), 963–975.

Odler, I. (2004). *Lea's Chemistry of Cement and Concrete*. (P. C. Hewlett, ed.), Elsevier Science and Technology Books.

Huizhen, L. (1992). "Effect of Structure and Composition on Reactivity of Zeolite-Tuff Used as Blending Material for Portland Cement." *9th International Congress on the Chemistry of Cement*, New Dehli, India, 129–134.

Hussain, S. E., Rasheeduzzafar, Al-Musallam, A., and Al-Gahtani, A. S. (1995). "Factors Affecting Threshold Chloride for Reinforcement Corrosion in Concrete." *Cement and Concrete Research*, 25(7), 1543–1555.

Inglezakis, V. J. (2005). "The concept of 'capacity' in zeolite ion-exchange systems." *Journal of colloid and interface science*, 281(1), 68–79.

Inventory of U.S. Greenhouse Gas Emissions and Sinks: 1990-2011. (2013). Retrieved January 26, 2014, from http://www.epa.gov/climatechange/Downloads/ghgemissions/US-GHG-Inventory-2013-Main-Text.pdf

Isaia, G. ., Gastaldini, a. L. ., and Moraes, R. (2003). "Physical and pozzolanic action of mineral additions on the mechanical strength of high-performance concrete." *Cement and Concrete Composites*, 25(1), 69–76.

Jankovic, A., Valery, W., and Davis, E. (2004). "Cement grinding optimisation." *Minerals Engineering*, 17(11-12), 1075–1081.

Janotka, I., and Krajči, L. (2008). "Sulphate resistance and passivation ability of the mortar made from pozzolan cement with zeolite." *Journal of thermal analysis and calorimetry*, 94, 7–14.

Janotka, I., Osaky, M., Križma, M., and Bágel', Ľ. (2011). "Performance Study of Slovak Natural Zeolite - Containing Cement Compositions." *Proceedings of the 13th International Congress on the Chemistry of Cement*, 1-7.

Johnson, M., O'Connor, D., Barnes, P., Catlow, C. R. a., Owens, S. L., Sankar, G., Bell, R., Teat, S. J., and Stephenson, R. (2003). "Cation Exchange, Dehydration, and Calcination in Clinoptilolite: In Situ X-ray Diffraction and Computer Modeling." *The Journal of Physical Chemistry B*, 107(4), 942–951.

Kadri, E. H., Aggoun, S., Schutter, G., and Ezziane, K. (2009). "Combined effect of chemical nature and fineness of mineral powders on Portland cement hydration." *Materials and Structures*, 43(5), 665–673.

Kadri, E.-H., and Duval, R. (2009). "Hydration heat kinetics of concrete with silica fume." *Construction and Building Materials*, 23(11), 3388–3392.

Kantro, D. L. (1974). "Tricalcium Silicate Hydration in the Presence of Various Salts." *ASTM Symposium on Acceleration of Setting and Hardening in Cement Pastes-Causes and Effects*, Washington, D.C., 312–320.

Karakurt, C., and Topçu, İ. B. (2011). "Effect of blended cements produced with natural zeolite and industrial by-products on alkali-silica reaction and sulfate resistance of concrete." *Construction and Building Materials*, 25(4), 1789–1795.

Kesraoul-oukl, S., Cheeseman, C., and Perry, R. (1993). "Effects of Conditioning and Treatment of Chabazite and Clinoptilolite Prior to Lead and Cadmium Removal." *Environmental Science & Technology*, 27(6), 1108–1116.

Khaleghian-Moghadam, R., and Seyedeyn-Azad, F. (2009). "A study on the thermal behavior of low silica X-type zeolite ion-exchanged with alkaline earth cations." *Microporous and Mesoporous Materials*, 120(3), 285–293.

Kielland, J. (1937). "Individual activity coefficients of ions in aqueous solutions." *Journal of the American Chemical Society*, 59, 1675–1678.

Kitsopoulos, K. P. (1999). "Cation-exchange capacity (CEC) of zeolitic volcaniclastic materais: Applicability of the ammonium acetate saturation (AMAS) method." *Clays and Clay Minerals*, 47(6), 688–696.

Klieve, J. R., and Semmens, M. J. (1980). "An evaluation of pretreated natural zeolites for ammonium removal." *Water Research*, 14, 161–168.

Knowlton, G. D., White, T. E. D. R., and Mckague, H. L. (1981). "Thermal study of types of water associated with clinoptilolite." *Clays and Clay Minerals*, 29(5), 403–411.

Kosanovic, C., Bronic, J., Cizmek, A., Subotic, B., Smit, I., Stubicar, M., and Tonejc, A. (1995). "Mechanochemistry of zeolites : Part 3 . Amorphization of zeolite ZSM-5 by ball milling." *Zeolites*, 15(June 1994), 51–57.

Kosanovic, C., Subotic, B., Smit, I., Cizmek, A., Stubicar, M., and Tonejc, A. (1997). "Study of structural transformations in potassium-exchanged zeolite A induced by thermal and mechanochemical treatments." *Journal of Materials Science*, 32, 73–78.

Kumar, S., Kumar, R., Bandopadhyay, a., Alex, T. C., Ravi Kumar, B., Das, S. K., and Mehrotra, S. P. (2008). "Mechanical activation of granulated blast furnace slag and its effect on the properties and structure of portland slag cement." *Cement and Concrete Composites*, 30(8), 679–685.

Lawrence, P., Cyr, M., and Ringot, E. (2003). "Mineral admixtures in mortars." *Cement and Concrete Research*, 33(12), 1939–1947.

Lawrence, P., Cyr, M., and Ringot, E. (2005). "Mineral admixtures in mortars effect of type, amount and fineness of fine constituents on compressive strength." *Cement and Concrete Research*, 35(6), 1092–1105.

Lerch, W. (1946). "The Influence of Gypsum on the Hydration and Properties of Portland Cement Pastes." *American Society for Testing Materials*, 12, 1–41.

Liebig, E., and Althaus, E. (1998). "Pozzolanic Activity of Volcanic Tuff and Suevite: Effects of Calcination." *Cement and Concrete Research*, 28(4), 567–575.

Lilkov, V., Petrov, O., Petkova, V., Petrova, N., and Tzvetanova, Y. (2011). "Study of the pozzolanic activity and hydration products of cement pastes with addition of natural zeolites." *Clay Minerals*, 46(2), 241–250.

Lilkov, V., Petrov, O., and Tzvetanova, Y. (2011). "Rheological, porosimetric, and SEM studies of cements with additions of natural zeolites." *Clay Minerals*, 46(2), 225–232.

Lilkov, V., Rostovsky, I., and Petrov, O. (2011). "Physical and mechanical characteristics of cement mortars and concretes with addition of clinoptilolite from Beli Plast deposit (Bulgaria), silica fume and fly ash." *Clay Minerals*, 46(2), 213–223.

Lothenbach, B., Scrivener, K., and Hooton, R. D. (2011). "Supplementary cementitious materials." *Cement and Concrete Research*, 41(12), 1244–1256.

Martinezramirez, S., Blancovarela, M., Erena, I., and Gener, M. (2006). "Pozzolanic reactivity of zeolitic rocks from two different Cuban deposits: Characterization of reaction products." *Applied Clay Science*, 32(1-2), 40–52.

Matias, P., Lopes, J. M., Ayrault, P., Laforge, S., Magnoux, P., Guisnet, M., and Ribeiro, F. R. (2009). “Effect of dealumination by acid treatment of a HMCM-22 zeolite on the acidity and activity of the pore systems.” *Applied Catalysis A: General*, 365(2), 207–213.

McCarthy, G. J., Johansen, D. M., Steinward, S. J., and Thedchanamoorthy, A. (1988). “X-ray diffraction analysis of fly ash.” *Advances in X-ray analysis*, 331–342.

Menendez, G., Bonavetti, V., and Irassar, E. F. (2003). “Strength development of ternary blended cement with limestone filler and blast-furnace slag.” *Cement and Concrete Research*, 25, 61–67.

Mertens, G., Snellings, R., Van Balen, K., Bicer-Simsir, B., Verlooy, P., and Elsen, J. (2009). “Pozzolanic reactions of common natural zeolites with lime and parameters affecting their reactivity.” *Cement and Concrete Research*, 39(3), 233–240.

Mielenz, R. C., Greene, K. T., and Schieltz, N. C. (1951). “Natural Pozzolans for Concrete.” *Economic Geology*, 46, 311–328.

Minard, H., Garrault, S., Regnaud, L., and Nonat, A. (2007). “Mechanisms and parameters controlling the tricalcium aluminate reactivity in the presence of gypsum.” *Cement and Concrete Research*, 37(10), 1418–1426.

Moosberg-Bustnes, H., Lagerblad, B., and Forssberg, E. (2004). “The function of fillers in concrete.” *Materials and Structures*, 37, 74–81.

Morel, F. M. M., and Herring, J. G. (1993). *Principles and Application of Aquatic Chemistry*. John Wiley & Sons, 588.

Mozgawa, W., Król, M., Pichór, W., and Nocum-Wczelik, W. (2011). “Immobilisation of selected ions in natural clinoptilolite incorporated in cement pastes.” *Intercem 2011 Barcelona*.

Mumpton, F. A. (1999). “La roca magica : Uses of natural zeolites in agriculture and industry.” *Proceedings of the National Academy of Science*, 96, 3463–3470.

Murakami, K., and Tanaka, H. (1969). “Supplementary Paper II-2: Contribution of Calcium Thiosulphate to the Acceleration of the Hydration of Portland Cement and Comparison with Other Soluble Inorganic Salts.” *Proceedings of teh 5th International Congress on Cement Chemistry*, 422–436.

Naceri, A., and Hamina, M. C. (2009). “Use of waste brick as a partial replacement of cement in mortar.” *Waste management (New York, N.Y.)*, Elsevier Ltd, 29(8), 2378–84.

Naiqian, F., and Tingyu, H. (1998). “Mechanism of natural zeolite powder in preventing alkali—silica reaction in concrete.” *Advances in Cement Research*, 10(3), 101–108.

Naranjo, A., Lukefahr, E. (2012). "Where has the fly ash gone?" *Construction Materials and Tips, Texas Department of Transportation*, 1-3.

Niemuth, M. D., Barcelo, L., and Weiss, J. (2012). “Effect of fly ash on optimum sulfate levels measured using heat and strength at early ages.” *Civil Engineering Materials*, 1(1), 1–18.

Oey, T., Kumar, A., Bullard, J. W., Neithalath, N., and Sant, G. (2013a). “The Filler Effect: The Influence of Filler Content and Surface Area on Cementitious Reaction Rates.” *Journal of the American Ceramic Society*, 96(6), 1978–1990.

Oey, T., Kumar, A., Bullard, J. W., Neithalath, N., and Sant, G. (2013b). “The Filler Effect: The Influence of Filler Content and Surface Area on Cementitious Reaction Rates.” *Journal of the American Ceramic Society*, 96(6), 1978–1990.

Ortega, E. A., Cheeseman, C., Knight, J., and Loizidou, M. (2000). “Properties of alkali-activated clinoptilolite.” *Cement and Concrete Research*, 30(10), 1641–1646.

Pabalan, R. T., and Bertetti, F. P. (2001). “Cation-Exchange Properties of Natural Zeolites.” *Reviews in Mineralogy and Geochemistry*, 45(1), 453–518.

Pane, I., and Hansen, W. (2005). “Investigation of blended cement hydration by isothermal calorimetry and thermal analysis.” *Cement and Concrete Research*, 35(6), 1155–1164.

Paya, J., Monzo, J., Borrachero, M. V., Peris, E., and Gonzalez-Lopez, E. (1997). “Mechanical treatments of fly ashes. Part III: Studies on strength development of ground fly ashes (GFA) - Cement mortars.” *Cement and Concrete Research*, 27(9), 1365–1377.

Perez-Ramirez, J., Kapteijn, F., Groen, J. C., Domenech, A., G, M., and Mouljin, J. A. (2003). “Steam-activated FeMFI zeolites. Evolution of iron species and activity in direct N2O decomposition.” *Journal of Catalysis*, 214(1), 33–45.

Perraki, T., Kakali, G., and Kontoleon, F. (2003). “The effect of natural zeolites on the early hydration of Portland cement.” *Microporous and Mesoporous Materials*, 61(1-3), 205–212.

Perraki, T., Kakali, G., and Kontori, E. (2005). “Characterization and pozzolanic activity of thermally treated zeolite.” *Journal of Thermal Analysis and Calorimetry*, 82(1), 109–113.

Perraki, T., Kontori, E., Tsivilis, S., and Kakali, G. (2010). "The effect of zeolite on the properties and hydration of blended cements." *Cement and Concrete Composites*, 32(2), 128–133.

Poon, C. S., Kou, S. C., and Lam, L. (2006). "Compressive strength, chloride diffusivity and pore structure of high performance metakaolin and silica fume concrete." *Construction and Building Materials*, 20(10), 858–865.

Poon, C. S., Lam, L., Kou, S. C., and Lin, Z. S. (1999). "A study on the hydration rate of natural zeolite blended cement pastes." *Construction and Building Materials*, 13, 427–432.

Princigallo, A., Lura, P., van Breugel, K., and Levita, G. (2003). "Early development of properties in a cement paste: A numerical and experimental study." *Cement and Concrete Research*, 33(7), 1013–1020.

Fernández, R., Vigil de la Villa, R., Garcia, E. V.-C., Fernández, R., Villa, R. V. de la, Garcia, R., and Villar-Cociña, E. (2011). "Characterization and pozzolanic activity of a calcined natural zeolite." *13th International Congress on the Chemistry of Cement*, 1–7.

Rahhal, V., and Talero, R. (2005). "Early hydration of portland cement with crystalline mineral additions." *Cement and Concrete Research*, 35(7), 1285–1291.

Ramachandran, V. S. (2001). "Thermal Analysis." *Handbook of Analytical Techniques in Concrete Science and Technology*, V. S. Ramachandran and J. J. Beaudoin, eds., Norwich, New York, 990.

Ramezanianpour, A. a., Ghiasvand, E., Nickseresht, I., Mahdikhani, M., and Moodi, F. (2009). "Influence of various amounts of limestone powder on performance of Portland limestone cement concretes." *Cement and Concrete Composites*, 31(10), 715–720.

Reynolds, Jr., R. (1989). "Principles of Powder Diffraction." *Modern Powder Diffraction*, Mineralogical Society of America, Washington, D.C.

Rivera, A., Rodriguez-Fuentes, G., and Altshuler, E. (2000). "Time evolution of a natural clinoptilolite in aqueous medium : conductivity and pH experiments." *Microporous and Mesoporous Materials*, 40, 173–179.

Rodriguez-Camacho, R. E., and Uribe-Afif, R. (2002). "Importance of using the natural pozzolans on concrete durability." *Cement and Concrete Research*, 32, 1851–1858.

Rosell-Lam, M., Villar-Cociña, E., and Frías, M. (2011). “Study on the pozzolanic properties of a natural Cuban zeolitic rock by conductometric method: Kinetic parameters.” *Construction and Building Materials*, 25(2), 644–650.

Rus, D., Vez, D., Krstulovic, R., and Zelic, J. (2000). “The role of silica fume in the kinetics and mechanisms during the early stage of cement hydration.” *Cement and Concrete Research*, 30, 1655–1662.

Sabir, B. ., Wild, S., and Bai, J. (2001). “Metakaolin and calcined clays as pozzolans for concrete: a review.” *Cement and Concrete Composites*, 23(6), 441–454.

Salvestrini, S., Sagliano, P., Iovino, P., Capasso, S., and Colella, C. (2010). “Atrazine adsorption by acid-activated zeolite-rich tuffs.” *Applied Clay Science*, 49(3), 330–335.

Schindler, A. K., and Folliard, K. J. (2005). “Heat of Hydration Models for Cementitious Materials.” *ACI Materials Journal*, 102(1), 24–33.

Shao, Y., Lefort, T., Moras, S., and Rodriguez, D. (2000). “Studies on concrete containing ground waste glass.” *Cement and Concrete Research*, 30(1), 91–100.

Shi, C., and Day, R. L. (2000). “Pozzolanic reaction in the presence of chemical activators Part II . Reaction products and mechanism.” *Cement and Concrete Research*, 30, 607–613.

Shi, C., Wu, Y., Riefler, C., and Wang, H. (2005). “Characteristics and pozzolanic reactivity of glass powders.” *Cement and Concrete Research*, 35(5), 987–993.

Snellings, R., Mertens, G., Cizer, Ö., and Elsen, J. (2010). “Early age hydration and pozzolanic reaction in natural zeolite blended cements: Reaction kinetics and products by in situ synchrotron X-ray powder diffraction.” *Cement and Concrete Research*, 40(12), 1704–1713.

Snellings, R., Mertens, G., and Elsen, J. (2009). “Calorimetric evolution of the early pozzolanic reaction of natural zeolites.” *Journal of Thermal Analysis and Calorimetry*, 101(1), 97–105.

Snellings, R., Mertens, G., and Elsen, J. (2012). “Supplementary Cementitious Materials.” *Reviews in Mineralogy and Geochemistry*, 74(1), 211–278.

Snellings, R., Mertens, G., Gasharova, B., Garbev, K., and Elsen, J. (2010). “The pozzolanic reaction between clinoptilolite and portlandite: a time and spatially resolved IR study.” *European Journal of Mineralogy*, 22(6), 767–777.

Sprynskyy, M., Buszewski, B., Terzyk, A. P., and Namieśnik, J. (2006). “Study of the selection mechanism of heavy metal (Pb^{2+}, Cu^{2+}, Ni^{2+}, and Cd^{2+}) adsorption on clinoptilolite.” *Journal of colloid and interface science*, 304(1), 21–8.

Tao, Y., Kanoh, H., Abrams, L., and Kaneko, K. (2006). “Mesopore-modified zeolites: preparation, characterization, and applications.” *Chemical reviews*, 106(3), 896–910.

Taylor-Lange, S. C., Riding, K. a., and Juenger, M. C. G. (2012). “Increasing the reactivity of metakaolin-cement blends using zinc oxide.” *Cement and Concrete Composites*, 34(7), 835–847.

Thomas, J. J., Jennings, H. M., Chen, J. J., Quentin, S., and Falla, V. (2009). “Influence of Nucleation Seeding on the Hydration Mechanisms of Tricalcium Silicate and Cement.” *Journal of Physical Chemistry C*, 113, 4327–4334.

Thompson, B. (2013). “Overview of Traditional/Classical Statistical Approaches.” *The Oxford Handbook of Quantitative Methods, Volume 2 - Statistical Analysis*, 7–24.

Thongsanitgarn, P., Wongkeo, W., Sinthupinyo, S., and Chaipanich, A. (2011). “Effect of Limestone Powders on Compressive Strength and Setting Time of Portland-Limestone Cement Pastes.” *Advanced Materials Research*, 343-344, 322–326.

Triantafillidis, C. S., Vlessidis, A. G., Nalbandian, L., and Evmiridis, N. P. (2001). “E ffect of the degree and type of the dealumination method on the structural , compositional and acidic characteristics of H-ZSM-5 zeolites.” *Microporous and Mesoporous Materials*, 47, 369–388.

Tsivilis, S., Chaniotakis, E., Kakali, G., and Batis, G. (2002). “An analysis of the properties of Portland limestone cements and concrete.” *Cement and Concrete Composites*, 24(3-4), 371–378.

Tuan, N. Van, Guang, Y., and Dai, B. D. (2011). “Study the Hydration Process of Cement Blended with Rice Husk Ash by Means of Isothermal Calorimetry.” *13th International Congress on the Chemistry of Cement*.

Unveren, E., Gunduz, G., and Cakicioglu-Ozkan, F. (2005). “Isomerization of Alpha-Pinene Over Acid Treated Natural Zeolite.” *Chemical Engineering Communications*, 192, 386–404.

USGS, "Mineral Yearbook Zeolites (Advance Release)," (2011) http://minerals.usgs.gov/minerals/pubs/commodity/zeolites/myb1-2011-zeoli.pdf

USGS, "Mineral Commodity Summaries, Zeolites," (2012). http://minerals.usgs.gov/minerals/pubs/commodity/zeolites/mcs-2012-zeoli.pdf

Vizcayno, C., de Gutiérrez, R. M., Castello, R., Rodriguez, E., and Guerrero, C. E. (2010). "Pozzolan obtained by mechanochemical and thermal treatments of kaolin." *Applied Clay Science*, 49(4), 405–413.

Wan, H., Shui, Z., and Lin, Z. (2004). "Analysis of geometric characteristics of GGBS particles and their influences on cement properties." *Cement and Concrete Research*, 34(1), 133–137.

Wang, S., and Peng, Y. (2010). "Natural zeolites as effective adsorbents in water and wastewater treatment." *Chemical Engineering Journal*, 156(1), 11–24.

Ward, J. W. (1968). "Spectroscopic study of the surface of zeolite Y. II. Infrared spectra of structural hydroxyl groups and adsorbed water on alkali, alkaline earth, and rare earth ion-exchanged zeolites." *The Journal of Physical Chemistry*, 72(12), 4211–4223.

De Weerdt, K., Haha, M. Ben, Le Saout, G., Kjellsen, K. O., Justnes, H., and Lothenbach, B. (2011). "Hydration mechanisms of ternary Portland cements containing limestone powder and fly ash." *Cement and Concrete Research*, 41(3), 279–291.

De Weerdt, K., Kjellsen, K. O., Sellevold, E., and Justnes, H. (2011). "Synergy between fly ash and limestone powder in ternary cements." *Cement and Concrete Composites*, 33(1), 30–38.

Xie, J., and Kaliaguine, S. (1997). "Zeolite ball milling as a means of enhancing the selectivity for base catalyzed reactions." *Applied Catalysis A: General*, 148(2), 415–423.

Yilmaz, B., Ertun, T., Ucar, A., Oteyaka, B., and Once, G. (2009). "A study on the effect of zeolites (clinoptilolite) on volcanic tuff blended cement pastes and mortars." *Magazine of Concrete Research*, 61(2), 133–142.

Yilmaz, B., Öteyaka, B., Ertün, T., Uçar, A., and Önce, G. (2009). "A study on the effect of zeolites (clinoptilolite) on volcanic tuff blended cement paste and mortars." *Magazine of Concrete Research*, 61(2), 133–142.

Zielinski, P. a., Van Neste, a., Akolekar, D. B., and Kaliaguine, S. (1995). "Effect of high-energy ball milling on the structural stability, surface and catalytic properties of small-, medium- and large-pore zeolites." *Microporous Materials*, 5(3), 123–133.